Cranfield University

Stephen Jude Buggy

Composite material process monitoring using optical fibre grating sensors

School of Engineering
PhD Thesis

Cranfield University

Engineering Photonics Group

School of Engineering

PhD Thesis

2008

Stephen Jude Buggy

Composite material process monitoring using optical fibre grating sensors

Supervisors: Prof. R. P. Tatam, Dr. S. W. James

June 2008

This thesis is submitted in partial fulfilment of the requirement for the degree of Doctor of Philosophy.

Abstract

In this thesis a long period grating (LPG) based sensor is investigated as a possible alternative to current process monitoring sensors used in the manufacture of composites to monitor cure. An LPG is demonstrated as a means of monitoring the cure of a UV-cured epoxy resin. The wavelength shift of the attenuation bands were measured during the cure of the resin and compared with measurements made using a fibre optic Fresnel based refractometer. The results showed a good correlation (6×10^{-3} rius) and illustrate the potential of the techniques for non-invasive composite material cure monitoring. Alternative fibre grating methods; a chirped LPG sensor, an in-fire Mach-Zehnder interferometer and a tilted fibre Bragg grating sensor, are also presented to demonstrate the versatility of grating based sensors for flow, high sensitivity refractive index and multi-parameter sensing, respectively. Demonstrations of LPG sensors in industrial applications are also presented and highlight the technical issues of integrating such devices in composite components and composite manufacturing processes.

Acknowledgements

This work has tested me. If it was not for the love and support provided by my beautiful wife Sarah, it would have been impossible.

My supervisors, Professor Ralph Tatam and Dr. Stephen James, have been very generous with their guidance and support during my PhD for this I am very grateful.

I thank everyone at the Engineering Photonics Group at Cranfield University. For help, assistance and most importantly, for giving me a laugh; Dackson, Dan, Giorgios, Pierre, Helen, Imran, Jane, Jin, Lu, Renata, Ricardo, Richard, Richard, Riyadh, Roger, Roy (honorary member), Sammy, Tom.

I must make special mention of Steve Staines for his engineering wizardry and assistance.

And Dr. Edmond Chehura, whose technical ability, unending patience and often hilarious discussions have aided me throughout my time at Cranfield.

From the School of Applied Sciences I must thank Athanasios Dimopoulos with whom I worked with closely on this project and Professor Ivana Partridge and Dr. Alexandros Skordos.

Thanks must also go to the project partners with particular mention of Dr. Adam Johnstone of Siemens Magnet Technology and Dr. Andrew Twin of Oxford Instruments Nanoscience.

Thank you to my family.

Daisy.....(and Fionn)

List of contents

Introduction 1

1.1 Introduction to composites

Fibre reinforced composite materials are of fundamental importance across a broad range of sectors, particularly the aerospace, marine and automotive sectors [1]. The combination of a high strength fibre network, e.g. carbon or Kevlar and supporting matrix material, either a thermoset, e.g. epoxy or thermoplastic, e.g. polypropylene, creates a material with a high strength to weight ratio [2]. They are typically used in safety critical and high technology applications. The nature of the manufacturing processes involved creates expensive components. This may be explained in part by the inconsistent nature of the process which can lead to; component warpage from residual stresses developed during the cure cycle [3], figure1.1, and voids created from poor impregnation of fibre matrices [4]. It is critical that these effects are avoided to reduce the possibility of in-service failure. In order to reduce costs of manufacture and create quality components it is critical to monitor the resin cure process. Resins require a cure cycle to take them from a liquid state to a vitrified or glass-like state. It is this process that requires feedback from the resin system to ensure that a fibre matrix is fully impregnated and that stresses do not build up within the component due to inhomogeneous cure.

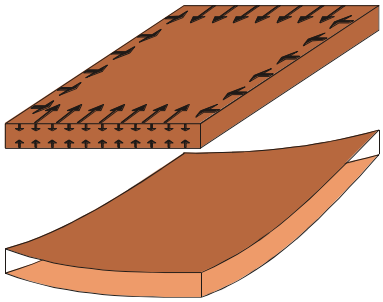

Figure 1.1 Graphical representation of composite warpage.

1.2 Process monitoring

Current on-line monitoring techniques, e.g. spectroscopy and dielectric analysis, have two main inherent disadvantages with respect to their usage. Mould mounted sensors typically monitor the surface resin close to the mould and hence do not accurately monitor the full component. Current embedded sensors, e.g. dielectric, with dimension typically 25mm x 10mm x 0.07 mm [5], have limited use due to their potential to create structural defects in the component As a result although the data from such sensors provides valuable information about the cure process, these types of sensor cannot be employed in safety critical and aerospace components. Traditional methods, e.g. thermal analysis, utilise only composite or resin samples and inherently do not reflect the real process parameters.

1.3 Optical process monitoring

The relatively small dimensions of optical fibres, typically a diameter of 125µm, make them far more attractive for embedded sensor applications in composite materials compared with traditional sensing techniques. They may be readily incorporated into composite parts and have been shown to have a negligible effect on component strength. Fibre optic techniques are already used for in-situ monitoring [7, 8]. However these techniques rely upon single parameter data to determine degree of cure and often require speciality fibres. This project aims to solve these issues by developing a new multi-parameter sensor that will provide data about penetration of resin in the mould

and monitor the refractive index change of the resin which may be related to the degree of cure. Further the advantage of using these new embedded sensors within a composite structure allows the possibility of future health usage monitoring of parameters such as strain and/or temperature.

One such multi-parameter sensor is the long period grating (LPG) [9]. LPGs are formed by modulation of the refractive index of the core of an optical fibre, figure 1.2.

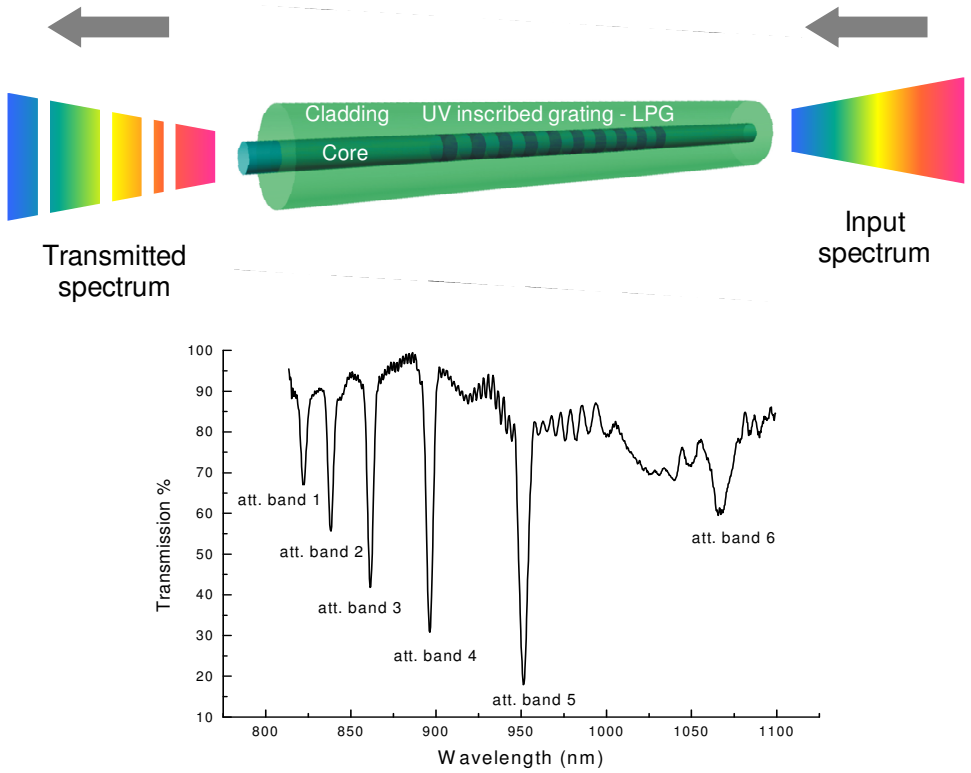

Figure 1.2 Schematic diagram of LPG with typical spectrum showing attenuation bands.

These periodic perturbations, typically with a period of between 10μm and 1000μm, cause light to be coupled from the fundamental core mode to a discrete set of cladding modes. This creates, what are termed as attenuation bands in the transmission spectrum of the fibre and it is these bands that are exploited to facilitate the signal processing of the sensor elements as they exhibit a sensitivity to a number of parameters e.g. temperature, strain and refractive index. In fact it is possible to design an LPG to exhibit

measurand insensitive bands dependant on an application [9]. LPGs have been used to monitor the flow of resins in moulds [10] but as yet have not been exploited as refractometers for measuring degree of cure. They exhibit a significant sensitivity to external refractive index with no requirement for cladding removal. Further, they can fulfil a role as lifetime usage sensors post-cure as they can be designed to be temperature and strain sensitive.

Many optical techniques have been used to monitor resin cure. The majority have employed the use of spectroscopic techniques to yield information about changes in molecular structure during cure. For example, Fourier Transform Infra-red spectroscopy (FTIR) has long been used as a method of analysis and the use of optical fibres to deliver infra-red (IR) light to and from a sample seems a natural progression. The attraction of the use of LPGs as an alternative cure monitoring sensor is their inherent ability to sense refractive index changes. In addition, they can also be used as multi-parameter sensors with sensitivity to temperature and strain. For example, it is possible to discriminate these measurands by utilising a temperature insensitive band to measure refractive index. If considered in this way, the LPG can be utilised as a post processing sensor for structural health and usage monitoring, thus making the LPG a very attractive sensor to industry.

1.4 The Aims and objectives of the work

The focus of this thesis is on the use of long period gratings as fibre optic refractive index sensors for the purpose of cure monitoring of resin systems. Optical refractometry is not new; there are many reports of the use of optical fibres as refractive index sensors in the literature. It has long been known that refractive index can reveal information about a material's molecular structure through the Lorentz-Lorenz relation [11]. The use of refractive index as a cure parameter has also been published [12]. However, the use of an LPG sensor as a cure sensor has not been reported previously. The work explored in this thesis includes the demonstration of the use of an LPG as a refractive index sensor during the cure of an epoxy and the comparison of these results with more traditional techniques. The LPG sensor and adaptations of these sensors are also compared with a Fresnel based refractometry technique. The application of such devices

with real matrices is shown to be problematic due to their high refractive index. For the first time the integration of LPGs in an industrial sense is reported with work involving the application of LPGs as temperature sensors in superconducting magnets and flow and cure sensors in RTM and vacuum bagging trials.

1.5 Thesis layout

The introductory chapter, chapter 2, introduces composite materials with a discussion on the makeup of such materials and the methods of manufacture. This leads to a short discussion on the need for cure monitoring and the current methods employed for this purpose. Finally optical techniques are reviewed with a principle focus on refractive index measurement and a look at the limited work on using LPGs as cure monitoring sensors.

The theoretical background to LPG devices is discussed in chapter 3. This includes a description of a simple Matlab model which is used later in the work to simulate the response of an LPG to changes to the surrounding refractive index. The methods used to manufacture the devices are also explained and the principle techniques utilised in house to manufacture the LPGs used throughout the work are detailed further. Finally characterisation data is demonstrated and compared with the results of previously published work with LPGs.

The application of an LPG as a cure monitoring sensor is demonstrated with a UV epoxy in chapter 4. The experiments demonstrate the capabilities of such sensors with composites. The work is developed further with a parallel refractometry system using Fresnel refractometry to analyse the changing refractive index of a resin during cure. The Fresnel system is used to analyse composite resin systems and the initial results on using LPG sensors with high index resins are reported.

Methods termed advanced fibre grating techniques are reported in chapter 5. This encompasses three different grating applications for the purpose of refractive index monitoring; chirped LPGs, in-fibre Mach-Zehnder devices and tilted fibre Bragg

gratings. The results of these techniques are demonstrated using an ultraviolet cured epoxy resin.

Chapter 6 and 7 covers the industrial application trials of long period gratings in composite systems. Chapter 6 details the work with two industrial collaborators; Oxford Instrument Nanosciences (OINS) and Siemens Magnet Technology (SMT). Both tests involve the integration of fibre gratings in superconducting magnets. These are systems where a resin is used as a structural component together with the superconducting windings to create a mechanically strong composite. The results reveal the data captured during routine post processing testing. Two main stream resin impregnation processes are detailed with grating sensors in chapter 7. Resin transfer moulding or RTM and vacuum bagging are both systems where a fibre network is placed in a mould and impregnated with a resin under pressure (or vacuum). LPGs were integrated within the process to demonstrate the viability of such devices as flow sensors, tracking the progression of the resin in the mould and cure sensors.

The final chapter, chapter 8, brings to a close the thesis with a summary of the results and conclusions from the work. Methods of developing the techniques discussed in the thesis and other possibilities for future work finalise the work presented.

1.6 References

1. Degamber, B. and Fernando, G. F. (2002). Process Monitoring of Fiber-Reinforced Polymer Composites. *MRS Bulletin*, May, p. 370-380.
2. Gay, Daniel. (2002). Composites materials (4th ed), CRC press, Florida.
3. Zarrelli, M. et al. (2006). Warpage induced in bi-material specimens: Coefficient of thermal expansion, chemical shrinkage and viscoelastic modulus evolution during cure. *Composites: Part A*, 37, p. 565–570.
4. Jinlian, H. et al. (2004). Study on void formation in multi-layer woven fabrics. *Composites: Part A*, 35, p. 595–603.

5. Kazilas, M.C. and Partridge I.K. (2005). Exploring equivalence of information from dielectric and calorimetric measurements of thermoset cure—a model for the relationship between curing temperature, degree of cure and electrical impedance. *Polymer,* 46, p. 5868–5878

6. O'Brien, D. J. and White S. R. (2003). Cure Kinetics, Gelation, and Glass Transition of a Bisphenol F Epoxide, *Polymer engineering and science*, 43 (4), p. 863-874.

7. Li, C., Cao, M., Wang, R., Wang, Z., Qiao, Y., Wan, L., Tian, Q., Liu H., Zhang, D., Liang T. and Tang C. (2003). Fiber-optic composite cure sensor: Monitoring the curing process of composite material based on intensity modulation, *Composites Science and Technology*, 63(12), p. 1749-1758.

8. Afromowitz, M. A. and Lam, K.-Y. (1990). The Optical Properties of Curing Epoxies and Applications to the Fiber-Optic Epoxy Cure Sensor, *Sensors and Actuators*, A21-A23, p. 1107-1110 .

9. James, S. W. and Tatam, R. P. T. (2003), 'Optical Fibre Long-period Grating Sensors: Characteristics and Application', *Measurement Science and Technology*, Vol. 14, pp. R49-R61.

10. Kueh, S.R.M., Parnas, R.S., Dunkers, J.P., Advani, S.G., Furrows, P.S., Jones, M.E., and Bailey, T.A. (2000). Long period gratings as flow sensors for liquid composite molding, In: *Nondestructive Evaluation of Aging Materials and Composites IV*, Newport Beach, California, Vol. 3993, Mar 8-9 2000, SPIE, Bellingham, p. 240-250.

11. Batsanov, S. S. (1961). Refractometry and Chemical Structure, Consultants Bureau Enterprises, USA.

12. Lam, K.-Y. and Afromowitz, M.A. (1995). Fiber-optic epoxy composite cure sensor. I. Dependence of refractive index of an autocatalytic reaction epoxy system at 850 nm on temperature and extent of cure, *Applied Optics*, 34(25), p. 5635-8.

Optical techniques for cure monitoring

2

2.1 Introduction to composites and manufacturing methods

A composite material consists of a reinforcement material, typically glass or carbon fibres and a thermoset or thermoplastic resin described in a general sense as a matrix. The combination of these two parts creates a composite material that exhibits excellent strength to weight characteristics and good damage tolerance. These characteristics are the reasons these materials are used extensively in safety critical and high technology applications e.g. aerospace, figure 2.1, automotive, marine and civil engineering. The manner in which the materials are combined is critical to the success of the final component. New technology composites termed AFRCs (advanced fibre reinforced composites) extend the concept of composites further by design of the arrangement and make-up of the reinforcement fibres and maximising the fibre density (volume fraction) without negatively impacting the final materials performance.

Figure 2.1. All composite fuselage section of Boeing Dreamliner [1].

Together with precise chemo-rheologically based modelling of the matrix, AFRCs are contributing more and more to the world of engineering materials because of the ability to 'design' a material, e.g. critical wing components of the Airbus A380. With this comes a need to understand both the fundamentals of the materials and the process involved in bringing them together. The work presented in this chapter focuses primarily on using optical techniques to monitor a single aspect of this process, the cure of the resin (sometimes termed the matrix) system.

Before discussing the process it is perhaps pertinent to look at the individual constituents of composites briefly. The two main constituents are (i) the reinforcement and (ii) the resin or matrix

2.1.1 The reinforcement

The origins of fibre reinforcement in the modern composite lie with synthetic fibres originally developed for the textile industry [2]. The further development of composite specific fibres e.g. carbon and boron with the mechanical strength properties of traditional materials and yet with much less density, led to the interest in composites in safety critical applications. The added attraction of the fibres permits their use in creating complex shapes through specific winding and or weaving processes. Typical properties are shown below, table 2.1, compared with more traditional materials.

Table 2.1 Fibre properties [3].

Materials	E_{11} (GPa)	σ_{11} failure (MPa)	Maximum strain (%)	Density (g/cm^3)	T_{max} (°C)
Fibres					
Boron	400	3600	1	2.53	500
Graphite: stiff (Hercules IMT)	300	5313	1.8	1.78	500
Graphite: strong (Hercules AS-4)	248	4071	1.65	1.8	500
Kevlar 49	138	3034	2.3	1.44	160
Kevlar 29	97	3275	3.9	1.44	160
S-glass	85	4585	5.7	2.48	650
E-glass	72	3448	4.8	2.54	550
Bulk materials					
Steel-SS410	200	1000	20	7.8	780
Aluminium (2024)	73	469	20	2.8	330
Wood (hickory)	15	76	0.5	0.7	100
Plate glass	70	70	0.1	2.5	500

The orientation of the fibres is perhaps the most important design parameter that affects a composites mechanical behaviour. In general there are three types of fibre orientation: 1D, Planar (2D) and 3D. The orientation is part of the design process and the design decision is affected by the end use of the composite component. The 'layup' or orientation of the reinforcement directly affects a composite component's mechanical properties.

A pictorial representation of two commonly used structure types is given in figure 2.2.

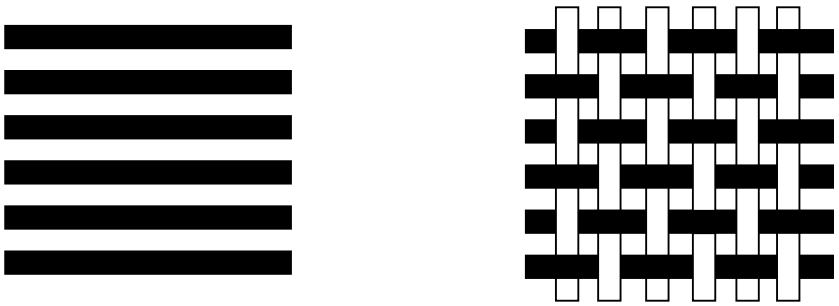

(a) (b)

Figure 2.2 Two examples of reinforcement fibre layouts. (a) unidirectional or linear and (1D) and (b) woven (2D).

Ultimately 1D layups show the greatest mechanical properties but in a single direction. 2D have good properties in both directions whilst 3D or random reinforcements show the lowest mechanical strength properties but exhibit no uniaxial properties and can therefore be designed for structures bearing 3D loads. Fibre volume fraction, V_f is a useful parameter that provides an overall indication of a composite materials strength characteristics. V_f is given by [4]:

$$Vf = \frac{Volume\ of\ \ fibre}{Total\ volume} \qquad 2.1$$

In general a high value for V_f signifies good strength characteristics since it indicates the quantity of the fibres (and hence strength and stiffness) in a composite. A typical value expected for aerospace components is 0.62 (or 62%) [3]. Too great a value for V_F can create resin penetration problems which lead to void formation and stress concentration, the consequence of which may lead to component failure under use. This is an engineering trade-off. Furthermore, the amount of fibres that are able to be 'packed' into a composite is directed by the manner in which they are arranged, i.e. 1D or 2D.

2.1.2 The resin or matrix

The matrix is essentially the body of a composite and it serves two purposes:

1. It holds the fibres together and in place
2. It ensures an even distribution of strain on the reinforcement fibres.

Matrices may be separated into two main groups, thermosets and thermoplastics. Most composites are thermoset based although toughened resin systems are a combination of the two. Typical matrices used in composites are epoxy, polyester, phenalic, cyonacryalate, PEEK, nylon and PPE (polypropylene). A comparison chart for the two resin types is given in table 2.2.

Table 2.2 Table showing simplified characteristics of resin matrices [5].

Resin type	Process temperature	Process time	Use temperature	Solvent resistance	Toughness
Thermoset	Low	High	High	High	Low
	↑	↓	↑	↑	↓
Thermo plastic	High	Low	Low	Low	High

The numerous process methods of combining fibre reinforcement with a matrix are driven by the constituent materials and to some extent the end product. Thermoplastics are generally speaking high molecular weight systems that through the application of heat become workable with sufficiently low viscosities to enable, with difficulty, the wetting of a reinforcement matrix. Thermosets however, are low molecular weight resins with lower viscosities at a similar process stage to that of thermoplastics and thus are more able to permeate reinforcement networks. An irreversible chemical reaction initiated by a catalyst or hardener enables the thermoset to become a dense, inter-linked molecular framework. In essence thermoplastics are melted and combined with a reinforcement to create a composite whilst thermosets are reacted and combined. The manufacturing temperatures of thermoplastics are typically greater (180 - 400°C) than those of equivalent thermosets (20 - 200°C); this potential disadvantage may be offset by their ability to be recycled and to a certain degree re-worked.

2.1.3 The manufacturing process

The manufacturing of composite components seeks to combine the strength properties of the fibre network with the bulk and adhesive nature of the resin effectively creating a new material. The main manufacturing methods are [2-5]; lay-up (hand, spray-up), pultrusion and liquid injection moulding (LIM), e.g. bag moulding and resin transfer moulding (RTM). Hand lay-up involves the placement of fibres which may be pre-impregnated with resin onto an open mould. Compaction of the fibres is done using rollers which squeeze out pockets of air and the curing is done in ambient conditions. This method is used in the aerospace and maritime industries. Spray-up is a semi-mechanised method of applying a reinforcement material in the form of chopped fibres

or roving with a resin through a spray gun onto an open mould. Again cure is achieved in ambient conditions. Typical applications are shower units, furniture and truck panels. For both these processes the typical materials used are epoxies or polyester resins and glass fibre reinforcement. Pultrusion is a method used for large scale manufacture of continuous composite forms, e.g. fishing rods. Fibres are passed through a resin impregnation tank and either pulled through a heated die that forms and cures the material into the component form. Components are then cut from the continuous form on the line to the required lengths. Some examples of the manufacture process are illustrated in figure 2.3.

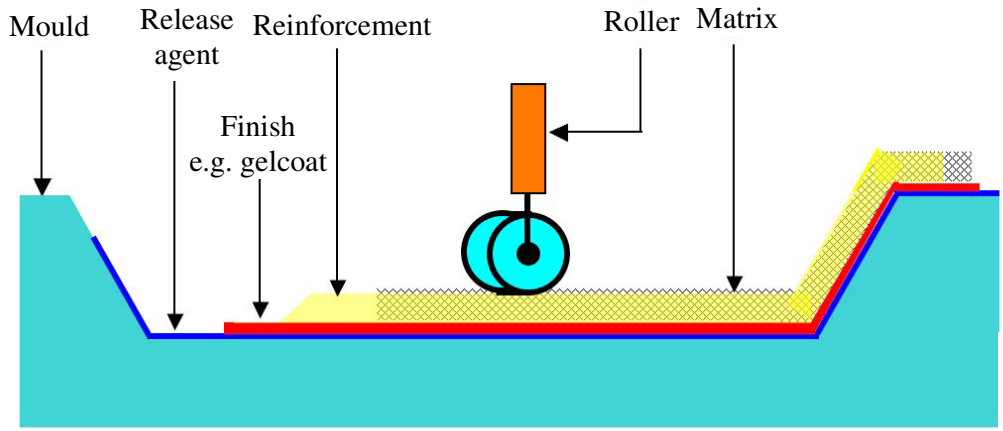

Figure 2.3 (a)

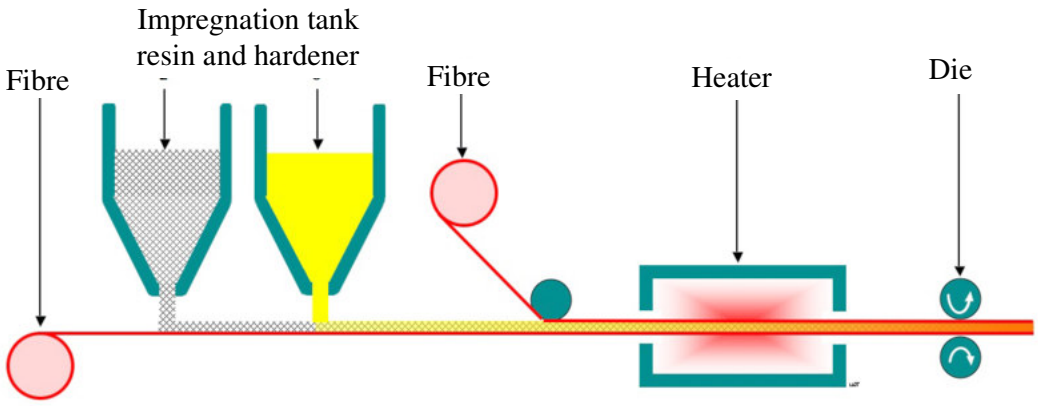

(b)

Figure 2.3 (a) hand lay-up, (b) pultrusion

Bag moulding and resin transfer moulding (RTM) are two forms of closed moulding methods where a mould and reinforcement are sealed and the resin is either transferred to the mould prior to cure or pre-impregnated reinforcement material is used. Bag moulding requires the addition of vacuum, pressure or placement in an autoclave as an additional process to consolidate the fibres and remove any entrapped air and is often termed vacuum infusion. The RTM tooling typically achieves the consolidation through the application of mechanical pressure from a clamping press which seals the mould. A simplified diagram of the RTM process is shown in figure 2.4. Both the RTM process and the vacuum infusion process are used as test beds in the work presented later in this thesis. The implementation of optical sensors for the purpose of flow and cure monitoring forms a large part of the research and the results from these trials are discussed in detail in chapter 6.

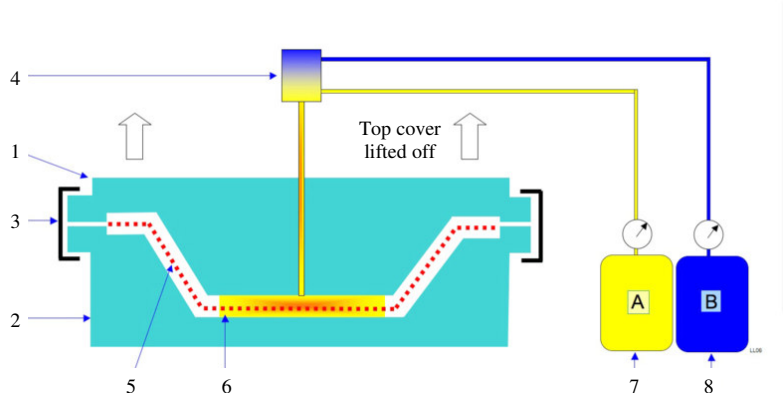

Figure 2.4 Simplified diagram of Resin Transfer Moulding process. 1 - top plate, 2 - mould, 3 - clamps, 4 - mixer, 5 - reinforcement, 6 - injected matrix, 7 - hardener, 8 - resin.

2.2 The need for cure monitoring

All manufacturing processes require control, in fact composites provide an example manufacturing medium that without control would create a worthless end product. The array of materials and processes open to a composite designer mean great variability with process parameters. These parameters must be controlled and monitored to ensure the final component is devoid of defects, is structurally sound and geometrically correct.

With AFRCs these considerations are without compromise as the end product is typically used in safety critical applications. Of particular concern in the manufacture of composites are effects which are attributed to the cure cycle, these are [4]:

- Void formation
- Warping or warpage
- Residual stresses
- Proper cure
- Component quality
- Consistency or repeatability

These areas are possible to address through the application of a cure sensor. Void formation can occur where a resin has not fully wet a reinforcement network. This can result in fibre to fibre contact under load and lead to failure. Residual stresses occur due to the different material properties of the ingredient materials and a phenomenon called shrinkage. Shrinkage occurs because the resin system shrinks when changing from a liquid to a resin. Large stresses can lead to warpage of a component when a component is cooled down. Quality and consistency are rather general terms which cover an important area because of the final application of typical composite components. Because AFRCs work in high tolerance environments variations between component batches are not acceptable, e.g. aerospace components. Components should be fully cured and of the correct dimensions consistently.

In this chapter the typical or industrially utilised sensor types are briefly discussed before a review of optical techniques is introduced. The latter part of this chapter deals with refractometry techniques leading to a section detailing the short body of work on the use of long period gratings as cure sensors.

2.3 Cure monitoring techniques

The multifarious methods of monitoring the cure of thermosets may be divided into three main areas; thermal monitoring, excitation field methods and optical techniques. Invariably each method offers particular advantages or disadvantage over another and is based on a particular parameter associated to the cure mechanism. The purpose for all the techniques is central however and that is to have the ability to quantify the cure state of the resin system. Data from the techniques may also be employed to create cure kinetic models [6]. Correlating a parameter, measurable during cure, to the cure state from developed cure kinetic models allows the possibility to optimise the cure process. Of particular interest in this work are the optical techniques and these are discussed in more detail in section 2.4. A brief discussion follows on thermal and excitation field methods as these techniques are used by industry and they form a benchmark for comparison with optical methods.

2.3.1 Thermal monitoring methods

There are two main thermal monitoring techniques: differential scanning calorimetry (DSC) and differential thermal analysis (DTA) [7]. DSC is based on the heat flow in a resin sample during a cure cycle. The measurement is usually contrasted with a reference sample. It essentially provides data about the exothermic or endothermic reactions taking place by monitoring the amount of heat added to or extracted from the sample to maintain a cure cycle temperature. Points of measurable heat flow indicate the phase transitions of the material. A basic system is illustrated in figure 2.5. DTA is a similar method but in this case a constant heat flow is maintained and the temperature variations of the sample are compared with that of the reference. The methods are coupon or small sample based and although provide accurate quantitative data about a resin cure process they cannot be directly correlated with real component large scale heat flows. The cure kinetic models of the resin systems used throughout this work were developed as part of this project by the School of Applied Sciences and were based partly on DSC measurement [8].

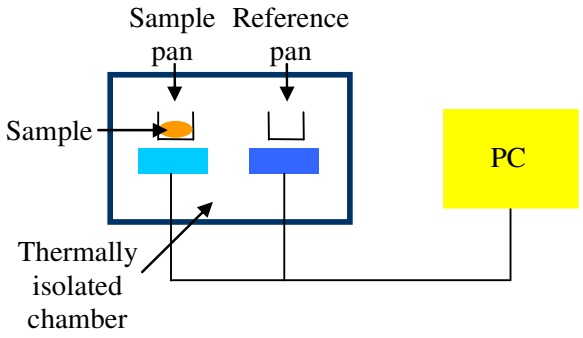

Figure 2.5 Simplified schematic of differential scanning calorimeter [8].

2.3.2 Excitation Field Methods

Resin cure monitoring has been demonstrated using many techniques including: acoustic (ultrasound) [9,10], electric (dielectric) [11], magnetic (nuclear magnetic resonance) [9,10] and mechanical (torsion braid analysis) [12]. Ultrasonic techniques analyse the velocity and attenuation of an acoustic wave that propagates through a sample. The acoustic wave experiences changes in phase and attenuation due to the changing molecular density of the resin during cure. Thus, analysis of the wave passing through a sample can provide data indicative of the state of cure. Figure 2.6 illustrates a simple ultrasonic system for resin cure monitoring [9].

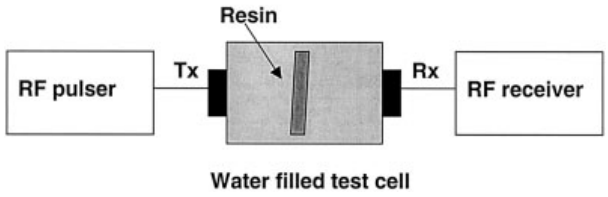

Figure 2.6 Ultrasonic cure monitoring method from [9].

Dielectric cure monitoring analyses the effect that a curing sample has on an electric field. Dielectric cure monitoring utilises the response of an E-field reacting with a dielectric material. Dipoles are generated in a material due to the presence of the field; on an atomic scale (by electron clouds or atomic shifts) or on a molecular scale (molecular shifts). However, as the field tends towards higher frequencies, the dipole response will lag behind the applied field. The point at which the dipole can no longer

react in time with the field is termed the relaxation frequency. The relaxation frequencies for separate atomic level structures provide an indication of atomic or molecular mobility and density, and hence an indication of degree of cure. Carbon fibre composites need to be insulated from such systems to prevent short circuit problems. Dielectric measurements from isothermally cured epoxy are shown in figure 2.7 [11].

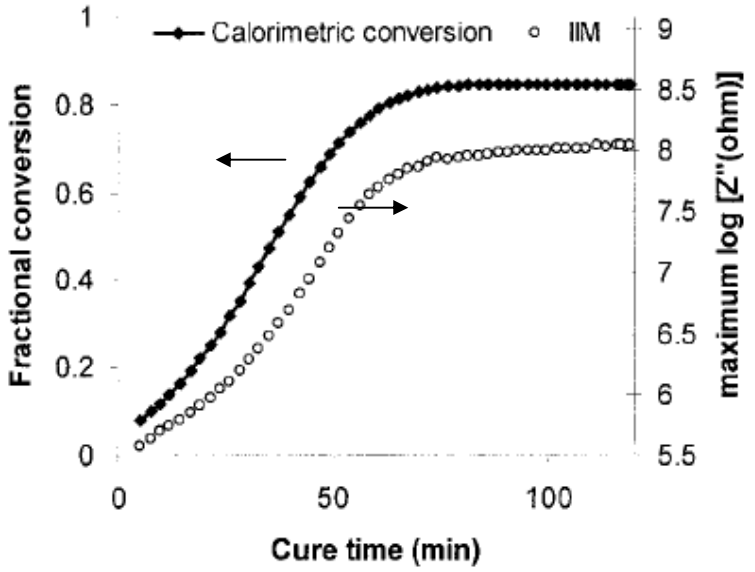

Figure 2.7 Cure conversion (shown as fractional conversion in the axis title) and dielectric measurement (imaginary impedance maximum) of an RTM6 epoxy for isothermal cure at 150°C [11].

NMR methods measure the mobility of nuclei, particularly hydrogen nuclei in samples. This has a particular advantage in epoxy systems where hydrogen performs a key role in the cure process. A sample is maintained in a background magnetic field and a radio frequency pulse of radiation is applied at right angles, figure 2.8. The pulse causes the nuclei to rotate with reference to the background magnetic field at an angle proportional to the pulsed radiation. When the pulse is removed the nuclei relax back to the background state, called free induction decay (FID), in a characteristic time. The time taken for FID is a function of the physical state of the molecules, for solid materials FID times of the order of 10-20μs are typical whilst liquids have times of a few seconds. Analysis of FID time can provide information about nuclei mobility during the cure process [10].

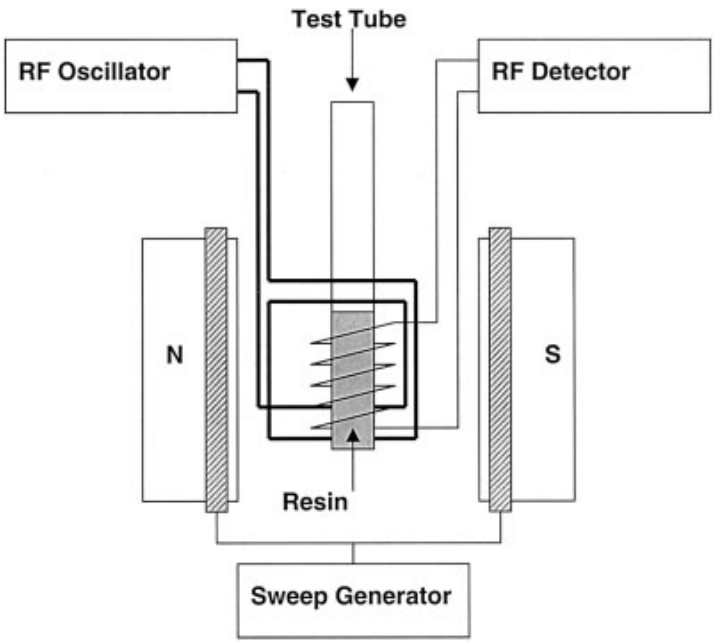

Figure 2.8 NMR schematic setup employed by Challis *et al* [9].

Mechanical methods include torsional braid analysis (TBA). With TBA a glass braid is impregnated with the resin system undergoing the test and allowed to cure under isothermal conditions. During the cure process the braid undergoes torsional tests to determine the elastic modulus of the sample. The elastic modulus is known to change with cure and reveal the changing mechanical properties as the resin forms monomer chains which consequently crosslink [12].

Table 2.3 Summary of cure monitoring methods

Technique	Method	Notes	References
DSC (differential scanning calorimetry)	Heat flow	Sample testing	7
DTA (differential thermal analysis)	Temperature change	Sample testing	6
Ultrasonic	Acoustic wave propagation	Sample testing	8,9
Dielectric cure	Dipole moment	Carbon fibre compatibility issue	10
NMR (nuclear magnetic resonance)	Nuclei rotation	Sample testing	8,9
TBA (torsional braid analysis)	Elastic modulus	Sample testing	11

These methods allow for coupon or sample assessment of resin systems but do not lend themselves to in situ monitoring. A simple comparative table is shown in table 2.3. Optical cure techniques have opened up the possibilities of in situ monitoring and a discussion of some of these methods is presented in the next section.

2.4 Optical cure monitoring

The need for cure monitoring of composites is primarily to improve the production process to obtain consistent components and reduce costs. Optical methods show distinct advantages over more traditional techniques for monitoring the cure of resin systems. Spectroscopic techniques allow for accurate determination of cure with the measurements achieved by small scale samples [13]. These are offline measurements and although these provide accurate data about a bulk matrix do not reflect the real composite component. Non-invasive methods of determining cure are more attractive, e.g. surface measurements of components [13] or the use of in-situ optical fibre sensors [14]. These measurements provide more insight into the component and the actual industrial process. The review presented here gives a broad outline of optical techniques considered to date as possibilities for the monitoring of cure.

2.5 Spectroscopy

In general the components of a thermoset plastic are a bulk resin and a hardener. These components react at room temperature or more usually through the application of heat and change from a liquid to a solid. The reaction involves the breaking and reforming of bonds, creating very long polymeric chains (polymerisation). Later reactions in the cure process involve further cross linking of these chains to form a rigid, heavily cross linked, dense network of molecules. Traditional optical sensing methods use spectroscopy to monitor the vibration energy exhibited by these molecular bonds as a guide to cure. As the cure continues the characteristic vibrations associated with a particular molecular bond species will grow or reduce as a function of cure time. Illustrated in figure 2.9, is the simplified reaction process of polyethylene were, the ethylene molecules, C_2H_4, are added with an initiator (hardener), in this case H_2O_2 that

provides free and reactive -OH radicals. With the application of heat and/or pressure these radicals break the double C=C bonds of the C_2H_4 molecule. This leaves an un-reacted end which is now free to break other C=C bonds in a similar manner. The process then continues to form a long polyethylene molecule through this chain reaction.

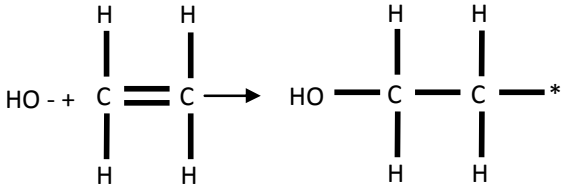

Figure 2.9 Showing ethylene C_2H_4 molecule reacting with free hydoxyl radical –OH from the H_2O_2 initiator.

A more typical matrix used in the manufacture of AFRCs are epoxy resins. The structure of a DGEBA (diglycidyl ether bisphenol – A) epoxy and amine hardener, DDM (4,4'-Diamino diphenyl methane) is shown in figure 2.10 and the simplified representation of a epoxy and amine resin system is illustrated in figure 2.11. It shows the predominant curing reactions and source of bond vibrations that can be monitored using spectroscopic techniques.

DGEBA (diglycidyl ether bisphenol – A)

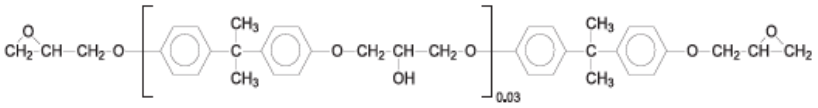

DDM (4,4'-Diamino diphenyl methane)

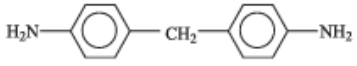

Figure 2.10 Structure of DGEBA epoxy and DDM hardener [6].

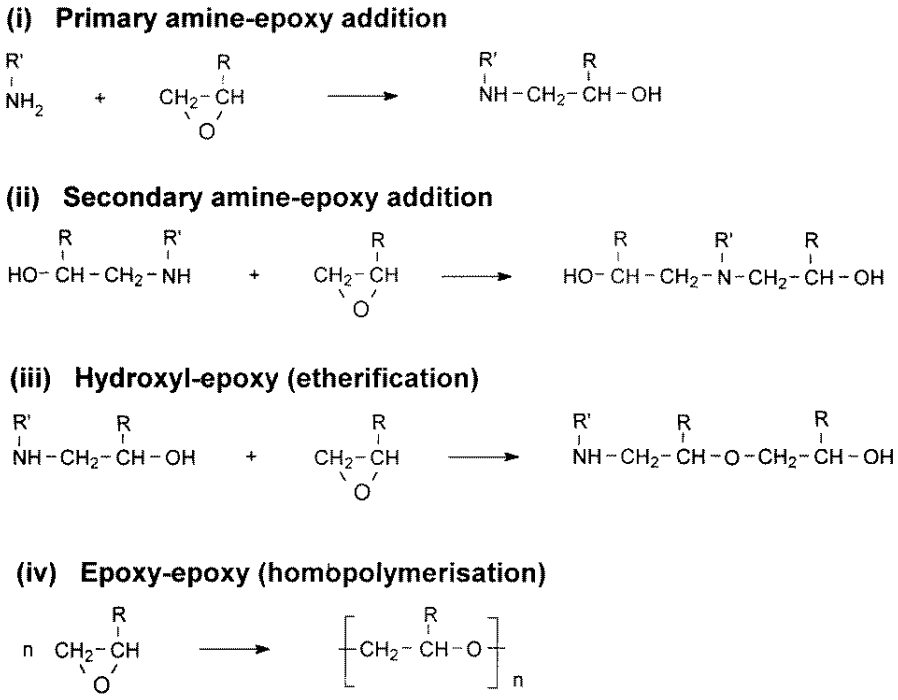

Figure 2.11 Generalised reaction scheme for epoxy/amine systems [6].

The next few sections discuss the application of spectroscopy to cure monitoring. The spectroscopy methods detailed are FTIR, Raman and fluorescence.

2.5.1 Infra-red spectroscopy

Fourier transform infrared (FTIR) spectroscopy utilises the interaction of infra-red radiation with matter. The infrared energy is absorbed causing the chemical bonds to vibrate. Chemical bonds within specific molecular groups termed functional groups within larger molecular structures tend to absorb energy at specific wavelengths, for example the first overtone stretching vibration of the aromatic C-H bond in a typical epoxy, absorbs at 1.668μm (5995cm^{-1}) [6]. This correlation permits the chemical structure of unknown molecules to be identified by infrared. The near infrared spectra of a curing epoxy are shown in figure 2.12 with the depletion of an amine resulting in the decrease of a spectral peak at 6600cm^{-1} [15]. This depletion is then used to track the progress of the cure reaction.

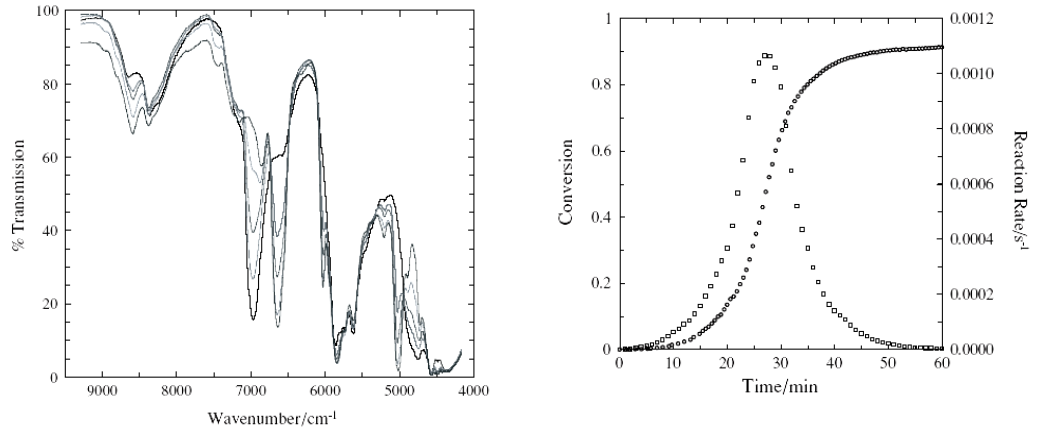

(a) (b)

Figure 2.12 (a) FTIR spectra for isothermal cure (160°C) microwave curing of an epoxy-amine systems (RTM6) recorded at 0, 15, 25, 27 and 60 minutes. The spectra show the depletion of the amine peak at 6600cm^{-1} and growth of the hydroxyl peak at 7000cm^{-1}. (b) Conversion (circles) and reaction rate (squares) calculated from depletion of amine peak in NIR spectra. [15]

Beers law allows infrared spectroscopy to be extended further by relating the concentration of a specific functional group in a sample to absorbance. It is given by [16]:

$$A = \varepsilon l c \qquad 2.2$$

where A is the absorbance, ε is the absorbivity, a proportional constant that is wavelength and molecule specific, l is the path length and c is the concentration. Thus spectroscopy can be used to determine specific functional groups in a sample and concentrations of such groups. For this reason it lends itself to cure monitoring as the molecular structure of a resin changes during the polymerisation process and more or less of a functional group becomes apparent. The predominant infrared window for FTIR is the mid infred (MIR) which is used to analyse the fundamental vibrations of functional groups. The MIR region covers the wavelengths from 2500nm (4000cm^{-1}) to 25000nm (400cm^{-1}). The high energy near infrared (NIR) region (from 2500nm to 500nm) excites overtones of these fundamental frequencies however the resultant spectra are more complex as the bands are not as well defined (broader) and overlap. However the advantages of working in this region are the optical components in this region are less costly and more available. Their application to in situ sensing is also more predominant in the literature as standard silica fibre may be used to transmit and

collect the infrared light. Although spectroscopy is not novel in itself its application to cure monitoring is. Qualitative analysis of samples has been reported as far back as 1963 [17]. However more recent work demonstrated FTIR with an epoxy system, TGDDM (tetraglycidyldiamino diphenylmethane) resin and DDS (diaminodiphenylsulfone) hardener using partially cured samples at various stages of the cure. The technique was transmission based and although informative did not monitor the cure process real time and no allowance was made for sample variation. A real time and quasi industrial based cure monitor was reported by Danneberg *et al* [18] in the MIR. A prism was used in close contact to the curing materials surface which was attached directly to the mould. A highly specialised composite resin was tested in the work but it demonstrated the potential of FTIR for quasi-online measurements. Of more interest in the work reported in this thesis are optical fibre based systems that endeavour to demonstrate real-time cure monitoring with an in situ capability.

MIR based systems require specialised fibres that bring technical challenges as well as costs, although improved spectroscopic analyses are possible due to the higher absorption at fundamental vibrations. Chalcogenide based systems are typical [13] although fluoride and sapphire based fibre systems have also been reported [19]. FTIR analysis was reported of a DGEBA (diglycidyl ether bisphenol – A) based resin [13]. The fibre sensor was constructed from chalcogenide fibre and consisted of aligning two fibre faces with a 30μm separation to allow the resin to fill the gap, figure 2.13. Careful control of the path length is then critical for these measurements during cure. The absorption due to the C-H stretching frequency at 1603cm^{-1} was used as a reference and the curing reaction was determined by analysis of the epoxy ring vibration at 1131cm^{-1}. The result was used as a cure parameter and compared favourably up until 75% conversion.

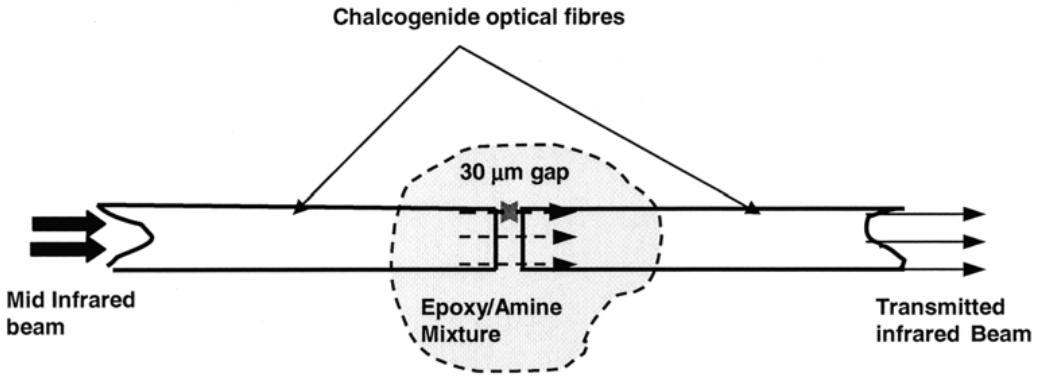

Figure 2.13 A transmission based FTIR optical fibre probe with optical fibres axially aligned and embedded into an epoxy/amine system [13].

A similar fibre optic technique using a sapphire fibre to monitor an epoxy has also been achieved [19]. The sensor data was related to mechanical tests undertaken after cure. The analysis revealed that a shorter cure time could be employed to achieve the required mechanical performance. It clearly demonstrated the benefit of the use of fibre optic sensors, the information gained allowed a reduction of 25 % in the production time. There is great variation in the application of spectroscopic techniques with optical fibre and the different types of fibre optic sensors used in spectrometric techniques can be categorised as [6];

Transmission – analysis of the transmitted light through a sample.

Reflection – analysis of the reflected light, which may incorporate both specular and diffuse (largely determined by surface topology) reflections.

Evanescent – light propagating through unclad or thinly clad waveguides is directly affected by changes to the surrounding medium because it exhibits propagating energy profiles that extend into the medium (evanescent tail).

In some cases all three categories are present within a specific probe type, however most systems purport to use a specific type.

A fibre optic method to acquire spectroscopic data from a TGDDM/DDS resin using a transmission based approach has been reported [20]. Plastic clad silica fibre was used to access the spectral change during cure in real time. Cure monitoring was achieved by monitoring the decrease of the primary amine band at 5067cm^{-1} up to the gelation point, where the resin is defined as having a rubber like state.

An evanescent sensor using a speciality, high index (1.618) silica fibre was used to monitor the cure of a DGEBA based epoxy by Dunkers *et al* [21]. Three 130μm fibres were grouped together to create a mini-bundle which was illuminated using a larger fibre bundle. The fibre refractive index was matched to that of the epoxy, to promote the evanescent tail of the propagating light energy through the bundle sensor and into the resin. The primary and secondary amines (at 6650cm-1 and 6580cm-1) provided the simplest means of monitoring the reaction but it was noted that the amine band quickly disappears prior to cure. Although the reaction was monitored no attempt was made to correlate the results with cure conversion. Tapanes *et al* [22] utilised the NIR with a side polished fibre optic probe to monitor an MY720 araldite. The fibre's cladding was removed to access the evanescent tail at the core/cladding interface, figure 2.14.

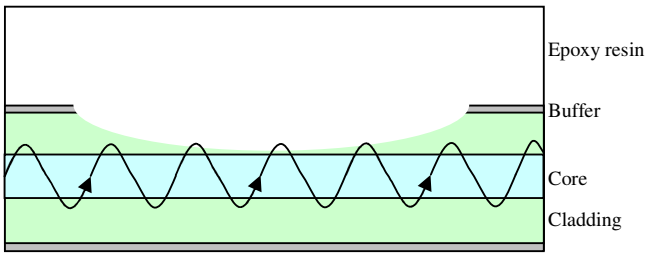

Figure 2.14 Etched fibre showing access to evanescent tail of core mode [22].

Degamber and Fernando [23] demonstrated the use of a fibre optic FTIR within a microwave oven. The microwave oven was used to decrease the longer production time associated with the use of a traditional autoclave system. The resin used was a MY721 araldite based system and both reflectance and transmission optical fibre FTIR probes were used. The degree of cure was calculated using the change in the epoxy peak at 4532cm^{-1} and the reference peak at 4619cm^{-1} (a combination of the C-H and C=C bond stretching). The cure conversion equation was given as:

$$\alpha = 1 - \frac{\left[A_{Ep} / A_{CH} \right]_t}{\left[A_{Ep} / A_{CH} \right]_0} \qquad 2.3$$

where α is the conversion, $[A_{Ep}/A_{CH}]_t$ is the ratio of the area of the epoxy peak to the peak corresponding to the C-H bond at time t and $[A_{Ep}/A_{CH}]_0$ is the ratio corresponding to the uncured resin (t = 0).

2.5.2 Raman spectroscopy

Raman spectroscopy methods monitor the interaction of high energy monochromatic excitation light with functional groups in a sample by analysing the scattered light. The scattered light may exhibit no frequency shift (Rayleigh) or exhibit frequency shifts proportional to the molecules' Raman vibrations. The strongest scattering is at frequencies lower than that of the incident radiation and termed Stokes Raman scattering. Apparent advantages over IR spectroscopy are: comparatively well resolved spectra, simple sample preparation, short measurement times and the option of using standard silica based fibre for detection.

Lyon *et al* [24] reported the use of a Raman based system to measure vibrations of the resin backbone molecule groups of a DGEBA based epoxy. The work was done in parallel with an IR based method for calibration to determine a quantitative analysis of the curing reaction. A 50mW laser diode working at 820nm excited the sample through a bifurcated optical fibre probe arrangement, figure 2.15 to enable excitation and detection of the sample. The epoxide peak at 1240cm^{-1} was normalised and used as a cure parameter and indicated a linear relationship with the measurements using IR spectroscopy. Mention is also made of the ability to use the Raman signal as an indicator of temperature.

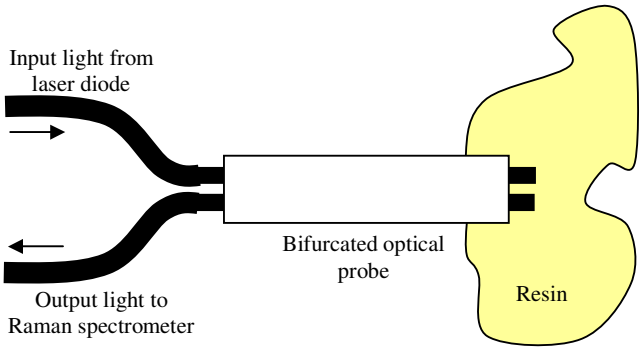

Figure 2.15 Bifurcated optical fibre probe arrangement for Raman spectroscopy [24].

Skrifvars *et al* [25] demonstrate the use of Raman spectroscopy as an alternative to FTIR. The Raman system used an 830nm laser diode at 200mW on the sample. The investigation looked at curing polyesters, tracking the change in the styrene C==C band intensity at 1630cm^{-1} with reference to the C==O band at 1730cm^{-1}. Problems with the measurement were highlighted by a dark coloured sample exhibiting high absorption of the excitation light. Previous work by DeBakker *et al* [26] with TGDDM epoxy and DDS highlighted a problem of Raman spectroscopy with epoxies where they exhibit strong fluorescence and swamp the Raman signal. Samples thus required burning out of the fluorescence before the Raman signal could be interpreted. The system used a Nd-YAG source at 1064nm and 800mW. The cure was monitored using the –NH_2 group in DDS at 3367cm^{-2} which was seen to decrease with time as the cure progressed (normalised with the CH_2 alkyl methylene groups in TGDDM). The results were compared with an NIR technique and showed good agreement in the early stages of the cure but less agreement during the latter part of the cure.

2.5.3 Fluorescence spectroscopy

Fluorescence spectroscopy utilises the re-radiated fluorescence from reactive agents (molecules that exhibit fluorescence) when illuminated with light energy at a particular wavelength. Paik and Sung [27] demonstrated a sensor using this phenomenon using a 420nm light source. Three implementation methods were tested to gather fluorescent data, figure 2.16. A bare fibre core, a cleaved surface probe and a stripped cladding mirrored probe were inserted into the sample. This intrinsic method required no

fluorescent additive but did require the curing agent diaminodiphenyl sulfone (DDS) as it has a measureable fluorescence. The red shift of the fluorescence during cure is attributed to the extent of the DDS reaction and thus provides an indication of cure. The results compared favourable with FTIR and DSC measurements but they report that extrinsic fluorescence measurements reveal more information about a resins network formation. However Wang *et al* [28] reject the principle of intrinsic fluorescence because of inconsistencies of measurements between different batches.

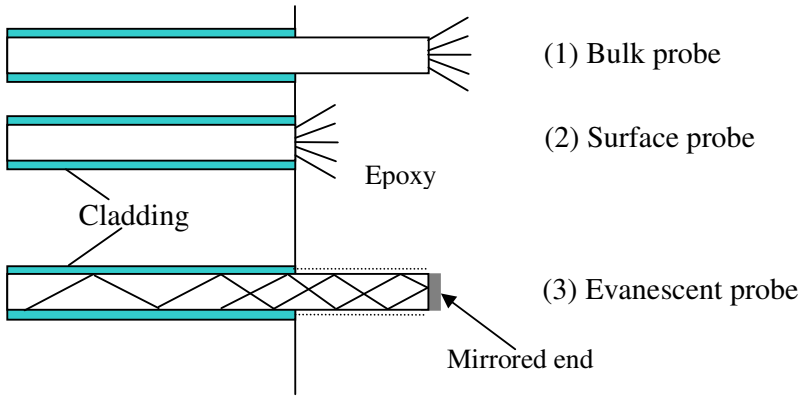

Figure 2.16 Fluorescence probes proposed by Paik and Sung [27].

Levy and Schwab [29] describe a fluorescence based fibre optic sensor that provides an intensity signal that is used to determine chemorheological states of a curing resin and a wavelength signal that is correlated with cure conversion. A helium-cadmium source at 441.6nm provided excitation energy which was delivered to a tool mounted sensor through fibre. The method requires the presence or addition of what are termed viscosity-dependent fluorescence (VDF) probes. These probes fluoresce with increasing viscosity and are thus ideal as indicators of the change in viscosity during cure. Wavelength measurements of the fluorescence reveal a correlation with the later stages of cure, greater than 80% degree of cure.

Pyrene additives were used by Benito *et al* [30] as an indicator of the cure process at the silica fibre/epoxy interface of a DGEBA (Diglyciclyether of bispenol A)) and EDA (Ethylendiamine) resin and compared with FTIR and DSC (Differential Scanning Calorimetry) measurements. Pyrene was used as an indicator because it has a long

fluorescence life time and reacts easily with amine groups providing a mechanism for actively monitoring an amine/epoxy reaction. The work was focussed on the matrix filler interface and revealed information purely about this location within a composite and not the bulk properties of the curing sample. An optical fibre was used to excite and collect in situ fluorescence at an excitation wavelength of 340nm. Although the technique may not be applicable in an industrial sense because of the requirement to add probes it did reveal a discrepancy between bulk measurements of the resin and that of the fibre/matrix interface.

A specialised fibre optic fluoro-sensor is reported by Woerdeman *et al* [13,31,32]. An evanescent wave fibre sensor, figure 2.17, was employed with a lead oxide based glass with a sufficiently high refractive index (1.62) to enable measurements with epoxies (1.48 – 1.58). Two polarity sensitive fluorescent probes were used (di-10-ASPPS and DMANS) for comparison and the combined results were compared with a conventional fluorimeter. The excitation wavelength was constant for all experiments at 488nm. The attractiveness of the polarity sensitive probes over others, e.g. viscosity-sensitive is their wavelength sensitivity that negates the use of a reference. The origins of the shifts are due to dipole mobility which becomes more restricted as the resin cures. The results compared favourably with the fluorimeter although a smaller wavelength shift was measured using di-10-ASPPS.

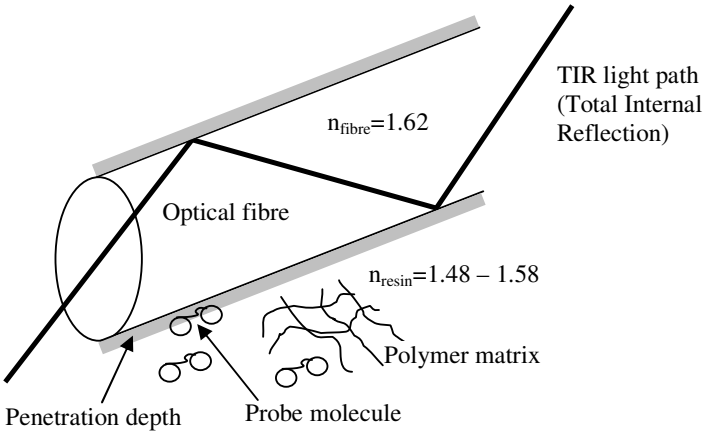

Figure 2.17. Evanescent wave sensor where fluorescent probes in the resin surrounding the sensor fibre are excited by the evanescent wave at the fibre resin interface [13,31,32].

2.6 Optical ultrasonic methods

Fibre optic ultrasonic techniques have also been demonstrated as cure monitors. Typically, an optical fibre interferometer is used to detect acoustic waves [33,34]. The ultrasonic pulses are generated by piezoelectric devices and serve to interrogate the mechanical properties of a curing resin. The ends of two fibres are cleaved and mirrored to act as a reference and sensing arm of an interferometer. Active homodyne detection [35] using a piezoelectric fibre stretching coil is employed to remove low frequency noise, figure 2.18. Pulsed light from high powered lasers, e.g. Nd:YAG laser at 1060nm, 1300mJ with a pulse width of 10ns have also been used to generate the acoustic waves in a sample [36]. Velocity and attenuation results from a curing epoxy are shown in figure 2.19. No correlation was made with the cure conversion of a resin although the trend appeared to indicate the cure process.

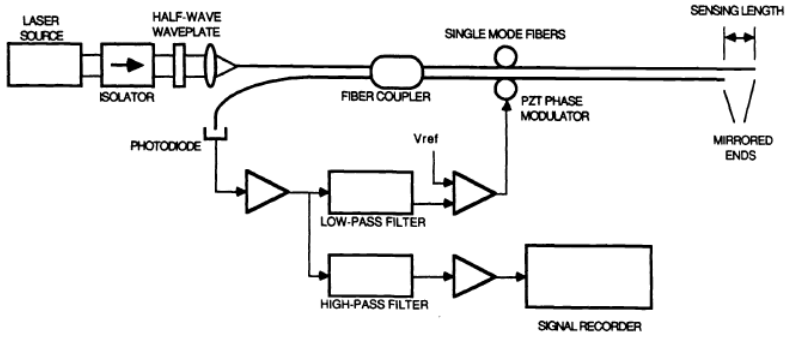

Figure 2.18 A fibre optic Michelson ultrasonic sensor [33].

A similar system using optical fibres to deliver the high energy pulses is described by Dorighi *et al* [37]. A fibre optic Fabry Perot interferometer was used to detect the ultrasonic signal velocity and attenuation. The signal's velocity showed a clear dependence on the degree of cure. The results were compared with a piezoelectric sensor and found to be comparable. A summary of the predominant methods of cure monitoring using optical means is shown in table 2.4.

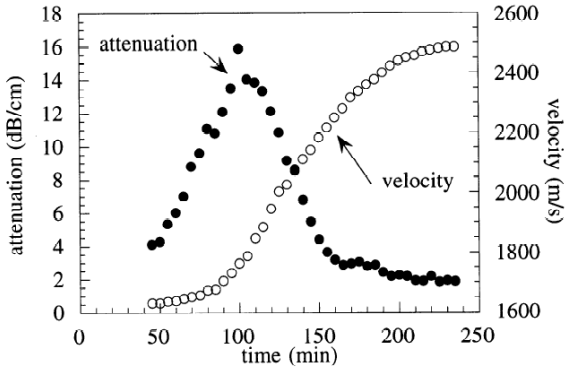

Figure 2.19 Results from [33] showing attenuation and velocity of optically induced ultrasonic waves during the cure of an epoxy detected using an optical fibre interferometer.

Table 2.4 Summary of optical cure monitoring methods

Technique		Method	Notes	References
FTIR (Fourier transform infra-red spectroscopy)	MIR	IR absorbtion	Expensive, primarily sample testing, compatability with silica based fibre	5,14,19,20,21,22
	NIR	IR absorbtion	Expensive, primarily sample testing, requires specialized optical fibres	11,17,18
Raman spectroscopy		Raman	Expensive, simpler than FTIR, compatability with silica	24,25
Fluorescence spectroscopy		Fluoresecence	Requires addition of fluorescent indicator	26,27,28,29,30,31
Fibre optic ultrasonic		Acoustic wave propagation	High power laser systems, complex analysis	32,33,34,35,36

2.7 Optical fibre refractometers

Why refractive index measurements? Refractive index constitutes a fundamental optical characteristic of a material and, for many applications in science and engineering, it is a necessary measurand. Correspondingly, there are many techniques for measuring a material's refractive index, with the application and method invariably being determined by the substance being measured. Many expressions exist to relate the refractive index of amorphous materials to density the simplest but least accurate being [38]:

$$n' - 1 = G\rho \qquad 2.4$$

where n' is the refractive index, ρ is the material density and G is constant for a given material. However a more exact and fundamental relationship is derived from the Lorentz-Lorenz relation [39] and given as [40]

$$\frac{n'^2 - 1}{n'^2 + 2} = L\rho \qquad 2.5$$

where $L=1000N_A\alpha/3\varepsilon_0 M$ and is constant for a given material. N_A is the Avogadro constant (6.023 x 10^{23} $mol^{-1)}$, α is the mean polarisability, ε_0 is the free space permittivity and M is the molecular weight. This gives an explicit dependence of the refractive index for a particular wavelength on the density. From this dependence and the density change exhibited by polymers during the cure process a possible method of assessing the cure state of a resin is available by measuring the refractive index during cure.

2.7.1 Refractometry

The traditional device used is the well known Abbe Refractometer [41] which utilises the sharp variation in the reflected and transmitted intensities of incident light on a prism with an angle of incidence approaching the critical angle. Such devices, although accurate, are precluded from use in many applications due to their bulk and method of use. However they still provide a benchmark method for determining the refractive index of extrinsic samples of liquids. Optical fibre sensors offer a number of significant advantages over these more traditional methods including immunity to hazardous environments (e.g. chemical, extreme temperatures or nuclear radiation), size (a standard optical fibre has an outer diameter of 125μm) and precision (interferometric techniques). Optical fibre based refractometers can be divided into two main areas, those which utilise the fibre as a transmission system to and from a measurement region or sensor head, or those that utilise the fibre itself as a sensor. These may also be described as extrinsic and intrinsic sensors. It is the latter that is considered here.

2.7.2 Optical fibre based refractometers

Takeo *et al* [42] proposed a bent (u-shaped) optical fibre, figure 2.20. The fibre in the region of the bend was stripped of its cladding to expose the core modes to variations in the surrounding refractive index. The operation of the sensor utilised the changes in the attenuation of the transmitted light in response to changes in surrounding refractive index. This method demonstrated an accuracy of 1 x 10^{-3} rius (refractive index units). Although this lends itself well to point sensing the sensor requires the fibre cladding to be stripped which may significantly compromise the mechanical strength of the sensor.

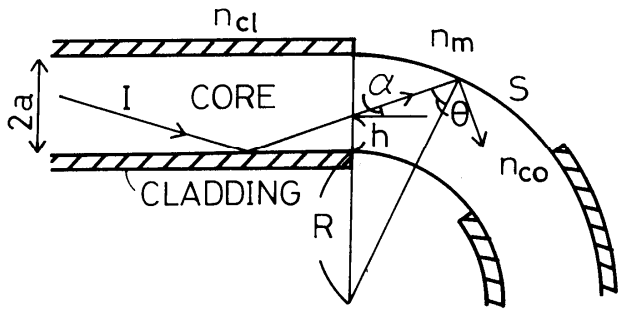

Figure 2.20 Optical fibre bent with radius R and removed cladding. Light ray *I* is incident at angle θ to the sensor surface [42].

Harmer [43] demonstrated a similar sensor type using multiple bends to improve the resolution. The use of plastic optical fibres, with their inherent high signal attenuation, limited the range of these sensors. Takeo *et al* [44] further improved this method by employing OTDR (Optical Time Domain Reflectometry) to create a quasi-distributed or multi point sensor. Smela *et al* [45] demonstrated an optical fibre refractometer where two fibres are wound together, with the coupling between the fibres determined by the change in refractive index of the surrounding environment. The use of the sensor as a detector of impurities or concentration was proposed. Kumar *et al* [46] reported the use of tapered fibres as refractive index sensors using plastic clad silica core fibre. The design of the taper determines the sensors refractive index sensitivity as indicated in figure 2.21 and equation 2.6 and 2.7.

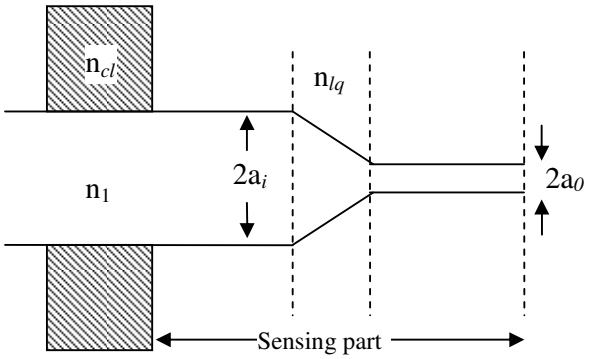

Figure 2.21 Geometry of tapered sensing probe of Kumar *et al*, n_1 is the core index, n_{lq} is the liquid refractive index and n_{cl} is the cladding index [46].

$$R = \frac{a_i}{a_0} \qquad 2.6$$

$$P = P_0 \left[\frac{n_1^2 - n_{lq}^2}{R^2 (n_1^2 - n_{cl}^2)} \right] \qquad 2.7$$

By correct choice of the diameters for the taper, a_i and a_o, given by R in the equation, a lower limit of refractive index measurement, $n_{lq} = 1$ is achieved with an upper limit bounded by n_1. The power loss, P (P_0 is the input power), through the fibre sensor provided an indication of surrounding refractive index, where the taper was used to couple light from fibre to fibre. Guo and Albin [47] proposed the use of fibre tapers without the cladding removed as evanescent wave sensors. The tapering ratio determines the sensor's sensitivity and, as with the unclad tapers, a specific sensor design would be required for specific refractive index ranges. They report that the sensor showed very poor resolution at refractive indices approaching that of the cladding. Un-clad tapers show a higher sensitivity five times greater than clad tapers although they suffer from an inherent fragility.

Hernandez *et al* [48] take the tapered fibre idea a step further by coating the cleaved end of a fibre taper with a mirror, thus creating a reflection sensor, where the fibre tip acts as a probe sensor, figure 2.28. A resolution of 4×10^{-4} rius was reported, again showing very similar characteristics to the transmission taper. A disadvantage with transmission sensors is that a return path is necessary.

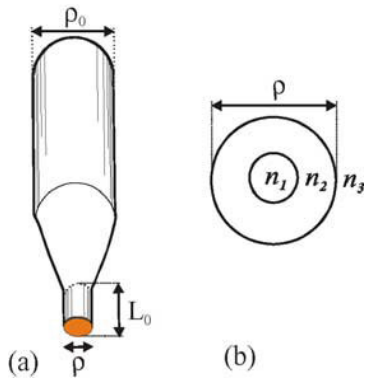

Figure 2.28 (a) Tapered multimode fibre taper with mirrored tip. ρ_0, ρ and L_0 are the fibre diameter and tip diameter and the length of the uniform section. (b) Cross section of the taper with n_1, n_2 and n_3 the refractive index of the taper tip, the fibre and the sample, respectively. [48]

Ravishankar *et al* [49] demonstrated the use of the refractive index sensor as a liquid level sensor, and also highlighted a technique where measurement of refractive indices higher than that of the core is possible. Their design used two parallel fibre end faces coupling light from one fibre to the other through a gap filled with the material to be measured, figure 2.22. They report an accuracy of $6x10^{-3}$ rius (Refractive Index Units), which is comparable with previously published figures.

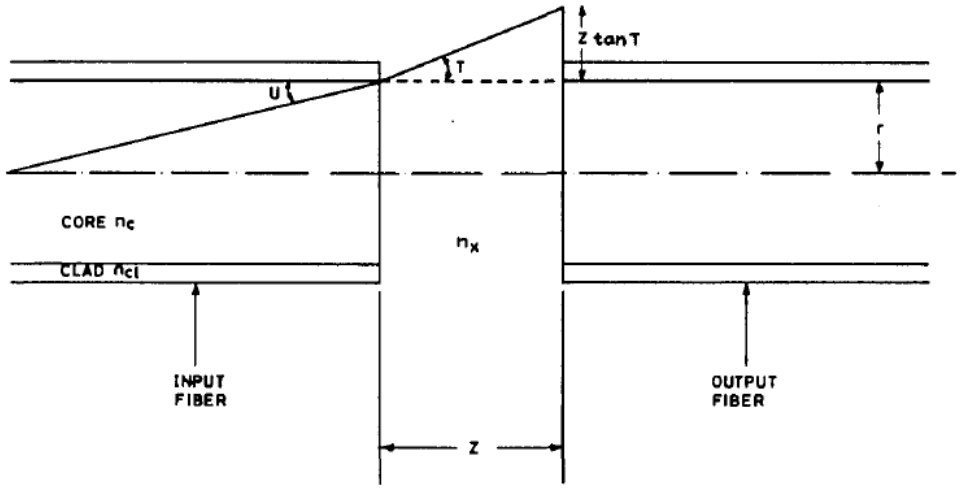

Figure 2.22 Coupling between two multimode optical fibres separated by a distance z, filled with a medium of refractive index n_x [49].

An interesting refractive index sensing technique was proposed by Ilev [50], combining the displacement sensing capabilities of an optical fibre [51,52] with an intensity modulation of light due to refractive index change. Displacement sensors usually utilise the intensity change in light coupled between two collinear fibres in response to one being displaced relative to the other. The method proposed by Ilev utilised the coupling of light back into a transmitting fibre by retro-reflection from a corner cube prism. As the refractive index is changed, the angle of incidence changes and in order to maintain maximum coupling the prism is displaced. The amount of displacement provides an indication of refractive index.

Suhadolink *et al* [53] reported the use of the displacement technique for the measurement of the refractive index of liquids. Here, two optical fibres were placed side by side and a moveable mirror used to couple light from one to the other, figure 2.23. The reduction in coupling caused by a change in the refractive index of the surrounding medium was compensated for by movement of the mirror, the displacement providing a measurement of refractive index change. Such displacement-based systems provide higher refractive index sensitivity for media whose refractive index approaches that of the core of the fibre. However, a major disadvantage is the moving parts involved.

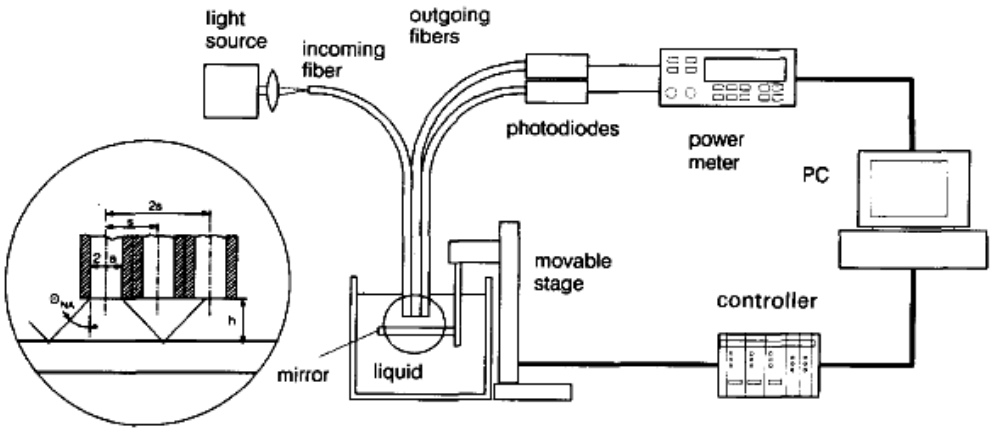

Figure 2.23 Experimental setup of reflection refractometer of [53]. Inset shows one incoming and two outgoing fibres. Two outgoing fibres are used to remove uncertainty in the results from intensity variations from the laser.

More complex refractive index sensors exploit interferometric techniques. A Mach Zehnder (MZ) configuration was proposed by Heideman *et al* [54] to detect changes in the refractive index surrounding a de-clad fibre that formed the sensing arm of the MZ, figure 2.24. The phase change imposed on light passing through the sensor arm indicated a relative change in refractive index. A sensitivity of $1x10^{-3}$ rius is reported which is comparable to the bent sensors discussed initially.

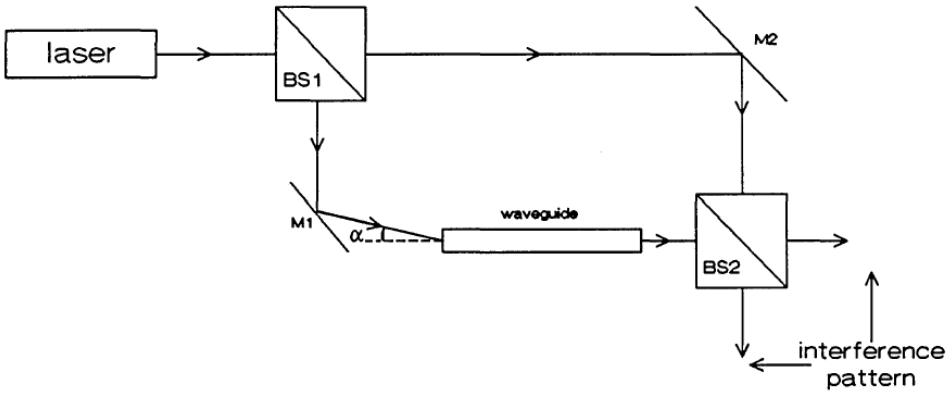

(a)

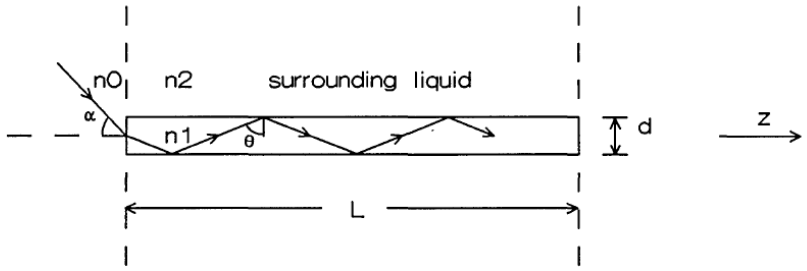

(b)

Figure 2.24 (a) Mach-Zehnder interferometer configuration with a laser as the light source, two beam splitters BS1 and BS2, two mirrors Ml andM2, and a waveguide in the signal arm of the interferometer. The coupling angle α is adjustable. (b) De-clad fibre waveguide showing ray path of light. n_0 is the air refractive index, n_1 is the core refractive index, n_2 the refractive index of the surrounding liquid, θ the glancing angle, d the fibre diameter, z the propagation direction. [54]

A simple pH sensor using a coupler was proposed by Attridge *et al* [55] which indicated the sensor's ability to measure the refractive index. Here a directional coupler's phase matching characteristics were altered by the change in refractive index of a pH-sensitive surrounding medium. This arrangement, although robust and having a fast response time, showed poor refractive index resolution due, in part, to higher order coupling.

Surface plasmon resonance (SPR) is a phenomenon being utilised to create new types of sensor, including refractive index sensors. SPRs are confined to the surface of, and occur at, the interface between a non-dielectric material and a vacuum or a dielectric. Light stimulates the free electrons within a non-dielectric material at optical frequencies, to create a plasmon oscillation. Slavik *et al* [56,57] reports the use of a single mode fibre to excite surface plasmon waves on a thin metal film, figure 2.25. The propagation characteristics of the plasmon wave are strongly determined by the refractive index of the immediate surrounding material. Thus refractive index can be determined, either by monitoring the changes in amplitude of the transmitted light, or measuring changes in excitation wavelengths. A clear disadvantage of this reported work is its very narrow working range e.g. 1.343 – 1.352 for an SPR sensor with gold film used in conjunction with an overlay to enhance the refractive index sensitivity. The operating region can be selected by the use of different overlay materials.

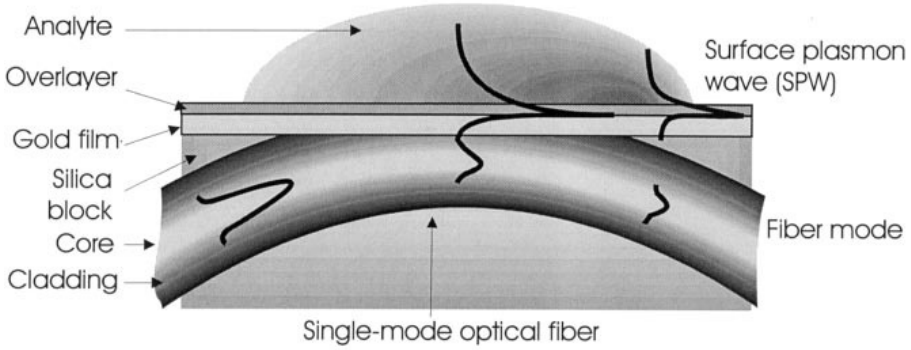

Figure 2.25 Surface plasmon resonance optical fibre sensor. [56,57]

Tijhuang *et al* [58] wished to improve on previous techniques by increasing the measurement range of refractive index sensors and to remove the obstacle of complex fibre designs. They reported the use of the Fresnel reflection of an amplitude modulated laser source from the cleaved end of a multimode fibre, the Fresnel reflectivity dependent upon the difference between the refractive index of the fibre and that of the surrounding medium. The system illustrated a higher sensitivity to refractive index change than previous work.

Chang *et al* [59] reported a Fresnel reflection based system that determines the refractive index from the Fresnel reflection of the cleaved end of an optical fibre. With this cleaved face acting as a probe, a change in refractive index results in a change in the intensity of the reflected light. It is possible to use this amplitude response to directly calculate refractive index. However, as with many optical fibre sensors, as the refractive index of the sensed material approaches that of the fibre, the resolution capability of the sensor drops. A detection capability of 2 x 10^{-5} rius is reported.

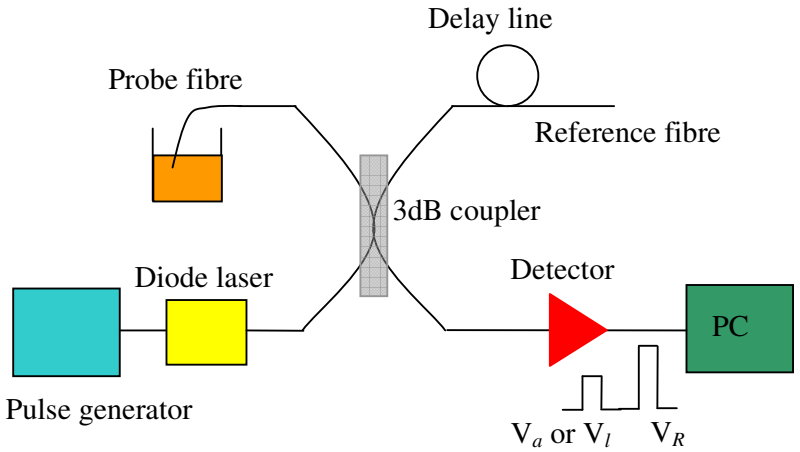

Figure 2.26 Experimental set-up of Fresnel based refractometer. [60]

A similar configuration was reported by Kim and Su [60] utilising simultaneous illumination by two wavelengths, figure 2.26. In both systems a reference arm is necessary to allow for changes with laser power, this is decoupled from the probe signal by incorporating a long section of fibre into the reference arm, thus introducing a time delay between the signal and reference. A variation of this setup is used as a comparative measurement system with the grating devices used in the experimental work detailed in later chapters. A more detailed description is given in chapter 3.

Plastic optical fibres (POF) are large diameter step-index multimode fibre, with typical core diameters of 1-mm and cladding thicknesses of 20μm [61]. POF typically has much higher attenuation than glass fibre, 1 dB/m or higher, but are much cheaper to produce and handle. POFs have also been reported as refractive index sensors as shown earlier with work by Takeo *et al* [42]. Ribeiro *et al* [62] exploited evanescent wave techniques and light scattering mechanisms with roughly polished POFs. Here the

cladding or sidewalls of POFs were polished down to the core leaving a rough surface, figure 2.27. The propagating core mode is then scattered by surface indentations. The optical attenuation is determined by the refractive index of the surrounding medium. The sensor is sensitive over the range of refractive index from that of the cladding to that of the core and a resolution of $1x10^{-3}$ rius was reported.

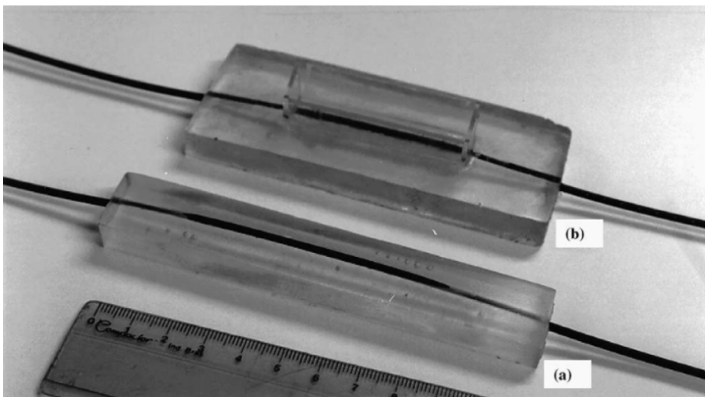

Figure 2.27 The POF sensor element manufactured by means of the side polishing technique on a resin block embedded fibre: (a) the sensor element; (b) the sensor element with a bonded cuvette around the exposed core. [62]

Table 2.5 Summary of refractometric methods

Technique	Method	Notes	References
Abbe refractometer	Critical angle	Sample testing	40
Bent fibre	Core mode interaction	Fragile sensor	41,42, 43, 44, 45
Tapered fibre	Power loss	Fragile sensor	46, 47, 48
Coupled fibres (displacement sensors)	Power loss	Intensisty based, complex sensor	49,50, 51, 52,53
Interferometers	Interferometric	Complex	54
pH based	pH	Poor resolution	55
SPR (surface Plasmon resonance)	SPR excitation	Narrow refractive index range	56,57
Fresnel	Fresnel reflection	Point sensor, intensity based	58,59, 60
POF (plastic optical fibre)	Core mode interaction, tapered	High losses, less sensitivity	61,62
Side polished	Core mode interaction	Intensity based, fragile sensor	63

Sheeba *et al* [63] demonstrate a side polished fibre technique for the sensing of pollution in coconut oils, again utilising refractive index. The system is intensity based, making use of the evanescent wave set up in the core/cladding interface. Again the cladding is polished to the core allowing the evanescent field to interact with the external environment. It demonstrates the ability to use the refractive index information to sense other parameters, in this case adulterants in coconut oil. Table 2.5 summarises the optical fibre based refractometric methods discussed.

2.8 Refractive index as a cure parameter

An optical fibre Fresnel based refractometer was proposed by Afromowitz and Lam [64] in 1990 as a cure sensor. The in-situ sensor used an LED at 850nm and a polyimide coated silica multimode fibre (200/240). A lock-in detection system was employed with a chopped signal at 1 kHz. The system did not have a reference port and no measures were taken to remove unwanted back reflections through the coupling network. A calibration scheme was employed to determine the refractive index measurements. Experimental results on an epoxy (EPON 828) were presented. The work highlighted the issue in correlating refractive index directly with cure conversion, figure 2.29, concluding that the early to mid stages of the cure may be approximated as a linear relationship but later work suggests that beyond the gel point the resin begins to shrink but local viscosity changes restricts this movement [64,65]. As a result the refractive index correlation with cure is more complex.

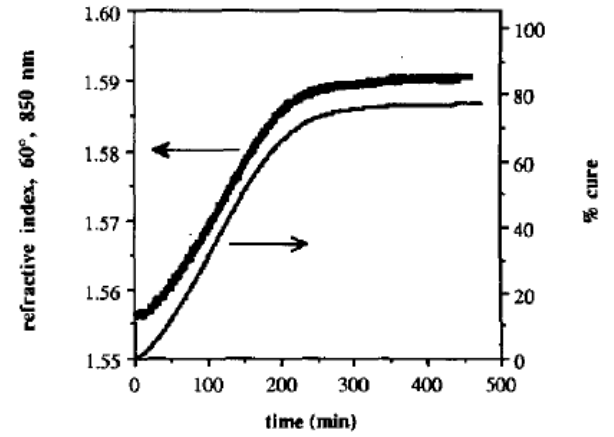

(a)

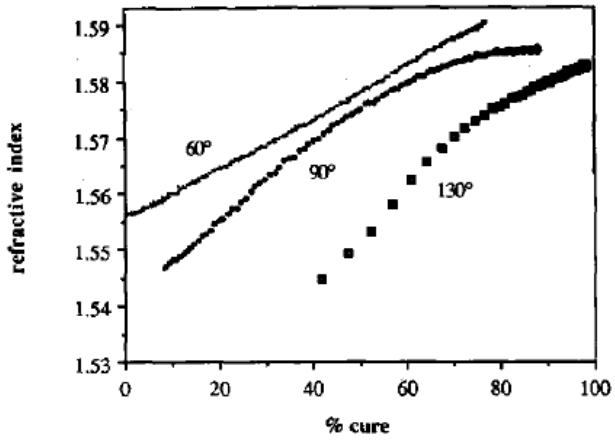

(b)

Figure 2.29 (a) Refractive index response of a curing epoxy shown with cure conversion determined by DSC for an isothermal cure at 60°C. (b) Correlation of refractive index response with three isothermal cure runs at 60°C, 90°C and 130°C [64,65].

An interferometric system was reported with a UV curable epoxy [66]. The advantage of the technique over spectroscopic methods is one of speed, having the ability to measure the quick transients experienced during the photocure process. A Helium-Neon source is used to illuminate both a sample and reference cell. The results (shown as $\Delta n/\Delta t$) were shown to be reproducible but were not compared with standard techniques. Cusano *et al* [67] demonstrated a Fresnel system to monitor a curing thermoset (EPON 828) in isothermal conditions. Again the Fresnel system was not referenced but in this work the refractive index was calculated using Fresnel equations.

A proposed equation relating the refractive index change to cure conversion is given as:

$$\alpha(t) = \left(\frac{n(t) - n_0}{n_\infty - n_0} \right) \alpha^{DSC\_MAX} \qquad 2.8$$

Where t is the cure time, n_0 is the start refractive index, n_∞ is the end refractive index and α^{DSC_MAX} is the maximum conversion obtained from the DSC measurements.

2.9 Optical fibre grating techniques

Of particular interest to the work detailed in this thesis are fibre grating refractometers. Optical fibre gratings have found a multitude of uses in the telecommunications industry, and as sensing elements. The first fibre grating stemmed from work by Ken Hill *et al* [68] working with photosensitive fibre in 1978. The reflection of laser light from an optical fibre was noted to increase with time. The phenomenon was later explained by the development of a grating structure, which was inscribed in the fibre by a standing wave pattern formed by the forward propagating light and the Fresnel back reflection from the far end of the fibre. The importance of such a phenomenon was instantly recognised for both telecommunications and sensing applications however the difficulty in reproducing the grating was significant. In the decades since, the writing techniques have improved. Meltz *et al* [69] described a method for writing a Bragg grating into an optical fibre by irradiating the side of an optical fibre with UV radiation at 244nm. UV inscription has become the most common method of manufacture. The manufacture of gratings is discussed in more detail in chapter 3.

An FBG and simplified spectral response is shown in figure 2.30. The wavelength of the reflected light is determined by the period of the grating given by the Bragg wavelength, equation 2.9:

$$\lambda_B = 2 n_{eff} \Lambda \qquad 2.9$$

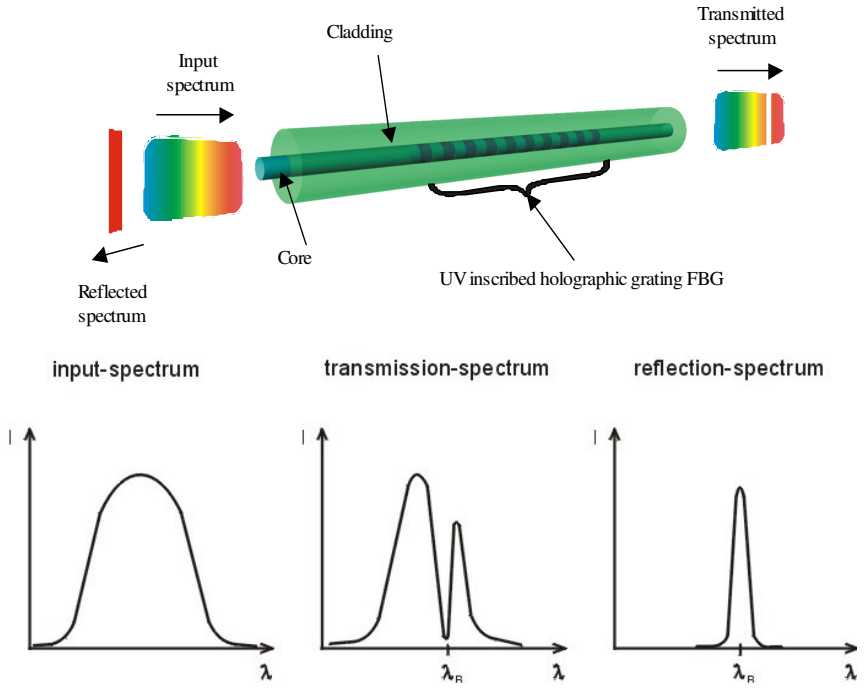

Figure 2.30 Schematic diagram of an FBG with simplified spectrum

where, Λ is the period of the FBG, n_{eff} is the effective refractive index of the counter propagating Bragg wavelength (determined from the core and cladding refractive index) and λ_B is the Bragg wavelength.

The sensing qualities of an FBG are evident from this equation with changes to the period, Λ, and/or n_{eff}, reflected by changes in the Bragg wavelength. Strain and temperature effects on the FBG alter the period and refractive index of the fibre and this has led to the prolific use of the device as a strain and temperature sensor. Side polishing the cladding of the fibre to allow the core modes propagating field to interact with the external environment allows the FBG to sense refractive index changes in the environment. The n_{eff} term in the Bragg equation is then bounded by the cores refractive index and that of the external environment, thus changes to the external refractive index will be reflected as shifts in the Bragg wavelength [70].

A Long Period Grating (LPG), figure 2.31, also has a periodic refractive index modulation of the core of an optical fibre, but has a number of significant differences to an FBG. While the FBG period is typically sub-micron, an LPG has a period in the range 100μm to 1mm [71]. As a result, the LPG has a radically different spectral response. The FBG couples a forward propagating mode of the core of the fibre to a

backward propagating mode, and its reflection and transmission spectra have one significant feature, i.e. a reflection peak at the Bragg wavelength, with this wavelength missing form the transmission spectrum.

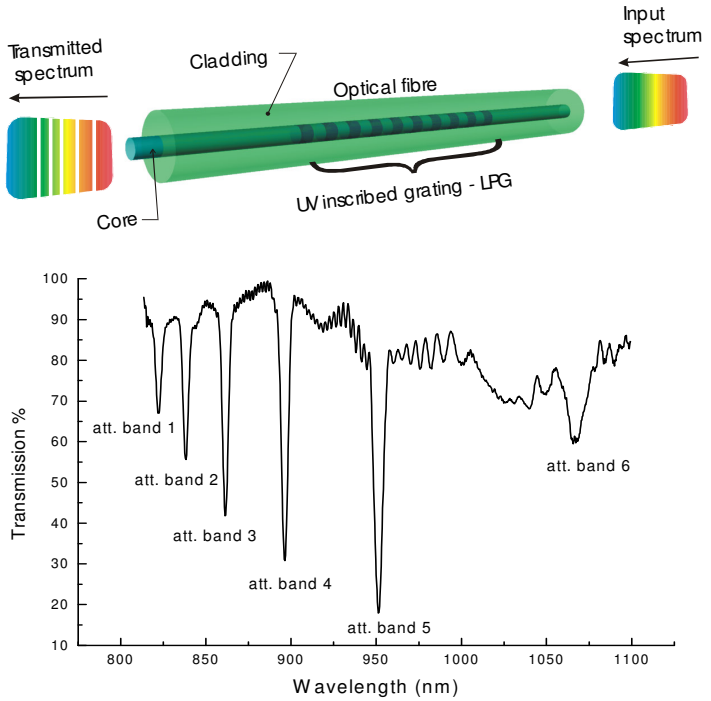

Figure 2.31 Schematic diagram of LPG with typical spectrum

An LPG acts to couple the forward propagating mode of the core of the fibre to a series of co-propagating cladding modes. The coupling to the cladding modes results in a discrete set of attenuation bands in the LPG's transmission spectrum. The central wavelengths of the attenuation bands are given by:

$$\lambda^i = \left[n_{eff} - n^i_{cl} \right] \Lambda \qquad 2.10$$

where λ^i is the central wavelength of the attenuation band with the ith cladding mode, Λ is the period of the LPG, n_{eff} is the effective index of the guided core mode, and n^i_{cl} is the refractive index of the ith cladding mode.

As in the case of the FBG, changes in the period or in the difference between the core and cladding mode effective indices will result in a change in the attenuation band's central wavelengths. LPGs are thus sensitive to physical parameters such as strain and temperature and the surrounding refractive index. The inherent refractive index sensing properties of an LPG are evident from the characteristic equation with the central wavelength of the attenuation bands affected by the cladding modes effective refractive index. The effective refractive index of these modes are bounded by that of the cladding and the external refractive index hence changes to the external refractive index will result in changes to the cladding modes properties and will result in shifts to the central wavelength. An important feature of LPGs is their multi-parameter sensing ability. It is possible through choice of LPG period and fibre type to have attenuation bands that are insensitive to certain measurands, e.g. a particular band may have refractive index sensitivity but be temperature insensitive. A more in depth discussion on the theory of LPGs is discussed in chapter 3.

2.9.1 FBG refractometers

The first use of an FBG as a refractometer was reported by Asseh *et al* [72] using an etched FBG. Etching, as with side polishing, allows the evanescent field to interact with the surrounding medium, figure 2.32. Here the Bragg wavelength determined from the characteristic equation of an FBG is now shown to be dependent upon the refractive index of the surrounding medium, as the effective index of the propagating mode is influenced by the surrounding refractive index. It was shown that the sensitivity was dependent upon the thickness of the remaining cladding. The optimum cladding thickness was 1μm. This creates a very fragile sensor, with a resolution of 2.5×10^{-4} rius at 1330 nm.

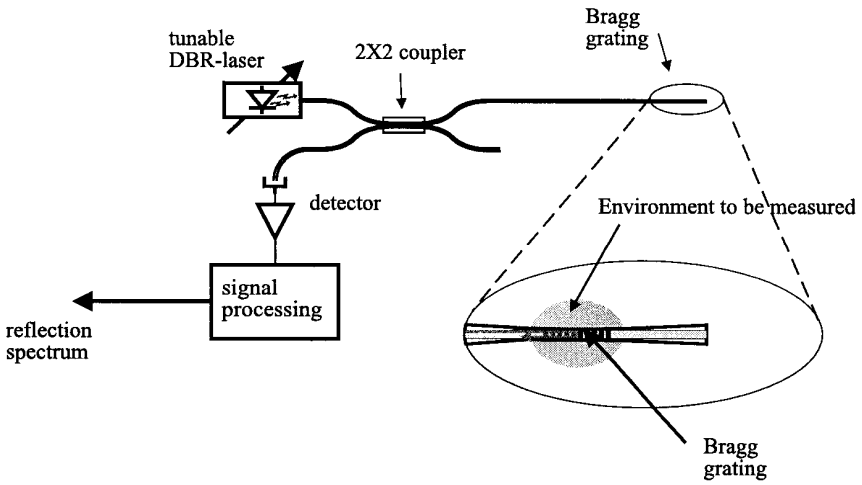

Figure 2.32 Light from a tuneable DBR (distributed Bragg reflector) laser is coupled to the grating through a directional coupler. The fibre cladding at the position of the grating was etched to access the evanescent tail of the core mode. [72]

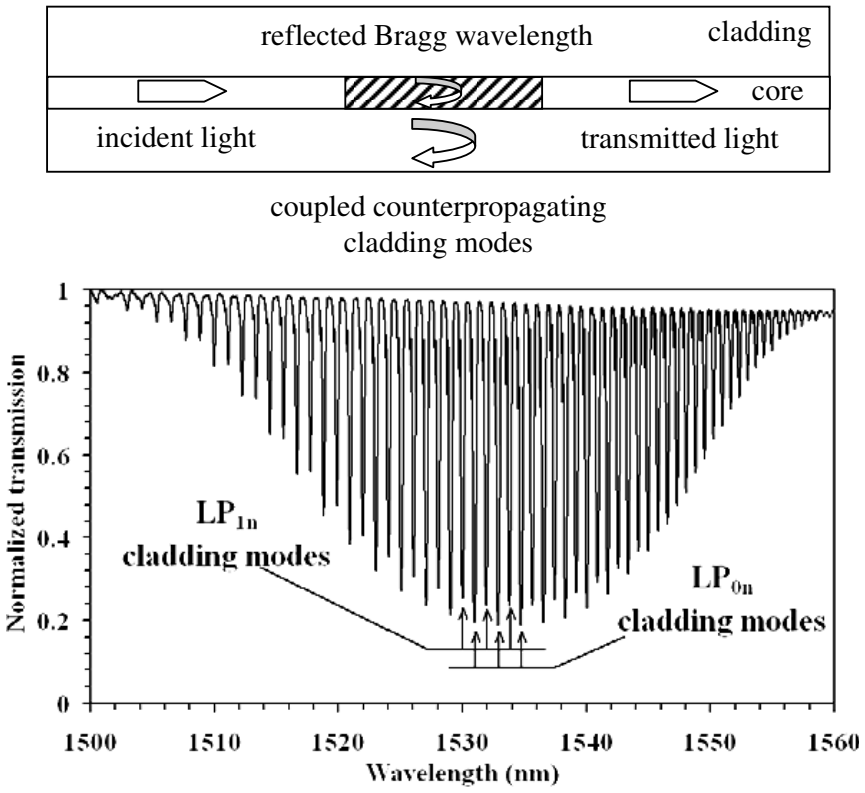

Figure 2.33 Schematic diagram of Tilted Fibre Bragg Grating (TFBG) and typical spectrum. Note the grating planes are tilted relative to the axis of the fibre. [73]

Laffont and Ferdinand [73] report the use of tilted FBGs, figure 2.33, as refractive index sensors. The transmission spectra of tilted FBGs exhibit discreet losses due to coupling to backward propagating cladding modes. As with LPGs, these modes are sensitive to changes in temperature strain and refractive index. The complex spectrum necessitates a more complex analysis, in this case, determining the envelope of spectra structure and monitoring the changes in area bounded by this envelope. A sensitivity of 1 x 10^{-4} rius was quoted.

2.9.2 LPG refractometers

The primary focus of the work presented in this thesis is on the use of LPGs as resin cure monitors by availing of their unique sensitivity to refractive index change without the need for removal of the cladding. The refractive index sensitivity of LPGs has been well reported [74]. Patrick *et al* [75] analysed the response of an LPG to the external index of refraction. An LPG of 275µm period was tested with a range external refractive indices from 1 to 1.72 over a wavelength range from 1100nm to 1700nm. The wavelength response confirmed that the LPGs high sensitivity region occurs as the external refractive index of the surround approaches that of the cladding and further, that the LPG has little or no sensitivity to refractive index above that of the core, figure 2.34.

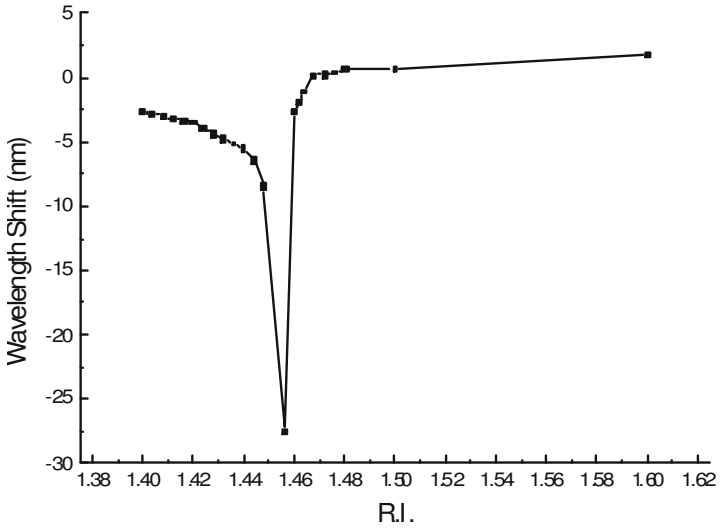

Figure 2.34 Typical refractive index response of an LPG's attenuation band [71].

Falciai *et al* [76] adapted the refractive index sensing qualities of LPG's to demonstrate a solution concentration sensor. The refractive index of calcium chloride, sodium chloride and ethylene glycol aqueous solutions were tested from pure distilled water to a saturated state. The method showed a similar resolution capability when compared with an Abbe refractometer of 1.5 x 10^{-3}.

Lee *et al* [77] demonstrated an interferometric LPG method which Brakel *et al* [78] later used for refractive index measurement. The technique utilised two separate fibre types to create a temperature insensitive sensor, figure 2.35. The LPG couples light from the fundamental mode to the cladding modes which propagate to the end of a silvered cleaved fibre end and are reflected back. This light is then re-coupled back to the core and creates a channelled spectrum within the attenuation bands of the transmission spectrum. An in-fibre Mach-Zehnder interferometer is created and the fringe like spectra exhibit wave length shifts in response to changes in temperature and refractive index.

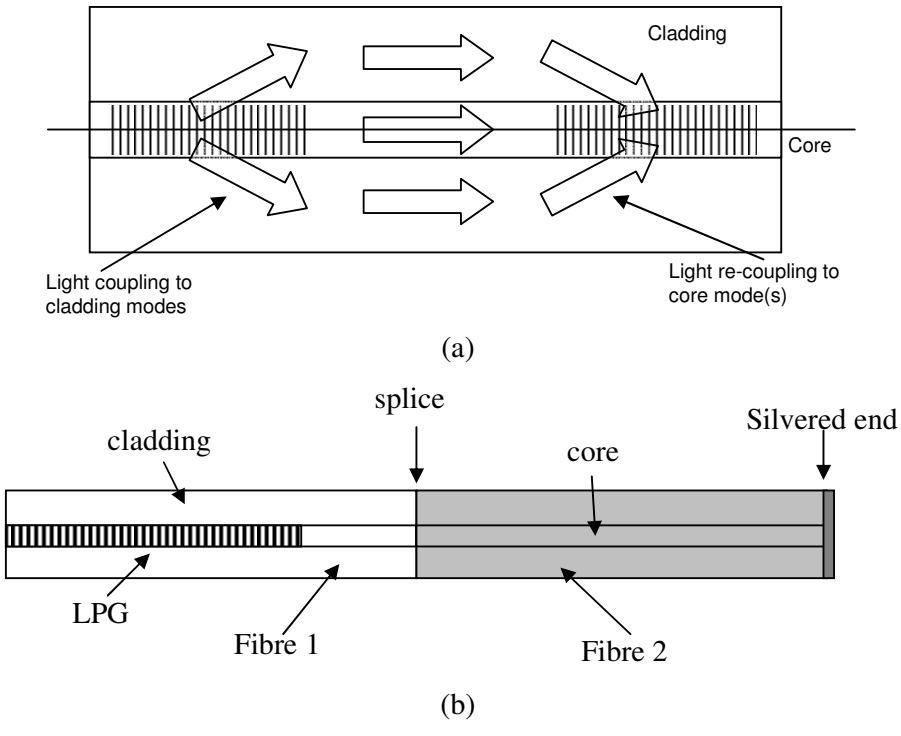

Figure 2.35 (a) Schematic diagram of cascaded LPG, showing Mach-Zehnder type interferometer. [79] (b) Structure of temperature compensation method for LPG proposed by Brakel *et al*. [78]

To remove the temperature effects, Brakel *et al* used two fibre types that exhibited a difference in the phase gradient per unit length. The phase change with temperature for both fibres added together should equal zero to compensate for temperature. The result was a temperature insensitive refractive index sensor.

Gwandu *et al* [79] also demonstrated the use of a cascaded LPG device written in double clad fibre for the simultaneous measurement of both refractive index and temperature. This was based on work published by Han [81] using cascaded LPGs written on double clad fibre. The core mode couples to cladding modes in both the outer and inner cladding. However the inner cladding modes are insensitive to refractive index change and thus respond only to temperature change, while the outer cladding modes are sensitive to both. Thus by monitoring the appropriate bands it is possible to separate both responses.

Yin *et al* [82] proposed the use of ultra-thin LPGs, fibres of 30μm diameter. The thin cladding wall increases the sensitivity of the LPG to surrounding refractive index. The coupled cladding modes evanescent field extend further into the external medium and thus respond more sensitively to changes in its refractive index. An interesting application involved coating an ultra thin LPG with a nematic liquid crystal which exhibited a refractive index change in response to incident polarised optical radiation. The LPG attenuation bands were shifted by changing the refractive index of the external medium with an argon laser and thus were used as a tuning mechanism. A wavelength shift of 3nm for 900mW of argon laser power was reported.

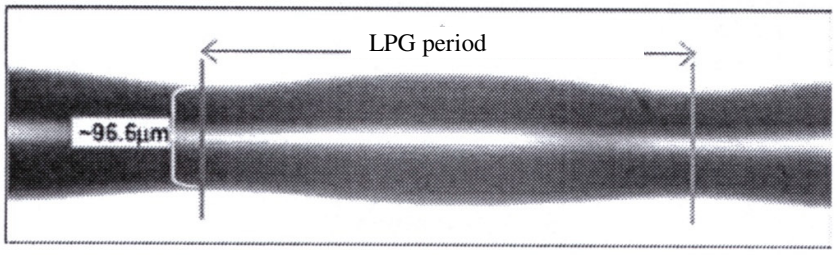

Structurally induced deformation of a LPG on B-Ge co-doped fiber by using CO_2 laser.

Figure 2.36 An LPG created using a CO_2 laser with deformation of the cladding [83].

Table 2.6 Summary of optical grating refractometry methods

Technique	Method	Notes	References
FBG (fibre Bragg grating)	Evanescent	Removed cladding, fragile sensor	72
TFBG (tilted fibre Bragg grating)	Evanescent	Complex spectra, multi-parameter sensor	73
LPG (long period grating)	Evanescent	Unstripped fibre, multi-parameter sensior	74,75,76, 82, 83
MZ – LPG (Mach-Zehnder LPG)	Interferometry	Complex spectra	77,78,79,80
Thinned LPGs	Evanescent	Fragile sensors, increased sensitivity	81

Chong *et al* [83] report an LPGs sensitivity to refractive index this time using a structurally induced grating written with a CO_2 laser. The typical method of manufacture of fibre gratings uses a UV source to form localised areas of refractive index difference. The method here describes using the CO_2 laser was used to form periodic decreases of the cladding diameter on a point by point basis to build up the LPG. Cladding diameters of 96.6µm are shown for a 125µm, figure 2.36. The beam diameter of the CO_2 laser restricted the manufacture of LPGs to periods greater than 400µm and lengths of 8.5mm. Methods of manufacture of LPGs are discussed in more detail in chapter 3. A summary of the optical fibre grating techniques used for refractive index measurements is shown in table 2.6.

2.10 Long period grating cure sensors

Although the use of LPGs as sensing devices has seen much work on their application in many fields, e.g. temperature sensors, their application as resin flow and cure sensors has been limited. A proposal to use LPGs as flow sensors was demonstrated by Dunkers *et al* [84] and Kueh *et al* [85]. Two LPGs were incorporated in three separate liquid composite moulds (LCM) tests, each test using a different reinforcement lay-up with different fibre volume fraction and fibre direction: random mat with a V_f of 0.17, unidirectional mat transversely oriented with a V_f of 0.6 and unidirectional mat axially oriented with a V_f of 0.6. The setup is shown in figure 2.37. The LPGs were enclosed between two reinforcement layers. A corn syrup was used to simulate the resin with an unspecified refractive index higher than that of the cladding.

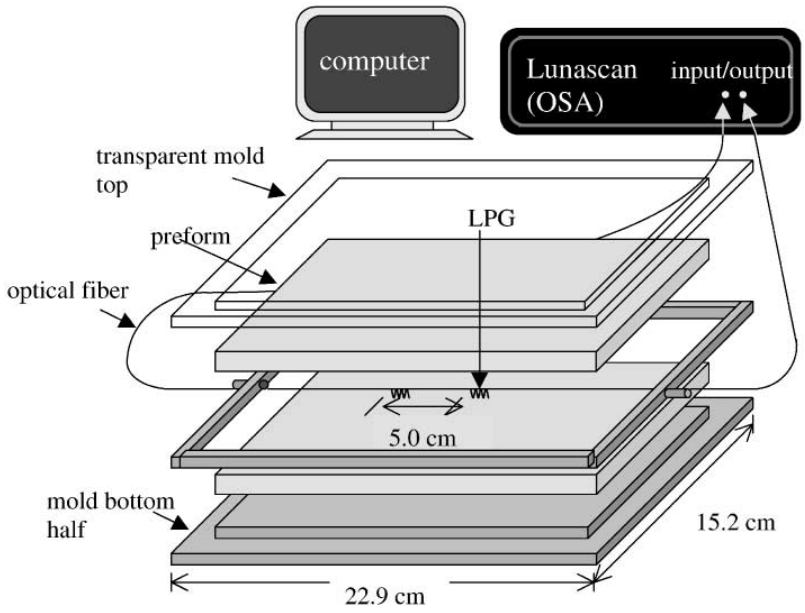

Figure 2.37 LPG flow and cure sensor setup [84].

Two attenuation bands were analysed which corresponded with the individual LPGs. The results illustrated the effects of high V_f materials to the spectra of LPGs. Simple on/off analysis was employed with each band exhibiting transmission gain as the resin covered each LPG. The results provided some information about the problem of incorporating bare silica LPG sensors in composite materials. The resultant spectra were poor due to possible microbending effects caused by the reinforcement coming into direct contact with the fibre. These issues are discussed further in chapter 6. The LPGs used with the random mat layup exhibited loss of attenuation bands. The spectra of those LPGs with the axially laid and transverse unidirectional mat were cleaner, i.e. exhibited more discernible bands. A method of protecting the LPGs involved placing them in 40mm long glass capillary tubes of 445µm inner diameter and 650µm outer diameter. Although the technique preserved the LPG band structure it defeated the critical advantage of optical fibre sensors in their ability to integrate within a structure without affecting the structural integrity. Similar work was repeated with a single LPG and corn syrup used as a simulation resin [86]. Random mat, woven fibre and 'braided and stitched' fibre were used as the reinforcement material. Again the LPG band analysis involved a simple on/off monitoring where the presence of the resin resulted in a change to the spectral location or transmission of the band. Although the work did not

relate the spectral shift or transmission change to flow parameters, the results highlighted the problem of placing LPGs in reinforcement materials of complex geometries with the loss of spectral bands for high V_f materials. Poor spectral information resulted when high V_f material was used (>0.5) and with different injection pressures.

A cure and flow sensor using the same LPG sensor for both measurements has been reported with a resin transfer moulding process (RTM) [87]. An epoxy with a refractive index of 1.45 is used with a random mat reinforcement. Although the cure progression is shown with a slight decrease in wavelength the results are confusing. The flow results show the disappearance of the band when the reinforcement material is fully wet however the cure results show a clear band that is monitored during the cure process and is shown to exhibit both wavelength shift and transmission change. Further the reinforcement material has apparently no direct effect on the unreinforced LPG spectrum. This contradicts previously published work and experimental observations which are discussed in detail in chapter 6. A demonstration of an in-fibre Mach-Zehnder interferometer based on the use of two LPGs has also been shown to have a response to the refractive index change of a UV-cured resin [88]. This is discussed in more detail in chapter 5.

2.11 Summary

It is important to have a quantitative process monitoring capability of AFRCs particularly as such materials become more commonplace in high technology applications. Traditional monitoring techniques although important and useful do not have sufficient in-situ capability to fulfil a real time monitoring capability. Refractive index measurements during the cure stage of a resin may provide a process parameter to enable monitoring and a review of optical fibre technologies illustrated the many techniques available to access this information. However the most elegant candidate appears to be grating based devices and more particularly LPGs. The use of such devices as cure sensors is limited in practice and forms the basis of later work in this thesis.

2.12 References

1. http://www.boeing.com/commercial/787family/gallery/k63211-1.html (accessed 26th May 2008).
2. Harris Bryan (1998). *Engineering Composite Materials*, Maney publishing, London.
3. Gutowski Timothy G. (1997). *Advanced Composites Manufacturing,* Wiley-Interscience, New York.
4. Gay, Daniel, Hoa, Suong V, and Tsai Stephen W. (2002). *Composite Materials: Design and Applications* (4th ed.), CRC press, Florida.
5. Schwartz Mel (1983). *Composite Materials Handbook* (2nd ed.), McGraw Hill, USA.
6. Degamber, B. and Fernando, G. F. (2002), 'Process Monitoring of Fiber-Reinforced Polymer Composites', *MRS Bulletin*, Vol. May, p. 370-380.
7. Kazilas, M. C. (2003), Acquisition and Interpretation of Dielectric Data for Thermoset Cure Monitoring (unpublished PhD thesis), Cranfiield University, Cranfiield University.
8. Dimopolous A. (2008). Effect of carbon nanotubes on epoxy, Cranfield University, Cranfield.
9. Challis, R. E., Unwin, M. E., Chadwick, D. L., Freemantle, R. J., Partridge, I. K., Dare, D. J. and Karkanas, P. I. (2003), ' Following network formation in an epoxy/amine system by ultrasound, dielectric, and nuclear magnetic resonance measurements: a comparative study', *Journal of Applied Polymer Science,* 88(7), p. 1665-1675.
10. Cocker, R.P., Chadwick, D.L. Dare, D.J. and Challis, R.E. (1998), 'A low resolution pulsed NMR and ultrasound study to monitor the cure of an epoxy resin adhesive', *International Journal of Adhesion and Adhesives*, 18, p. 319-331.
11. Skordos, A. A., and Partridge, I. K. (2004), 'Determination of the Degree of Cure under Dynamic and Isothermal Curing Conditions with Electrical Impedance Spectroscopy', *Journal of Polymer Science: Part B: Polymer Physics*, 42, p. 146–154.

12. Lee, J. K. And Gillham, J. K. (2003), 'Evolution of properties with increasing cure of a thermosetting epoxy/aromatic amine system: physical ageing', *Journal of Applied Polymer Science*, 90(10), p. 2665-2675.
13. Fouchal, F, Knight, J. A. G. And Dickens, P. M. (2004), 'Monitoring the polymerization of a diglycidyl ether bisphenol-A/2,20-dimethyl-4,40-methylenebis (cyclohexylamine) matrix with a Fourier transform infrared optical fibre sensor', *Proceedings of the Institution of Mechanical Engineers*, 218, p. 331-342.
14. Mijovic, J. And Andjelic, (1995), 'ln situ real-time monitoring of reactive systems by remote fibre-optic near-infra-red spectroscopy', *Polymer*, 36(19), p. 3783-3786.
15. Nesbitt, A., Navabpour, P., Degamber, B., Nightingale, C., Mann, T., Fernando, G. and Day, R. J., (2004), 'Development of a microwave calorimeter for simultaneous thermal analysis, infrared spectroscopy and dielectric measurements', *Measurement Science and Technology*, 15, p. 2313–2324.
16. Smith, Brian C., (1995), *Fundamentals of Fourier Transform Infrared Spectroscopy*, CRC press, Florida.
17. Danneberg H., (1963), 'Determination of functional groups in epoxy resins by near-infrared spectroscopy', *Polymer Engineering and Science*, 3(1), p.78-88.
18. Dunkers, J.P., Flynn, K.M. and Parnas, R.S. (1997), 'Mid-infrared attenuated total internal reflection cure sensor for control of resin transfer moulding of a pre-ceramic polymer', *Composites - Part A: Applied Science and Manufacturing*, 28(2), p. 163-170.
19. Druy, M.A., Glatkowski, P.J., and Stevenson, W.A. (1991), 'Cure monitoring of polymeric composites with fiber optics and FTIR spectroscopy', *Proceedings of the Conference on Optical Fiber Sensor-Based Smart Materials and Structures*, Blacksburg, VA, USA, Apr 3-4 1991, p. 169.
20. George, G.A., Cole-Clarke, P., St. John, N. and Friend, G. (1991), 'Real-time monitoring of the cure reaction of a TGDDM/DDS epoxy resin using fiber optic FT-IR', *Journal of Applied Polymer Science*, 42(3), p. 643-657.
21. Dunkers, J. P., Flynn, K. M., Huang, M. T. and McDonough W. G. (1998), 'Fourier Transform Near-Infrared Monitoring of Reacting Resins Using an

Evanescent Wave High-Index Fiber-Optic Sensor', *Applied Spectroscopy*. 52, p. 552-556

22. Tapanes, E.E., Hill, A.J. and Rossiter, P.L. (1993), 'Real-time, in-situ cure monitoring of advanced aerospace composites using a fibre optic sensor based on FTIR spectroscopy', *Proceedings of the 1993 9th International Conference on Composite Materials, ICCM/9. Part 2 (of 6)*, Vol. 2, Jul 12-16 1993, p. 457.
23. Degamber, B. and Fernando, G.F. (2002), 'Remote Process Monitoring Using Optical Fibre Sensors', *First IEEE International Conference on Sensors - IEEE Sensors 2002*, Orlando, FL, USA, Vol. 1, Jun 12-14 2002, , Institute of Electrical and Electronics Engineers Inc., p. 1537-1542.
24. Lyon, R.E., Chike, K.E. and Angel, S.M. (1994), 'In situ cure monitoring of epoxy resins using fiber-optic Raman spectroscopy', *Journal of Applied Polymer Science*, 53(13), p. 1805-1812.
25. Skrifvars, M., Niemela, P., Koskinen, R. and Hormi, O. (2004), 'Process cure monitoring of unsaturated polyester resins, vinyl ester resins, and gel coats by Raman spectroscopy', *Journal of Applied Polymer Science*, 93(3), p. 1285-1292.
26. Debakker, C. J., George, G. A., St. John, N. A. And Fredericks, P.M. (1993), 'The kinetics of the cure of an advanced epoxy resin by Fourier transform Raman and near-IR spectroscopy', *Spectrochimica Acta, Part A (Molecular Spectroscopy)*, 49A(5-6), May-June, p. 739-52
27. Paik, H.-J. and Sung, N.-H. (1994), 'Fiberoptic intrinsic fluorescence for in-situ cure monitoring of amine cured epoxy and composites', *Polymer Engineering and Science*, 34(12), p. 1025-1032.
28. Wang, F. W., Lowry, R. E. and Fanconi B. M. (1986), 'Novel fluorescence method for cure monitoring of epoxy resins', *Polymer*, 27, p. 1529-1532.
29. Levy R. L. and Schwab S. D. (1991), 'Monitoring the composite curing process with a fluorescence-based fiber-optic sensor', *Polymer Composites* ,12, p.96-101.
30. Gonzalez-Benito, J., Olmos, D., Sanchez, P.G., Aznar, A.J. and Baselga, J. (2003), 'Kinetic study of the cure process at the silica microfibres/epoxy interface using pyrene fluorescence response', *Journal of Materials Processing Technology,* 143-144(1), p. 153-157.

31. Woerdeman, D.L. and Parnas, R.S. (1995), 'Cure monitoring in RTM using fluorescence', *Plastics Engineering*, 51(10), p. 25-27.

32. Woederman D. L., Flynn K. M., Dunkers J. P. and Parnas R. S. (1996), 'The use of evanescent wave fluorescence spectroscopy for control of the liquid molding process', *Journal Reinforced Plastics and Composites*, 15, 922-943.

33. Davis, A., Ohn, M.M., Liu, K., and Measures, R.M. (1991), 'Study of an opto-ultrasonic technique for cure monitoring', Fiber Optic Smart Structures and Skins IV, Sep 5-6 1991, Vol. 1588, Publ by Int Soc for Optical Engineering, Bellingham, WA, USA, Boston, MA, USA, p. 264-274.

34. Ohn, M.M., Davis, A., Liu, K., and Measures, R.M. (1993), 'Embedded fiber optic detection of ultrasound and its application to cure monitoring', Fiber Optic Smart Structures and Skins V, Sep 8-9 1992, Vol. 1798, Publ by Int Soc for Optical Engineering, Bellingham, WA, USA, Boston, MA, USA, pp. 134-143.

35. Jackson, D. A., Priest, R., Dandridge, A. And Tveten, A. B. (1980), 'Elimination of drift in a single mode optical interferometer using a piezoelectrically stretched coiled fibre', *Applied Optics*, 19, p. 2926-2929.

36. Mitra, B., Shelamoff, A. and Booth, D.J. (1998), 'Optical fibre interferometer for remote detection of laser generated ultrasonics', *Measurement Science & Technology*, 9(9), p. 1432-1436.

37. Dorighi, J., Krishnaswamy, S. and Achenbach, J. (1997), 'Fiber optic ultrasonic system to monitor the cure of epoxy', *Research in Non-Destructive Evaluation*, 9(1), p. 13-24.

38. Gladstone, J.H. and Dale T. P. (1858), Researches on the refraction, dispersion and sensitiveness of liquids, Transactions *of the Royal Society (London)*, A148, p. 887.

39. Born, M. and Wolf E. (1999), *Principles of Optics: Electromagnetic Theory of Propagation, Interference and Diffraction of Light (7th Edition)*, Cambridge University Press, Cambridge.

40. Meeten, G. H. and North, A. N. (1991), 'Refractive index measurement of turbid colloidal fluids by transmission near the critical angle', *Measurement Science & Technology,* 2, p. 441–7.

41. Bellingham and Stanley, Abbe 60 Series Refractometer: Operators Manual, available at: www.bellinghamandstanley.com
42. Takeo, T. and Hattori, H. (1982), 'Optical fiber sensor for measuring refractive index', *Japanese Journal of Applied Physics. Pt. 1*, 21(10), p. 1509-1512.
43. Harmer, A.L. (1983), 'Optical fibre refractometer using attenuation of cladding modes', First International Conference on Optical Fibre Sensors, 26-28 April 1983, IEE, London, UK, p. 104-8.
44. Takeo, T. and Hattori, H. (1992), 'Silica glass fiber photorefractometer', *Applied Optics*, 31(1), p. 44-50.
45. Smela, E. and Santiago-Aviles, J.J. (1988), 'A versatile twisted optical fiber sensor', *Sensors and Actuators*, 13(2), p. 117-29.
46. Kumar, A., Subrahmanyam, T.V.B., Sharma, A.D., Thyagarajan, K., Pal, B.P. and Goyal, I.C. (1984), 'Novel refractometer using a tapered optical fibre', *Electronics Letters*, 20(13), p. 534-5.
47. Guo, S. and Albin, S. (2003), 'Transmission property and evanescent wave absorption of cladded multimode fiber tapers', *Optics Express*, 11(3), p. 215-223.
48. Monzon-Hernandez, D., Villatoro, J. and Luna-Moreno, D. (2005), 'Miniature optical fiber refractometer using cladded multimode tapered fiber tips', *Sensors and Actuators, B: Chemical*, 110(1), p. 36-40.
49. Ravishankar, M.K. and Pappu, S.V. (1986), 'Fiber-optic sensor-based refractometer-cum-liquid level indicator', *Applied Optics*, 25(4), p. 480-2.
50. Ilev, I.K. (1995), 'Fiber-optic autocollimation refractometer', *Optics Communications*, 119(5-6), p. 513-16.
51. Murphy, P.J. and Coursolle, T.P. (1990), 'Fiber optic displacement sensor employing a graded index lens', *Applied Optics*, 29(4), p. 544-7.
52. Breen, S., Paton, B.E., Blackford, B.L. and Jericho, M.H. (1990), 'Fiber optic displacement sensor with sub-angstrom resolution', *Applied Optics*, 29(1), p. 16-18.
53. Suhadolnik, A., Babnik, A. and Mozina, J. (1995), 'Optical fiber reflection refractometer', Sensors and Actuators, B: Chemical: Proceedings of the 2nd

European Conference on Optical Chemical Sensors and Biosensors, EUROPT(R)ODE II, Apr 19-21 1994, Vol. B29, No. 1-3, pp. 428-432.

54. Heideman, R.G., Kooyman, R.P.H., Greve, J. and Altenburg, B.S.F. (1991), 'Simple interferometer for evanescent field refractive index sensing as a feasibility study for an immunosensor', *Applied Optics*, 30(12), p. 1474-9.

55. Attridge, J.W., Leaver, K.D. and Cozens, J.R. (1987), 'Design of a fibre-optic pH sensor with rapid response', *Journal of Physics E (Scientific Instruments)*, 20(5), p. 548-53.

56. Slavik, R., Homola, J. and Ctyroky, J. (1999), 'Single-mode optical fiber surface plasmon resonance sensor', *Sensors and Actuators B (Chemical)*, B54(1-2), p. 74-9.

57. Slavik, R., Ctyroky, J. and Homola, J. (2000), 'Fiber optic surface plasmon resonance sensor with a Bragg grating', Proceedings of SPIE - The International Society for Optical Engineering: 3rd Conference on Photonics, Devices, and Systems (PHOTONICS PRAGUE '99), Jun 21-Jun 23 1999, Vol. 4016, pp. 154-158.

58. Tjhuang, T.T., Teo, S.K., Mendis, F.V.C. and Selvan, B. (1985), 'Refractometry through optical frequency-domain reflectometry', *Electronics Letters*, 21(14), p. 613-14.

59. Chang, K.-A. , Lim, H.-J., and Su, C. B. (2002), 'A Fibre Optic Fresnel Ratio Meter for Measurements of Solute Concentration and Refractive Index Change in Fluids', *Measurement Science and Technology*, 13, p. 1962-1965.

60. Kim, C.-B. and Su, C. B. (2004), 'Measurement of the Refractive Index of Liquids at 1.3 and 1.5 Micron Using a Fibre Optic Fresnel Ratio Meter', *Measurement Science and Technology*, 15, p. 1683-1686.

61. Bartlett, R.J., Philip-Chandy, R., Eldridge, P., Merchant, D.F., Morgan, R. and Scully, P.J. (2000), 'Plastic optical fibre sensors and devices', *Transactions of the Institute of Measurement and Control*, 22(5), p. 431-457.

62. Ribeiro, R.M., Canedo, J.L.P., Werneck, M.M. and Kawase, L.R. (2002), 'An evanescent-coupling plastic optical fibre refractometer and absorption meter based on surface light scattering', *Sensors and Actuators A (Physical)*, A101, (1-2), p. 69-76.

63. Sheeba, M., Rajesh, M., Vallabhan, C.P.G., Nampoori, V.P.N. and Radhakrishnan, P. (2005-), 'Fibre optic sensor for the detection of adulterant traces in coconut oil', *Measurement Science & Technology*, 16(11), p. 2247-50.

64. Afromowitz, M. A. and Lam, K.-Y. (1990), 'The Optical Properties of Curing Epoxies and Applications to the Fiber-Optic Epoxy Cure Sensor', *Sensors and Actuators*, A21-A23, p. 1107-1110.

65. Cusano, A., Breglio, G., Giordano, M., Calabro, A., Cutolo, A., and Nicolais, L. (2000), 'An Optoelectronic Sensor for Cure Monitoring in Thermoset-based composites', *Sensors and Actuators*, 84, p. 270-275.

66. Lam, K.-Y. and Afromowitz, M.A. (1995), 'Fiber-optic epoxy composite cure sensor. I. Dependence of refractive index of an autocatalytic reaction epoxy system at 850 nm on temperature and extent of cure', *Applied Optics*, 34(25), p. 5635-8.

67. Dudi, O., A1 - Grubbs, W. T. (1999), 'Laser Interferometric Technique for Measuring Polymer Cure Kinetics', *Journal of Applied Polymer Science*, 74, p. 2133-2142

68. Cusano, A., Breglio, G., Giordano, M., Nicolais, L., and Cutolo, A. (2004), 'Multifunction Fiber Optic Sensing System for Smart Applications', *IEEE/ASME Transactions on Mechatronics*, 9(1), p. 40-49.

69. Hill, K.O., Fujii, Y., Johnson, D. C. and Kawasaki B. S. (1978), 'Photosensitivity in optical fiber waveguides: Application to reflection filter fabrication', *Applied Physics Letters,* 32(10), p. 647.

70. Meltz, G., Morey, W.W., Glenn, W.H., and Fritz, D.J. (1993), 'UV-induced Bragg gratings in optical fibers and thin-film waveguides', Photosensitivity and Self-Organization in Optical Fibers and Waveguides, 17-18 Aug. 1993: Proceedings of the SPIE - The International Society for Optical Engineering, Vol. 2044, Quebec, Que., Canada, pp. 236-45.

71. Schroeder, K., Ecke, W., Mueller, R., Willsch, R. and Andreev, A. (2001), 'A fibre Bragg grating refractometer', *Measurement Science and Technology*, 12(7), p. 757-64.

72. James, S. W. and Tatam, R. P. T. (2003), 'Optical Fibre Long-period Grating Sensors: Characteristics and Application', *Measurement Science and Technology*, 14, p. R49-R61.

73. Asseh, A., Sandgren, S., Ahlfeldt, H., Sahlgren, B., Stubbe, R. and Edwall, G. (1998), 'Fiber optical Bragg grating refractometer', *Fiber and Integrated Optics*, 17(1), p. 51-62.

74. Laffont, G. and Ferdinand, P. (2001), 'Tilted short-period fibre-Bragg-grating-induced coupling to cladding modes for accurate refractometry', *Measurement Science & Technology*, 12(7), p. 765-70.

75. Sarfraz, K. (2003), Fibre Optic Long Period Fibre Gratings for Sensing Applications (unpublished PhD thesis), Cranfield University, Cranfield University.

76. Patrick, H. J., Kersey, A. D., and Bucholtz, F. (1998), 'Analysis of the Response of Long Period Gratings to External Index of Refraction', *Journal of Lightwave Technology*, 16, p. 1606-1642.

77. Falciai, R., Mignani, A.G., and Vannini, A. (2001), 'Long period gratings as solution concentration sensors', 5th European Conference on Optical Chemical Sensors and Biosensors, Apr 16-19 2000, Vol. 74, Elsevier Science B.V., Lyon, p. 74-77.

78. Byeong Ha Lee, Youngjoo Chung, Won-Taek Han, and Un-Chul Paek (2000-), 'Temperature sensor based on self-interference of a single long-period fiber grating', 13th International Conference on Optical Fibre Sensors, 12-16 April 1999: IEICE Transactions on Electronics, Vol. E83-C, Inst. Electron. Inf. & Commun. Eng, Kyongju, South Korea, p. 287-92.

79. Van Brakel, A. and Swart, P.L. (2005), 'Temperature-compensated optical fiber Michelson refractometer', *Optical Engineering*, 44(2), p. 020504.

80. Gwandu, B.A.L., Shu, X., Allsop, T.D.P., Zhang, W., Zhang, L., Webb, D.J. and Bennion, I. (2002), 'Simultaneous refractive index and temperature measurement using cascaded long-period grating in double-cladding fibre', *Electronics Letters*, 38(14), p. 695-696.

81. Young-Geun Han, Byeong Ha Lee, Won-Taek Han, Un-Chul Paek and Youngjoo Chung (2001-), 'Fibre-optic sensing applications of a pair of long-period fibre gratings', *Measurement Science & Technology*, 12(7), p. 778-81.

82. Yin, S., Chung, K.-W. and Zhu, X. (2001), 'A novel all-optic tunable long-period grating using a unique double-cladding layer', *Optics Communications*, 196(1-6), p. 181-186.

83. Chong, J.H., Shum, P., Hartono, H. and Aleta, Y. 'Investigations on the Characteristics of Point-by-Point Co2 Laser Induced Long-Period Grating on Optical Fiber', p. 1283-1285. Information, Communications and Signal Processing, 2003 and the Fourth Pacific Rim Conference on Multimedia. Proceedings of the 2003 Joint Conference of the Fourth International Conference on Volume 2, Issue , 15-18 Dec. 2003 Page(s): 1283 - 1285 vol.2

84. Dunkers, J.P., Lenhart, J.L., Kueh, S.R., van Zanten, J.H., Advani, S.G. and Parnas, R.S. (2001), 'Fiber optic flow and cure sensing for liquid composite molding', *Optics and Lasers in Engineering*, 35(2), p. 91-104.

85. Kueh, S.R.M., Parnas, R.S., Dunkers, J.P., Advani, S.G., Furrows, P.S., Jones, M.E., and Bailey, T.A. (2000), 'Long period gratings as flow sensors for liquid composite molding', Nondestructive Evaluation of Aging Materials and Composites IV, Mar 8-Mar 9 2000, Vol. 3993, Society of Photo-Optical Instrumentation Engineers, Bellingham, WA, USA, Newport Beach, CA, USA, pp. 240-250.

86. Zhu, Y, Wang, C., Wang, J., He, W. And Gao, Guoqiang (2005), 'Long-period gratings in-situ sensing for flow monitoring in liquid composite molding', *Journal of Material Science Technology*, 21(2), p. 234-238.

87. Yoon, Y., Chung, S., Lee, W. And Lee, B. (2004), 'A study on the measurement technique of resin flow and cure during the Vacuum Assisted Resin Transfer Moulding process using the Long Period Fibre Bragg Grating sensor', *Advanced Composites Letters*, 13(5), p. 237-243.

88. Buggy, S.J., Murphy, R.P., James, S.W. and Tatam, R.P., 'Cure monitoring of a UV cured epoxy resin using a long period grating Mach-Zehnder interferometer', Presented at the Third European Workshop on Optical fibre Sensors, Napoli, Italy, July 4-7, 2007.

Long period gratings – theory, fabrication and characterisation

3

3.1 Introduction

A long period grating (LPG) sensor is an optical fibre based device with sensing virtues that are to a large extent determined by the geometrical structure and optical properties of the host fibre. The LPG has, since its inception in 1996 [1], found a host of applications as a sensor for temperature [2,3], strain [3,4], bend radius [5,6], chemical concentration [7,8] refractive index [9,10] measurement, and bio-medical [11,12] applications. In this chapter an appreciation of the origin of this sensing ability is presented through a basic summary of optical fibres and a short theoretical overview of the LPG. The methods used to fabricate LPG devices are also summarised and a concluding section demonstrates the temperature, strain and chemical concentration characteristic of an example LPG. Because LPGs are optical fibre based devices an introduction on the propagation of light energy in a fibre optic will aid a later discussion on the interaction of propagating light with an LPG device.

3.2 Optical Fibres

An optical fibre consists of a core material of refractive index, n_1 surrounded by a cladding of lower index, n_2 [13]. This refractive index difference may be gradual, graded index fibres, or more typically may have a step profile, step index fibre. A typical step index optical fibre is illustrated in figure 3.1. The core of an optical fibre may be considered as the light conduit of the optical fibre and it is surrounded by a protective cladding as the insulator. The physics behind the behaviour of light within an optical fibre may be explained by two means. Firstly, using 'ray theory' where the light is considered as a "line corresponding to the direction of flow of radiant energy" [14] bouncing along the core/cladding interface of the optical fibre. Secondly in terms of electromagnetic wave energy, where use is made of Maxwell's equations and the boundary conditions imposed on a propagating electromagnetic wave by the optical fibre.

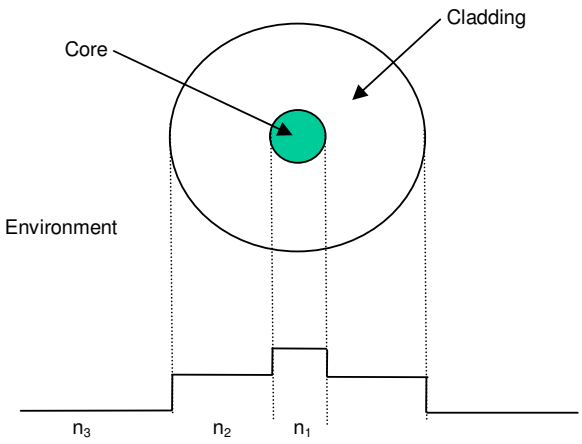

Figure 3.1. Step index optical fibre. n_1 is the core refractive index, n_2 the cladding refractive index and n_3 the refractive index of the environment.

The two are not necessarily contradictory although the ray model is a simpler representation of light energy propagation and valid when $\lambda \rightarrow 0$ [15]. A more correct description, for cases when the optical fibre radius is of the same order as that of the

optical wavelength, is in terms of electromagnetic modes which are solutions to Maxwell's equations for a given optical fibre and wavelength.

3.2.1 The ray model approach

A ray of light is shown in figure 3.2 travelling through an optical fibre waveguide at an angle such that it bounces along the interface between the core and the cladding and thus propagates along the z-axis. This propagation angle is governed by Snells law and represents a guided mode. The angle, ϕ, at which propagation is possible, is given by [14].

$$n_1 \sin \phi_c = n_2 \qquad 3.1$$

where ϕ_c is termed the critical angle and n_1 and n_2 are the core and cladding refractive index respectively and $\phi < \phi_c$.

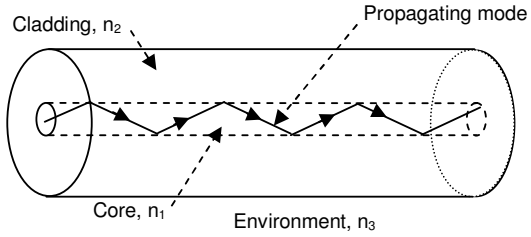

Figure 3.2. Simple model of ray tracing through an optical fibre

This phenomenon is called total internal reflection [16]. In order for total internal reflection to occur the core refractive index must be higher than that of the cladding. The wave guiding properties of an optical fibre are governed by its geometry (core and cladding dimensions and shape) and material properties (difference in between core and cladding refractive index). The number of modes supported by an optical fibre can be approximated by [15].

$$M \approx \frac{V^2}{2} \qquad 3.2$$

where M is the number of modes and V is the normalised frequency and given by [15]:

$$V = \left(\frac{2\pi}{\lambda}\right) a\sqrt{(n_2^2 - n_1^2)} \qquad 3.3$$

where, a is the radius of the fibre core. Step index fibres are single mode when V<2.40522. A fibre that supports one mode is termed single mode and it is clear from equation 3.3, that it is possible to reduce the diameter of the core to a point where a single mode is supported at a particular wavelength.

3.2.2 Electromagnetic theory

There are many references that describe the propagation of electromagnetic waves [17,18]. The pertinent points with reference to propagation in an optical fibre are detailed here. From Maxwell's equations, the wave equation for electromagnetic radiation propagating in an optical fibre in cylindrical co-ordinates for the z components of E and H, E_z, H_z, can be written as:

$$\frac{\partial^2 \psi}{\partial r^2} + \frac{1}{r}\frac{\partial \psi}{\partial r} + \left(k^2 - \beta^2 - \frac{1}{r^2}\right)\psi = 0 \qquad 3.4$$

Where $\psi = E_z, H_z$ and r is the radial coordinate, β the propagation constant and $k^2 = \omega^2 n^2/c$, ω is the angular frequency, $\omega = 2\pi f$. The propagation constant, β, is a parameter that determines a mode's phase and amplitude variation in the z direction. Further derivation of the radial (E_r and H_r) and azimuthal (E_φ and H_φ) field components is possible as they may be expressed in terms of E_z and H_z [18]. From equation 3.4, a finite set of solutions are possible for a given waveguide at a particular frequency with each solution corresponding to a guided mode with a propagation constant β. The propagation constant is given as:

$$\beta = \frac{\omega n_{eff}}{c} = \frac{2\pi n_{eff}}{\lambda} \qquad 3.5$$

where n_{eff} is termed the effective refractive index of the propagating mode. For propagation modes within the core a discrete set of values for β are confined to: [19,20]

$$n_2 k_0 < |\beta| < n_1 k_0 \qquad 3.6$$

where, k_0 is the free space propagation constant, $k_0=2\pi/\lambda$. Radiation modes are also solutions to the boundary conditions [16] and represent non-propagating modes that radiate energy from the core, their discrete propagation constants are confined to:

$$|\beta| < n_3 k_0 \qquad 3.7$$

A long period grating is an optical fibre based grating that enables coupling between the core and the cladding. If the cladding is surrounded by a lower refractive index, e.g. air, the cladding can support cladding modes and their discrete propagation constants are confined to:

$$n_3 k_0 < |\beta| < n_2 k_0 \qquad 3.8$$

A β-plot is shown in figure 3.3 to illustrate the range of solutions for the propagation constant.

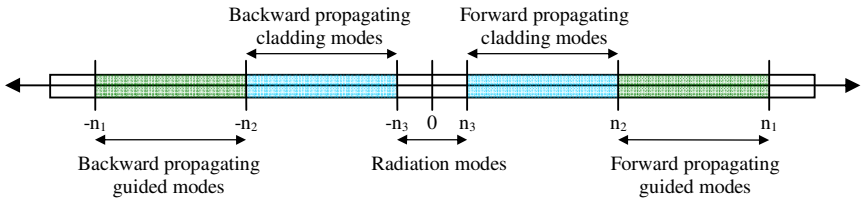

Figure 3.3 Propagation constant or β- plot showing modal distribution in an optical fibre.

3.3 Long period gratings – theory

A grating is a periodic structure that causes light or incident electromagnetic energy to behave a certain way dependent on the periodicity of the grating. An LPG is a fibre based grating and consists of a periodic perturbation of the refractive index of the core, with a period typically from 100μm to 1mm [21]. In an optical waveguide, if there is sufficient modal overlap between a core and cladding mode then there can be a transfer of energy from the core mode to the cladding modes, figure 3.4. The index perturbation of an LPG can be designed to enhance this effect by phase matching to a discrete set of cladding modes. The cladding is a very poor waveguide and coupled light is subsequently lost through absorption and scattering losses. This is apparent as loss bands in the transmission spectrum.

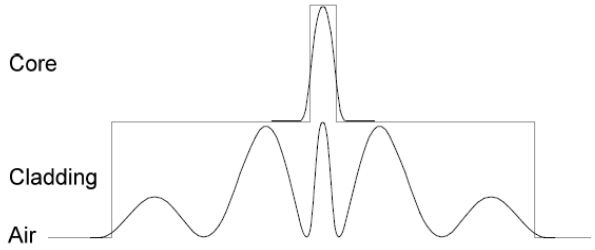

Figure 3.4 Simplified side view of the intensity profile of the core and cladding modes showing modal overlap [22].

A diagram of a long period grating is shown in figure 3.5 and a typical transmission spectrum is shown in figure 3.6 with the attenuation bands that are characteristic of LPG spectra.

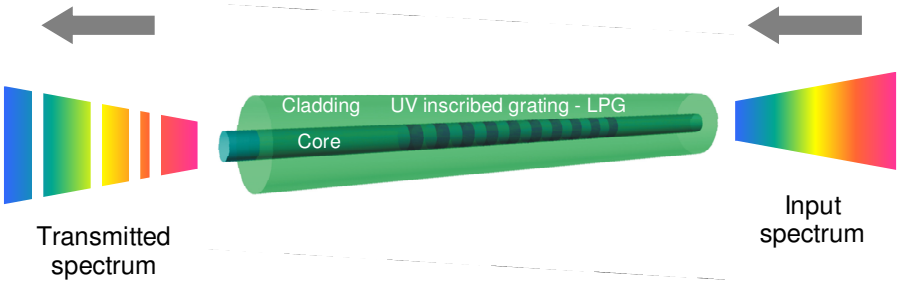

Figure 3.5. Diagram of an LPG

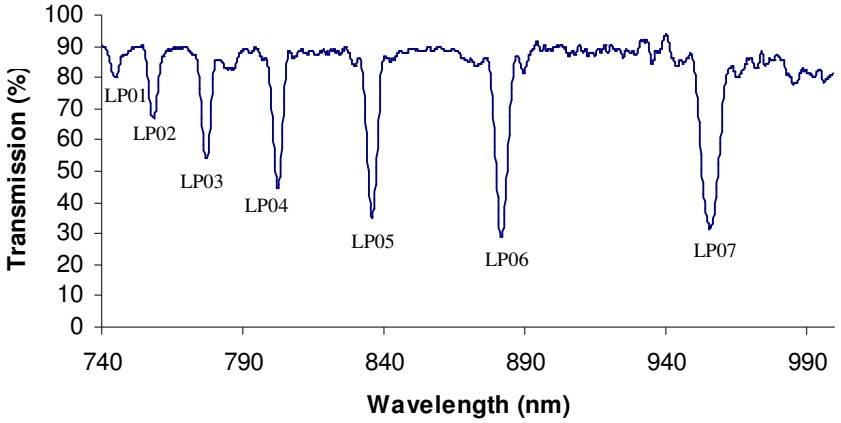

Figure 3.6. Plot of the transmission spectrum of an LPG written for this work of period 400μm and length 40mm fabricated in Fibercore PS750. The bands are annotated with their associated coupled cladding modes.

The central wavelength of each attenuation band is sensitive to the period of the LPG and difference between the refractive index of the fundamental core mode and individual cladding modes, termed the differential refractive index [21]. The discrete wavelength at which coupling occurs is given by [1]:

$$\lambda^i = \left[n_{eff} - n^i_{clad}\right]\Lambda \qquad 3.9$$

Where λ_i is the central wavelength of the attenuation band, n_{eff} is the effective refractive index of the core mode, n^i_{clad} is the effective refractive index of the i^{th} cladding mode and Λ is the period of the LPG. Coupled mode theory may be used as a tool to explain the exchange in power between the core and cladding modes [23,24]. The core and cladding are considered separately as two waveguide structures and, under phase matched conditions, light couples from one to the other. Higher diffraction orders are described by [25]:

$$\lambda^i = \frac{\left[n_{eff} - n^i_{clad}\right]\Lambda}{N} \qquad 3.10$$

where *N*=1,2,3...is an integer representing the diffraction order. Higher order coupling attenuation bands modes have been reported for both temperature and strain responses [25].

3.3.1 Coupled mode theory

In an unperturbed optical fibre, the light propagates in the core without any appreciable loss. In the presence of a perturbation however, power may be exchanged between different modes. An LPG written at some point in the optical fibre is a waveguide perturbation that causes the energy in the core mode to couple to cladding modes. The mechanism can be described using coupled mode theory. The relationship between two propagating modes, A and B, in the presence of a perturbation is of the type [26]:

$$\frac{dA}{dz} = \kappa_{ab} B e^{-i\Delta z} \tag{3.11}$$

$$\frac{dB}{dz} = \kappa_{ba} A e^{+i\Delta z} \tag{3.12}$$

This describes the modal amplitude in terms of the propagating axis. κ_{ab} and κ_{ba} are termed the coupling coefficients and establish the strength of interaction between the modes. They are determined by the physical dimensions and type of perturbation and by the individual mode profiles. Δ is the phase mismatch constant, it indicates that total power exchange between the modes occurs when it is equal to zero.

The coupled mode equation that describes the more particular interaction between the core mode and cladding modes of an LPG is given as [27]:

$$\frac{dA_{core}}{dz} = i\kappa_{core\_core} A_{core} + i\sum_{v} \frac{m}{2} \kappa_{1v-01}^{clad-core} A_{v}^{clad} \exp(-i\delta_{1v-01}^{clad-core} z) \tag{3.13}$$

$$\delta_{1v-01}^{clad-core} \equiv \left(\beta_{01}^{core} - \beta_{1v}^{clad} - \frac{2\pi}{\Lambda} \right) \tag{3.14}$$

Equation 3.13 describes the amplitude evolution of the core mode, A_{core} along the axial length of the fibre , z. κ_{core_core} is termed the dc self coupling constant of the core mode,

$\kappa_{1v\text{-}01}$ is the core mode to v^{th} cladding mode coupling coefficient, A_v the v^{th} cladding mode amplitude. $\delta_{1v\text{-}01}$ is termed the detuning parameter or phase mismatch constant [27] and defines a resonant condition when the propagation constants of the core mode and v^{th} cladding mode are matched by a $2\pi/\Lambda$ term. This is described as the LPGs grating vector where Λ is the period of the grating. This interaction is termed phase matching. Yariv [26] describes the process as one where a driving mode interacts with the perturbation to create a polarization wave that in turn drives the second mode. At resonance, when both modes are phase matched, the detuning parameter becomes zero. It is at this point the band depth is at a maximum and determines the central wavelength of the band. The transmission spectrum of an LPG may then be determined from the coupled mode equations [28,29]:

$$T = \frac{P^{(v)}(L)}{P_{01}(0)} = \frac{\sin^2\left[\kappa_{1v-01}^{clad-core} L \sqrt{1+\left(\frac{\delta_{1v-01}^{clad-core}}{\kappa_{1v-01}^{clad-core}}\right)^2}\right]}{1+\left(\frac{\delta_{1v-01}^{clad-core}}{\kappa_{1v-01}^{clad-core}}\right)^2} \qquad 3.15$$

This describes the power transfer between the core mode and individual (v^{th}) cladding modes. At resonance when the detuning parameter is zero and complete energy transfer takes place between the core and cladding mode equation 3.15 simplifies to:

$$T_v = 1 - \sin^2(\kappa_{1v-01}^{clad-core} L) \qquad 3.16$$

where, T_v is the minimum transmission of the v^{th} band, L is the length of the grating and $\kappa_{1v\text{-}01}$ is the coupling coefficient of the v^{th} cladding mode.

3.3.2 Coupling coefficients

The coupling coefficients are determined by the overlap of the modal profiles of the core and cladding modes, the overlap integral, and the amplitude of the index

modulation of the grating. The tangential coupling coefficients are stronger than the longitudinal coefficients and may be determined from [30]:

$$\kappa_t^{clad-core} = \omega \iint dxdy \Delta\varepsilon E_{t\_core} \cdot E_{t\_clad}^{*} \qquad 3.17$$

where E_{t_core} and E_{t_clad} are the tangential field components of the electric field profile of the core and cladding modes. This may be confirmed by considering the simplified modal profile of the modes shown previously in figure 3.4. $\Delta\varepsilon$ describes the index variation of the grating which can be approximated by [27]:

$$\Delta\varepsilon \cong 2\varepsilon_0 n \Delta n \qquad 3.18$$

where n is the dc refractive index, Δn is the refractive index change of the grating. The longitudinal coupling coefficients are negligible contributors to the coupling process as the longitudinal field components are 2-4 orders of magnitude smaller than the transverse components [27]. For an axially symmetric grating only cladding modes of azimuthal order $l=1$, have non-zero coupling constants where there is sufficient mode field overlap. Higher order cladding modes, $l>1$, are possible to couple to with asymmetric grating profiles [31]. The coupling constants for the first 168 cladding modes, $l=1$, of a 1550nm single mode fibre are shown in figure 3.7.

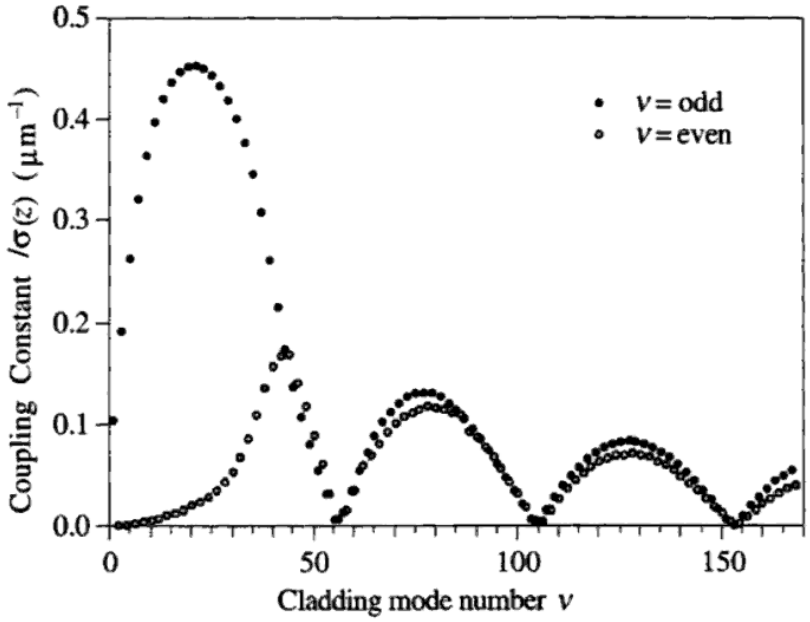

Figure 3.7. Grating normalised coupling coefficients $\kappa_{v-01}^{clad-core}$ for the first 168 cladding modes for l=1 in a typical optical fibre. Reproduced from [26].

From figure 3.7, it is clear that for the first 40 modes the odd ordered modes have higher coupling coefficients. The dispersion equation used in calculating the coupling coefficients is based on a three layer interpretation [32] where there is no separation between the EH and HE modes. The solution to the dispersion relation reveals that the odd modes represent HE modes and the even modes represent the EH modes. It is evident then that the fundamental core mode, HE_{11} couples to the fundamental cladding modes, HE_{11} and further HE_{1n} modes where n is an integer. The theory presented here is revisited in section 3.4 where a simple matlab model is constructed of an LPG.

3.3.3 Origins of temperature sensitivity

The temperature sensitivity of an LPG can be attributed to changes to the grating period and changes in the core and cladding mode effective indices. Changes to these parameters cause spectral shifts of the attenuation bands. The origin of this wavelength shift may be accessed by chain-rule differentiating equation 3.9 with respect to temperature [2],

$$\frac{d\lambda}{dT} = \frac{d\lambda}{d(\delta n_{eff})}\left[\frac{dn_{eff}}{dT} - \frac{dn_{cl}}{dT}\right] + \Lambda\frac{d\lambda}{d\Lambda}\frac{1}{L}\frac{dL}{dT} \qquad 3.19$$

where T is temperature, δ_{eff} is the effective differential refractive index between the core mode and the cladding modes and L is the length of the grating. The right hand side of the equation contains two terms that may be separated as two contributing terms to the wavelength response. The first term represents a thermo-optic effect and is described as the material contribution. It is due to the thermally induced change in differential refractive index. This contribution strongly depends on the order of the cladding mode with different characteristics evident from lower order modes to those of a higher order. It is also defined by the composition of the fibre, e.g. different fibre types having different thermo-optic coefficients. The second term on the right hand side of equation 3.19 is the waveguide contribution, as it depends on changes to the LPG period. For lower order modes this term is positive, while for the higher order modes where the effective modal index approaches that of the cladding, it can be negative. At this point temperature changes due to the thermo optic effect of the cladding dominate the changes to the LPG period. Thus LPGs can be made temperature insensitive by careful design of the LPG period, or have a positive or negative temperature response [2]. Grating periods of 100μm or less have been shown to exhibit a negative $d\lambda/d\Lambda$ [33]. Co-doping a fibre with a negative thermo-optic co-dopant in a germanosilicate fibre to suppress or enhance temperature sensitivities has also been reported [34] A typical temperature response of an LPG, manufactured in Corning SMF-28 fibre, is illustrated in figure 3.8. It shows that the temperature responses are linear and exhibit different coefficients for each band. LPGs fabricated in standard telecommunications optical fibre exhibit temperature sensitivities in the range 3nm/100°C to 10nm/100°C [21]. This is an order of magnitude larger than the sensitivity of FBG sensors [35]. The transmission loss of an attenuation band with respect to temperature can be obtained from [34]:

$$\frac{dP_0}{dT} = -\frac{\kappa L\sin(2\kappa L)}{I}\left(\frac{dI}{dT} - \frac{I}{\lambda_0}\frac{d\lambda_0}{dT}\right) \qquad 3.20$$

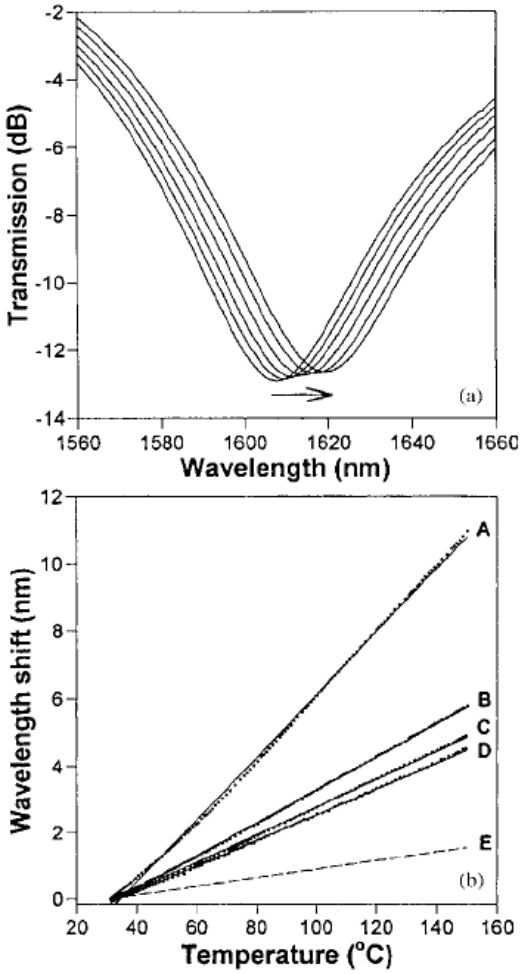

Figure 3.8 (a) Wavelength shift of an LPG attenuation band with temperature. The LPG was fabricated with period of 280 μm in Corning SMF-28 fibre. The spectra correspond to temperatures of 22.7, 49.1, 74.0, 100.9, 127.3 and 149.7°C. (b) Shift in the wavelengths of four attenuation bands, A–D, as a function of temperature. The dashed line is the shift for an FBG fabricated at1550 nm for comparison. [3].)

Where P_0 is the attenuation band loss, κ the coupling coefficient of the bands coupled mode and I the overlap integral. It shows that an attenuation bands transmission response to temperature is governed by the overlap integral and wavelength shift. Typically these effects have different polarities leading to a negligible transmission loss response with temperature.

3.3.4 Origins of strain sensitivity

By differentiating equation 3.9 with respect to strain, a similar expression indicating the LPG's response to strain can be obtained [2]

$$\frac{d\lambda}{d\varepsilon} = \frac{d\lambda}{d(\delta n_{eff})}\left[\frac{dn_{eff}}{d\varepsilon} - \frac{dn_{cl}}{d\varepsilon}\right] + \Lambda\frac{d\lambda}{d\Lambda} \qquad 3.21$$

where ε is the strain. Again, the first term on the right hand side of the equation is the material contribution and the second is the waveguide contribution. For LPGs with a periodicity > 100μm the material contribution is negative and the waveguide contribution is positive. By careful design of LPGs and appropriate choice of fibre type, a sensor with positive, negative or zero sensitivity to strain can be created [21]. Thus the ability to design a LPG's response to strain and temperature opens up the possibility of multi-parameter devices with the option of isolating either of the measurands. A typical response to strain is shown in figure 3.19, in which the wavelength shifts of a number of the attenuation bands of an LPG of period 280 μm, written in Corning SMF 28 fibre, are plotted as a function of strain.

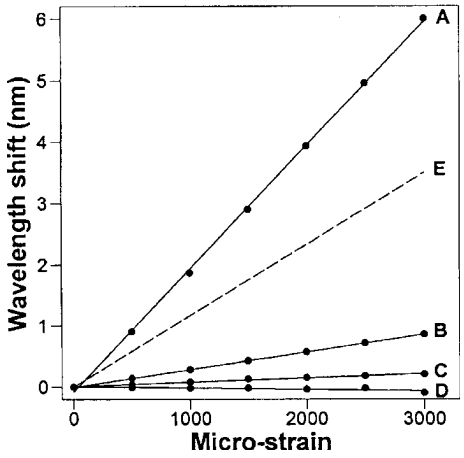

Figure 3.9 Shift in the wavelengths of four attenuation bands, A–D, as a function of strain. The dashed line is the strain-induced wavelength shift for an FBG fabricated at 1550 nm for comparison. From [3].

3.3.5 Origins of refractive index sensitivity

The effective refractive indices of the cladding modes of an LPG are dependent on the refractive index of the surrounding medium. From equation 3.9, a change in the cladding's refractive index will result in a change of the central wavelength of the attenuation bands. Thus a change in refractive index surrounding the LPG will result in a wavelength shift of an attenuation band. The response has been mathematically treated by Allsop *et al* [25]. The wavelength shift for refractive index change is shown as:

$$\frac{d\lambda}{dn_{sur}} = \frac{d\lambda}{d\delta n_{eff}} \frac{d\delta n_{eff}}{dn_{sur}} \qquad 3.22$$

$$\frac{d\lambda}{d\delta n_{eff}} = \frac{\lambda}{\left(\delta n_{eff} - \delta n_g\right)} \qquad 3.23$$

The first term on the right hand side of equation 3.22 is expressed in equation 3.23 and shows a dependence on δn_{eff} and the differential group index, δn_g. δn_g dictates the spectral behaviour of the band and is dependent on the spectral properties of the fibre as well as the period of the fibre [25]. The second term is found not to dictate the shift of the attenuation band.

Equation 3.22 governs the spectral response of an LPG for a surrounding index that allows propagation of the cladding modes, that is when $n_{sur} < n_{clad}$.

Because each band represents the effect of coupling to a distinct cladding mode, the different bands exhibit different sensitivities. It indicates that higher order cladding modes exhibit higher sensitivities. The sensitivity increases as the surrounding refractive index approaches that of the cladding [9]. It is this particular property which will be utilised in this project to monitor the cure of resins. This is illustrated in figure 3.14. However this highlights an issue of LPG sensing; the host fibre (fibre onto which the LPG is written) needs to be of a similar refractive index to that of the refractive index to be measured.

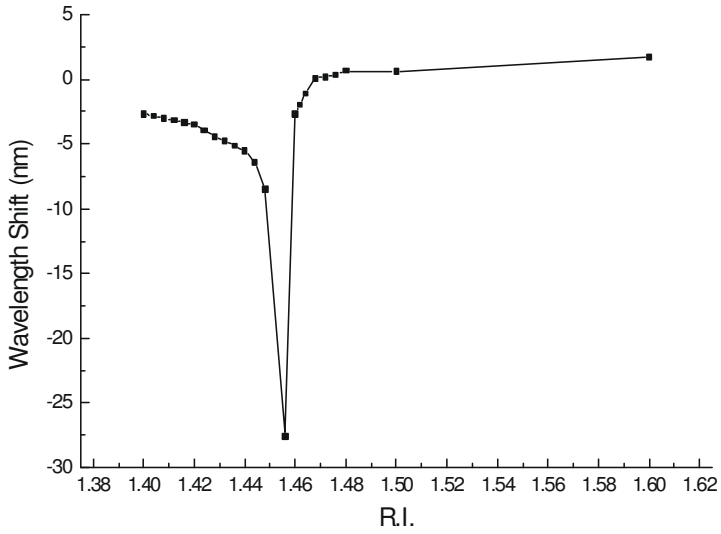

Figure 3.10 Refractive index dependence of the 5th attenuation band of an LPG of period 400μm and 40mm length [21].

3.4 Modelling LPGs

A Demonstration of the mathematical principles that describe an LPG is achieved using a model written in Matlab. The literature highlights two methods of achieving this:

(1) The two layer approach – Using this approach the core is ignored for the calculation of the cladding modes, figure 3.11 (a). The approach ensures that the dispersion equations to solve for the cladding modes are simple.

(2) The three layer approach – Erdogan [27,36] proposed the use of a three layer method, originally derived by Tsao [32]. In this case, figure 3.11(b) the core is accounted for in the calculations of the cladding modes as a significant portion of a cladding modes field profile exists in the core. The dispersive relation for calculating the cladding modes is correspondingly more complex. Much literature has been published on techniques for the analysis of cladding modes [37-40] in three layer structures.

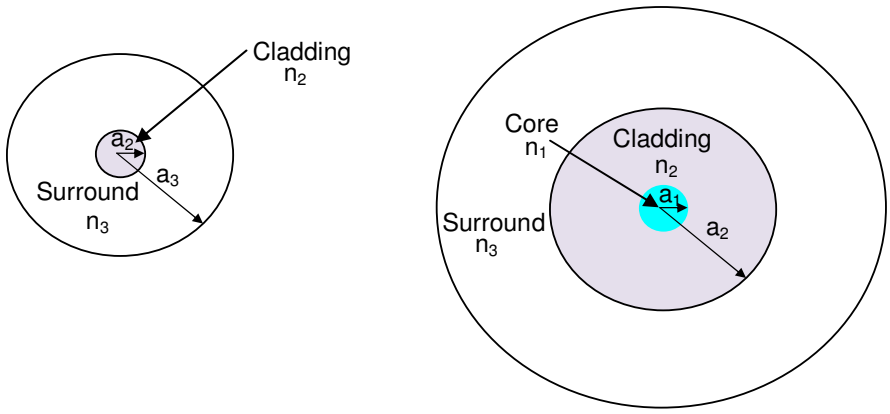

(a) (b)

Figure 3.11 (a) and (b) show the two and three layer model of an optical fibre. Core refractive index, n_1, cladding refractive index, n_2, surround refractive index n_3, core radius, a_1 and cladding radius, a_2.

For a qualitative analysis of the response of an LPG to refractive index change during cure the first method was employed and is described here.

3.4.1 Two layer model

The modelling process may be deconstructed to five succinct steps. A number of assumptions are made here. Firstly that the gratings are assumed to have a circularly symmetric refractive index profile, have no tilt and be of uniform period and secondly that the index perturbation, σ is small, $\sigma << 1$ which is the case for ultraviolet induced gratings.

1) Calculation of the propagation constants of the fundamental core mode.
2) Calculation of the propagation constants of the possible cladding modes.
3) Calculation of the electric field mode profiles of the core and the cladding.
3) Calculation of the overlap integral and hence coupling coefficients between the core and cladding modes.
4) Determination of the transmission spectrum.

3.4.1.1 Core mode

When a waveguide is termed weakly guiding the assumption is that $\Delta << 1$, where

$$\Delta = \frac{n_{core} - n_{clad}}{n_{core}} \qquad 3.24$$

Under these conditions certain modes may be grouped together as they exhibit closely matched propagation constants and parallel electric field profiles. The approximated modes are termed linearly polarised modes and designated as LP_{km} where k represents the azimuthal order and m the radial order. The fundamental mode of a single mode fibre is termed LP_{01} and corresponds with the HE_{11} mode in exact mode notation.

The dispersion relation for the LP (see note below) core modes of an optical fibre using the weakly guiding approximation [41] is given as [15]:

$$\frac{J_k(ua)}{(ua)J_{k-1}(ua)} = \frac{K_k(wa)}{(wa)K_{k-1}(wa)} \qquad 3.25$$

where J is a Bessel function of the first kind, K is a modified Bessel function of the second kind, k represents the azimuthal order of the mode (LP_{km}), a is the core radius and u and w the normal phase parameters in the core of an optical fibre.
For the fundamental mode this may be expressed as [27]:

$$V\sqrt{1-b}\,\frac{J_1\left(V\sqrt{1-b}\right)}{J_0\left(V\sqrt{1-b}\right)} = V\sqrt{b}\,\frac{K_1\left(V\sqrt{b}\right)}{K_0\left(V\sqrt{b}\right)} \qquad 3.26$$

where V is the V number of the fibre and b is the normalised effective index given by:

$$b = \frac{n_{eff}^2 - n_2^2}{n_1^2 - n_2^2} \qquad 3.27$$

Thus by solving equation 3.26 to obtain *b* for a single mode fibre, n_{eff} can be determined for the propagating core mode. The solution to the dispersion relationships are in terms of *ua* for equation 3.25 and *b* for equation 3.26 from which the effective index of the mode may be calculated. This may be done graphically or numerically. A bisection method was used in the Matlab program.

3.4.1.2 Cladding modes

The two layer model assumes the cladding is the propagating medium and the surround, n_3 is the cladding of infinite dimensions. The core is neglected in calculating the possible cladding modes. This assumption is made on the basis that the core dimension is small relative to the cladding and that the majority of the cladding mode profile propagates in the cladding, however as noted previously [27] a significant portion of the mode field is present in the core. This assumption then is flawed as the calculated effective indices of the possible cladding modes will be influenced by the core. Therefore only qualitative conclusions may be inferred from the modelled results. The cladding modes effective indices for HE modes may be calculated from [15, eqn 8.27]

$$\frac{J_{k-1}(ua)}{(ua)J_{k-1}(ua)} = -(1-\Delta)g + \frac{k}{(ua)^2} - \sqrt{(k^2h^2 + \Delta^2 g^2)} \qquad 3.28$$

$$g = g_k(wa) = \frac{K_k^{'}(wa)}{(wa)K_k(wa)} \qquad 3.29$$

$$\Delta = \frac{(n_1^2 - n_2^2)}{2n_1^2} \qquad 3.30$$

As with the solution to the core modes the dispersion relations provide solutions for *ua* from which the effective index of the cladding modes may be found. For a given fibre (core and cladding refractive index and radial dimensions) and LPG period only a finite set of cladding modes need be considered and as discussed in section 3.3.2 only the first 40 cladding modes exhibit significant coupling with the fundamental core mode.

3.4.1.3 Coupling coefficients

The calculation of the coupling coefficients involves the determination of the overlap integral between the core mode and the individual cladding modes. Only transverse coupling coefficients are considered as the longitudinal coefficients are typically 2-4 orders of magnitude smaller. The transverse coupling coefficients are calculated as [27]:

$$\kappa_{v-01}^{clad-core}(z) = \frac{\omega \varepsilon_0 n_1^2 \sigma(z)}{2} \int_0^{2\pi} d\varphi \int_0^{a1} r dr (E_r^{clad} E_r^{core*} + E_\varphi^{clad} E_\varphi^{core*}) \qquad 3.31$$

Where κ_{v-01} is the core to cladding mode coupling coefficient from the v^{th} mode to the LP_{01} core mode, $\sigma(z)$ is the grating profile, φ and r are the azimuthal and radial components. From this it is clear that both the grating profile and the modal shape play an important role in calculating the coupling coefficient. Intuitively, the modal similarity and symmetry between two modes will lead to a higher coupling coefficient than two modes that have a dissimilar mode profile. However coupling to modes with asymmetric field profiles can be achieved through careful design of the grating, $\sigma(z)$. For a symmetric grating only non- zero coupling coefficients are those between the LP_{01} mode and the l=1 cladding modes, i.e. HE_{1n} and EH_{1n} modes, where n is an integer < 1. As the central wavelength of the individual bands are determined by the effective mode indices only and not the coupling coefficients, the coefficients were not calculated in the model. Only the wavelength shift response of an attenuation band with changing refractive index is of interest. An array of values corresponding to the first 20 modes was constructed based on the coefficients calculated in figure 3.8.

3.4.1.4 LPG simulation

A simple model was constructed using equations 3.26 and 3.28 to calculate the effective indices of the fundamental core mode and the first 10 cladding modes of an optical fibre. Figure 3.12 shows the calculated effective refractive indices of the core mode and first 10 cladding modes with wavelength. The fibre modelled had a cut-off wavelength

of 650nm with the parameters shown in table 3.1. The parameters represent a Fibercore SM-750 fibre that is used throughout this thesis as a host fibre for many of the experimental LPGs.

Table 3.1 Fibre and LPG parameters

Core radius (a_1) = 2.8μm
Cladding radius (a_2) = 62.5μm
Core refractive index (n_1) = 1.458
Cladding refractive index (n_2) = 1.454
Surround refractive index (n_3) = 1
Cut-off wavelength = 650nm
LPG period = 400μm
LPG length = 40mm

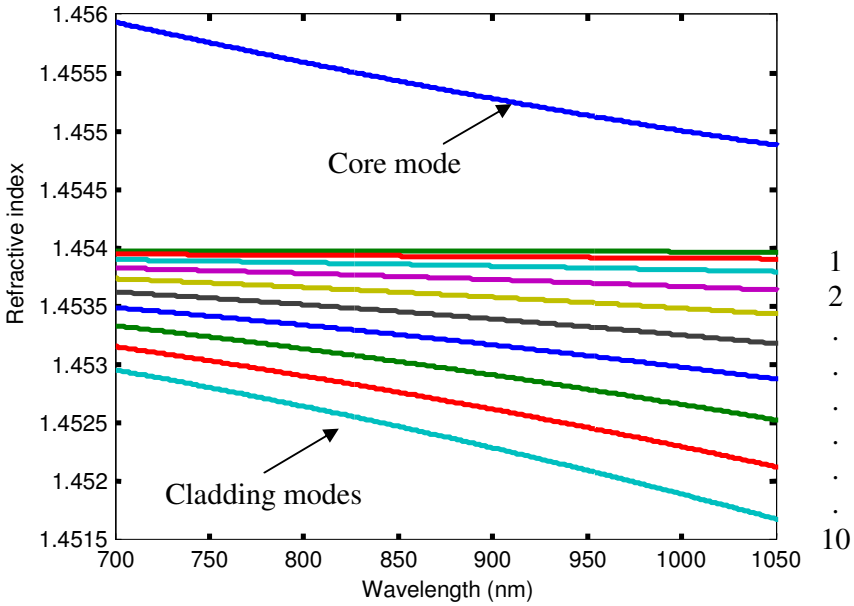

Figure 3.12 Calculated effective refractive indices of the core mode and cladding modes of LPG with parameters of table 3.1.

The calculated effective indices of the modes can then be used to determine the spectral location of the attenuation bands of the LPG using equation 3.9. Figure 3.13 shows the change in spectral location of the resonant wavelength with LPG period. Thus different cladding modes are coupled to through choice of the LPG period.

A transmission spectra can then be calculated using equation 3.14, 3.15 and using the coupling coefficients shown in figure 3.7. A transmission spectrum for an LPG of the parameters given in table 3.1 is shown in figure 3.14. The small spectral features either side of the attenuation bands are attributed to the model.

The matlab program is used to predict the wavelength response of a curing resin, the results of which are discussed in section 4.3.

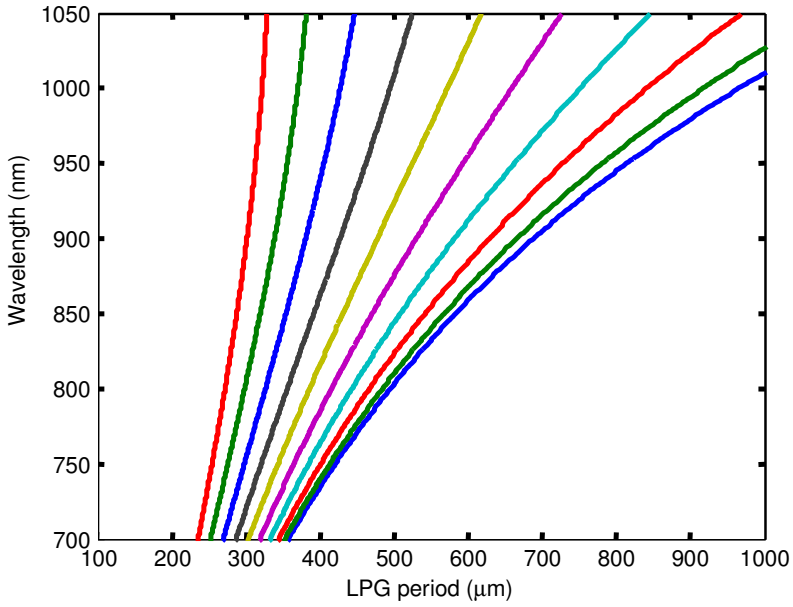

Figure 3.13 Central wavelength of the first 10 attenuation bands (corresponding to the first 10 cladding modes) with LPG period.

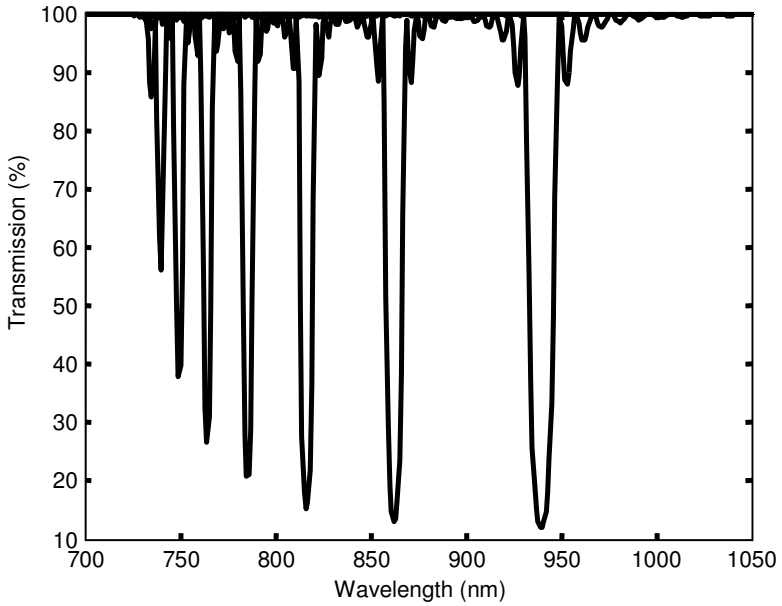

Figure 3.14 Transmission spectrum of LPG with the parameters shown in table 3.1.

3.5 LPG Fabrication

The fabrication of LPGs in optical fibre has been achieved by either physical deformation of the fibre or direct modulation of the core refractive index. These methods are discussed in the next section.

3.5.1 Mechanically induced LPGs

A number of methods for mechanically inducing an LPG have been reported. The initial work by Hill and Bilodeau [42] with mode converters in optical fibre utilised a mechanically formed device to create an 'internally written' grating. This was achieved by compressing a grooved plate on a fibre and then illuminating the fibre with light from an Ar-ion laser, of wavelength 480nm, for a period of 1 hour. The mechanism produced a band with a transmission loss of 3dB band. The placement of a fibre on periodically located (700μm to 1100μm) copper wires placed on a glass plate has also been reported, figure 3.15 [43]. The fibre was subjected to a weight of 3.4kg with the

load spread by an acrylic plate. Spectral bands with drop outs of -10dB or more were achieved.

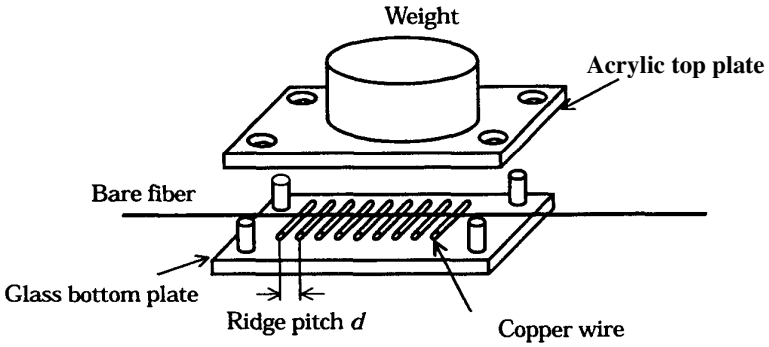

Figure 3.15 Mechanically induced LPG with copper wires and applied weight. From [43]

A similar technique, figure 3.16, with glass plates and metal wires utilised the shrinkage of the epoxy during cure to compress the periodically placed wires onto the bare fibre, rather than a localised weight. An epoxy with a high thermal expansion coefficient was used that allowed the LPG to be thermally tuned. It was demonstrated as a robust thermally tuneable loss filter [44].

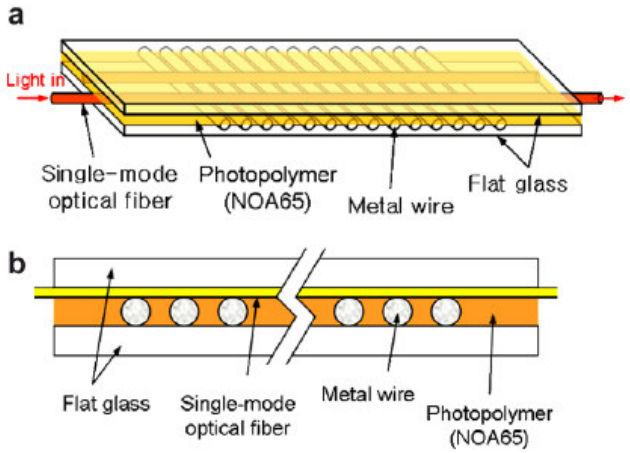

Figure 3.16 Mechanically induced LPG utilising shrinkage forces of epoxy during cure to compress glass plates together. From [44].

The resultant attenuation bands exhibited maximum transmission losses of -9dB for jacketed fibre and -12dB for fibre with the jacket removed. Grooved plates have also been used to create an LPG [45]. A more complex method of producing an LPG involves placing a fibre on a tube with machined v-grooves, figure 3.17. The fibre was then held in place and held in tension by a suspended weight (w1 in figure) at one end and by winding a nylon string over the fibre and tube. The resultant attenuation bands had a dependence on the number of turns of nylon string wrapped around the fibre with bands of transmission losses in excess of 20dB reported [46].

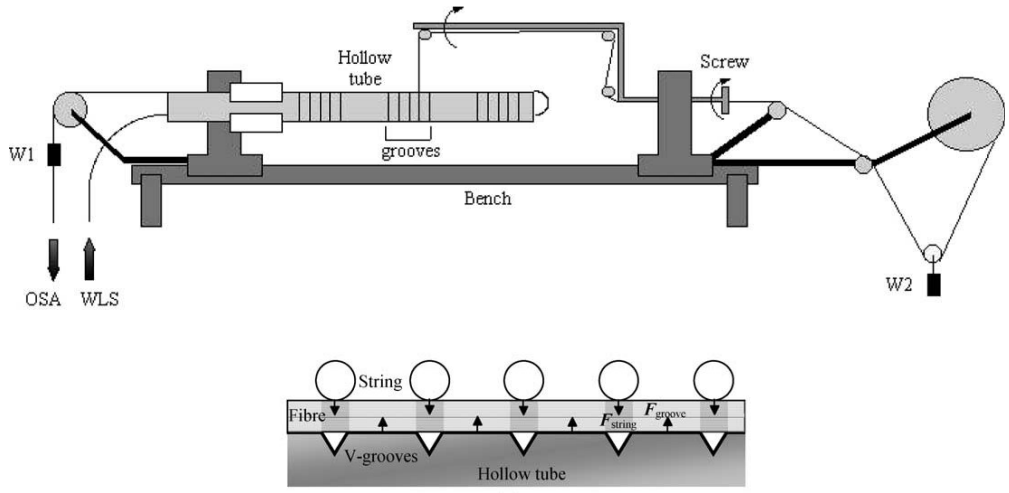

Figure 3.17 Mechanically induced LPG with fibre periodically deformed with nylon string and v-grooves. From [46].

3.5.2 Arc induced LPGs

The basic principle of this method involves periodically arcing across sections of a fibre to cause localised refractive index changes through deformation of the fibre. In this work LPGs have been written in nitrogen doped silica fibre using the electric arc writing technique [47]. The nitrogen has a high thermal diffusion coefficient and thus only arcs of low heat and a short time are necessary to impart abrupt changes in refractive index. A technique was employed by arcing across a section of fibre and then

axially moving the arc probes lengthwise along the optical axis of the fibre and thus writing the LPG by what is termed a point by point process. Because the diffusion process occurs at temperatures in excess of 1200°C and has no effect at lower temperatures, arc induced gratings are advantageous as high temperature sensors.

An arc writing method has also been reported utilising a translation stage to move a fibre axially through arc probes whilst the fibre is maintained at constant axial tension by a hanging weight [48]. An arc discharge of 10mA for 1 second over a 150μm section is reported. The bands exhibited high transmission losses (20dB) in the 1200nm - 1500nm region. The LPG devices were characterised for temperatures up to 800°C (0.11nm/°C) and showed no change in spectral response to temperature. The work reported that high quality gratings were achievable with no appreciable change in the fibre diameter for each arced section for a light axial tension using a 5.1g weight. The coupling mechanism was attributed to stress relaxation in the glass during the arc stage and formation of new stresses at cooling. This results in localised changes in density and hence refractive index. A similar process was reported in [49]. Devices termed 'ultra short period' LPGs have been reported using this technique [50] with 4 or 5 grating planes of 500μm period producing attenuation bands with transmission losses in excess of 30dB. The effect may be attributed to the strong localised refractive index change due to the writing process. The arc current was set at 15mA, 20kHz for an arc duration of 375ms. The resultant LPGs exhibit a high insensitivity to bend with a negligible spectral response for curvatures up to 10^{-1}. The thermal response agreed well with previously published work.

3.5.3 CO_2 laser technique

A two mode spatial mode converter was reported by deforming a silica fibre using the output from a CO_2 laser [51], this mode converter was an early LPG. The deformation caused a periodic refractive index change of $\Delta n = 0.1$, an order of magnitude greater than non-deforming photo-induced techniques (discussed in the next section). The technique used a CO_2 laser to make periodic cuts on the surface of the stripped fibre. The periodic cuts were subsequently annealed by arcing across the cuts to relax

localised stress regions induced by the glass cutting. The resultant deformation profile is a sinusoidal corrugation, figure 3.18. Also shown are cut grooves from a CO_2 laser of about 15-50μm depth and 400μm period [52].

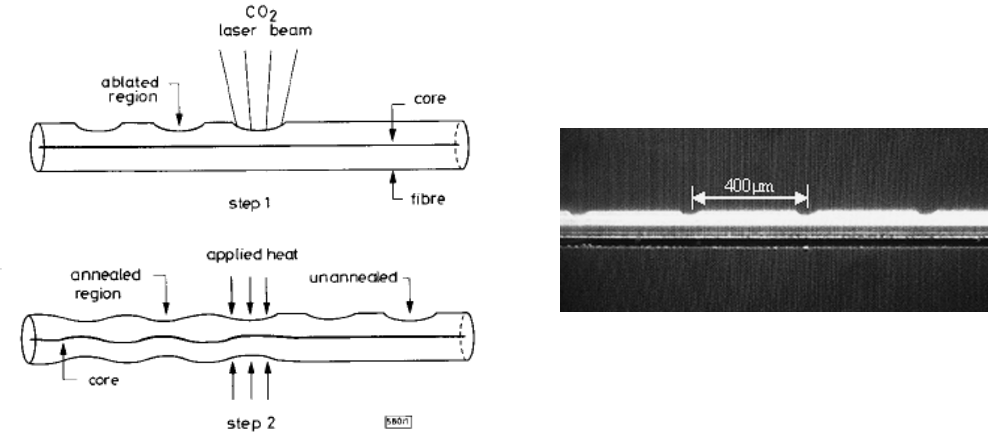

(a) (b)

Figure 3.18 (a) CO_2 written LPG showing cutting and arcing process to create sinusoidal corrugation [51]. (b) Cut sections of fibre as a result of CO_2 laser writing process. From [52].

The device was then demonstrated to be an efficient (99%) LP_{01} to LP_{11} mode converter for a period of 265μm which corresponds to the intermodal beat length of the two modes. The first LPG written in this manner was demonstrated by using the output from a 10.6um CO_2 laser using a single pulse of 300ms at 0.5W) [53]. The laser was focused down to a spot size of 140μm onto the fibre axis. LPGs written using fibre loaded with hydrogen were compared with non-hydrogen loaded fibre. The results indicated that hydrogen loaded fibre required far less gratings planes and shorter pulse durations of 200ms to achieve similar attenuation losses of 10dB. The changes in the refractive index were reported to be due to residual stress relief and densification of the glass. A similar technique was employed to manufacture 500μm period LPGs in B_2O_3-doped glass [54].

A multiple pulse technique has also been used with a CO_2 laser with a focused beam size of 400μm at 1.8W [55]. The beam was focussed onto the fibre axis and multiple pulses were incident on the fibre until consistent microbends were formed. The fibre was held under constant axial tension using a 2.6g load. LPGs of differing periods were

manufactured, 420µm to 500µm with lengths ranging from 6.72mm to 8mm. Attenuation bands in excess of -30dB were reported and temperature sensitivities of 0.04nm/°C which is comparable to LPGs manufactured using similar techniques [54].
LPGs have been written using multiple pulse scanning method with a galvanometric mirror, figure 3.19 [56]. The scheme used a dithering technique to modulate a scanning laser to create the periodic deformations on the fibre.

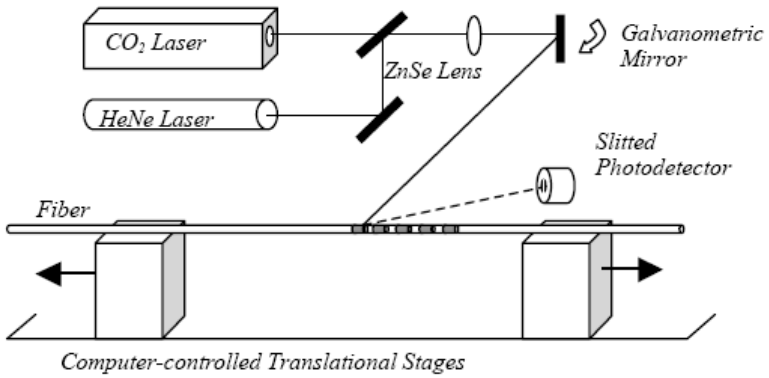

Figure 3.19 Galvanometric based scanning system for CO^2 based LPG writing method. [56]

The technique also employed two translation stages one moving away from the other at a constant velocity and the diameter of the fibre at the focus point then determined by the exposure time. The method reported a better background loss than focussed techniques. These are attributed to the abrupt changes to the fibre profile. Attenuation bands in excess of 30dB were reported with LPGs of 600µm and 18mm of length.

3.5.4 Direct modulation of the core

Since the inception of in fibre gratings with the early work by Hill [57] and Meltz [58], use of ultraviolet radiation has become the standard method of manufacture for optical fibre gratings. Other methods include infrared radiation [59], ion implantation [60] and, with the new interest in photonic crystal fibres and polymer fibres, new techniques are being developed applicable to these technologies, e.g. acoustic deformation [61]. The reason for the predominance of the ultraviolet inscription method both industrially and in academic research centres is its relative simplicity compared to other techniques and

its ability to be modified to allow for multiple designs of gratings. The ultraviolet writing process is possible due to the photosensitivity of optical fibres. The ultraviolet energy causes specific bonds, caused by germanium defects inherent within the glass, to break. These bonds exhibit an absorption peak at 240nm and when broken release a free electron that may recombine anywhere within the glass matrix. This mechanism creates a change in density, due to molecular rearrangement, and hence increases the refractive index locally [31]. Increasing the photosensitivity of the glass has been achieved through co-doping fibre with boron and germanium [62] and by hydrogen loading [63]. Methods to inscribe gratings in Ge-doped fibre using ultraviolet radiation typically use wavelengths between 193 and 266nm [31]. There are two methods which are typically used, the amplitude mask technique and the point by point technique.

The amplitude mask technique requires a mask to be written usually in copper, chrome-plated silica [28] or indirect methods involving patterned mirrors [64] or microlens arrays [65]. The method simplifies the manufacturing process by permitting basic alignment of the fibre and laser system and a reduced stability requirement. Multiple grating planes are written simultaneously allowing for rapid manufacture. The mask method typically produces high quality gratings that can be manufactured repeatedly although different designs of LPGs require different mask designs. This technique was the predominant method employed in the manufacture of gratings used in the work presented in this thesis and will be discussed further in the next section.

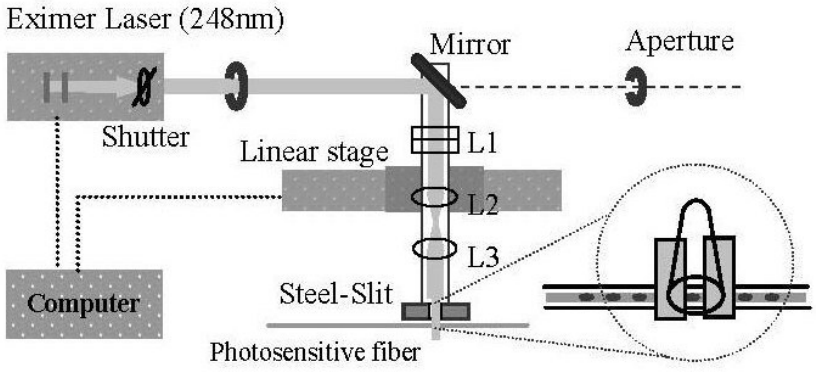

Figure 3.20 Point by point method described by [66].

The point by point method, figure 3.20, conversely allows for more flexibility [66] of the grating design however the tighter tolerances on the laser and focusing optics creates a more complex writing process with much longer writing times.

3.6 Experimental LPG fabrication

The fabrication of gratings in-house was achieved using the UV writing technique and the methods used are detailed here.

3.6.1 Fibre preparation

Two types of fibre are used in the experimental section of this work for writing LPGs. A photosensitive boron-germanium co doped fibre from Fibercore (Fibercore PM750) with a cut-off wavelength of 730nm and a non-photosensitive optical fibre (Fibercore SM750) also with a cut-off wavelength of 650nm that is made photosensitive by hydrogen loading [63]. This was achieved by placing the fibre in a sealed pressure vessel that maintained the optical fibre in a hydrogen atmosphere at 200 psi for at least two weeks.

The fibre jacket is removed using a chemical etching technique. The jacket must be removed because it absorbs ultraviolet energy and prevents the light impinging on the glass. The fibre is placed on a microscope slide and then covered to the desired length with a thin layer of 'Nitromors' (a dichloromethane and methanol based paint stripper). After 1 minute the jacket is gently removed using lens tissue and the bare fibre cleaned with lens tissue and Isopropyl alcohol (IPA). Previous work has indicated prolonged exposure to stripping materials can affect the fibre mechanical strength [67]. The fibre is then allowed to be connected to an on line monitoring system using FC/PC Bullet connectors.

3.6.2 Amplitude mask

This fabrication method uses ultraviolet radiation incident on a fibre through an amplitude mask to create the refractive index pattern on the host fibre. A typical manufacture set-up is shown in, figure 3.21.

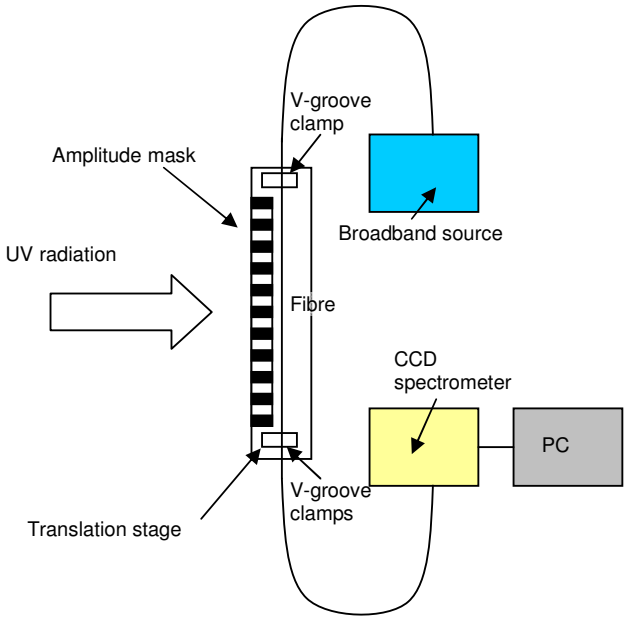

Figure 3.21 Manufacture setup for amplitude mask method of writing LPGs. The translation stage traverses the fibre across the ultraviolet beam.

The amplitude mask is laser machined from copper foil (~100µm), with a 50% duty cycle, and 400µm period. It is fixed 5mm in front of a V-groove clamp on a translation stage that holds the fibre in place during the writing cycle. The ultraviolet radiation is generated from an injection seeded frequency-quadrupled Spectra physics, Quanta-Ray, GCR 100 series Nd:YAG laser that operates at 266nm with a pulse width of 5ns, beam width of 10mm and a repetition rate of 10Hz. Prior to fabrication the laser is allowed to warm up for 1 hour to allow the laser to stabilise. The 10mm radius beam had an incident power on the fibre of 55-65mW, measured using a thermal head power meter. The fibre was prepared and placed in the V-grooves of the translation stage with the stripped fibre almost touching the mask. The translation stage traverses the fibre and mask in front of the ultraviolet laser beam with a maximum exposure of 10mm on the

fibre at any one time. This is then traversed along the length of the fibre to create LPGs of any design length. The stage movements are programmed by a NEAT programmable motion control system with the ability to create programs to allow for variation in the fabrication conditions and characteristics of the LPG.

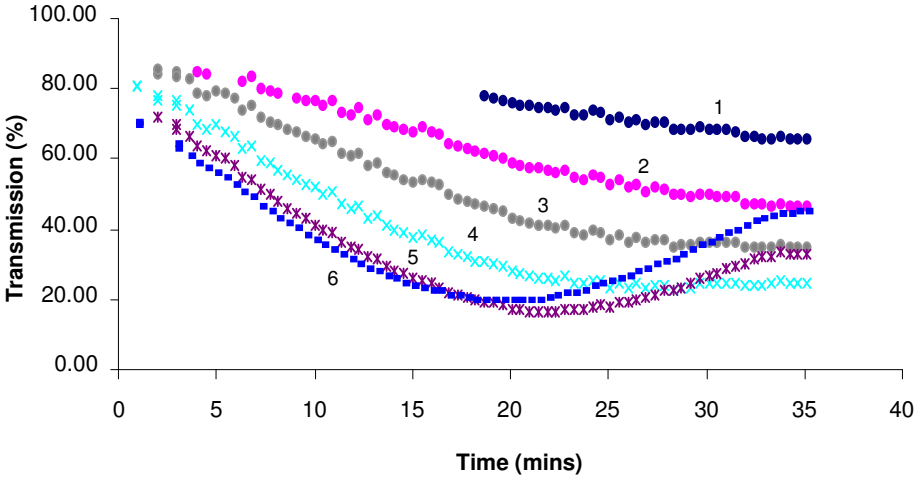

Figure 3.22 Plot of all six bands of an LPG fabricated in Fibercore PS750 fibre with a 400µm period over a 40mm length. Band 1, coupled to the HE_{11} cladding mode has the weakest transmission extinction whilst Band 6, HE_{12} cladding mode reaches a maximum extinction before re-coupling.

An online monitoring system to monitor the LPG during the writing process consists of an Ocean Optics, Tungsten Halogen light source; HL 2000 which is used to illuminate the LPG with a spectral range of 200-1700nm and an Ocean Optics S2000 CCD spectrometer with a 0.3nm resolution is used to capture the spectra. A Labview program accesses the spectra from the spectrometer and detects the attenuation bands using a peak detection algorithm. Peak detection is achieved by setting a threshold and the points below which are fitted with a polynomial, typically a 6^{th} order polynomial. The order of the polynomial is selected to best fit the data. The minimum point of the fitted polynomial is defined as the minimum point of the attenuation band. This permitted a developing band to be tracked during manufacture. Figure 3.22 shows the bands attenuation losses develop during manufacture of a 40mm, 400µm LPG in Fibercore PS750. After 20 minutes the longest wavelength bands (labelled bands 5 and 6) show the effects of over coupling; the attenuation loss starts to decrease as the cladding modes

associated to these bands start to re-couple back to the core mode. This is consistent with equation 3.16 which predicts sinusoidal dependence of minimum transmission depth with grating length. The online monitoring system can reduce writing times as specific bands may be tracked and once a required transmission depth is achieved the writing process can be halted.

3.6.3 Point by point method

The point by point technique is implemented by replacing the amplitude mask with a specially adapted Vernier calliper. The callipers provide a slit width that is adjustable with a 1μm resolution. This allows bespoke LPG designs to be created, e.g. apodised or chirped gratings. The calliper is held in a stationery position in front of the ultraviolet beam and the fibre is traversed behind it. A similar system was reported by Malo *et al* [68] and a schematic of the setup is shown in figure 3.23.

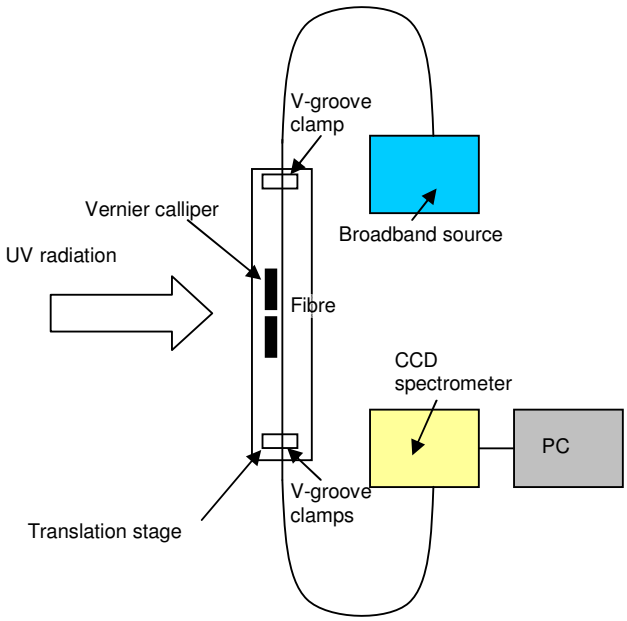

Figure 3.23 Experimental setup of a point by point writing technique. The Vernier callipers are fixed in position and the translation stage and fibre traverse the ultraviolet beam.

3.6.4 Annealing

The process of annealing fibres is necessary for two reasons [31]:

(1) To remove a thermally unstable component of the LPGs refractive index modulation that otherwise degrades slowly over time or at elevated temperatures.
(2) To aid the out diffusion of hydrogen in hydrogen loaded fibre – the hydrogen content determines the differential refractive index of the fibre.

Both the central wavelength of the attenuation bands shift and the transmission depth reduces in relation to this refractive index modulation change. The evolution of the spectra through diffusion of the hydrogen has been studied [70-71]. The minimum annealing time for hydrogen diffusion is given by [73]:

$$t(h) = 2.063\times10^{-4} \exp\left(\frac{4079}{T(K)}\right) \qquad 3.32$$

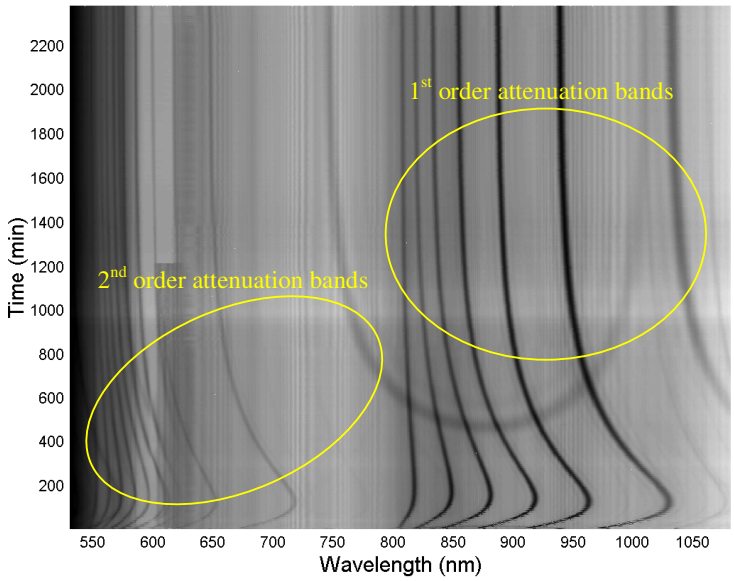

Figure 3.24 LPG spectra during hydrogen out diffusion. The image is grey scale with black representing 0% and grey representing 100%.

An example of the effects of out diffusion on an LPG spectrum is shown in figure 3.24. The bands show a large wavelength shift during the first 200 minutes; this is attributed to the quick diffusion of hydrogen in the cladding. A slower release of hydrogen trapped in the core explains the slow progression of the bands returning to their original spectral location [31].

The annealing process to remove the thermally unstable component of the refractive index change involves elevating the temperature of the fibre above its expected working temperature and holding at this temperature for a period of time. The annealing process exhibits a permanent change in the transmission spectrum of a grating, figure 3.25. The central wavelength of an attenuation band is shown to experience a permanent negative shift of 1nm. Equilibrium has not been reached in this case and further monitoring of the attenuation bands over a longer period would have revealed that after a finite time the bands no longer shift in terms of wavelength.

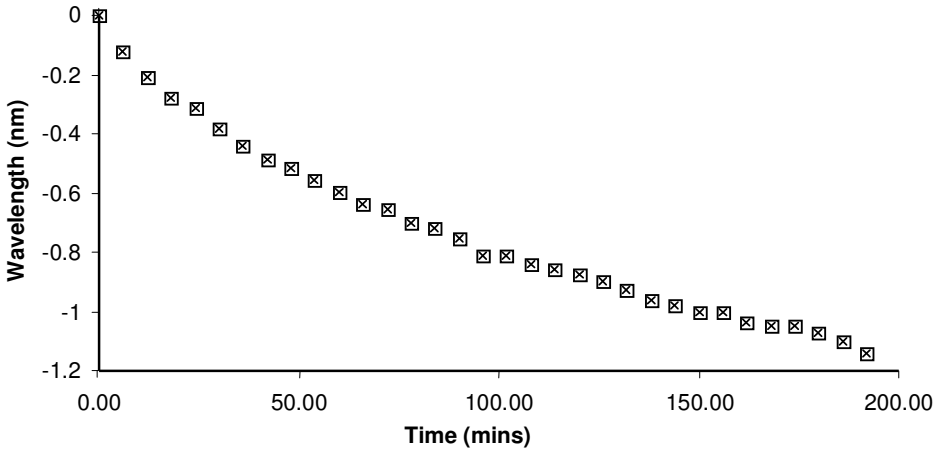

Figure 3.25 Plot of the shift in wavelength of the 4th attenuation band during annealing. LPG: period 400μm, length 40mm, fabricated in Fibercore PS750

The annealing process has also been shown to permanently alter the sensitivity of the LPG to measurands [19]. Figure 3.26 shows the reduced sensitivity of an attenuation band to temperature before and after an annealing process (LPG held at 200°C for 2 hours).

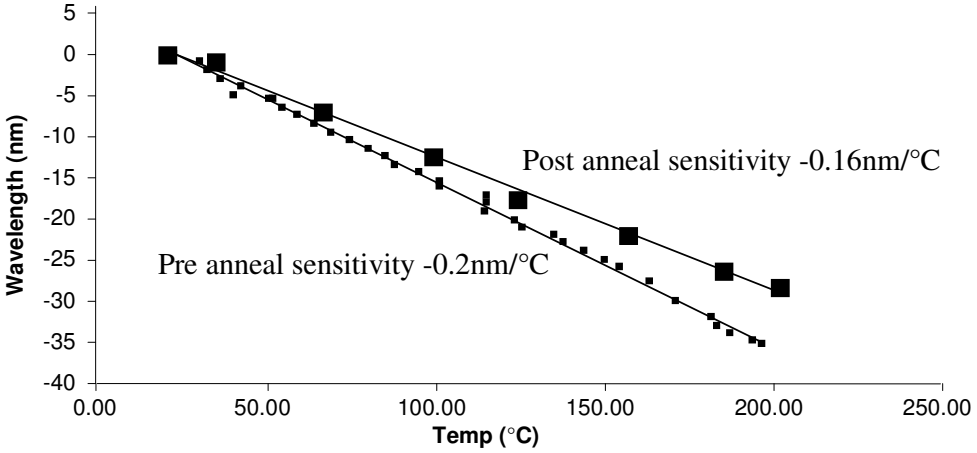

Figure 3.26 Wavelength shift of the 4th attenuation band of a LPG of period 400μm, 40mm in length with temperature. ■= post anneal, ▪ = Pre anneal

3.7 Characterisation of LPGs

An evaluation was made of the sensing capabilities of LPGs to environmental parameters such as temperature, strain and refractive index. The experimental characterisation of LPGs to these parameters is presented in this section. The LPGs were manufactured from boron-germanium co-doped photosensitive fibre (FibreCore PS750, cut-off at 650nm). They have a period of 400μm and a length of 40mm and were manufactured using the amplitude mask method described in section 3.6.2. All LPGs were annealed at 200°C for a period of two hours.

3.7.1 Temperature

The response of an LPG to a temperature change to its surrounding environment is manifest by a shift in wavelength of the attenuation bands. To investigate this shift an experiment was set up with an LPG placed within a Carbolite cylindrical furnace, figure 3.27. The Carbolite furnace is PID (proportional–integral–derivative controller) controlled with an accuracy of ±1°C. For a set temperature, a central section of 40mm in

length within the furnace exhibits a ±5°C variation. The fibre is pre-tensioned to untwist it and keep it straight as bends or twists will cause the attenuation bands to split [5,6], due to induced birefringence. It is fixed at both ends outside the furnace using cyanoacrylate glue. The thermally induced strain effects are assumed to be negligible because; silica has a very low coefficient of thermal expansion and the strain response of an LPG (detailed in section 3.7.2) is poor when compared with other optical sensors, e.g. FBGs.

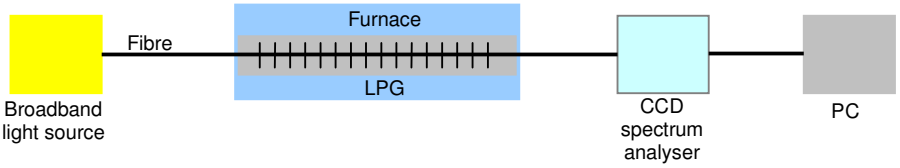

Figure 3.27 Experimental setup for temperature characterisation.

The wavelength responses of the three longer wavelength attenuation bands of an LPG are shown in Figure 3.28. The bands in this instance are denoted as 2, 3 and 4 and correspond to coupling to the HE_{12}, HE_{13} and HE_{14} cladding modes. Table 3.2 details their temperature sensitivities. These figures correspond with previous work on LPGs written in PS750 type fibre [19].

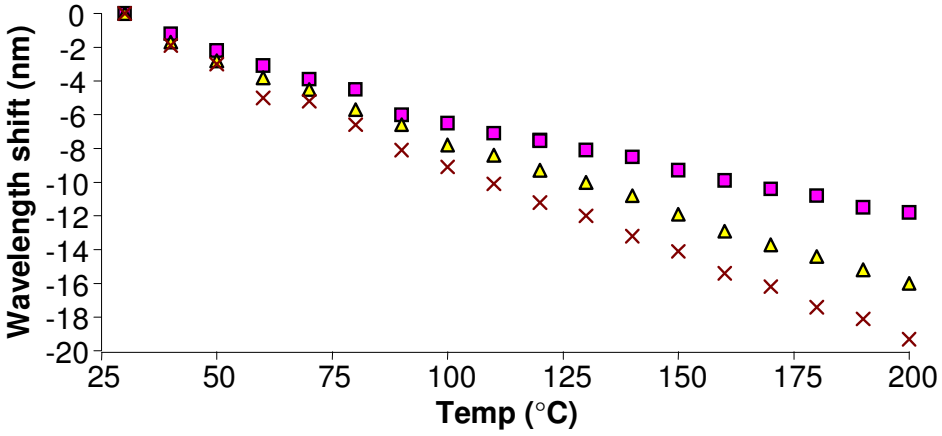

Figure 3.28 A plot showing the three highest attenuation bands of a 400µm period, 40mm length LPG. ■ = band 2, ▲= band 2, × = band 4.

Table 3.2 Temperature sensitivities for bands 2 - 4 for a 400μm period LPG of 40mm length in PS750 fibre.

Band	2	3	4
Temperature sensitivity	0.05nm/°C	0.09nm/°C	0.11nm/°C

3.7.2 Strain

As discussed in section 3.3.4, an LPG subjected to an axial strain exhibits a change in the central wavelength of the attenuation bands. To characterise this response in an LPG, the experimental layout illustrated in figure 3.29 was used. The LPG experiences axial strain by lateral movement of a manually controlled Vernier translation stage. The fibre is secured to V-grooves in the blocks and glued with cyanoacrylate. The fibre is stripped at the gluing points to remove the possibility of fibre slippage within the protective polyacrylate jacket. The furnace was set to maintain a constant temperature of 25°C.

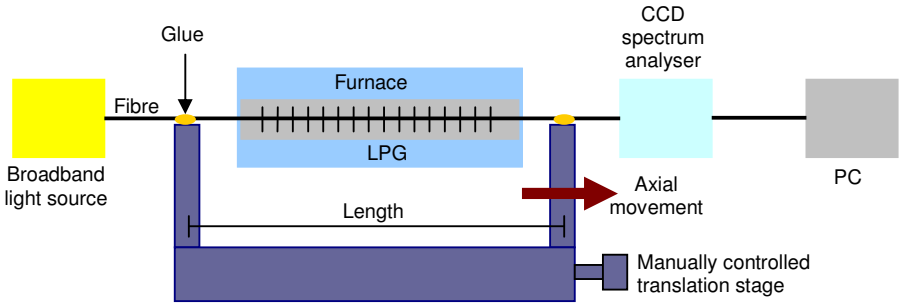

Figure 3.29 Experimental setup for strain characterisation

The separation between the fixing points was incremented by 50μm steps, corresponding to a strain resolution of 167με. The fibre was tested to breaking point and this point was found to be lower than that of fibre without an LPG. This is consistent with previous work looking at the reduction in mechanical strength of fibres subjected to the grating writing process. The mechanical integrity may be compromised because of ultraviolet induced defects created by the pulsed writing method. This method of manufacture has been shown to reduce the mechanical strength of fibres by a factor of 4 compared with those using continuous wave ultraviolet writing methods [67].

The distance between the glue points was measured at 30cm. The Vernier stage has a resolution of ±0.5μm corresponding to 1.67με. The initial tension is applied in 10μm steps until a change in wavelength is resolved from the CCD captured spectra, from then the measurements are made in 50μm steps. This point is assumed to be the zero strain level. The bands in this instance are denoted as 1, 2, 3, 4 and 5, corresponding to the first 5 lower order cladding modes. Figure 3.30 and table 3.3 shows the measured response and strain sensitivities. These figures are typical of a LPG response to strain. The strain sensitivity of LPG devices are at least an order of magnitude less sensitive compared with an FBG strain sensor, typically 1pm/με [20].

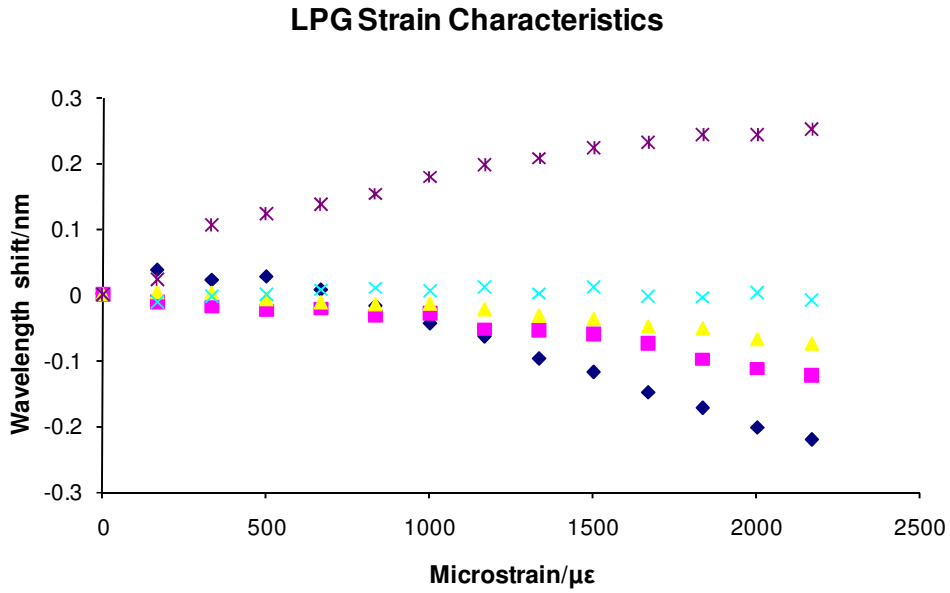

Figure 3.30 A plot showing the attenuation bands of a 400μm, 40mm length LPG response to axial strain. ◆ = band 5, ■ = band 4, ▲= band 3, × = band 2, ✳ = band 1

Table 3.3 Strain sensitivities for bands 1 through 5 for a 400μm period LPG of 40mm length in PS750 fibre.

Band	1	2	3	4	5
Strain sensitivity/ pm/με	0.11	0	-0.08	-0.13	-0.19

Band 1 shows a linear response to strain with a positive wavelength sensitivity coefficient, band 2 has a negligible response and bands 3-5 show a linear response with

a negative sensitivity coefficient. This demonstrates the multi-parameter sensing ability of LPGS, i.e. band 2, which has a negligible response to strain, can be used to access strain insensitive temperature data. The multi parameter capability has been exploited previously as a demonstration of a smart sensor [2].

3.7.3 Refractive Index

To characterise an LPGs response to changes to the surrounding refractive index, an experiment exploiting the refractive index dependence on the concentration of an ethylene glycol solution was used. The experimental setup is shown in figure 3.34.

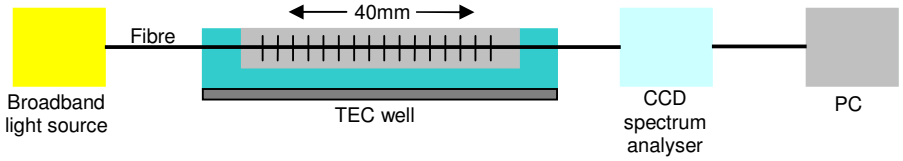

Figure 3.31 Experimental setup for refractive index characterisation.

A thermo-electrically cooled well was constructed to contain the ethylene-glycol solution. The temperature was maintained at 25 ± 0.5°C, to avoid errors resulting from the temperature sensitivity of the LPG and any thermo-optically induced change in the refractive index of the solution. Starting with a 0% ethylene-glycol solution and increasing the ethylene-glycol content by 10% each time; the well is filled and the LPG spectrum recorded. This corresponds with a variation in refractive index from 1.33 (distilled water) to 1.426 (ethylene-glycol). The results are shown in figure 3.32 and table 3.4 and are comparable with previously published work using an ethylene glycol solution [8,9]. The higher order mode, band 5 in this case corresponding to coupling to the HE_{15} cladding mode, shows a higher sensitivity to the change in refractive index. This may be explained by the shape of the mode profile for the higher order modes which exhibit an evanescent tail that extends further into the surrounding material.

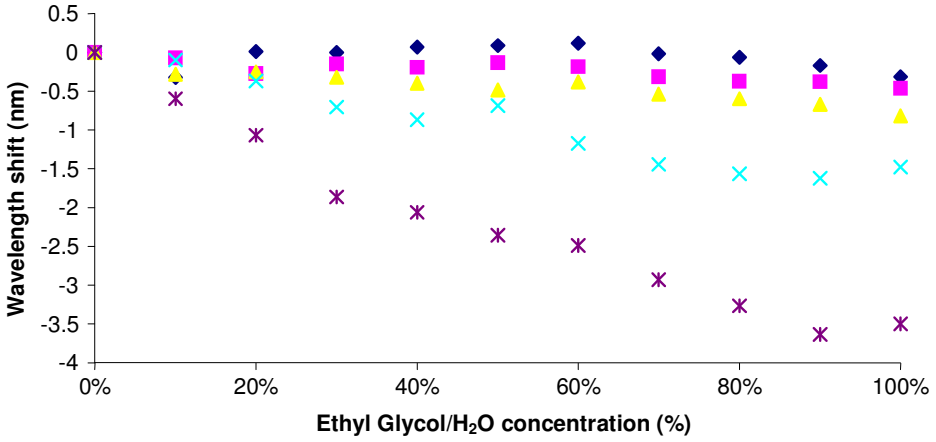

Figure 3.32 A plot showing the attenuation bands of a 400µm, 40mm length LPG response to axial strain. ◆ = band 1, ■ = band 2, ▲= band 3, × = band 4, ✳= band 5

Table 3.4 Refractive index sensitivities for bands 1 through 5 for a 400µm period LPG of 40mm length in PS750 fibre.

Band	1	2	3	4	5
refractive index sensitivity/ nm/%	0	-0.38	-0.65	-1.71	-3.53

3.8 Summary

This chapter provides a concise review of the theory, fabrication and characterisation of long period gratings. A theoretical overview provides the foundation of coupled mode theory which is the predominant modelling technique used to explain the coupling mechanism of an LPG. A simple Matlab model is introduced, based on this technique, to provide a qualitative analysis of LPG devices. The fabrication techniques reported in the literature to create LPGs are discussed together with the two main methods employed to fabricate LPGs as part of the project; the UV inscription method using an amplitude mask and the point by point method. Finally the characterisation results, of an LPG fabricated using the amplitude mask method, for temperature, strain and refractive index are presented and found to be comparable with previously published results.

3.9 References

1. Bhatia, V. and Vengsarkar, A. M. (1996), 'Optical fibre long period gratings sensors', *Optics Letters*, 21, p. 692 – 694.
2. Bhatia, V., Campbell, D. K., Sherr, D., D'Alberto, T. G., Zabaronick, N. A., Ten Eyck, G. A., Murphy, K. A. and Claus, R. A., (1997), 'Temperature insensitive and strain insensitive long period grating sensors for smart structures', *Optical Engineering*, 36, p. 1872-1876.
3. V. Bhatia, (1999), 'Applications of lpgs to single and multi-parameter sensing', *Optics Express*, 4(11), p. 457 – 466,.
4. Liu, Y, Zhang, L and Bennion, I, (1999), 'Fibre optic load sensors with high transverse strain sensitivity based on long-period gratings in B/Ge co-doped fibre', *Electronics Letters*, 35, p. 661-662.
5. Patrick, H. J., Chang C.C. and Vohra, S.T., (1998), 'Long period gratings for structural bend sensing', *Electron Letters*, 34, p. 1773-1775.
6. Ye, C.C., James, S.W. and Tatam, R.P. (2000), 'Long period fibre gratings for simultaneous temperature and bend sensing', *Optics Letters*, 25, p. 1007-1009.
7. Allsop, T., Zhang, L. and Bennion, I. (2001), 'Detection of organic aromatic compounds in paraffin by a long period fibre grating optical sensor with optimised sensitivity', *Optics Communication*, 191, p. 181-190.
8. R. Falciai, A.G. Mignani and A. Vannini, (2001), 'Long period gratings as solution concentration sensors', *Sensors and Actuators B*, 74, p. 74-77.
9. H. J. Patrick, A. D. Kersey and F. Bucholtz, (1998),'Analaysis of the long period fibre gratings to external index of refraction', *Journal of Lightwave Technology*, 16, p.1606-42.
10. R. Hou, Z. Ghassemlooy, A. Hassan, C. Lu And K. P. Dowker, (2001), 'Modelling Of Long Period Fibre Grating Response To Refractive Index Higher Than That Of Cladding', *Measurement Science And Technology*, 12, p. 1709-1713.
11. Allsop, T., Earthrowl-Gould, T, Webb, D. J. and Bennion, I. (2003), 'Embedded Progressive-Three-Layered Fiber Long-Period Gratings For Respiratory Monitoring', *Journal Of Biomedical Optics*, 8(3), p.552-8.

12. Delisa, M. P. Zhang, Z. Shiloach, M. Pilevar, S. Davis, C. C. Sirkis J. S. And Bentley, W. E. (2000), 'Evanescent Wave Long Period Fibre Bragg Grating As An Immobilised Antibody Bio Sensors', *Analytic Chemistry*, 72, p. 2895-2900.
13. Ramo, S., Whinnery, J. R., And Van Duzer, T. (1984), Fields And Waves In Communication Electronics (2nd Edition), John Wiley And Sons, California, USA.
14. Hecht, E. And Zajac, A. (1977), Optics (2nd Edition), Addison-Weley Publishing Company, New York, USA.
15. Gowar, J. (1983), Optical Communication Systems, Prentice Hall, London, UK.
16. Syms, R. And Cozens, J. (1992), Optical Guided Waves And Devices, Mcgraw-Hill, Berks., UK.
17. Born, M. And Wolf, E. (1959), Principles Of Optics, Cambridge University Press, Cambridge, UK.
18. Yariv, A. (1985), Optical Electronics, College Publishing, New York, USA.
19. Sarfraz, K. (2003), Fibre Optic Long Period Fibre Gratings For Sensing Applications (Unpublished Phd Thesis), Cranfield University, Cranfield, UK.
20. Bhatia, V. (1998), Properties And Applications Of Long Period Gratings (Unpublished Phd Thesis), Virginia Polytechnic And State University, Blacksburg, Virginia.
21. James, S. W. And Tatam, R. P. T. (2003), 'Optical Fibre Long-Period Grating Sensors: Characteristics And Application', *Measurement Science And Technology*, 14, p. R49-R61.
22. Dobbs, H. L. (2007), Fibre Gratings In Novel Optical Fibres For Applications In Sensing (Unpublished Phd Thesis), Aston University, Birminham, UK
23. Pierce, J. R. (1954), 'Coupling Of Modes Of Propagation', *Journal Of Applied Physics*, 25(2), p. 179-184.
24. Taylor, H. F. And Yariv, A. (1974), 'Guided Wave Optics', *Proceedings Of The IEEE*, 62(8), p. 1044-1060.
25. Allsop, T., Zhang, L., Webb, D.J. and Bennion, I. (2002), 'Discrimination between strain and temperature effects using first and second-order diffraction from a long-period grating', Optical *communications*, 211, p.103-108.

26. Yariv, A. (1973), 'Coupled-Mode Theory For Guided-Wave Optics', *IEEE Journal Of Quantum Electronics*, Qe-9(9), p. 919-933.
27. Erdogan, T. (1997), 'Cladding -Mode Resonances In Short- And Long- Period Grating Filters', *Journal Of The Optical Society Of America A*, 14(8), p. 1760-1773.
28. Vengsarkar, A. M., Lemaire, P. J., Judkins, J. B., Bhatia, V., Erdogan, T., And Sipe, J. E. (1996), 'Long Period Fiber Gratings As Band-Rejection Filters', *Journal Of Lightwave Technology*, 14(1), p. 58-65.
29. Hall, D.G. (1987), 'Theory Of Wave-Guides And Devices', Integrated Optical Circuits And Components, L.D. Hutchenson:Editor, Marcel-Dekker, New York, USA.
30. Kogelnik, H. (1990), 'Theory of optical waveguides', in Guided-Wave Optoelectronics, Tamir, T. Editor, Springer-Verlag, New York, USA.
31. Kashyap, R. (1999), Fiber Bragg Gratings, Academic Press, San Diego, USA.
32. Tsao C. (1992), Optical Fiber Waveguide Analysis, New York, Oxford, UK.
33. Bhatia, V. Campbell, D.K. D'Alberto, T. Ten Eyck, G.A. Sherr, D. Murphy, K.A. and Claus, R.O. (1997), 'Standard optical fiber long-period gratings with reducedtemperature sensitivity for strain and refractive-index sensing', Conference on Optical Fiber Communication, OFC 97.
34. Han, Y-G, Lee, B. H., Han, W-T, Paek U-C and Chung Y. (2001), 'Fibre-optic sensing applications of a pair of long-period fibre gratings', *Measurement Science And Technology*, 12, p. 778–781.
35. Meltz, G. And Morey, W. W. (1992), 'Bragg Grating Formation And Germanosilicate Fiber Photosensitivity', *Proceedings of the SPIE*, 1516, p.185–99.
36. Erdogan, T. (1997), 'Cladding Fiber Grating Spectra', *Journal Of Lightwave Technology*, 15(8), p. 1277-1294.
37. Koyamada Y., (2000), 'Analysis Of Core-Mode To Radiation-Mode Coupling In Fiber Bragg Gratings With Finite Cladding Radius', *Journal Of Lightwave Technology*, 18(9), p. 1220-1225.

38. Koyamada Y., (2001), 'Analysis Of Core-Mode To Radiation-Mode Coupling In Long Period Fiber Gratings', Ieee Phtonics Technology Letters, 13(4), p. 308-310.

39. Anemogiannis E., (2003), 'Transmission Characteristics Of Long Period Fiber Gratings Having Arbitrary Azimuthal/Redial Refractive Index Variation', *Journal of Lightwave Technology*, 21(1), p. 218-227.

40. Kong M., (2006), 'Field Solution And Characteristics Of Cladding Modes Of Optical Fibers', *Fiber And Integrated Optics*, 25, p. 305-321.

41. Gloge, D. (1971), 'Weakly Guiding Fibers', *Applied Optics*, 10(10), p. 2252-2258.

42. Bilodeau, F., Hill, K. O., Malo, B., Johnson, D. C., And Skinner, I. M. (1991), 'Efficient, Narrowband Lp_{01}<–>Lp_{02} Mode Convertors Fabricated In Photosensitive Fibre: Spectral Response', *Electronics Letters*, 27(8), p. 682-684.

43. Yokota M., Oka H., Yoshino T., 'Mechanically Induced Long Period Fiber Grating And Its Application For Distributed Sensing', 15th Optical Fiber Sensors Conference Technical Digest, OFS 2002, p. 135-138.

44. Sohn K. R., Peng G-D. (2007), 'Mechanically Formed Loss-Tunable Long-Period Fiber Gratings Realized On The Periodic Arrayed Metal Wires', *Optics Communications*, 278, p.77-80.

45. Unnikrishnan Nair B., Sudeep Kumar V. P., Mahadevan Pillai V. P., Nayar, V. U. (2007), 'Wavelength Shift Of Cladding Mode Resonances In A Mechanically Induced LPFG By Twisting The Fiber', *Fiber And Integrated Optics*, 26, p.159–172.

46. Rego, G. Fernandes, J.R.A. Santos, J.L. Salgado, H.M. Marques, P.V.S. (2003), 'New Technique To Mechanically Induce Long-Period Fibre Gratings', *Optics Communications*, 220, p.111–118.

47. Karpov, V.I. Grekov, M.V. Dianov, E.M. Golant, K.M. Vasiliev, S.A. Medvedkov, O.I. Khrapko, R.R. (1998), 'Mode-Field Converter And Long-Period Gratings Fabricated By Thermo-Diffusion In Nitrogen-Doped Silica-Core Fibers', OFC'98 Technical Digest.

48. Rego, G. Okhotnokov, O. Dianov, E. (2001), 'High-Temperature Stability Of Long Period Fiber Gratings Produced Using An Electric Arc', *Journal Of Lightwae Technology*, 19(10), p. 1574 – 1579.

49. Awang, I.K., Yun S.H., Gentzsch, E. and Kim B. Y. (1999), 'Profile-Controlled Long-Period Fiber Gratings Based On Periodic microbends', Optical Fiber Communication Conference and The International Conference On Integrated Optics And Optical Fiber Communication. OFC/IOOC '99, Technical Digest.

50. Nam S. H., Zhan C., Lee J. Hahn C., Reichard K, Ruffin P., Deng K-L. And Yin S. (2005), Bend-Insensitive Ultra Short Long-Period Gratings By The Electric Arc Method And Their Applications To Harsh Environment Sensing And Communication, *Optics Express*, 13(3), p731-737.

51. Poole C. D., Presby H. M., Meester J. P. (1994), Two Mode Fibre Spatial-Mode Converter Using Periodic Core Deformation, *Electronics Letters,* 30(17), p. 1437-1438.

52. Wang, Y.-P.; Jin, W.; Wang, D. N. (2007), 'Strain Characteristics of CO2-Laser-Carved Long Period Fiber Gratings', *IEEE Journal of Quantum Electronics*, 43(2), p.101 – 108.

53. Davis D.D., Gaylord T. K., Glystis E. N., Kosinski S. G., Mettler S. C. And Vengsarkar A. M. (1998), 'Long Period Fibre Grating Fabrication With Focused CO_2 Laser Pulses', *Electronics Letters*, 34(3), p.302-303.

54. Kim C.S. Han Y. G. Kim, J. H., Park H. S., Paek U. C. And Chung Y. (1999), 'Enhancement And Suppression Of The The Thermal Sensitivity Of Long Period Fiber Gratings Fabricated With A CO_2 Laser', Cleo Pacific Rim 1999, Wb3, p.131-132.

55. Chong J. H., Shum P., Hartono H. And Yohana A. (2003), 'Investigations On The Characteristics Of Point By Point Co2 Laser Induced Long Period Grating On Optical Fiber, 2003', Proceedings Of The 2003 Joint Conference Of The Fourth International Conference On Information, Communications And Signal Processing Volume 2, Issue , 15-18 Dec. 2003 Page(S): 1283 – 1285.

56. Perez E., Chan H. M., Tomov I. And Lee H. P. (2006),'Fabrication Of Ultra-Compact Long–Period Fiber Grating Through Differentially Scanned CO_2 Laser,

Passive Components and Fiber-based Devices III - Proceedings Of SPIE, 6351, p. 635131

57. Hill, K. O., Fujii, Y., Johnson, D. C. and Kawasaki, B. S. (1978), 'Photo-Sensitivity In Optical Fiber Waveguides: Application To Reflection Filter Fabrication', *Applied Physics Letters*, 32, p.647-649.
58. Meltz, G., Morey, W. W. and Glen, W. H. (1989), 'Formation Of Bragg Gratings In Optical Fibers By A Transverse Holographic Method', Optics Letters, 14, p.823-825.
59. Kondo, Y., Nouchi, K., Mitsuyu, T., Watanabem, Kazansky, P. And Hirao K. (1999), 'Fabrication Of Long-Period Fibre Gratings By Focused Irradiation Of Infra-Red Femtosecond Laser Pulses', *Optics Letters*, 24, p.646–8.
60. Fujumaki, M., Ohki, Y., Brebner, J. L. and Roorda, S. (2000), 'Fabrication Of Long-Period Optical Fibre Gratings By Use Of Ion Implantation', *Optics Letters*, 25, p. 88–90.
61. Diez, A., Birks, T. A., Reeves, W. H., Mangan, B. J. And Russell, P. St. J. (2000), Excitation Of Cladding Modes In Photonic Crystal Fibers By Flexural Acoustic Waves, *Optics Letters*, 25(20), p. 1499-1501.
62. Williams, D. L., Ainslie, B. J., Armitage, J. R., Kashyap, R. and Campbell, R. (1993), 'Enhanced UV Photosensitivity In Boron Codoped Germanosilicate Fibers, *Electronics Letters*, 29, p. 45–7.
63. Lemaire, P. J., Atkins, R. M., Mizrahi, V. and Reed, W. A. (1993), 'High Pressure H_2 Loading As A Technique For Achieving Ultrahigh UV Photosensitivity And Thermal Sensitivity In GeO_2 Doped Optical Fibre, *Electronics Letters*, 29(13), p. 1191-1193.
64. Patrick, H. J., Askins, C. G., Mcelhanon, R. W. and Friebele, E. J. (1997), 'Amplitude Mask Patterned On An Excimer Laser Mirror For High Intensity Writing Of Long Period Fibre Gratings', *Electronics Letters*, 33, p.1167–8.
65. Lu, S. Y., Tan, H. Y. And Demokan, M. S. (1999), 'Low-Cost Microlens Array For Long-Period Grating Fabrication', *Electronics Letters,* 35, p.79–80.
66. Wei, C. Y., Ye, C. C., James, S. W., Tatam, R. P. and Irving, P. E. (2002), 'The Influence Of Hydrogen Loading And The Fabrication Process On The

Mechanical Strength Of Optical Fibre Bragg Gratings Optical Materials 20 (4) 241-251

67. Wei, C.Y. Ye, C.C. James, S.W. Tatam, R.P. Irving, P.E. (2002), 'The Influence Of Hydrogen Loading And The Fabrication Process On The Mechanical Strength Of Optical Fibre Bragg Gratings, *Optical Materials*, 20(4), p. 241–251.

68. Malo, B., Hill, K. O., Bilodeau, F., Johnson, D. C. and Albert, J. (1993), 'Point-By -Point Fabrication Of Micro-Bragg Gratings In Photosensitive Fibre Using Single Excimer Pulse Refractive Index Modification Techniques, *Electronics Letters*, 29(18), p.1668-166.

69. Zhang, L. Y. Liu, Everall, L. Williams, J. A. R. And Bennion I. (1999), 'Design And Realization Of Long-Period Grating Devices In Conventional And High Birefringence Fibers And Their Novel Applications As Fiber-Optic Load Sensors', *IEEE Journal Of Selected Topics In Quantum Electronics*, 5(5), p. 1373 -1378.

70. Fujita, K., Masuda, Y., Nakayama, K., Ando, M., Sakamoto, K., Mohri, J., Yamauchi, M., Kimura, M., Mizutani, Y., Kimura, S., Yokouchi, T., Suzaki, Y. and Ejima S. *(*2005), 'Dynamic Evolution Of The Spectrum Of Long-Period Fiber Bragg Gratings Fabricated From Hydrogen-Loaded Optical Fiber By Ultraviolet Laser Irradiation', *Applied Optics,* 44(33), p. 7032-7038.

71. Guan, B. O., Tam, H.Y., Chan, H.W., Choy C-L and Demokan, M.S.U. (2001), 'Growth Characteristics Of Long-Period Gratings In Hydrogen-Loaded Fibre During And After 193 Nm UV Inscription', *Measurement Science Technology*, 12, p.818–823.

72. Mizunami, T., Fukuda, T., (2006), 'FEM Calculation And The Effects Of Hydrogen Diffusion In Fabrication Processes Of Long-Period Fiber Gratings, *Optics Communications*, 259, p.581–586.

73. Masuda, Y.; Nakamura, M.; Komatsu, C.; Fujita, K.; Yamauchi, M.; Kimura, M.; Mizutani, Y.; Kimura, S.; Suzaki, Y.; Yokouchi, T.; Nakagawa, K.; Ejima, S. (2004), 'Wavelength Evolution Of Fiber Bragg Gratings Fabricated From Hydrogen-Loaded Optical Fiber During Annealing', *Journal Of Lightwave Technology*, 22(3), p. 934-941.

Optical cure monitoring – experimental

4

4.1 Introduction

In this chapter the initial application of optical fibre based cure monitoring techniques is described. Laboratory trials were used to characterise the behaviour of the sensors prior to their application in an industrial trial. The chapter deals with the use of LPG sensors as resin cure sensors, utilising the sensitivity of such devices to changes in the surrounding refractive index. The refractive index change during the polymerisation process of matrices provides a parameter that is measurable during the cure process and may provide an indication of cure. A comparison is made with industrially recognised techniques, e.g. DSC (differential scanning calorimetry) and with cure kinetic modelling developed by the School of Applied Sciences at Cranfield [1,2]. An evaluation of the characteristics of LPG sensors during the cure process is made using a Fresnel based refractometer. Two systems were constructed each operating at a different wavelength, to investigate the response of the resins at different wavelengths and to aid with cross comparison of other optical fibre techniques, e.g. tilted fibre Bragg gratings, operating at similar wavelengths. These techniques are discussed in more detail in chapter 5.

The experimental results detailed here are considered in three sections, each with a separate focus. The first section introduces the concept of Fresnel refractometry which

is a benchmarking method used extensively to compare with the LPG results. The second section demonstrates the cure monitoring capabilities of LPG sensors. The inherent high sensitivity of LPGs to refractive indices that approach that of the cladding ensures that standard silica based optical fibre is not an ideal sensor host material for most structural resin systems used in the manufacture of composites (typical composite resin system index >1.5) [3]. A test resin is used initially to demonstrate the LPG devices. In this case an epoxy with a refractive index close to that of silica is used, EpoTek OG-134 (refractive index of 1.4@589nm) [4], a UV cured resin. This work allows for a clear understanding of the operation of the device and appreciation of the problems likely to be exhibited by the interaction of resin with an optical fibre sensor. The final section focuses on the results of measurements made on resin systems more appropriate to composites. The problems associated with the practical application of LPG sensors with such resins are highlighted.

4.2 Fresnel refractometry

4.2.1 Theory

The basic laws of reflection and refraction are detailed in many text books [5, 6] and are used to describe the effects of a plane wave incident on plane boundary between two homogeneous isotropic media. By using these laws it is possible to study the reflection effects of propagating light incident on a material and determine its refractive index at a particular wavelength. The equations that describe the amplitude reflectivity of an incident wave are (a descriptive diagram is shown in figure 4.1):

$$r_{\perp} = \frac{n_i \cos\theta_i - n_t \cos\theta_t}{n_i \cos\theta_i + n_t \cos\theta_t} \qquad 4.1$$

$$r_{\parallel} = \frac{n_t \cos\theta_t - n_i \cos\theta_i}{n_t \cos\theta_t + n_i \cos\theta_i} \qquad 4.2$$

Where $r_{\perp}$ is the amplitude reflection for light polarised perpendicular to the plane of incidence, $r_{||}$ is light polarised parallel to the plane of incidence, θ_i is the angle of

incidence, θ_t is the angle of transmission, n_i is the refractive index of the incident medium and n_t is the index of the transmission medium. At normal incidence (θ_i=0) which is the case for the fundamental mode of a single mode fibre, the equations are simplified to:

$$r_{\perp(\theta_i=0)} = \frac{n_i - n_t}{n_i + n_t} \qquad 4.3$$

$$r_{\parallel(\theta_i=0)} = \frac{n_t - n_i}{n_t + n_i} \qquad 4.4$$

$$r_{\perp} = -r_{\parallel} \qquad 4.5$$

The intensity reflection coefficient is given by:

$$R=|r|^2 \qquad 4.6$$

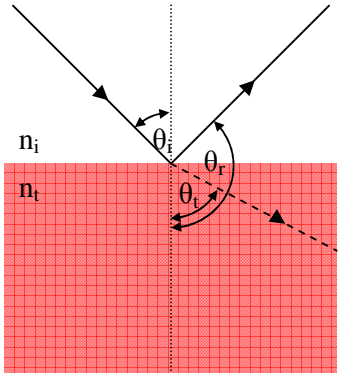

Figure 4.1 Schematic showing the incident, transmitted and reflected light at a plane boundary. θ_i is the angle of incidence, θ_t is the angle of transmission, θ_r is the angle of reflection, n_i is the refractive index of the incident medium and n_t is the refractive index of the transmission medium, where $n_t > n_i$.

Using equation 4.6, the reflected light amplitude from an incident surface can be related to the refractive index of the material. By comparing the reflection coefficient of a test material with that of a material of a known refractive index at a specific measurement wavelength, it is possible to directly measure the refractive index of the test material.

An application of this principle as an optical fibre Fresnel based refractometer has been published [7]. The setup is shown in figure 4.2.

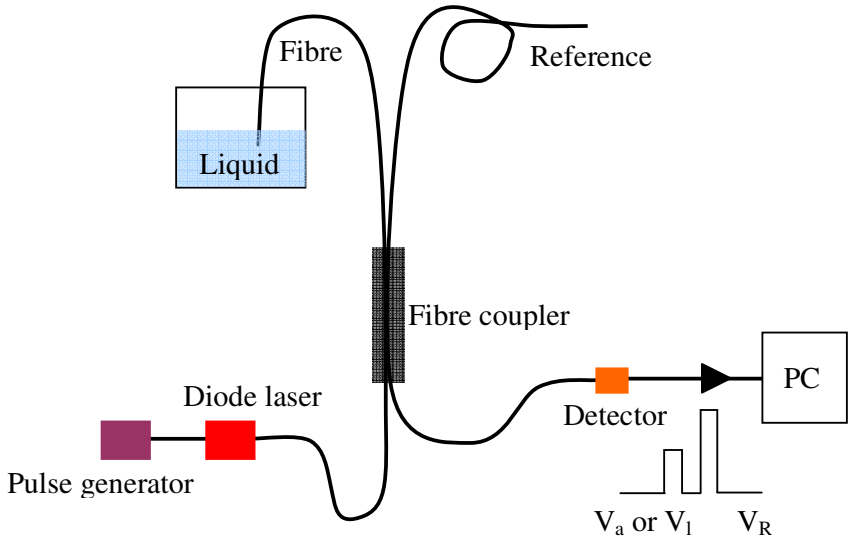

Figure 4.2 Fresnel refractometer [7]

The authors use a double pulsed technique, to account for variations in the laser power. This method uses a reference arm with an arbitrary length of fibre to separate the probe pulse from the reference pulse by a time of *2l/c,* where *l* is the length of fibre and *c* the free space speed of light. For a 1ms delay a 150km length of fibre is required to separate the pulses. The setup requires a trade off between either very long lengths of fibre or fast pulse generation and detection equipment, >1GHz. An adaptation was made to this setup for the experimental work in this thesis and is discussed in detail in section 4.2.2. The basic theory underpinning the basis of both techniques is discussed in this section.

The cleaved end of an optical fibre back reflects light propagating in the core. The reflected light is governed by the Fresnel equations. If the fibre tip is held in air and the back reflected light measured then the voltage signal from the detector is proportional to it and given as:

$$V_a \propto \frac{(n_f - n_a)^2}{(n_f + n_a)^2} \qquad 4.7$$

where n_f is the refractive index of the fibre core, n_a is the refractive index of the air (1.000 2739 [7]) and V_a is the voltage signal from the photodiodes for the fibre tip surrounded by air. If the fibre tip is then placed in a liquid of unknown refractive index the detector signal is proportional to:

$$V_l \propto \frac{(n_f - n_l)^2}{(n_f + n_l)^2} \tag{4.8}$$

where, n_l is the refractive index of the liquid and V_l is the voltage signal from the photodiode when the fibre tip is surrounded by the liquid. The ratio of these two results then makes it possible to calculate the unknown refractive index of the liquid. This is given by:

$$R = \frac{V_l}{V_a} = \frac{(n_f - n_l)^2}{(n_f + n_l)^2} \Big/ \frac{(n_f - n_a)^2}{(n_f + n_a)^2} \tag{4.9}$$

This can be rearranged to obtain:

$$n_l = n_f \left[\frac{1-\eta}{1+\eta} \right] \tag{4.10}$$

where

$$\eta = \left[\frac{n_f - n_a}{n_f + n_a} \right] \times \frac{1}{\sqrt{R}} \tag{4.11}$$

The effective refractive index of the core mode may be calculated from the group refractive index, n_g, which is given by:

$$n_g = \frac{c}{v_g} \tag{4.12}$$

The group velocity is defined as the inverse of the rate of change of the propagation constant with respect to the angular frequency.

$$v_g = \left[\frac{\partial \beta}{\partial \omega}\right]^{-1} \tag{4.13}$$

Where β is the modal propagation constant and ω is the angular frequency.

$$\beta = \frac{\omega}{c} n_f \tag{4.14}$$

We can then rewrite equation 4.13 as,

$$v_g = \left[\frac{\partial \frac{\omega}{c} n_f}{\partial \omega}\right]^{-1} = c\left[\frac{\partial \omega n_f}{\partial \omega}\right]^{-1} = c\left[n_f + \frac{\partial n_f}{\partial \omega}\omega\right]^{-1} \tag{4.15}$$

Putting this into equation 4.12 we get,

$$n_f = n_g - \omega \frac{\partial n_f}{\partial \omega} \tag{4.16}$$

This can be rearranged in terms of wavelength to give

$$n_f = n_g + \lambda \frac{\partial n_f}{\partial \lambda} \tag{4.17}$$

The accuracy of the calculation for n_l is governed by this calculated value for n_f.

4.2.2 Application

The optical fibre based Fresnel refractometer was achieved by creating a fibre network to allow illumination of a test material and collection of the reflected light, as shown in figure 4.3. The reflected light from the cleaved end of a fibre is typically 4% and to capture this back reflection the light was directly modulated in order to use lock-in detection. Two separate refractometers were constructed operating at different wavelengths; each of these is discussed in more detail in the following sections.

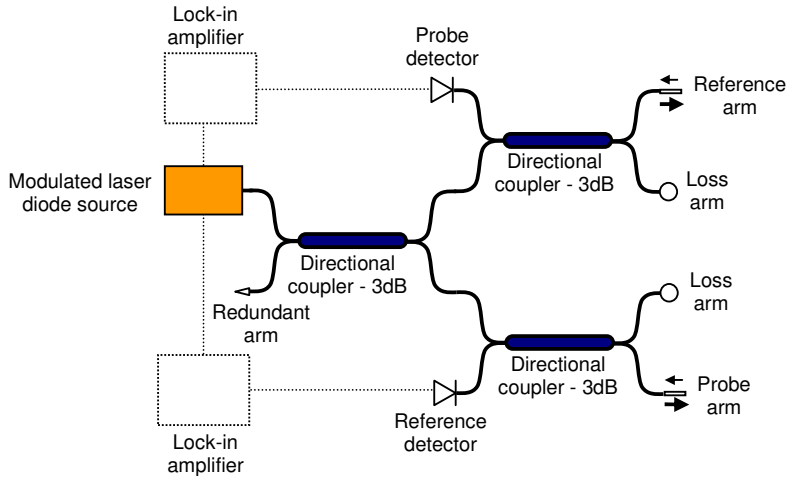

Figure 4.3 Experimental configuration. Lock-in amplifiers are synched to the chopper frequency to enable detection of modulated light.

The probe and reference arms are terminated by cleaved optical fibre ends. The optimum reflection is achieved for a right angled cleave. For both the probe and reference arm the associated coupler has an unused port, labelled as the loss arm in the diagram. These unused ports must be decoupled from the network to prevent light from reflecting back into the network. Stray reflections can induce incorrect refractive index measurements. This was achieved by a combination of three methods. Firstly the end of the fibre was crushed to cause scattering of the emitted light, secondly the end of the fibre was immersed in a refractive index matching gel and finally microbends were then imparted on the fibre by coiling the fibre into a small diameter (5mm) to introduce significant losses. Lock-in detection was achieved by directly modulating the light sources.

4.2.3 833nm Fresnel refractometer

A Fresnel system was created at 833nm to enable comparison of the refractive index measurements made with LPGs written on fibre with a cut-off wavelength at 650nm. The LPG bands appeared from 700 – 1000nm and were interrogated using a CCD spectrometer. The Fresnel system that was constructed to operate at a wavelength of 833nm is shown in figure 4.4. A coupler network was constructed using 3 3dB couplers in order to provide a probe arm, a reference arm and an input arm. A Sharp LT015MD0 laser diode was used to illuminate the network at 833nm. A chopper, amplitude modulated the input light at 270Hz and provided a modulation synch which was connected to the lock-in amplifiers. Detection was achieved using silicon photodetectors connected to the lock-in amplifiers. A labview program was written to communicate to the lock-in amplifiers through GPIB communication. This permitted simultaneous data logging for both the reference arm and probe arm. The setup is shown in figure 4.4.

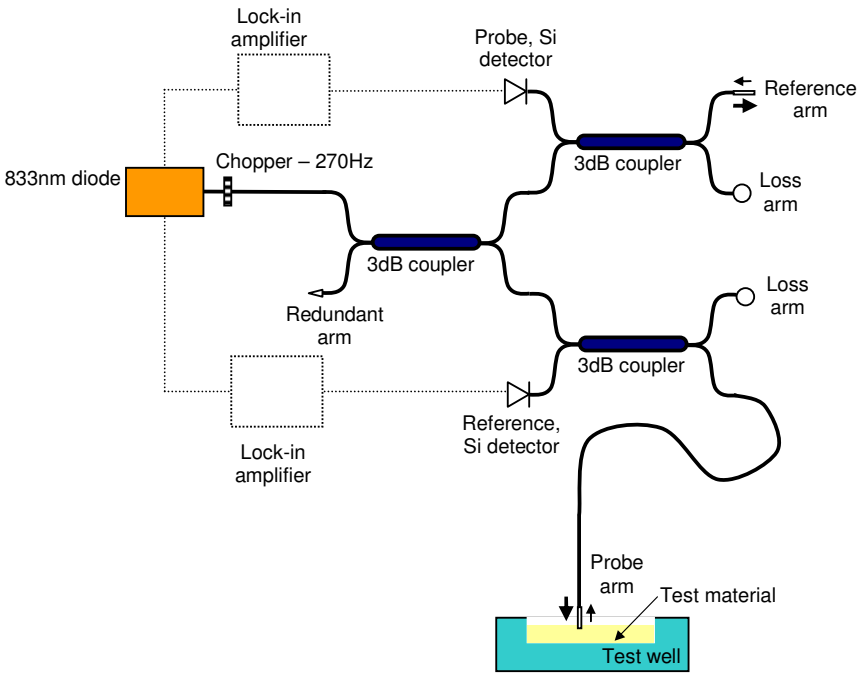

Figure 4.4 Experimental configuration of 833nm Fresnel refractometer.

4.2.4 1581nm Fresnel refractometer

A Fresnel system was created at 1581nm to enable comparison of the refractive index measurements made using a tilted FBG working at 1550nm. The experimental configuration is shown in figure 4.5. The output from an Anritsu MG9630A laser diode operating at 1581nm with 360μW output power was amplitude modulated at a frequency of 270Hz, 50% duty cycle and coupled into a network of 1550nm, 3dB, directional couplers. Lock-in detection was achieved using Thorlab PDA400 InGaAs detectors and EG&G lock-in amplifiers.

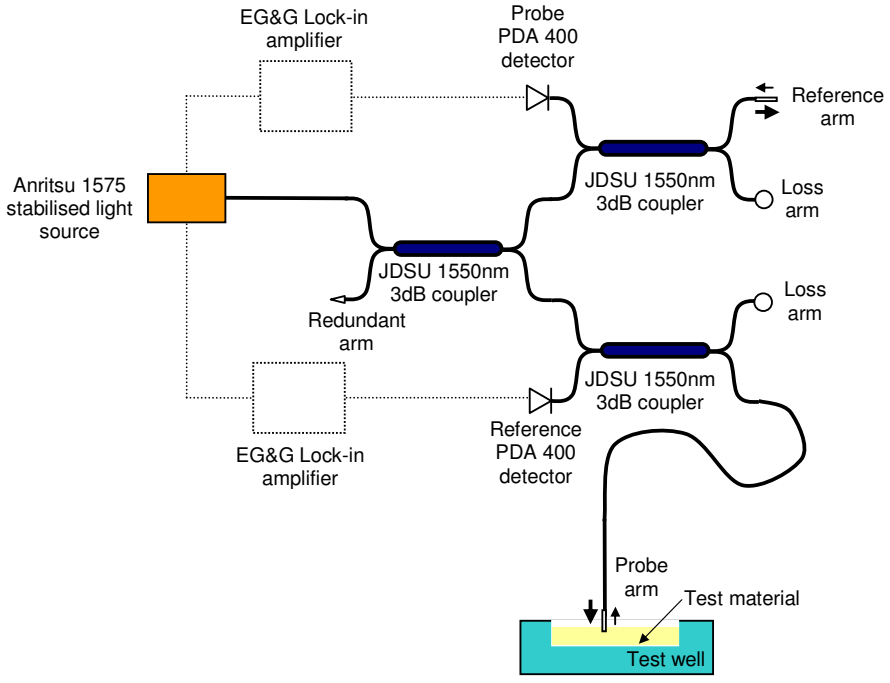

Figure 4.5 Experimental configuration of 1581nm Fresnel refractometer.

4.2.5 Fresnel network characteristics

The calibration data for the 833nm Fresnel refractometer is shown in figure 4.6 and 4.7. The root mean square deviation of the measurements (difference between calculated and actual refractive index value) about the mean is 0.000946 which suggests a resolution capability to the 3rd decimal point. However the offset error shown by the mean value of

0.003645 may indicate an unbalanced network or poor extinction of unwanted back reflections.

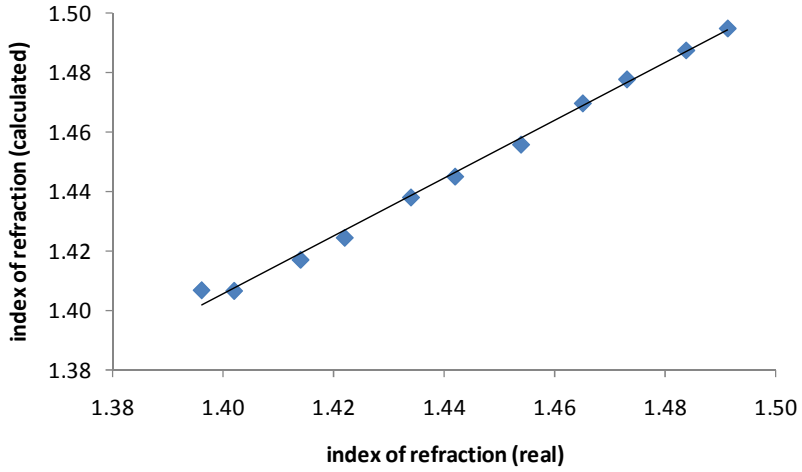

Figure 4.6 Calculated refractive index results of 833nm Fresnel network using Cargille index oil samples. A linear trend line is shown.

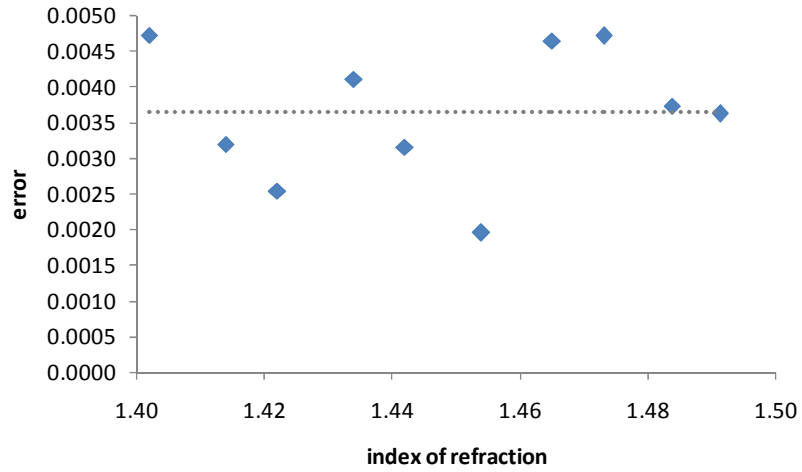

Figure 4.7 Calculated errors for refractive index values calculated using the 833 Fresnel network shown in figure 4.4. The mean is shown as a dotted line, 0.003645, root mean square deviation, 0.000946.

The calibration data for the 1575nm Fresnel refractometer is shown in figure 4.8 and 4.9. The root mean square deviation of the measurements about the mean is 0.001577 which suggests a resolution capability to the 3rd decimal point. Here, the offset error

shown by the mean value of -0.000652 is smaller than that of the 833nm network. The error distribution shows an increase in error at 1.44 which suggests the region in which the resin refractive index matches that of the fibre.

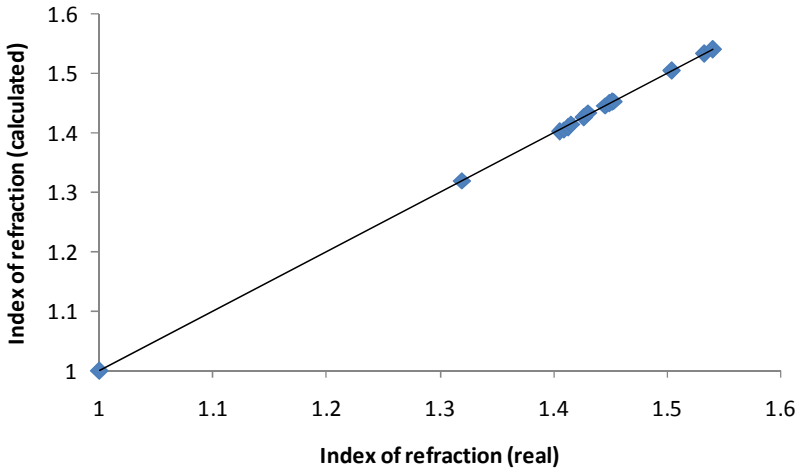

Figure 4.8 Calculated refractive index results of 1575nm Fresnel network using Cargille index oil samples. A linear trend line is shown.

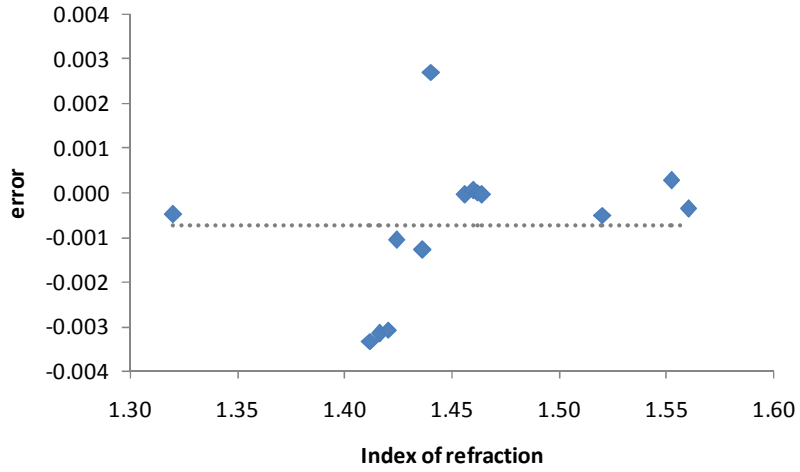

Figure 4.9 Calculated errors for refractive index values calculated using the 1575 Fresnel network. The mean is shown as a dotted line, -0.000652, root mean square deviation of 0.001577.

The resolution capabilities of the Fresnel network are 1 x 10^{-3} rius at 833nm and 1.6 x 10^{-3} rius at 1575nm.

4.2.6 Dispersion characteristics

To aid the correlation of the refractive index values measured using the different sensors working at different wavelengths (e.g. a refractive index sensitive LPG attenuation band at 970nm and the Fresnel refractometer operating at 833nm), a dispersion analysis was carried out on two transparent liquid resins, the Epotek OG-134 resin as mentioned previously and a structural resin that is investigated in more depth in section 4.4, MY750 (a typical composite epoxy system) . A Bellingham & Stanley Abbe refractometer with an Ando AQ4304 programmable broadband source was used to illuminate the resins at different wavelengths and a dispersion curve plotted showing the wavelength dependence of the refractive index of each of the resins. The measurements were made at room temperature (22°C) in a temperature controlled environment of ±2°C. A 3-term Cauchy dispersion curve was then fitted to the data points [6]. Using this curve, an estimation of the refractive index at different wavelengths (within the experimental wavelength range) can be made.

$$n(\lambda) = A + \frac{B}{\lambda^2} + \frac{C}{\lambda^4} + \ldots \qquad 4.15$$

A Cauchy fit is shown for the MY750 resin in figure 4.10 and the Epotek OG-134 resin is shown in figure 4.11.

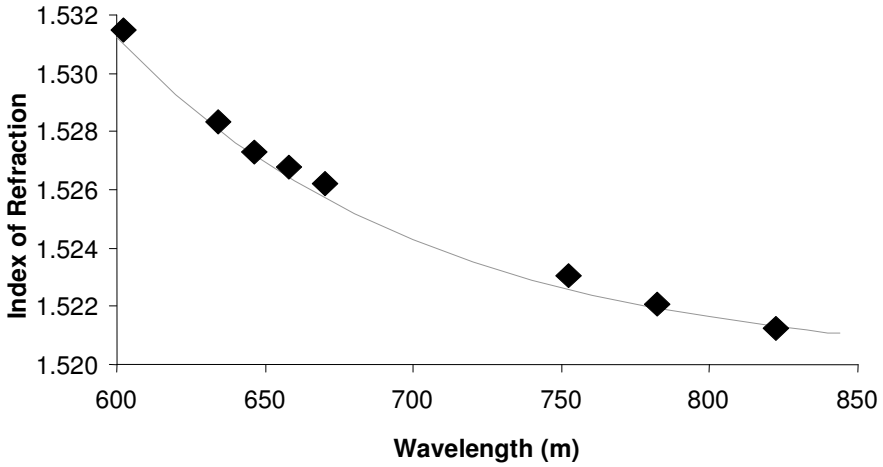

Figure 4.10 Dispersion analysis of MY750, ◆ = Calculated RI values at 22°C from Abbe refractometer, ▬ = 3-term Cauchy fit to experimental data.

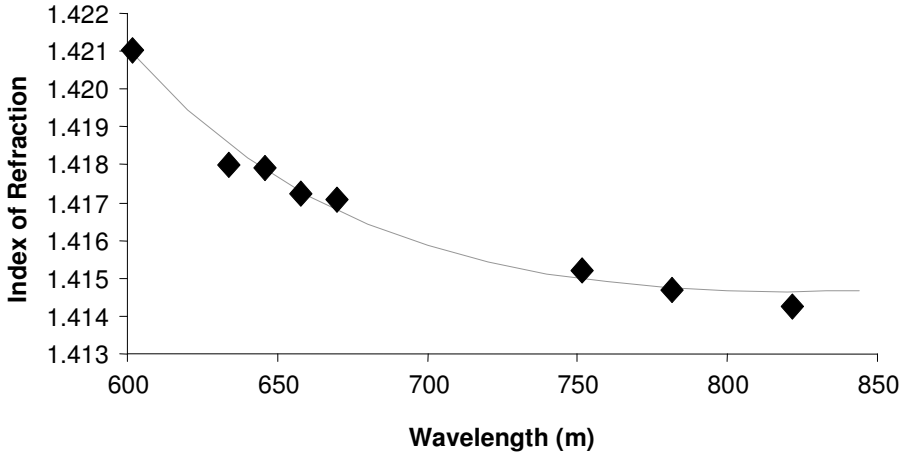

Figure 4.11 Dispersion analysis of OG-134, ◆ = Calculated RI values at 20°C from Abbe refractometer, ▬ = 3-term Cauchy fit to experimental data.

Table 4.1 lists the Cauchy coefficients for both resins. An error of $\pm 8 \times 10^{-4}$ ($^{\circ}C^{-1}$) can be allowed for thermo-optic changes ($\pm 2 \times 10^{-4}$ ($^{\circ}C^{-1}$)) and read off errors [8].

Table 4.1 Cauchy coefficients for MY 750 and OG 134 resins.

	Resins	
Coefficients	MY 750	OG 134
A	1.523	1.423
B	-5.8×10^{-15}	-1.13×10^{-14}
C	3.15×10^{-27}	3.82×10^{-27}

4.3 Experimental work with UV cured epoxy

To demonstrate the response of the LPG attenuation bands to changes in the refractive index of a curing resin surrounding it, a resin with a refractive index similar to that of the LPG cladding was used. This follows the discussion in chapter 3, whereby the LPG exhibits a high sensitivity to refractive indices approaching that of the cladding. In this case a UV cured epoxy resin from Epotek was used. OG-134 is an epoxy based resin

system used in the fibre optics industry. It is a clear resin that undergoes cure when exposed to UV radiation; a UV initiated catalyst begins the cure process. Typical UV cure processes are quick acting [9], in this work, the UV energy directed at the samples was restricted by distancing the lamp from the sample sufficiently to slow down the cure reaction. Both Fresnel systems described, operating at two separate wavelengths, are used as a benchmarking tool to demonstrate the capabilities of the LPG sensor.

4.3.1 Experimental setup

Two LPGs were used to investigate an LPG's response to the change in refractive index of a resin at two separate wavelengths. LPGs of length 40mm and 400µm period were fabricated in two different optical fibre types, one with a cut off wavelength of 650nm (Fibercore SM750) and the other with a cut off wavelength of 1275nm (Optical Fibres OF1310). The two separate wavelength regions were 800nm and 1550nm. At 800nm CCD spectrometers were utilised, this demonstrated that the system could be developed with simple and relatively inexpensive optical components. At 1550nm the LPG data could be compared with refractive index measurements reported at 1550nm, e.g. tilted FBGs, and discussed in section 5.3. The fibres were photosensitised by pressurising them in hydrogen for a period of 2 weeks at a pressure of 150bar at room temperature. Each LPG was manufactured by placing the fibre behind an amplitude mask that was illuminated by a UV laser beam at a wavelength of 266nm, provided by a frequency-quadrupled Nd:YAG laser, see chapter 3.

The transmission spectrum of the LPG written in the SM750 fibre, shown in figure 4.12 (a), was monitored by coupling the output from a tungsten-halogen white light source into the fibre and coupling the transmitted light to a CCD spectrometer (Ocean Optics S2000) with a resolution of 0.3nm. The transmission spectrum of the LPG written on OF1310 fibre was monitored using an Advantest Q8381 spectrum analyser with a resolution of 0.1nm, figure 4.12 (b). The spectral window of the CCD based spectrometer is from 600nm – 1100nm, therefore an optical spectrum analyser is required to interrogate the LPG written in OF1310 fibre.

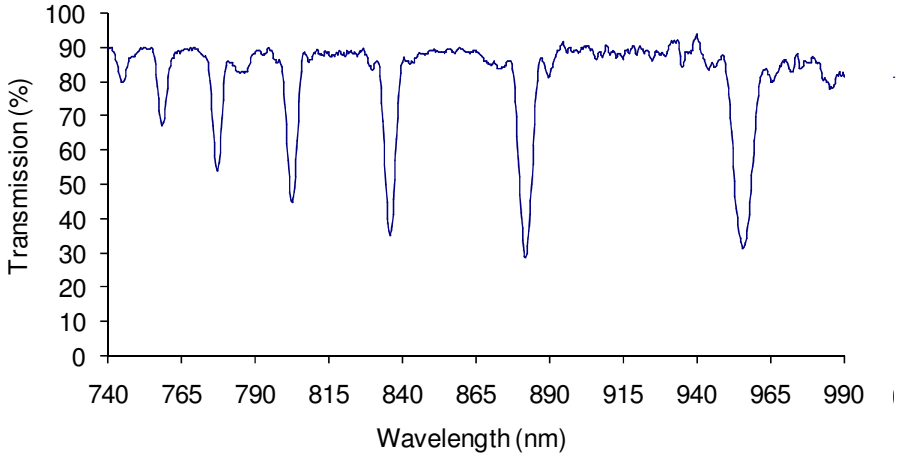

(a)

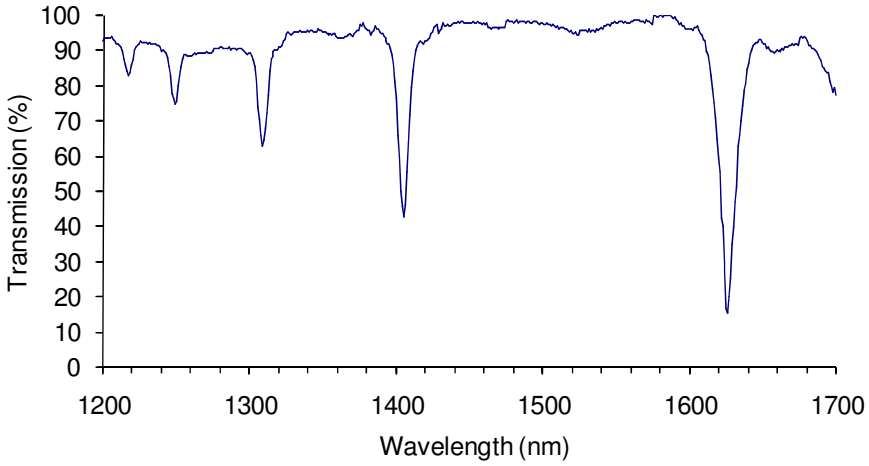

(b)

Figure 4.12 Transmission spectrum of an LPG of length 40mm and of period 400µm, fabricated in an optical fibre with a cut-off wavelength of 650nm (Fibercore SM750) (a) and 1310nm (OF1310)(b).

The responses of the LPG refractometers to the refractive index changes that occurred during the cure process were compared with refractive index measurements made using Fresnel based measurements, described in section 4.2 [7].

4.3.2 Differential scanning calorimetry and impedance spectroscopy

In order to relate the measured refractive index change during cure with cure conversion, it was necessary to compare the results with standard assessment techniques. Two methods were investigated, differential scanning calorimetry (DSC) and impedance spectroscopy.

DSC is a widely used technique for investigating the characteristics of polymers. DSC measures the heat absorbed or released by a sample undergoing cure and relates this to the cure reaction. In the case of thermosetting curing, the heat flow is proportional to the rate of reaction [10]. Normalisation and integration of the heat flow versus time curve using an appropriate baseline [11] yields the degree-of-cure evolution with time. A sample was prepared using the PTFE well and UV cured at a constant temperature of 29°C in a TA Instruments 2920 MDSC with an RCS cooling unit. The resin was irradiated under the same conditions as the refractometry experiments. This work was achieved with the aid of Athanasios Dimopoulos of the Composites Centre at the School of Applied Sciences, Cranfield University.

Impedance spectroscopy has been proposed as an online method for monitoring a polymer during cure [12, 13, 14]. The technique is based on changes in the electrical and dielectric properties of a polymer as the cure progresses. The molecular structure of a material undergoes significant change during cure and the material goes through phase transitions in the cure cycle, i.e. liquid to rubber to glass. Much information can be derived from impedance measurements but for the purposes of online monitoring in a control context it is necessary to relate a dielectric parameter directly to a material state index, i.e. cure conversion. In this experiment the imaginary impedance maximum (IIM) is used as a dielectric parameter to assess the cure state of the epoxy under cure. The IIM measurement can be directly related to the quantity and mobility of charged species which can be correlated to the cure reaction [14]. A sample was prepared and interrogated using a GIA (Pearson Panke) interdigitated dielectric sensor and interrogated using a Solartron Instruments 1260 frequency response analyzer over a frequency range of 1Hz to 1MHz. The analysis proposed in [14] was followed to assess the cure progression from the impedance data. The resin was irradiated under the same

conditions as the refractometry experiments. This work was achieved with the aid of Dr. Skordos of the Composites Centre at the School of Applied Sciences, Cranfield University.

4.3.3 Results

Figure 4.13 shows the refractive index of the curing resin measured by both of the Fresnel based refractometers (solid line - 833nm and dashed line - 1581nm). The datum is the time at which the UV lamp was switched on. At this time a clear decrease in refractive index was observed. This is due to an exothermic reaction initiated by the incident UV light [9]. The temperature of the resin was measured with a thermocouple, placed in the resin, which indicated a 6.5°C increase in temperature over the first 5 minutes. It was also noted that there was an ambient temperature increase of 3°C. This was measured with a thermocouple placed close to the sample. The thermocouple measurements are shown in figure 4.14. This may be due to infrared radiation from the UV lamp which causes the sample temperature to rise during the cure time.

4.3.3.1 Fresnel measurements

The measurements of the refractive index change, using the two Fresnel wavelength refractometers during the cure, show good agreement. After the initial decrease in refractive index corresponding to the initial exothermic peak, a turnaround point and rapid increase in refractive index is measured; this indicates the reaction process. This may be justified because, although there is a slight decrease in temperature of 1°C which may account for a small increase in refractive index ($1x10^{-4}$), the larger change in refractive index must be attributed to the increasing molecular density of the resin due to polymerisation. The rate of change of refractive index reduces after 90 minutes. The difference between the measurements made at the two wavelengths may be due to the poor spectral resolution achievable using the optical spectrum analyser (OSA). Because a tungsten halogen light source was used with a poor power output ($11mW/cm^2$), a spectral resolution of 5nm was specified on the OSA in order to determine the attenuation bands.

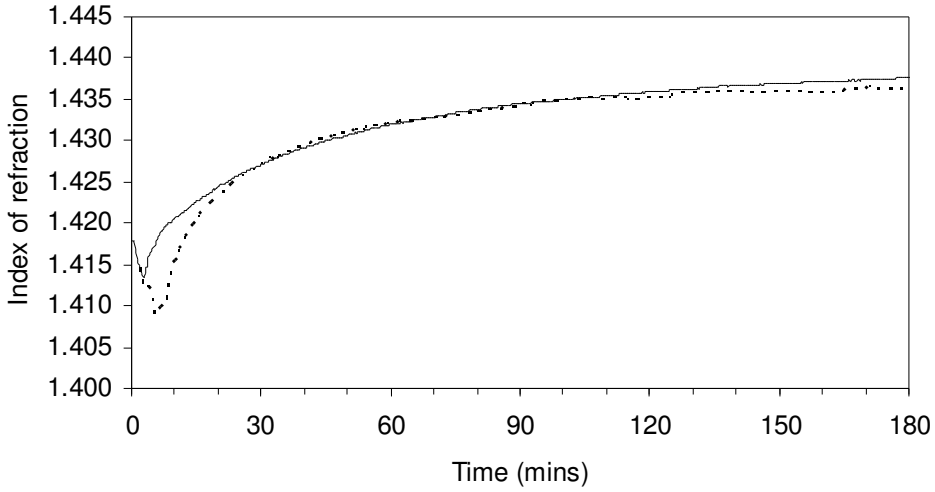

Figure 4.13 Refractive index change measured during the cure of the OG-134 epoxy resin, determined from the measurements made using the Fresnel refractometers operating at 833nm (solid) and 1581nm (dashed)

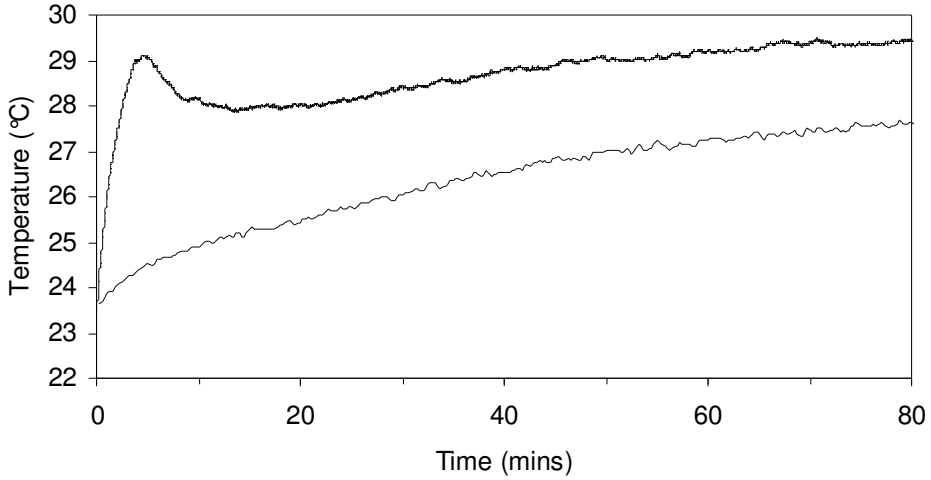

Figure 4.14 Temperature of the OG-134 epoxy resin measured during cure by two K-type thermocouples; one placed in the sample (solid) and the second placed close to the sample (dashed).

The model discussed in chapter 3 was used to predict the expected wavelength shift of an LPG band in response to the refractive change during cure. The refractive index measured during the cure of the resin using the Fresnel system was then input to the model to calculate the corresponding change in the cladding mode effective index, and

thus allow prediction of the change of the central wavelengths of the LPG attenuation bands. Figure 4.15 shows the predicted shift of the central wavelength of the attenuation band coupled to the higher order cladding mode, LP_{05} of an LPG fabricated in the SM750 fibre. The experimentally measured response of an LPG of the same design is also shown. The close agreement with the model highlights the ability of the LPG as an optical cure monitoring sensor. The contributions of strain and temperature to the measured wavelength shift are not included in the simplified model. Axial and transverse strain is known to develop during the cure for some resin systems [15], but has not yet been determined for the UV resin used here. In general, LPGs shows a high sensitivity to temperature, and a low sensitivity to strain. However as discussed in chapter 3, an LPG can be designed such that a temperature insensitive band may be used to measure the refractive index change. Temperature changes will also affect the refractive index of materials to a greater or lesser extent and these need to be considered when analysing the results. The effect of this was shown previously with the initial exothermic peak when the ultraviolet lamp was switched on. For isothermal curing this may be neglected as the sample is held at a constant temperature

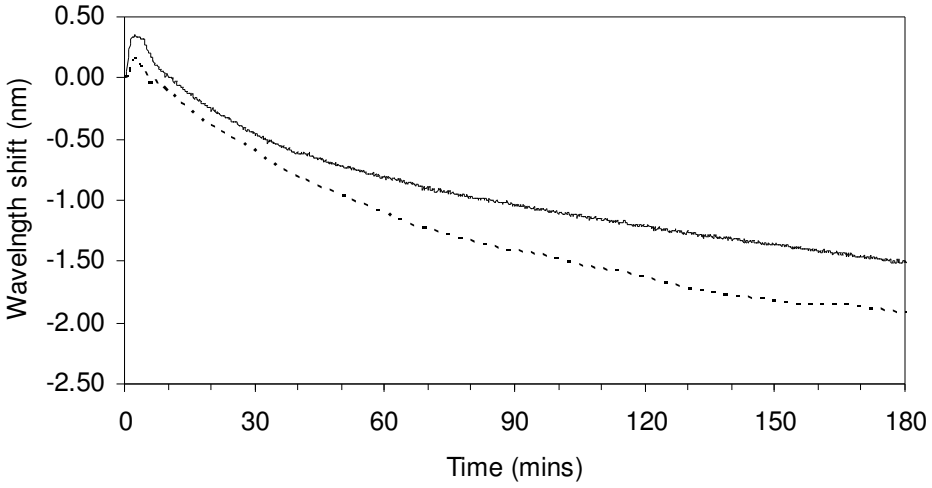

Figure 4.15 The experimental (solid) and theoretical (dashed) wavelength response of the 5th attenuation band of an LPG (central wavelength at 940nm), of length 40mm and of period 400μm fabricated in SM750 fibre, during the cure of the OG-134 epoxy resin.

4.3.3.2 LPG measurements

The wavelength responses of the LPGs were related to refractive index by immersing the fibre in a set of Cargille index oils over the range of indices to be measured and the wavelength response recorded. Figure 4.16 shows the refractive index calculated from the response of the attenuation bands coupled to the LP_{05} cladding mode of both LPGs (SM750 and OF1310 fibre). At both wavelengths, the initial decrease in refractive index, observed when the UV lamp is switched on, is followed by a rapid positive change in refractive index. The LPGs show a decrease in the rate of change of refractive index after 90 minutes, in agreement with the measurements made using the Fresnel refractometer. The discrepancies may be attributed to dispersion effects and to errors induced by the temperature sensitivity of the LPG. The results obtained using both the Fresnel technique and the LPG illustrates the dispersive properties of the resin; the refractive index at the longer wavelength was lower than at the shorter wavelength.

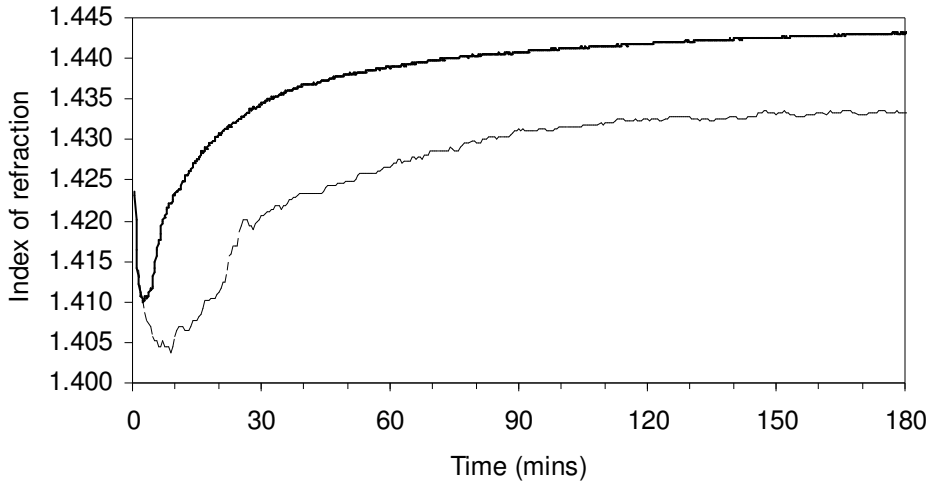

Figure 4.16 The evolution of the refractive index during cure of the OG-134 epoxy resin, determined from the wavelength shift of the 5th attenuation bands of the LPG based refractometers at 940nm (solid) and 1545nm (dashed).

Tables 4.2 and 4.3 compare the measurements made using the LPG and Fresnel techniques in the two wavelength regimes.

Table 4.2 Comparison of the refractive index change exhibited by EpoTek OG134 during cure, determined from the Fresnel (833nm) and LPG (fabricated in the PS750 fibre) methods. (Δ is the difference between the measurements made using the two methods).

	Optical technique		
Cure state	$Fresnel_{833}$	LPG_{940}	Δ
Wet (initial)	1.4178	1.4237	0.0059
Cured (final)	1.4376	1.4432	0.0056

Table 4.3 Comparison of the refractive index change exhibited by EpoTek OG134 during cure, determined from the Fresnel (1581nm) and LPG (fabricated in the OF1310 fibre) methods. (Δ is the difference between the measurements made using the two methods).

	Optical technique		
Cure state	$Fresnel_{1581}$	LPG_{1545}	Δ
Wet (initial)	1.4184	1.4190	0.0006
Cured (final)	1.4365	1.4332	-0.0033

The discrepancy between results obtained using the Fresnel and LPG based refractometers may be attributed to the temperature sensitivity of the LPG. The response of the attenuation bands to changes in temperature was not accounted for in the measurements.

A direct comparison of the refractive index change during cure and the results obtained using DSC and impedance spectroscopy are shown in figures 4.17 and 4.18. Both results show good agreement. They illustrate how as LPG based refractometer may be used to provide data for process monitoring of complex composite components. DSC or spectroscopic based kinetic modelling can be correlated with the wavelength response of an LPG to determine a state of cure.

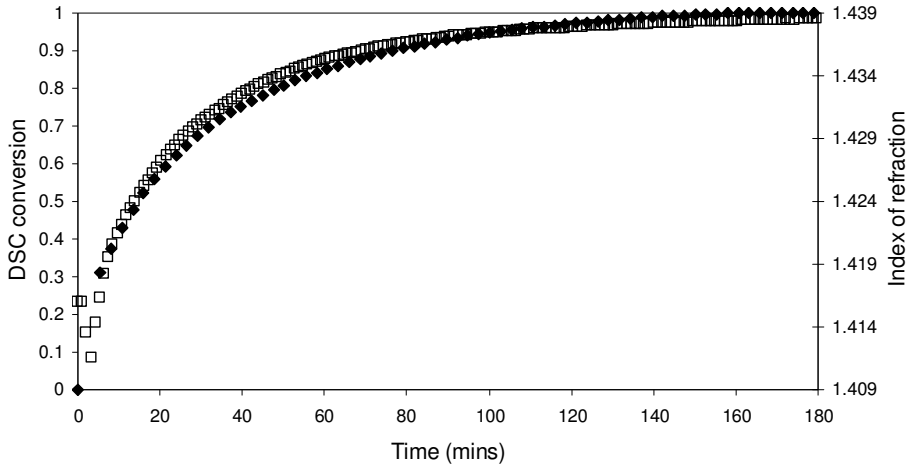

Figure 4.17 Index of refraction (□) and DSC conversion (◆) of UV cured epoxy.

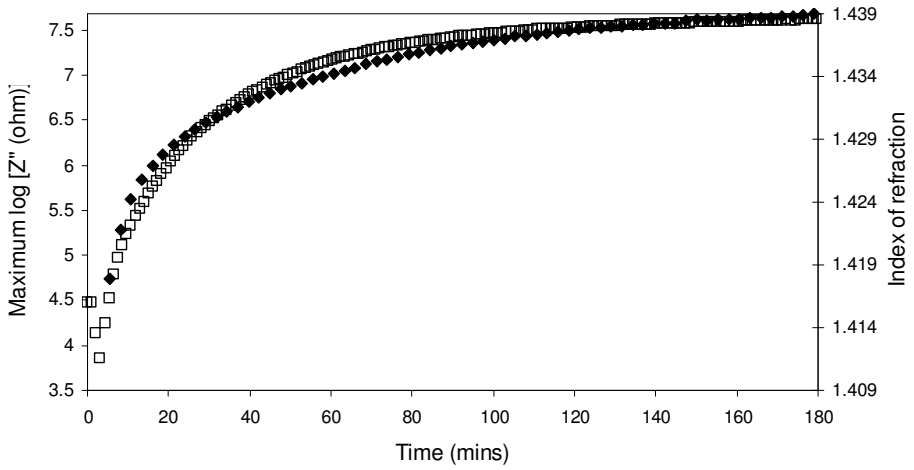

Figure 4.18. Index of refraction (□) and impedance spectroscopy measurements (◆) of UV cured epoxy.

4.3.4 Summary

In summary, optical fibre refractometers were demonstrated as cure monitoring sensors of a UV cured epoxy. The core-cladding mode coupling resonances of an LPG have been shown to be sensitive to the cure of an epoxy resin. The measurements made using an LPG were compared with those made using a fibre optic Fresnel reflection based technique, and were found to be in agreement to within 6 x 10^{-4} rius. However LPGs are sensitive to temperature and strain, which must be decoupled to accurately measure refractive index. The results were compared with traditional cure monitoring techniques and show close agreement with both DSC and impedance spectroscopy measurements. This leads to the possibility of using the sensors with cure-kinetic models to characterise and monitor the cure of resins and fibre reinforced resin systems [16].

4.4. Resins used for manufacture of composites

This research is focussed on utilising and developing optical fibre techniques, grating technology in particular, for monitoring the development of cure in composite resin systems. The initial development work summarised in section 4.3 demonstrated the capability of such techniques to monitor the cure of a simple epoxy system with a refractive index close to that of the fibre. This allowed the wavelength response of an LPG attenuation band to be utilised as a cure monitor by directly measuring the changing refractive index of the resin during cure. Composite resin systems are appreciably different. A fundamental difference and of critical importance in this case, is their high refractive index. The high refractive index of such resins precludes the use of standard telecom fibres as LPG sensor material as the refractive index change during cure is restricted to the low sensitivity region of the response curve. Summarised here is the experimental work on measuring the refractive index response of such resins during cure using Fresnel refractometry. The resins investigated in this work are listed below:-

MY 750 – Isothermal cure cycle of 40°C for 6 hours and 80°C for 3 hours.
A resin system used predominantly in vacuum impregnation processes particularly in the manufacture of magnetic coils. A transparent Bisphenol A (DGEBA) based resin,

pre-mixed (by the School of Applied Sciences to aid accurate cross comparison of results) with a commercial hardener (HY 5922). The liquid state of the resin at room temperature and low viscosity allows for ease of fibre penetration. The resin was supplied by Vantico Ltd.

Hexcel 8552 – Isothermal cure cycle of 180°C for 120mins.
The resin is a high performance toughened epoxy used in the aerospace industry. It is a semi-solid (at room temperature) opaque and dark yellow resin. The resin is a one part system, a tetrafunctional epoxy system pre-mixed with a diamino diphenyl sulphone curing agent and thermoplastic (Dapsone). The resin was semi-solid at room temperature therefore it was necessary to heat the resin to 80°C for a short period, 10mins; this was sufficient to decrease the viscosity of the material to allow the fibre to be inserted into the sample. The resin was supplied by Hexcel Ltd.

MTM 44 - Isothermal cure cycle of 130°C for 240mins or 180C for 120 minutes
The resin is a high performance toughened epoxy used in the aerospace industry developed for predominantly pre-impregnated composite processes. It is a semi-solid (at room temperature) dark brown resin. The resin is a one part system, a tetra-functional epoxy system pre-mixed with two aromatic polyamines curing agents and a toughening thermoplastic additive. The resin was difficult to handle in the laboratory experiments, and a similar procedure to that used for the HX 8552 resin was employed. The resin was supplied by ACG.

4.4.1 Cure kinetic modelling

Ideally, a model describing the cure of a resin system would determine the state of cure of a resin at any point during a cure cycle. This would be particularly advantageous for processing of resin systems in industry. In reality this is difficult to achieve due to the complex nature of the reaction mechanisms and, on a commercial level, the knowledge of the chemical make up of many resin systems are restricted. Modelling techniques have been developed using empirical data in order to characterise a resin system utilising two parameters (time or temperature and cure conversion). Determination of

the model parameters is achieved through analyses of resin samples. The simplest model can be expressed as an n^{th} order rate equation [1] and is given as:-

$$\frac{d\alpha}{dt} = k(1-\alpha)^n \qquad 4.16$$

Where α is the cure conversion, n is termed the reaction exponent and k is the rate constant obeying the Arrhenius equation:

$$k = Ae^{-\left(\frac{E}{RT}\right)} \qquad 4.17$$

Where A is termed rate prefactor and relates the rate constant with temperature, E is the activation energy, R is the universal gas constant and T is temperature (in Kelvin). A modification of 4.16 is necessary in order to describe a more typical reaction in resin systems termed autocatalysis. Equation 4.16 assumes a maximum reaction rate at the start of the cure, whereas in autocatalytic reactions, where the catalyst itself is generated by the cure reaction, the maximum reaction rate occurs some time after the cure has started. A modified form of equation 4.16 is described by [17]:

$$\frac{d\alpha}{dt} = (k_1 + k_2\alpha^m)(1-\alpha)^n \qquad 4.16$$

Where the rate constants k_1 and k_2 and exponential factors m and n are determined through curve fitting to cure measurement data obtained from DSC experiments. Modelling of the three structural resins was carried out using DSC measurements by Athanasios Dimopoulos at the School of Applied Sciences. The isothermal and dynamic cure kinetic models for MY750 are shown in figure 4.19 and 4.20. The isothermal models illustrate the importance of the cure temperature with cure, for example for an isothermal cure at 40°C the resin never reaches 100% cure. The models are developed using genetic algorithm techniques fitting experimental data with model parameters. Discrepancies between the model and experimental data may be explained by the initial assumption made in developing the models that the reaction rate during cure is a unique

function of cure conversion and temperature. This assumption begins to breakdown when complex resin systems are modelled where different cure mechanisms within a resin may exist.

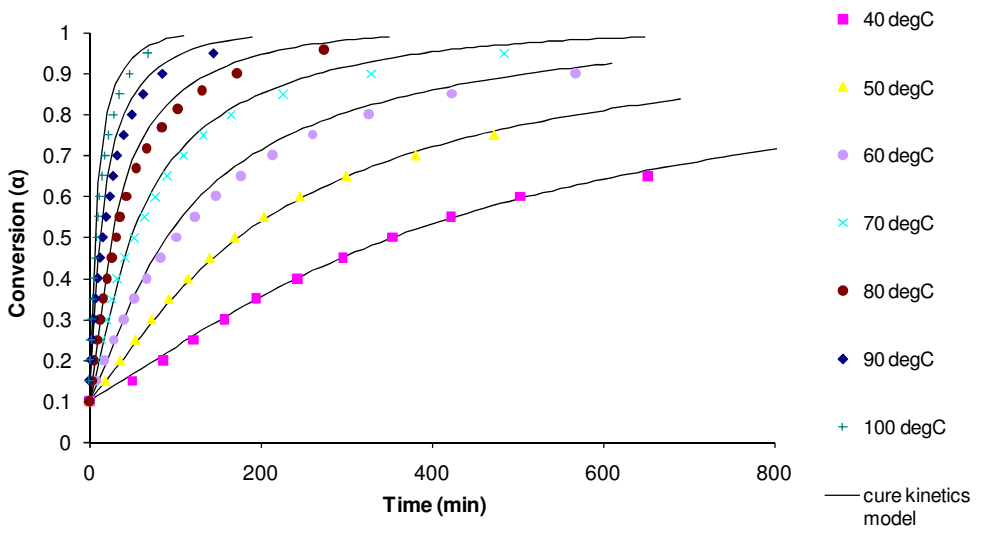

Figure 4.19 Isothermal cure kinetic model of MY750 from DSC analysis [1].

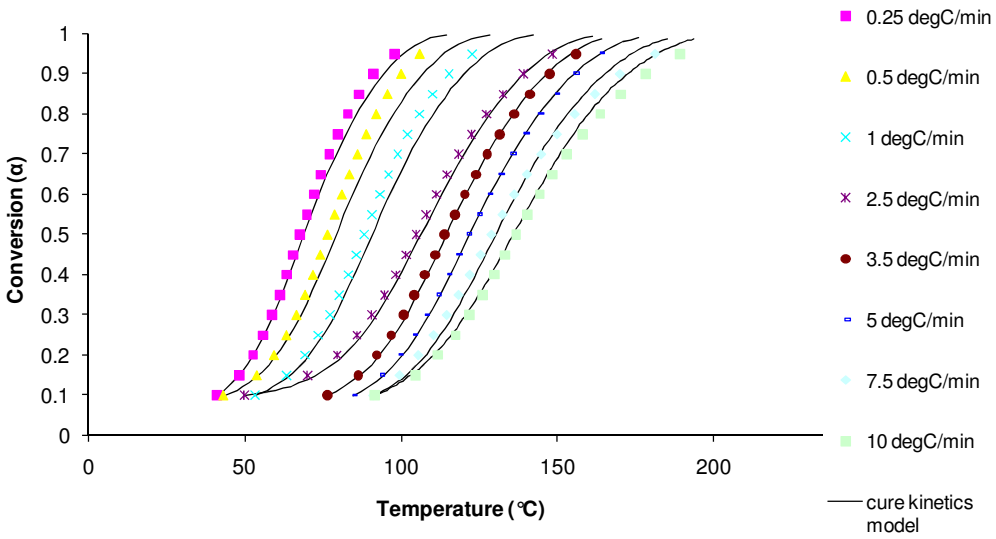

Figure 4.20 Dynamic cure kinetic model of MY750 from DSC analysis [1].

The dynamic cure results allow determination of the state of cure once isothermal conditions are met, for example for a 5°C/min heating rate once an isothermal cure

temperature of 100°C is reached the resin is already 20% cured. Clearly a fast heating rate ensures there is little cure conversion before isothermal conditions are met. Similar models were developed for the Hexcel 8552 and MTM-44 resins and are used to correlate the refractive index response with cure conversion.

Investigation of the refractive index change with cure can now be achieved through correlation with the cure kinetic models. Cusano *et al* [17], report an equation relating the refractive index change to degree of conversion by:-

$$\alpha_r = \frac{n_t - n_0}{n_\infty - n_0} \qquad 4.17$$

where α_r is the cure conversion (determined from refractive index measurements), n_t = the refractive index at time t, n_0 = index at the start of cure and n_∞ = the index at the end of cure. This assumes a linear relationship between degree of cure and refractive index during cure. Equation 4.17 assumes a 100% cure conversion is achieved for n_∞; this can be adapted for maximum conversion (determined experimentally by DSC) by:-

$$\alpha(T) = \alpha_r \alpha^{\max}(T) \qquad 4.18$$

where α(T) is conversion for isothermal cure at temperature T, α^{max}(T) is the maximum conversion obtained for an isothermal cure at temperature T.

4.4.2 Experimental configuration

The experimental setup is illustrated in figure 4.21. The cleaved tip of the fibre from the probe arm of the Fresnel refractometer was placed in the resin to be measured. The resin was contained within a PTFE well. A reusable PTFE well was designed as this allowed a cured sample to be removed easily to allow repeat measurements. A PID controlled Carbolite tube furnace was used to cure the resins. The furnace with an accuracy of ±1°C had a maximum working temperature of 900°C. A 40mm section at the centre of

the tube had a uniform temperature. Each resin required different isothermal cure conditions as previously indicated.

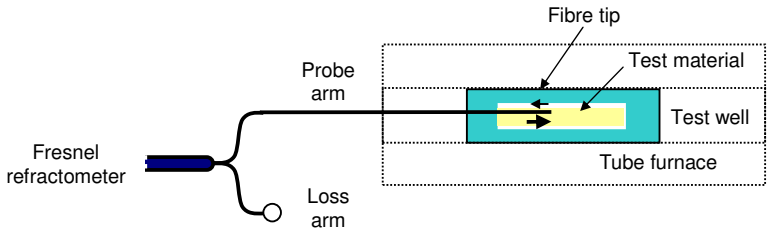

Figure 4.21 Experimental configuration.

4.4.3 Results

Each resin system was isothermally cured the parameters of which are detailed in table 4.4. Each resin is discussed in turn.

Table 4.4 Isothermal curing parameters for investigated resins

MY 750	120°C for 90 minutes or 80°C for 6 hours
HX 8552	180°C for 60 minutes
MTM 44	180°C for 60 minutes

4.4.3.1 MY 750

Figures 4.22 and 4.24 show the refractive index measured during the cure of two samples of the MY750 resin. Measurements were made using both Fresnel refractometer systems in order to investigate the response of the resin refractive index change at different wavelengths, 833nm and 1581nm.

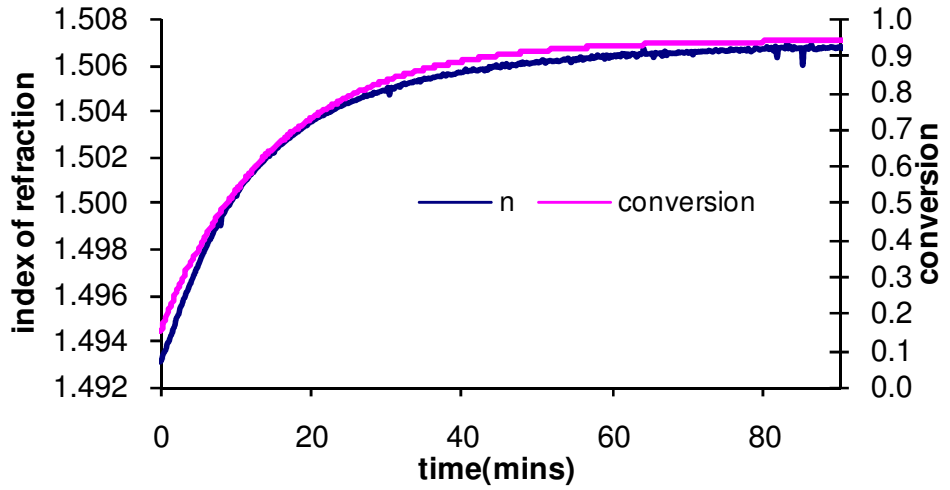

Figure 4.22 MY 750 refractive index response at 833nm and cure kinetic model for isothermal cure at 120℃ for 90 minutes.

The change in refractive index of the MY 750 resin shows a very similar response at both wavelengths. The measured refractive index change at 1581nm is lower. This corresponds with the dispersion relation using the Cauchy equation in section 4.2.5. Correlations of the refractive index response of both tests with a cure kinetics model are shown in figures 4.23 and 4.25. The experimental results show good agreement with the conversion curve and reinforce the possibility of using such measurements as a cure conversion indicator. Discrepancies are evident at the start and at the end of cure. These may be attributed to thermal effects which are transitory at the start of the cure during isothermal stabilisation.

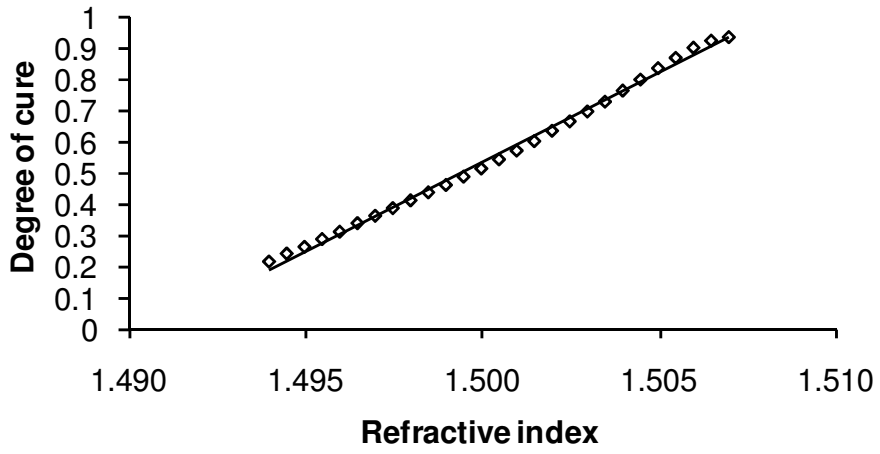

Figure 4.23 MY 750 correlation of refractive index response at 833nm and cure kinetic model for isothermal cure at 120°C for 90 minutes.

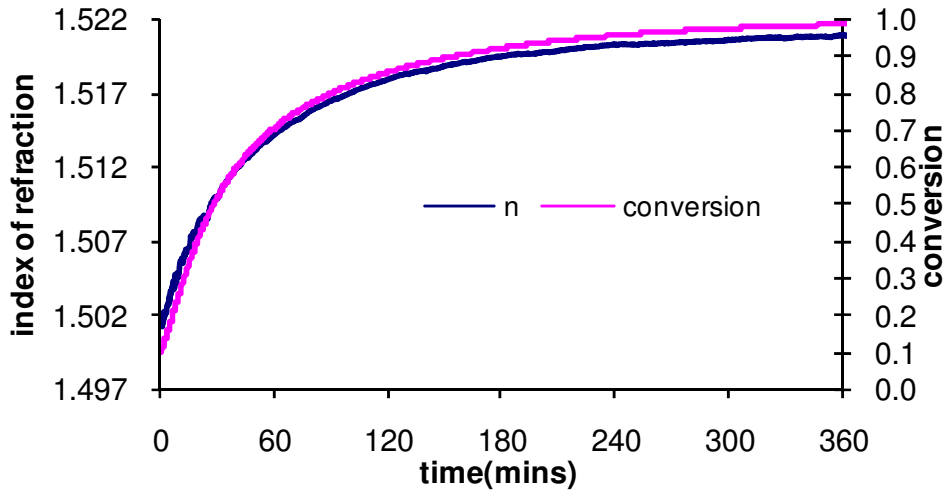

Figure 4.24 MY 750 refractive index response at 1581nm and cure kinetic model for isothermal cure at 80°C for 6 hours.

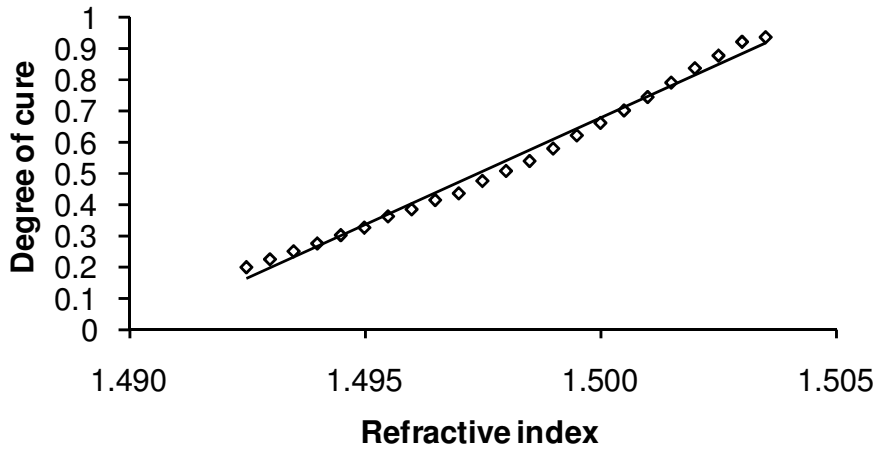

Figure 4.25 MY 750 correlation of refractive index response at 1581nm and cure kinetic model for isothermal cure at 80°C for 6 hours.

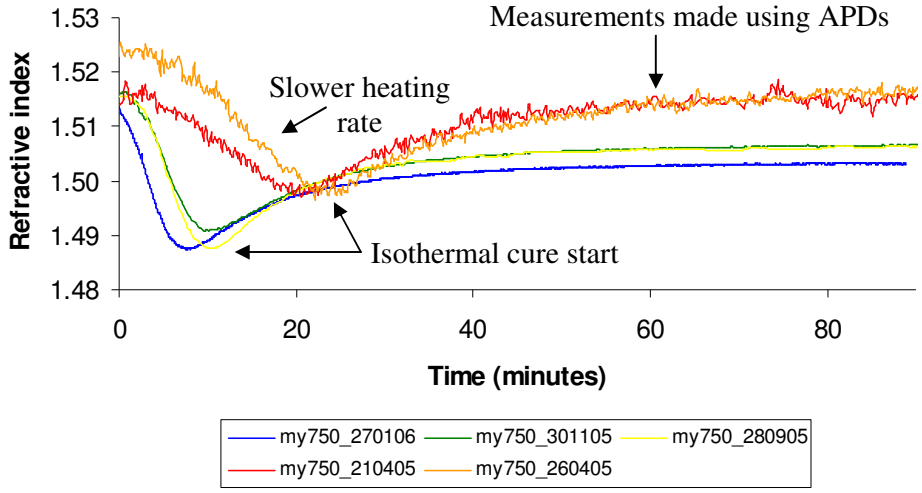

Figure 4.26 MY 750 refractive index response for repeated isothermal cures at 120°C for 90 minutes. The test dates are shown in the legend. All results are for refractive index measured at 833nm except (—, my750_270106) which is calculated at 1581nm.

Figure 4.26 shows a comparison of measured refractive index changes during isothermal cure cycles of repeated tests of MY750 resin. The figure shows two

measurements made using the 833nm refractometer where the resin was cured using a slower heating rate, 2.5°C/min. The apparent noise on the refractive index measurement may be attributed to the use of APDs, because these detectors contribute a high noise content, particularly at low speed modulation, less than 10kHz. Subsequent measurements were made using standard photodiodes. At time zero there is an initial decrease in refractive index which may be attributed to the thermo-optic effect. After a time which is found to be dependent on the initial heating rate, the reaction starts to dominate and the index curve exhibits a minimum. The higher heating rates varied from 7.1°C/min to 7.8°C/min and as a consequence the start of the isothermal cure begins earlier in the cure cycle; this explains the differences between the minima location between tests. At this time the resin has reached thermal equilibrium and the isothermal cure datum can be assumed. It is clear from the results that there is a measurable difference between results at 833nm and 1581nm and this may be attributed to the dispersion properties of the resin.

4.4.3.2 HX 8552

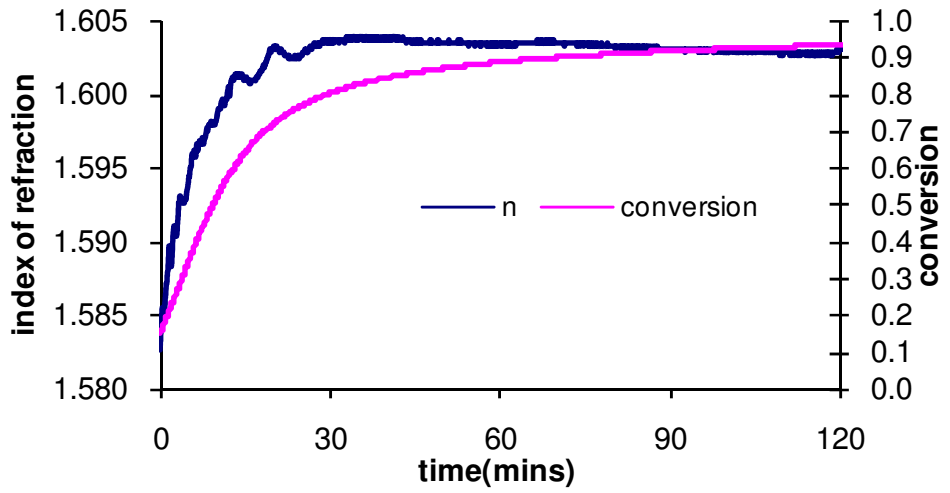

Figure 4.27 HX 8552 refractive index response at 1581nm and cure kinetics model for isothermal cure at 180°C for 2 hours.

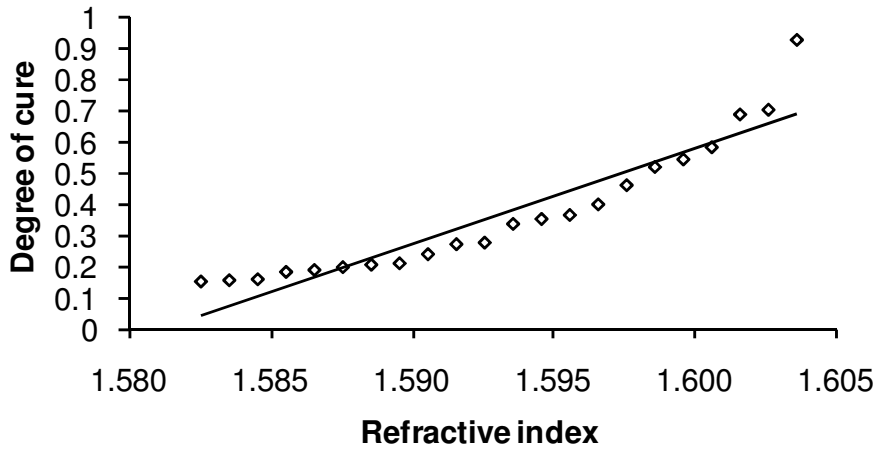

Figure 4.28 HX 8552 correlation of refractive index response at 1581nm and cure kinetics model for isothermal cure at 180°C for 2 hours.

Figure 4.27 shows a cure cycle for the Hexcel 8552 resin. The refractive index change during the isothermal cure at 180°C was measured at 1581nm. The tests reveal a significant amount of noise on the signal when compared with the measurements of the MY750 resin. As a result there is a poor correlation with the cure model as shown in figure 4.28. The explanation for this apparent noise may be attributed to the high volatile content of the resin. The resin requires degassing to remove volatiles generated during mixing with the hardener [1]. Attempts were made to de-gas the sample heating the samples at low temperatures to allow the gasses to pass through the sample; these proved unsuccessful. Volatiles are also generated during cure as by products of the reaction. These volatiles escape and move through the sample. It is safe to assume that they may cause erroneous signals to be generated at the fibre tip. This volatile noise affects the calculation of the refractive index measurements. Figure 4.29 provides evidence of this effect. The figure shows a SEM (scanning electron microscope) photograph of the fracture surface of a sample of cure Hexcel 8552 resin. Trapped volatiles are shown as voids in the fracture surface and are of a similar dimension to that of the fibre.

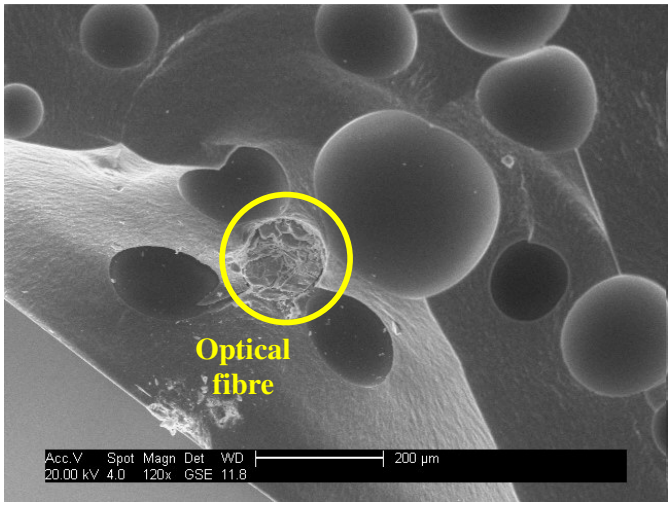

Figure 4.29 Fracture surface of HX 8552 post cure at 120 times magnification. The fracture tip of the Fresnel fibre is evident with trapped volatiles exhibited as voids of the same dimensional order to that of the fibre.

As a comparison, figure 4.30 shows the fracture surface of a sample of MY750 resin. This resin is a solvent free resin [1] and hence free of organic volatiles that are present in the other two resin systems discussed here. A smooth surface is apparent and the figure does not show signs of trapped volatiles [18,19]. This may explain the lack of noise on the Fresnel refractometery signal.

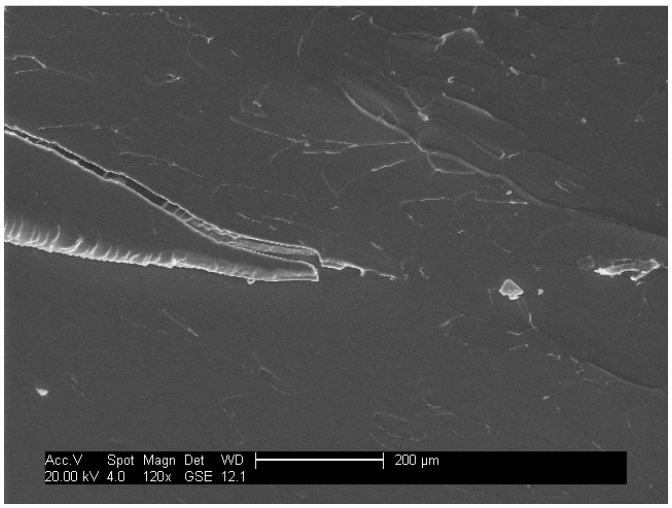

Figure 4.30 Fracture surface of MY 750 post cure. Small fracture fissures are evident but there is no sign of void formation due to trapped volatiles.

4.4.3.3 MTM44

Shown in figure 4.31 is the refractive index change of MTM44 resin during isothermal cure, measured using a Fresnel refractometry system operating at 1581nm. The results reveal a complicated pattern of refractive index change over the entire cure process. The refractive index response shows an apparent noisy signal up until 30 minutes, after which time the signal appears to reduce in noise content. The refractive index variation during cure does not appear to correlate linearly with the cure conversion model, figure 4.32. This may indicate a more complex reaction process.

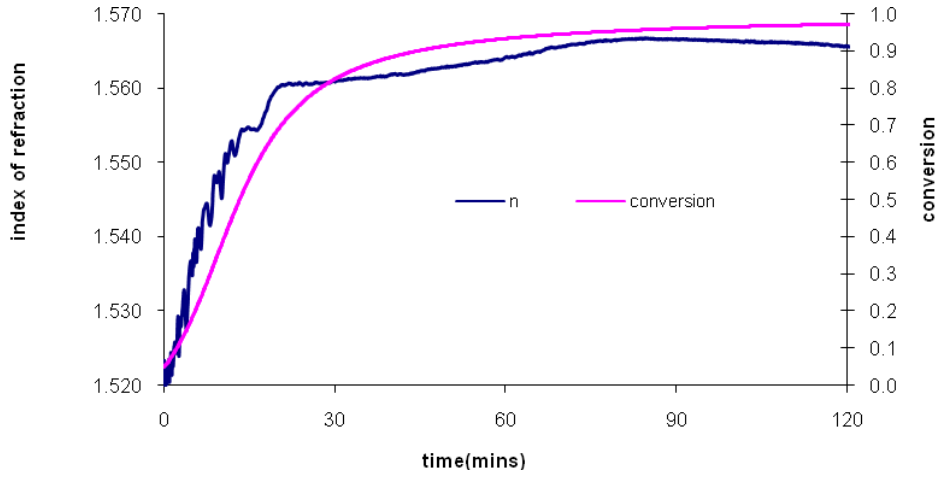

Figure 4.31 MTM 44 refractive index response and cure kinetic model for isothermal cure at 1581nm

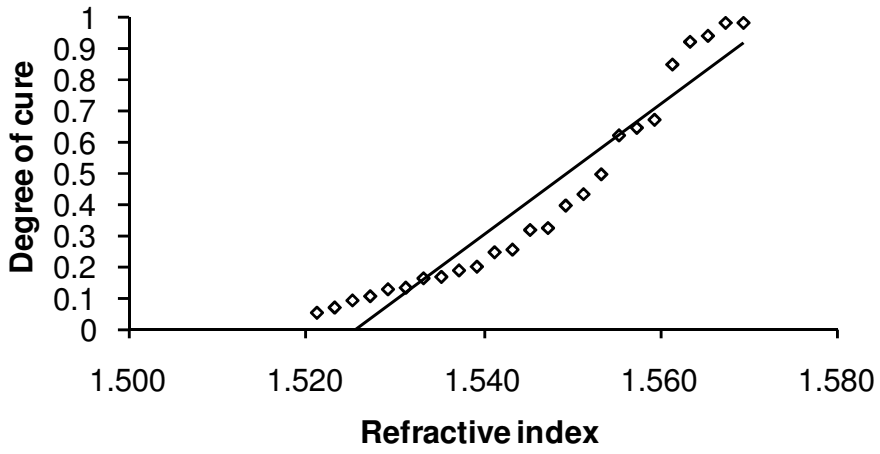

Figure 4.32 MTM 44 correlation of refractive index response at 1581nm with isothermal cure kinetics model.

DSC analysis for dynamic cure of mtm-44 reveals this to be the case, figure 4.33 [1]. The analysis clearly shows two reaction peaks which may be attributed to two or more reaction schemes [1].

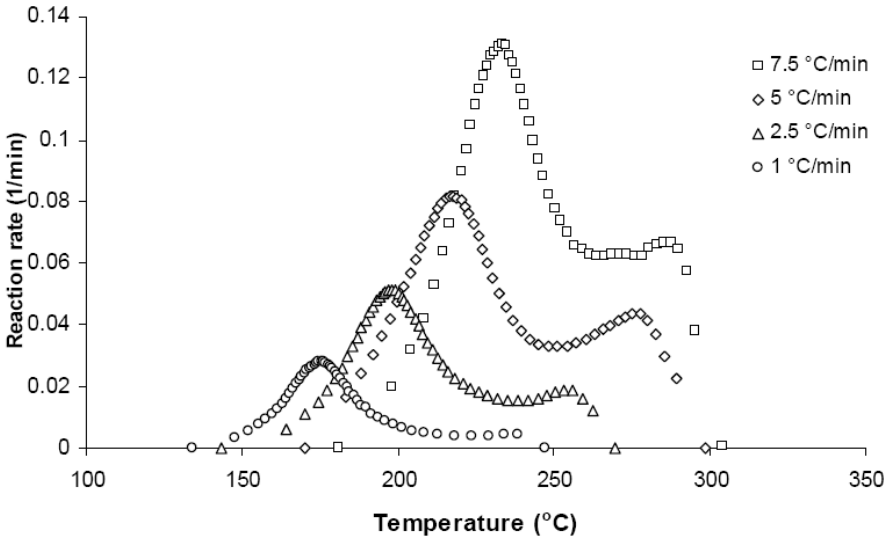

Figure 4.33 MTM 44 reaction rate with temperature for dynamic cure analysis using DSC.

Figure 4.34 reveals more information that may provide clues as to the origin of the complex refractive index response. The resin system contains a thermoplastic that phase separates from the thermoset for a specific conversion [1]. These phases will undergo different cure reactions and result in different by products during the cure. It may be surmised that, as the phase separated areas are of a similar order of magnitude in size to that of the fibre core, the exact location of the fibre tip is important in order to understand the nature of the refractive index change being measured. Therefore the noise on the refractive index measurements may be attributed to the phase separation at the fibre tip because the Fresnel reflections at the fibre/thermoplastic interface will be different to those from a fibre/thermoset interface.

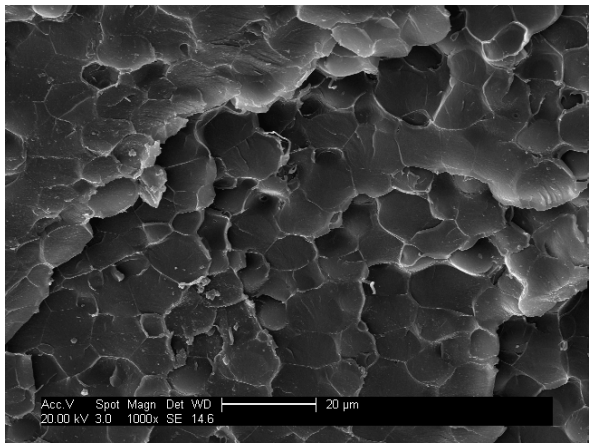

Figure 4.34 Fracture surface of MTM 44 post cure at 1000 times magnification. The resin is a mixure of thermoset and thermoplastic. The phase separation is evident as 'island' like structures in the picture.

On a macroscopic level, further evidence as to the origin of the noisy signal is indicated in figure 4.35, where the fibre is shown clearly protruding from the surface of a sample fracture. Large bubbles are shown which may be attributed to volatile out gassing during the initial stages of cure at low viscosity levels.

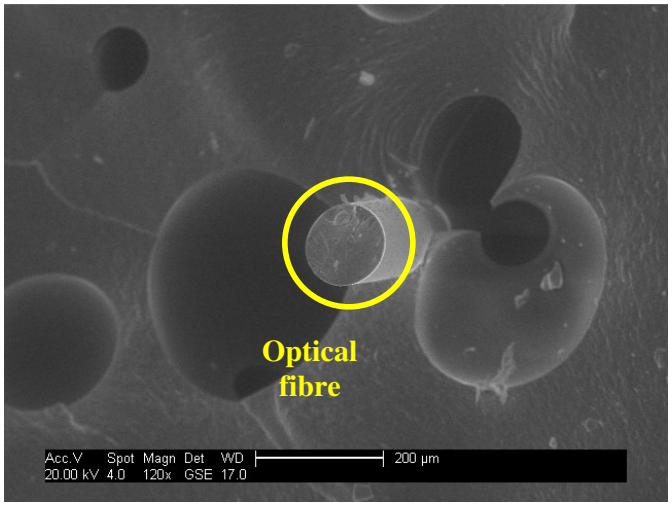

Figure 4.35 Fracture surface of MTM 44 post cure at 120 times magnification. The fracture tip (circled) of the Fresnel fibre is protruding from the surface. Evidence of trapped volatiles of the same dimensional order of the fibre is also visible.

Figure 4.36 shows two repeated refractive index measurements of the resin during cure. Both measurements indicate a significant amount of noise from about 5 minutes to 20 minutes during the initial stages of cure.

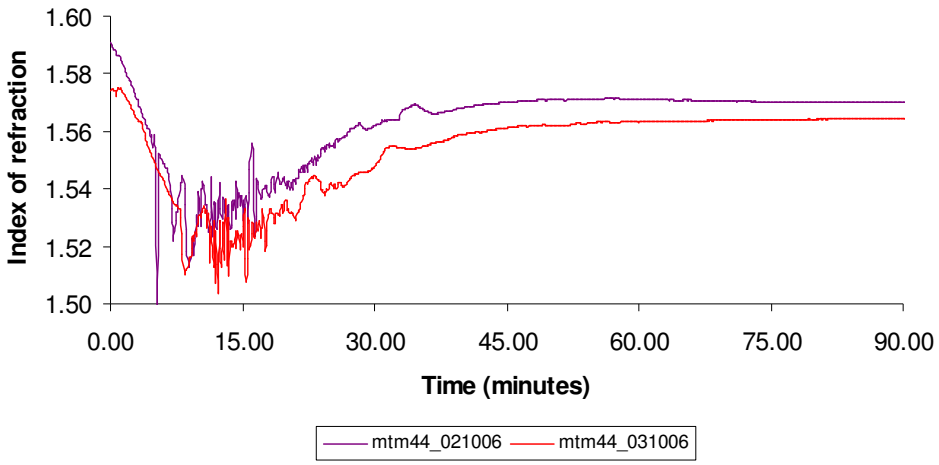

Figure 4.36 Multiple cure samples of MTM 44 showing refractive index response measured using the Fresnel refractometer at 1575nm. The test dates are shown in the legend. The initial noise phase (<30 minutes) may be attributed to the phase separation of the resin and out gassing effects.

As yet there is no published work that directly relates the refractive index change to the degree of cure. Lam and Afromowitz [20] propose that the change in the refractive index of an epoxy is linear with respect to cure up until the gelation point, beyond which the formation of a giant macromolecule and local viscosity impedes shrinkage in volume of the sample and thus the linearity assumption is no longer valid.

4.5 LPG based measurements of composite resins

Fresnel techniques for the measurement of a resin during cure provide a simple and effective method for single point cure monitoring. LPGs have a longer gauge length and also offer the possibility for multi-parameter sensing, e.g. strain and temperature. The effective use of LPGs however is restricted to fibres of indices similar to that of the resin being monitored, in order to access the high sensitivity region of the LPGs refractive index response. The application of an LPG for cure sensing was demonstrated using an ultraviolet cure epoxy resin and is discussed in section 4.3. For measurements of refractive index far removed from that of the cladding of the fibre the response of an LPG is poor. A demonstration of an LPG cure sensor in silica fibre for resins of high refractive index is discussed briefly here. In this case the high index resin used was MTM 44 because of its high measured refractive index.

4.5.1 Experimental setup

The experimental setup is shown in figure 4.37. Two LPG sensors of 40mm in length with a 400μm period were placed in a PTFE (Polytetrafluoroethylene) test well.

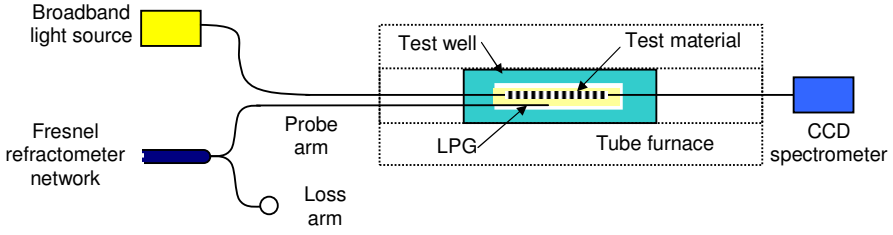

Figure 4.37 Experimental setup for cure monitoring of a resin using an LPG.

One of the LPGs was immersed in the test resin whilst the other was surrounded by air in order to act as a reference. Each of the LPGs were illuminated with a tungsten halogen broadband light source and interrogated using an Ocean Optics S2000 CCD spectrometer. A Fresnel refractometer operating at a wavelength of 1581nm was also used to determine the change in refractive index during an isothermal cure.

4.5.2 Results

The results presented in figure 4.38 show the wavelength response of the bands that exhibited the highest refractive cure response of the LPG sensors in the curing MTM 44 and in air. In this case these were the fifth attenuation bands which correspond to the coupling to the LP05 cladding mode at 900nm. A significant level of noise is shown to affect the signal during the isothermal cure stage. It is clear however that the band does exhibit a wavelength shift in response to the changing refractive index. The reference LPG exhibits a flat response from about 20 minutes which corresponds with the temperature fluctuations measured using a thermocouple. The attenuation band that corresponds to the LPG in the resin however continues to show a positive wavelength shift with increasing refractive index. As was shown in chapter 3, section 3.3.3, the refractive index sensitivity of an LPG is high when the medium surrounding an LPG has a refractive index that approaches that of the cladding [21]. To extend the measurement range to refractive indices higher than that of the cladding, it is necessary to exploit the refractive index dependence of the extinction ratio of the LPG attenuation bands to the external refractive index. For surrounding refractive indices higher than that of the cladding, leaky modes associated with Fresnel reflection at the glass/surround interface are evident as attenuation bands with a slightly longer wavelength and a reduced extinction ratio. These attenuation bands show a very weak wavelength sensitivity to changes in refractive index greater than that of the cladding, but the extinction ratios have been shown to increase as the surrounding refractive index increases beyond that of the cladding [21]. However it may be expected that as the LPG is operating in the poor sensitivity region, where the refractive index is higher than that of the cladding, the wavelength shift is positive for increasing refractive index [21].

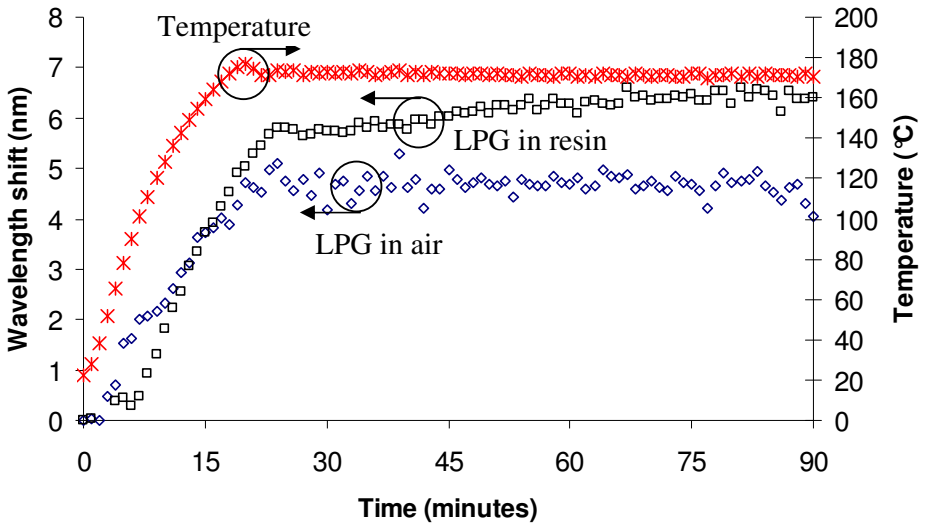

Figure 4.38 MTM 44 LPG wavelength response for isothermal cure at 1550nm

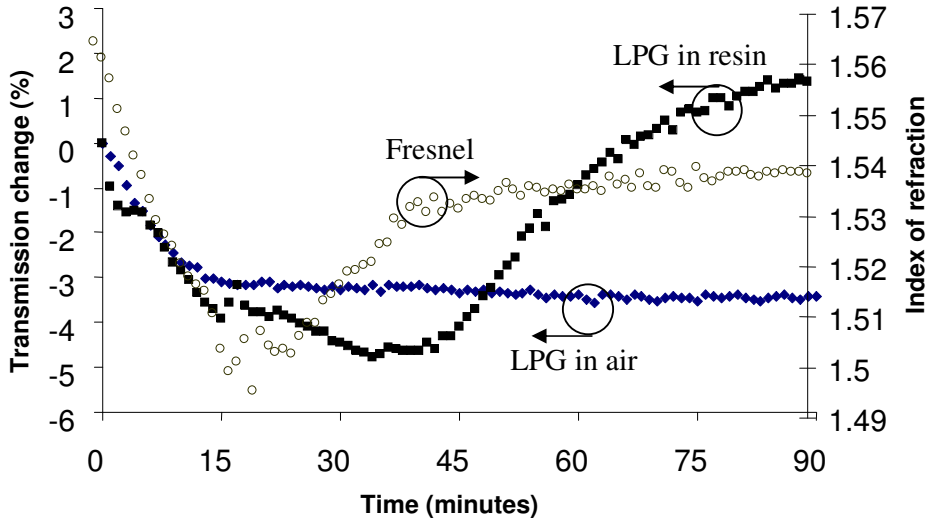

Figure 4.39 MTM 44 LPG transmission response for isothermal cure at 1550nm

As discussed previously the attenuation bands exist because of coupling to leaky modes. These modes have loss characteristics determined by Fresnel reflections at the cladding and surround interface. As a result it is possible to monitor the refractive index change during cure by monitoring the change in transmission loss of an attenuation band and this is demonstrated in figure 4.39. After about 20 minutes, the attenuation band of the

reference LPG shows no appreciable change in transmission. The Fresnel refractometer signal is noisy during the early stages of the cure, which may be due to the presence of volatiles as discussed in section 4.4.3.3 [19].The band for the LPG in resin however shows a decrease in transmission before reaching a minimum at around 40 minutes. This is followed by a gradual increase in transmission before flattening. What is interesting to note here is the difference between the amplitude minima of the LPG band (~40 minutes) and that of the Fresnel measurement (~20 minutes). The Fresnel measurements seem to show a distinct change in the rate of the reaction at 40 minutes and this coincides with the minima of the LPG sensor. Rheological measurements were made to detect the approximate gelation time, this is the time at which the resin changes from a liquid to a rubbery or gel like state. The measurements detect the change in viscosity of a sample during cure and reveal that a sudden increase in viscosity occurs at a specific time corresponding to the gelation time. Figure 4.40 show the results for rheological measurements for three different isothermal cure cycles [1]. For an isothermal cure at 180°C, the gelation time occurs at 20 minutes.

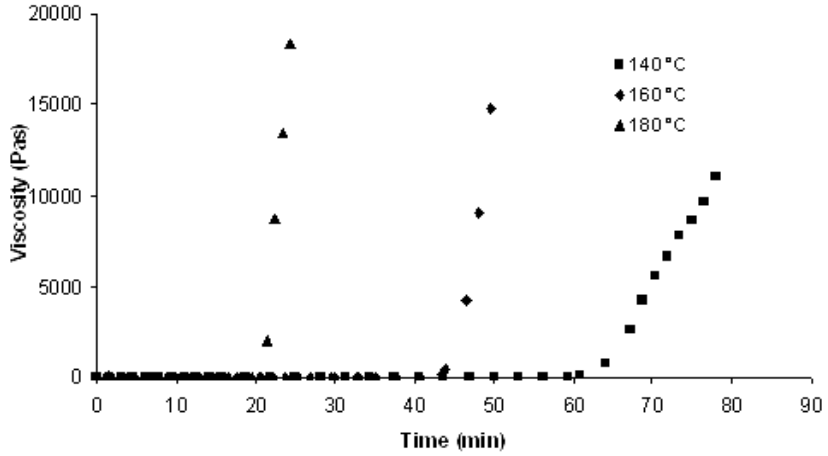

Figure 4.40 Rheological measurements on mtm-44 for isothermal cure

This coincides with the Fresnel and LPG measurement inflexion point. The change in extinction ratio of the LPG attenuation band also shows good correlation with cure conversion for the latter stages of the cure, calculated from the cure kinetics model. This is illustrated in figure 4.41.

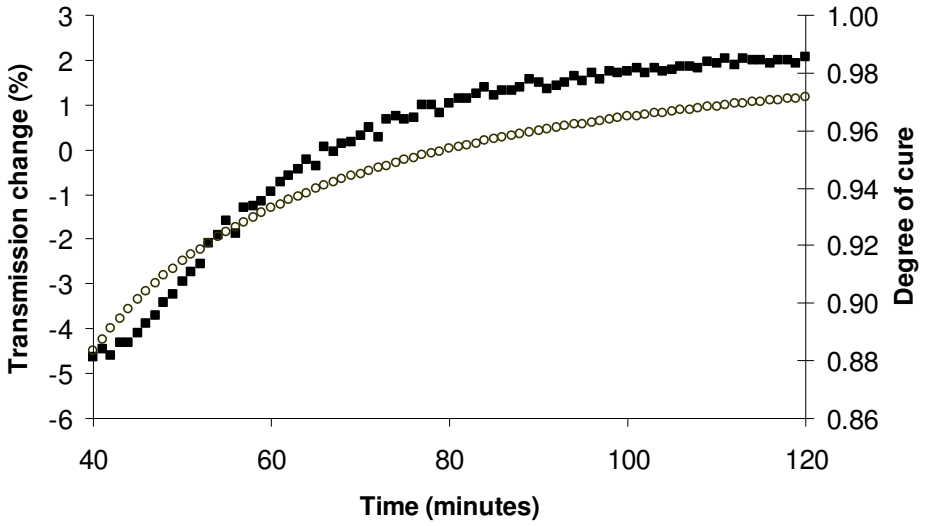

Figure 4.41 Extinction ratio (■) of the 5th attenuation band of a 650nm cut-off fibre, 400mm period LPG of 40mm length and refractive index change (○) measured with a Fresnel refractometer at 1581nm.

As discussed previously, the analysis of the resin details a very complex reaction mechanism with multiple reaction schemes. The LPG band may be responding to changes in refractive index corresponding to the different reactions and may indicate the phase separation point where the resin is no longer homogenous but separated into a thermoplastic and thermoset. An SEM photograph of the cured resin is shown in figure 4.42 and shows the phase separation between the thermoset and thermoplastic. Further work is needed to investigate the response of LPG sensors to complex non-homogenous resin systems.

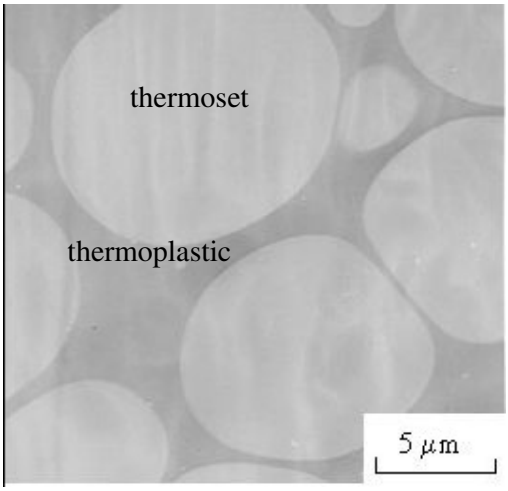

Figure 4.42 Phase separation of thermoset and thermoplastic in cured MTM 44 [1].

4.6 Summary

The application of LPGs for the purpose of cure monitoring was demonstrated with a UV cured epoxy system. The resin had a refractive index similar to that of the cladding of the fibre and this enabled the sensor to work within the high sensitivity region of the LPGs response to refractive index change. For comparative purposes two Fresnel refractometers were constructed and demonstrated to measure the change in refractive index of a resin during cure at 833nm and 1581nm. These wavelengths were chosen, firstly, to make use of relatively inexpensive optical components, e.g. CCD spectrometers, at 833nm and secondly to compare the results with more typical FBG techniques at 1550nm. The results were compared with the LPG data and showed very good agreement for the UV cured epoxy. The Fresnel refractometer was used to measure the change in refractive index of structural resins which have a refractive index above that of the cladding of the fibre. The point sensing capability of such a technique using an optical fibre may provide a simple method of accessing cure information from composite resin systems at specific locations in composite components. Although LPGs require a host fibre to have a matching refractive index to that of the resin, experimental evidence has shown a sensitivity to refractive index change both in terms of wavelength shift and transmission change.

4.7 References

1. Dimopolous A. (2008). Effect of carbon nanotubes on epoxy (Unpublished PhD Thesis), Cranfield University, Cranfield, UK.
2. Kazilas, M.C. and Partridge, I. K. (2005), 'Exploring equivalence of information from dielectric and calorimetric measurements of thermoset cure—a model for the relationship between curing temperature, degree of cure and electrical impedance', *Polymer*, 46, p. 5868.
3. Woederman, D. L. Spoerre, J. K. Flynn K. M. and Parnas R. S. (1997), 'Cure monitoring of the liquid composite molding process using fiber optic sensors', *Polymer Composites,* 18, p.133-150.
4. Epoxy Technology, http://www.epotek.com
5. Hecht, E. And Zajac, A. (1977), Optics (2nd Edition), Addison-Weley Publishing Company, New York, USA.
6. Born, M. And Wolf, E. (1959), Principles Of Optics, Cambridge University Press, Cambridge, UK.
7. Kim, C. B. and Su, C. B. (2004), 'Measurement of the refractive index of liquids at 1.3 and 1.5 micron using a fibre optic Fresnel ratio meter', *Measurement Science and Technology,* 15, p.1683-1686.
8. Li T. and Tan X. (1993), Stepwise interferometric method of measuring the refractive index of liquid samples, *Applied optics,* 32(13), p.2274-77.
9. Boey, F., Rath, S. K., Ng, A. K., Abadie, M. J. M. (2002), 'Cationic UV Cure Kinetics for Multifunctional Epoxies', *Journal of Applied Polymer Science*, 86, p. 518–525.
10. R. B. Prime, "Differential Scanning Calorimetry of the epoxy cure reaction," Poly. Eng. Sci. 13, (5) 365-371 (1973).
11. Bandar, U. (1986), 'A systematic solution to the problem of sample background correction in DSC curves', *Journal of Thermal Analysis,* 31, p. 1063.
12. Maffezzoli, A., Trivisano, A., Opalicki, M., Mijovic J. and Kenny J. M. (1994), 'Correlation between dielectric and chemorheological properties during cure of epoxy-based composites', *Journal of Material Science*, 29, p. 800-808.

13. Mijovic, J., Andjelic, S., Fitz, B, Zurawsky, W., Mondragon, I., Bellucci, F., Nicolais, L. (1996), 'Impedance Spectroscopy of reactive polymers. 3. Correlations between dielectric, spectroscopic and rheological properties during cure of a trifunctional epoxy resin', *Journal of Polymer Science: B: Polymer Physics,* 34, p. 379–388.

14. Skordos, A. A. and Partridge, I. K. (2004), 'Determination of the degree of cure under dynamic and isothermal curing conditions with electrical impedance spectroscopy', *Journal of Polymer Science: B*, 42, p. 146-154.

15. Chehura, E., Skordos, A. A., James, S. W., Partridge, I. K. and Tatam, R. P. (2005), 'Strain development in curing epoxy resin and glass fibre/epoxy composites monitored by fibre Bragg grating sensors in birefringent optical fibre', *Smart Materials and Structures,* 14, p. 354-362.

16. Skordos, A. A. And Partridge, I. K. (2001), 'Cure Kinetics Modelling Of Epoxy Resins Using A Non-Parametric Numerical Procedure', *Polymer Engineering And Science*, 41(5).

17. Cusano, A., Breglio, G., Giordano, M., Calabro, A., Cutolo, A., and Nicolais, L. (2000), 'An Optoelectronic Sensor for Cure Monitoring in Thermoset-based composites', Sensors and Actuators, 84, p. 270-275.

18. Pearce, P.J., Arnott, D.R., Camilleri, A., Kindermann, M.R., Mathys, G.I., Wilson, A.R. (1998), 'Cause and effect of void formation during vacuum bag curing of epoxy film adhesives', *Journal of Adhesion Science and Technology,*12(6), p. 567-584.

19. Yue, C. Y. (1988), 'Differential Scanning Calorimetric Determination Of The Volatile Content And Properties Of Epoxy Prepreg', *Journal of Materials Science Letters*, 7(8), p. 811-813.

20. Lam, K.-Y. and Afromowitz, M.A (1995), 'Fiber-optic epoxy composite cure sensor. I. Dependence of refractive index of an autocatalytic reaction epoxy system at 850 nm on temperature and extent of cure', Applied Optics, 34(25), p. 5635-8.

21. Patrick, H. J., Kersey, A. D., and Bucholtz F. (1998), 'Analysis of the Response of Long Period Fiber Gratings to External Index of Refraction', *Journal of Lightwave Technology,* 16, p. 1606-1612.

Advanced optical fibre monitoring techniques

5

5.1 Introduction

The investigation of alternative techniques for monitoring the cure of resins is discussed in this chapter. Two methods are introduced and discussed in the first part of this chapter and are variations of the LPG sensor; chirped LPGs are proposed for flow measurement and cascaded gratings are considered for cure monitoring with the aim of increasing sensitivity, and of potentially multiplexing the sensor elements.

The multi-parameter sensing capability of the LPG sensor could offer a means of measuring both resin flow and cure development. This is explored through the exploitation of the properties of a chirped LPG in section 5.2. Section 5.3 demonstrates the use of interferometric methods with LPGs, detailing the results of experimental work with cascaded LPGs. Cascaded LPGs offer several advantages over single LPG sensors. Firstly, they exhibit very high sensitivities to measurands and have been demonstrated as sensors to detect external refractive index [1], temperature and transverse load [2] and bending [3]. Secondly they can be multiplexed [4] and thus provide a distributed sensing capability.

Section 5.4 details a different type of core to cladding mode coupler, a tilted fibre Bragg grating (TFBG). A TFBG acts to couple light between the core mode and backward propagating cladding modes. The cladding modes interact with the surrounding environment and the effect of this has been exploited in recent publications with the TFBG devices used as band rejection filters [5], optical spectrum analyzers [6], fibre polarimeters [7] and, recently, as sensor elements [8, 9].

5.2 A long period grating based directional flow sensor

5.2.1 Introduction

The refractive index response of an LPG has been exploited to develop chemical concentration sensors [10], bio-sensors [11], flow sensors [12] and has been used to demonstrate a liquid level sensor [13]. Khaliq *et al* [13] demonstrated the use of a uniform period LPG as a liquid level sensor by monitoring the change in the transmission spectrum when the LPG was partially immersed in a liquid of refractive index lower than that of the cladding. The LPG attenuation bands were observed to split as a different phase matched resonant condition existed for the section of the fibre immersed in the liquid as compared to the section in air. The relative transmission depth for the split attenuation bands was shown to be a function of the proportion of the LPG immersed in the liquid. Here the concept of the LPG based liquid level sensor is developed further by demonstrating a sensor which also provides information on the direction of immersion, by exploiting the properties of a chirped LPG.

5.2.2. Chirped long period gratings

A chirped long period grating [14] has a periodicity that varies as a function of axial position along the length of the LPG. This results in a broadening of the attenuation bands and a decrease in their extinction, compared with that of a LPG of uniform period. The spectrum of a chirped LPG may be explained by considering it as a composite of separate LPGs of different periodicities. A representation of this is shown

in figure 5.1. The LPGs of different period Λ_1, Λ_2, and Λ_3 all form attenuation bands of differing central wavelengths given by equation 3.11 but repeated here as 5.1.

$$\lambda^i = \left[n_{eff} - n^i_{clad}\right]\Lambda \qquad 5.1$$

A composite band results from a superposition of all three bands as shown in figure 5.1 (a), this is a schematic of the broadening effect of a chirped LPG. The reduction in attenuation may be understood from the expression for the transmission minimum, T_i, of an LPG attenuation band given by [15]

$$T_i = 1 - \sin^2(\kappa_i L) \qquad 5.2$$

where κ_i is the coupling coefficient of the i^{th} cladding mode and L is the length of the LPG. T_i is shown to have a sine squared dependency on length. Considering the composite representation of a chirped grating, it is clear that chirping an LPG causes the attenuation bands to broaden. Furthermore, if each individual LPG has an associated length that is inherently less than the overall length, it may be expected that the overall transmission depth of a composite band is less than that of a non-chirped LPG.

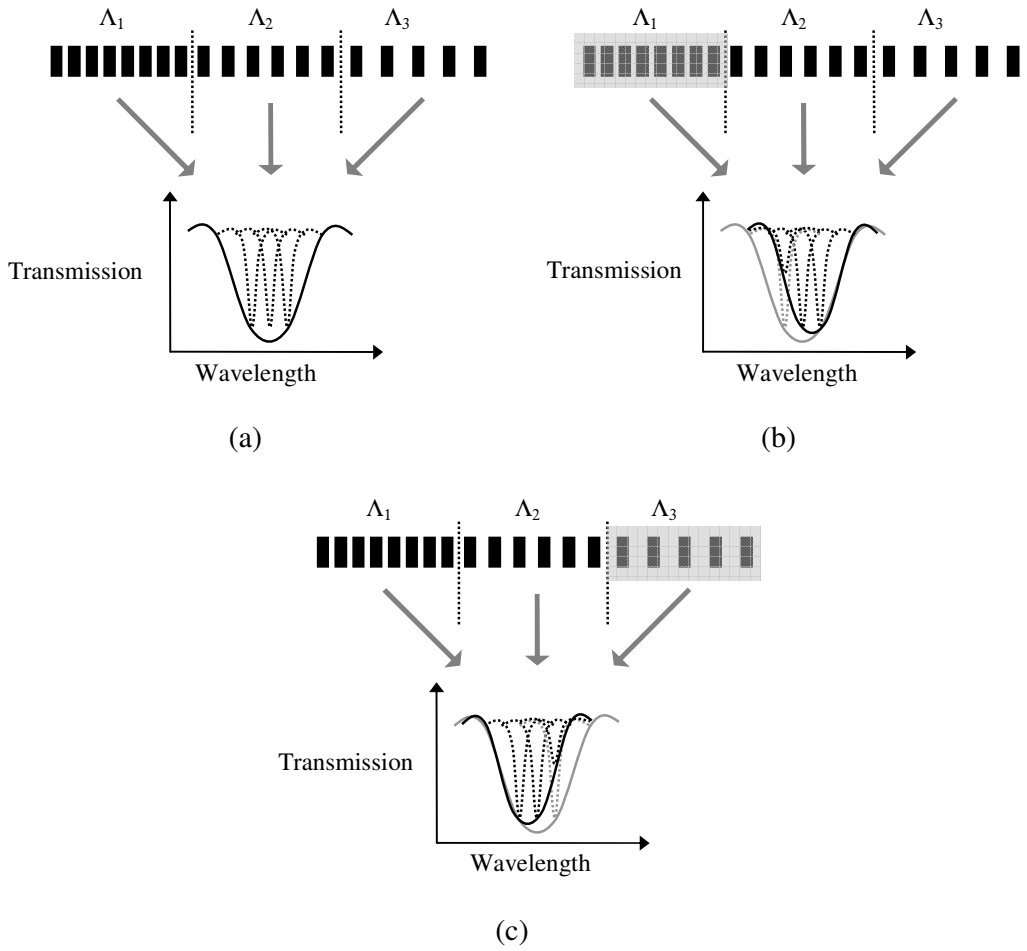

Figure 5.1 Simplified representation of a chirped LPG; (a) shows the composite band formed from the three different period LPGs, (b) the effect of covering the section of the LPG of period, Λ_1, (c) of covering the section of the LPG with a period of Λ_3.

If a section of the LPG is covered with an oil of refractive index higher than that of the cladding, e.g. the section of period Λ_1 as illustrated in figure 5.1 (b), the composite band experiences a reduction in the attenuation depth and a positive wavelength shift of the lower wavelength edge. This is because the LPG is operating in the low sensitivity region of the refractive index response curve, as discussed previously in section 3.3.3. The reduction in attenuation is due to the low coupling efficiency to leaky cladding modes [16]. The wavelength shift for high refractive index materials is negligible and in this case is ignored. The overall result is of a narrowing of the composite band from the lower wavelength side. The expected result for a similar covering of section Λ_3 is

shown in figure 5.1 (c). It exhibits a narrowing of the composite band however in this case it is from the longer wavelength side. This demonstrates the potential for the use of such devices as directional flow sensors.

5.2.3 Experiment

An LPG of length 40 mm was fabricated in hydrogen loaded single mode fibre with a cut off wavelength of 650nm (Fibercore SM750). The point by point method was used to create a small chirp to the period of the LPG. The chirp rate was chosen to ensure there was a broadening to the LPG band whilst maintaining a discernible band profile for ease of analysis. The fibre was placed behind a Vernier calliper with a fixed slit width of 200μm that was illuminated by a UV laser beam at a wavelength of 266nm, provided by a frequency quadrupled Nd:YAG laser. A computer controlled translation stage was used to move the fibre behind the slit to create a linearly chirped period that varied in the range 395μm to 405μm. The LPG was subsequently annealed at 100°C for 24 hours to ensure that the hydrogen had diffused out and that the spectrum was stable [17].

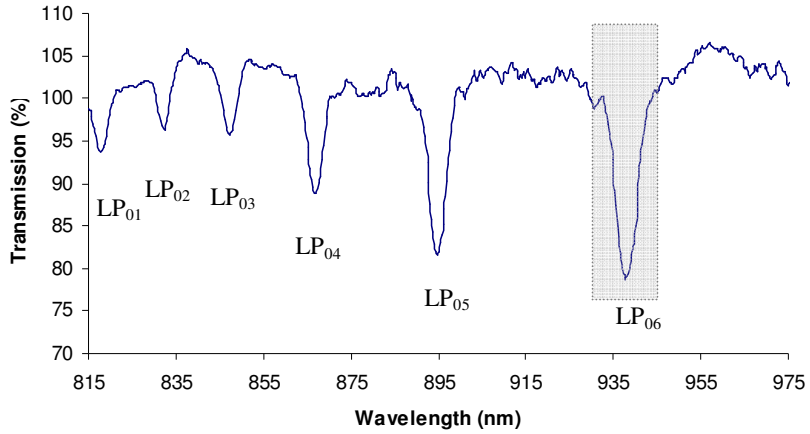

(a)

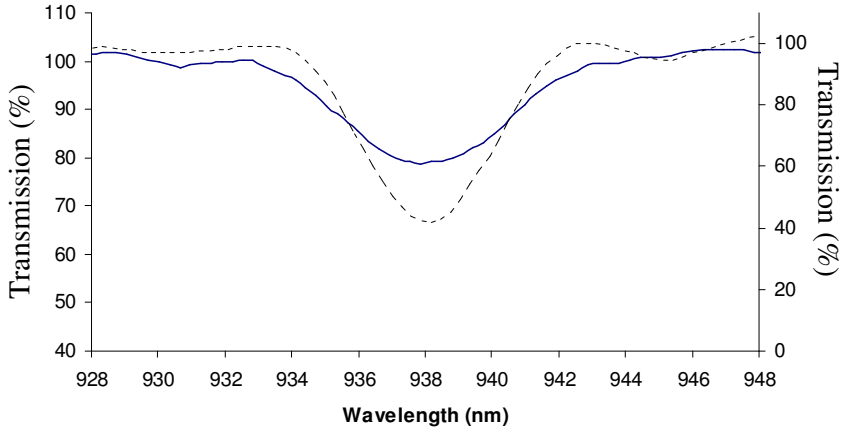

(b)

Figure 5.3 Transmission spectrum of a chirped LPG of length 40mm and linearly chirped period 395µm - 405µm, fabricated in Fibercore SM750. The band coupled to the LP_{06} cladding mode is highlighted and shown compared with a band in the same spectral location (b) of an LPG of uniform period 400µm (dashed).

The transmission spectrum of the chirped LPG, shown in figure 5.3, was monitored by coupling the output from a tungsten-halogen white light source into the fibre and coupling the transmitted light to a CCD spectrometer (OceanOptics S2000) with a resolution of 0.3nm. The experimental setup is shown in figure 5.4 (a). A feed syringe allowed a test syringe, graduated with 0.01ml marks, to be gradually filled with a Cargille refractive index oil of refractive index 1.56 ± 0.0002. The fibre was held in

place with rubber grommets to prevent the fibre from bending, which is known to distort the transmission spectrum [18]. The rubber grommets also provided a seal to ensure that there was no loss of liquid. The needle from the feed syringe was placed close to the wall of the test syringe to ensure there was no contact between oil and LPG before the oil reached the bottom of the test syringe. The experiment was repeated with the orientation of the chirp reversed to simulate the effect of the liquid flowing over the LPG from the opposite direction, as illustrated in figure 5.4 (b).

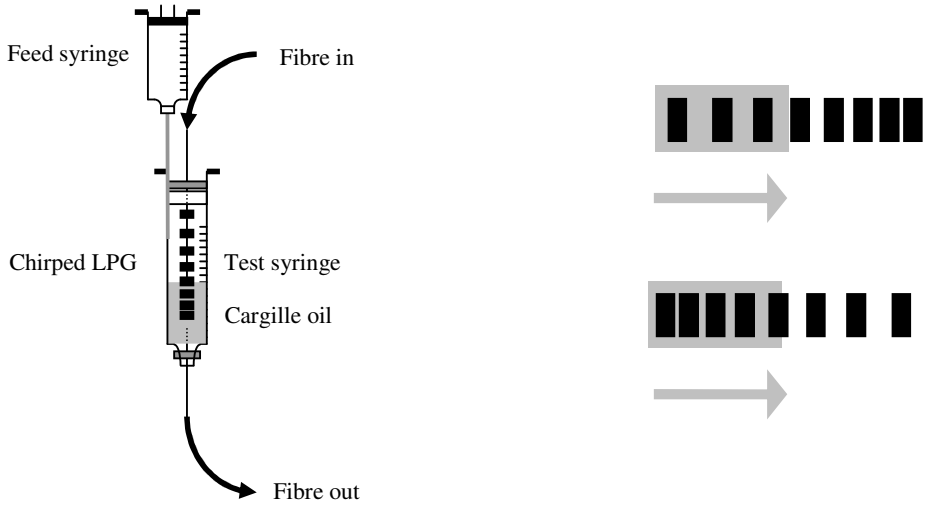

(a) (b)

Figure 5.4 Experimental setup for the investigation of a chirped long period grating flow sensor (a) and layout of chirped LPG for flow sensing, arranged with decreasing and increasing period relative to oil flow (b).

5.2.4 Results

As the test syringe was filled with the Cargille oil, the transmission spectrum of the LPG was recorded for each 2.7mm (due to each 5ml drop from the feed syringe) increment in the depth of the oil. Figure 5.5 shows the response of band 6 to the gradual immersion of the LPG in the oil for the different experiment orientations. With the LPG oriented with decreasing period relative to the oil level, experiment 1, (a), an apparent negative wavelength shift is measured.

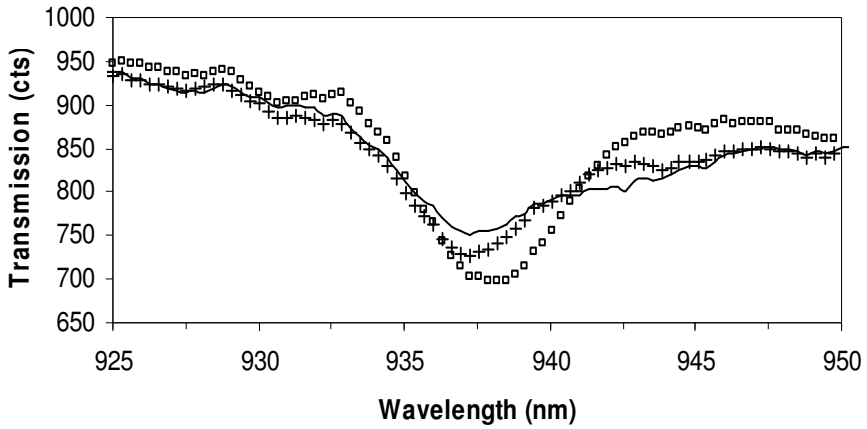

(a)

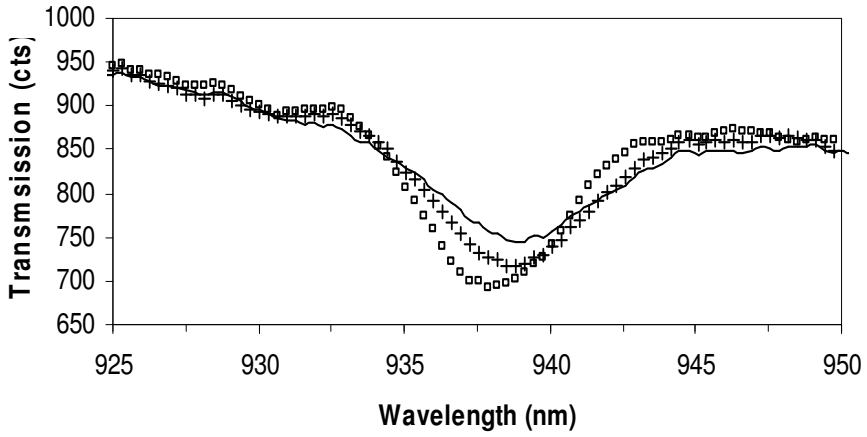

(b)

Figure 5.5. Change in shape of band 6 for gradual immersion in 1.56 Cargille index oil. Experiment 1 (a) and experiment 2 (b). 0% is no coverage, 50% half and 100% total coverage of 40mm grating length. □ - 0%, + - 50%, ─ - 100%.

This is caused by a reduction of the extinction at longer wavelengths due to the cladding/oil structure of the covered section no longer supporting propagating cladding modes. This agrees well with the discussion of section 5.2.2. The result for experiment 2 is shown in figure 5.5 (b) and an apparent positive wavelength shift is measured initially.

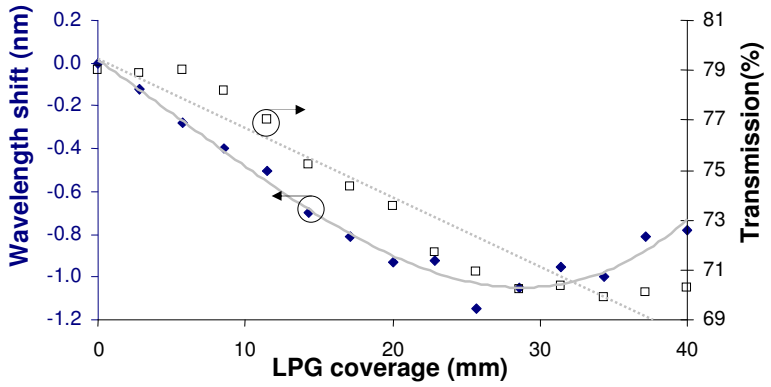

(a)

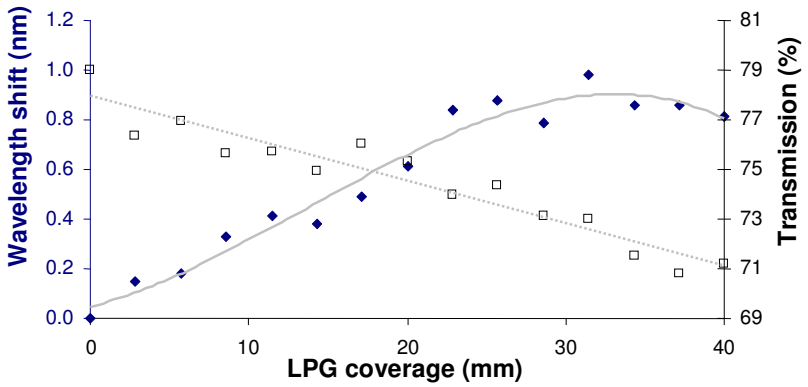

(b)

Figure 5.6 Wavelength shift (♦) of band 6 and transmission (□) against LPG coverage with Cargille index oil (1.56) for LPG arranged with decreasing period relative to direction of oil (a) and increasing period relative to direction of oil (b). The lines are shown only as a visual aid.

Figures 5.6 (a) and (b) show the wavelength shift of the central wavelength of attenuation band 6 and the associated minimum transmission value for each of the experiment orientations. The spectral location of the band minimum was calculated by fitting a 6^{th} order polynomial to the spectra. For both experiments, an apparent wavelength shift of approximately 1nm results, with directional information given by the direction of shift; experiment 1, (a), reveals a negative shift and experiment 2, (b), reveals a positive shift. The change in depth of the attenuation band provides no

directional information as would be expected with an 8% drop in attenuation for both orientations.

5.2.5 Discussion

The results presented in figures 5.5 and 5.6 show the wavelength shift and change in transmission of band 6 for the gradual immersion of the LPG in the Cargille oil. The apparent wavelength shift of the band is shown to be dependent on the direction of flow of the oil surrounding the fibre. The change in the extinction of the band is shown to have no directional dependence. When the LPG is fully immersed in the high index oil the cladding/oil structure no longer supports propagating cladding modes but leaky cladding modes exist due to Fresnel reflections from the cladding oil interface [15]. Coupling to such modes is weak when the index difference between the cladding and oil is small and results in attenuation bands with a poor extinction ratio [16]. The consequence of this and the broadening effect on the attenuation bands exhibited by chirped LPGs may contribute to errors in determining the wavelength of the band minimum. The measurement response indicates the possibility of using such sensor types for distributed sensing over the gauge length of the sensor.

5.2.6 Conclusion

A chirped LPG was demonstrated as a directional flow sensor with an oil of refractive index higher than that of the silica fibre. The central wavelength of an attenuation band is shown to have a directional dependence with immersion in the high refractive index oil.

5.3 Cure monitoring using a long period grating Mach-Zehnder interferometer

5.3.1 Introduction

The work presented in this section was completed with Dr. Richard Murphy, Engineering Photonics Group, Cranfield University.

When a pair of LPGs is written in series in an optical fibre, they form an in-fibre Mach-Zehnder interferometer (MZI), as illustrated in Figure 5.7 (a). This opens up the possibility of more sensitive measurements of refractive index change and multiplexing capabilities. The first LPG acts to couple a proportion of the propagating mode into the cladding. The cladding mode is re-coupled into the core by the second LPG, where it interferes with the core mode, introducing a sinusoidal channelled spectrum in the attenuation bands. The frequency of the channelled spectrum or fringe pattern in the spectrum of a cascaded LPG is determined by the separation of the LPGs. The phase is influenced by measurand-induced changes in the effective index of the cladding modes and the visibility is dependent upon factors such as the coupling efficiency of the LPGs and the cladding mode attenuation. Cascaded LPGs have been used to sense bending [3], external index of refraction [1,4], temperature and transverse load [2]. Here, an LPG based MZI is used to monitor the refractive index changes that occur during the cure of a UV cured epoxy resin (EpoTek OG-134).

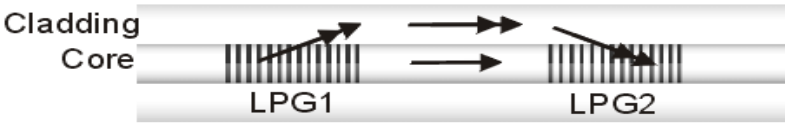

(a)

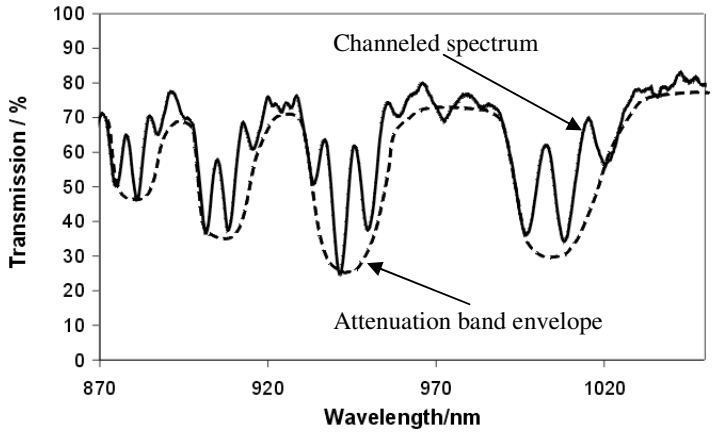

(b)

Fig 5.7 (a) Operation of cascaded LPGs as an MZI (b) channelled spectra in the attenuation bands [4].

5.3.2 Cascaded LPG theory

Assuming that the LPGs are identical, have a 3dB coupling strength, and that the attenuation of the cladding modes can be neglected, a channelled spectrum is imposed on the LPG spectra of a single LPG by the formation of an in-fibre Mach-Zehnder interferometer. An example of the channelled spectra is shown in figure 5.7. The transmission spectrum is given by [4]:

$$I = I_0(\lambda)\left(1-\cos\left(\frac{2\pi}{\lambda}(n_{eff\_core}-n^{i}_{eff\_clad})L+\Phi\right)\right) \qquad 5.3$$

$$\Phi = 2\tan^{-1}\left(\frac{\Delta\beta}{2s}\tan sd\right)-\Delta\beta d \qquad 5.4$$

$$\Delta\beta = \frac{2\pi}{\lambda}(n_{eff\_core}-n^{i}_{eff\_clad})-\frac{2\pi}{\lambda} \qquad 5.5$$

Where $I_0(\lambda)$ is the spectral form of the attenuation band envelope, n_{eff_core} and n_{eff_clad} are the effective refractive indices of the core and cladding modes, d is the grating length, L is the separation between the LPGs and s depends on the coupling coefficients and detuning parameter $\Delta\beta$, $s^2 = \kappa\kappa = (\Delta\beta/2)^2$. The channelled spectrum has a frequency content which is calculated by performing a Fourier Transformation of the intensity pattern to obtain a Fourier transformed spectrum, $F(I)$ an example of which is shown in figure 5.8. The Fourier transform is shifted to move the dc component of the array to the centre of the spectrum to aid visualisation (fftshift in matlab). The dc component is also truncated to aid visualisation. A real valued wavelength spectrum is transformed to a complex valued frequency spectrum containing phase information. One distinct peak is clearly visible on either side of the central DC peak. The amplitude of the DC peak is truncated in the interest of clarity. The side peaks represent the single frequency present in the induced fringe pattern, which is determined by the physical separation of the LPGs.

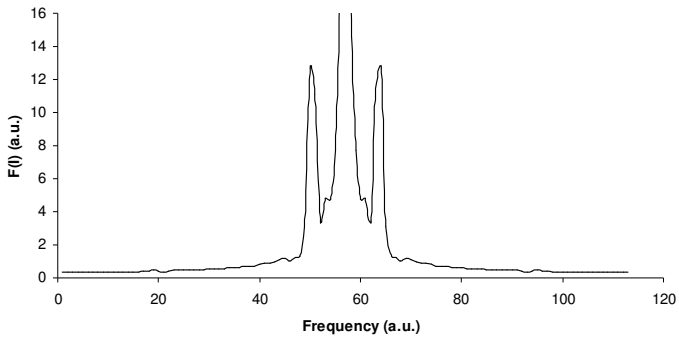

Fig 5.8 The Fourier transform of the intensity spectrum of an optical fibre containing a cascaded LPG MZI.

Phase information is calculated by taking the arc tangent of the real and imaginary components of the complex valued frequency spectrum, equation 5.6.

$$\Phi = \tan^{-1}\left[\frac{\Re(T(\omega))}{\Im(T(\omega))}\right] \qquad 5.6$$

Any change in refractive index or temperature results in a change in the effective refractive indices of the core and cladding modes. This appears as a change in the phase

of the fringe pattern, which may be determined using the methods discussed above [2,4]. Phase information obtained in this way is wrapped modulo 2π, resulting in discontinuities in the phase, which then require unwrapping to remove these discontinuities to produce a continuous measurement response.

5.3.3 Experiment

A Fresnel refractometer was used to provide an alternative measurement of the refractive index. The experimental configuration is shown in Figure 5.9. A refractometer operating at a wavelength of 833nm, as discussed in chapter 4 (section 4.2.3), was used for comparative measurements.

The cascaded LPG pair was fabricated in a hydrogen loaded single mode optical fibre with a cut-off wavelength of 650nm by UV exposure though a phase mask. The LPGs were each of length 20mm with a period of 400μm and were separated by 40mm.

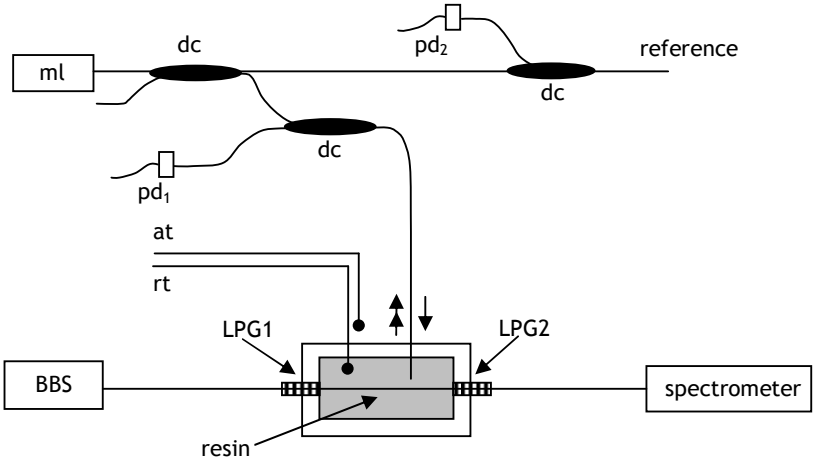

Fig 5.9 Experimental configuration. ml, modulated laser diode light source; pd, photodiode; dc, directional coupler; BBS, broadband source; LPG, long period grating; rt, thermocouple measuring the resin temperature; at, thermocouple measuring the ambient temperature.

A UV cured epoxy resin, EpoTek OG134, with an uncured refractive index of 1.4163 measured at 589nm [19], was used as the test resin. A UV lamp with an output power of 4W and with a spectral peak at 365nm was positioned to provide a fluence of

6.57mW/cm^2 in order to slow the cure reaction. Only the length of fibre separating the LPGs was immersed in the resin, as indicated in Figure 5.9. Thermocouples were placed to measure the resin temperature and ambient conditions. The cascaded LPG spectrum and the Fresnel reflection were recorded at 6 second intervals during the cure. The Fourier transform of the wavelength spectrum was analysed to yield the phase change.

5.3.4 Results and discussion

Figure 5.10 shows the calculated phase shift of the channelled spectrum during the 4 hour cure of the resin. This is compared with the measured refractive index change using a Fresnel refractometer. The measured phase shift showed a positive trend which concurred with the increase in refractive index during cure. The origin of the features at 35 minutes and 55 minutes are associated with small temperature fluctuations, as can be seen in Figures 5.12(a) and (b), where the temperature of the resin, monitored using a thermocouple, and the phase change are plotted on the same graph. The features in Figure 5.12 correspond to thermally induced refractive index changes. A decrease in temperature causes the resin to increase in refractive index due to the thermo-optic effect. This induces a positive phase shift [4] as the changing refractive index of the resin modifies the effective refractive index of the cladding mode. Importantly as the resin refractive index approaches that of the cladding there is an increased sensitivity to refractive index. This is accompanied by a decrease in the attenuation depth of the cladding modes, and an associated decrease in visibility, as shown in Figure 5.11.

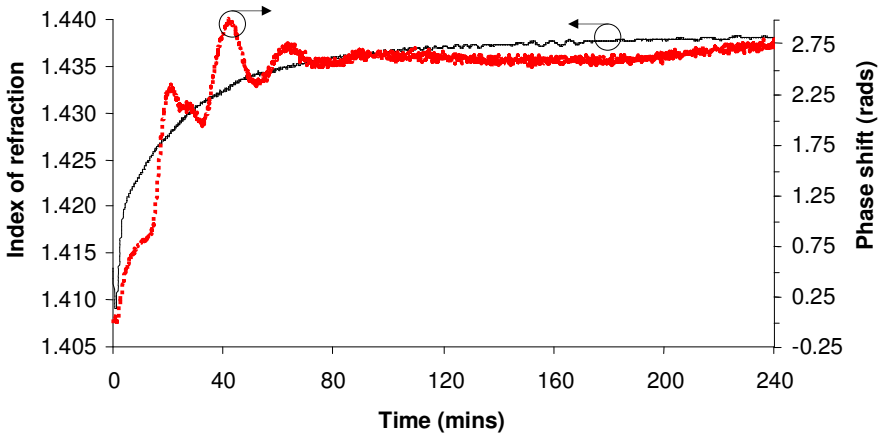

Fig 5.10 Phase shift of channelled spectrum (dashed) measured with LPG-MZI and Fresnel measured refractive index (solid) change during epoxy cure.

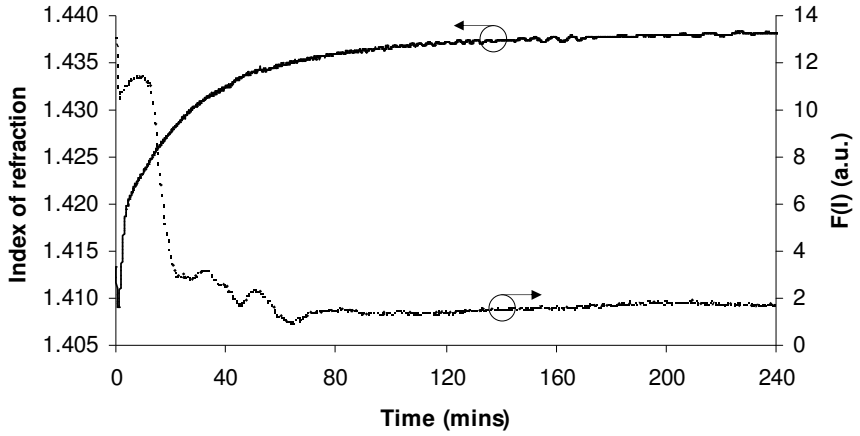

Fig 5.11 Frequency amplitude, F(I) (dashed) measured with LPG-MZI and Fresnel measured refractive index (solid) change during cure.

Figure 5.12 illustrates the potential for the use of an LPG MZI as a highly sensitive cure sensor. The exothermic reaction (see chapter 4, section 4.3) which occurred shortly after the resin was illuminated by the UV lamp is clearly identified. The high sensitivity of the system, exhibited as the refractive index of the resin approaches that of the cladding, may be useful for identifying the occurrence of exothermic or endothermic reactions within a complex component for monitoring systems where tight control of the temperature is required. The features highlighted indicate thermal fluctuations in the

resin that cause measured phase shifts. The apparent time delay between the measured results may be attributed to the location of the thermocouple relative to the fibre sensor. It is interesting to note that, despite the reduction in the visibility of the channelled spectrum, it is still possible to measure the change in phase.

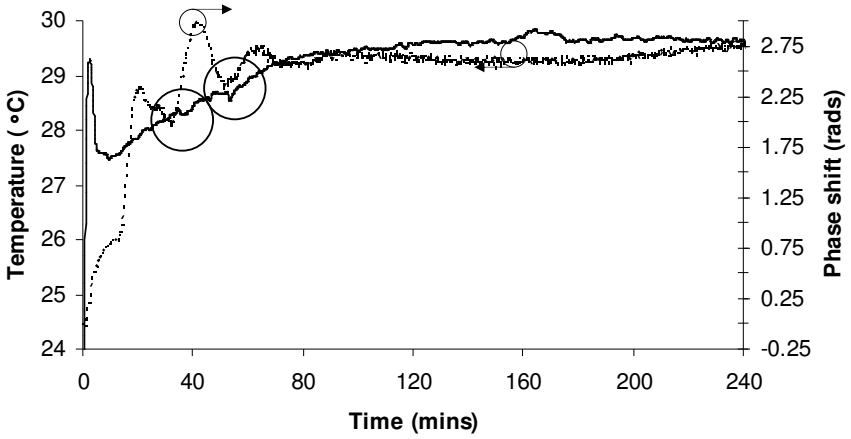

(a)

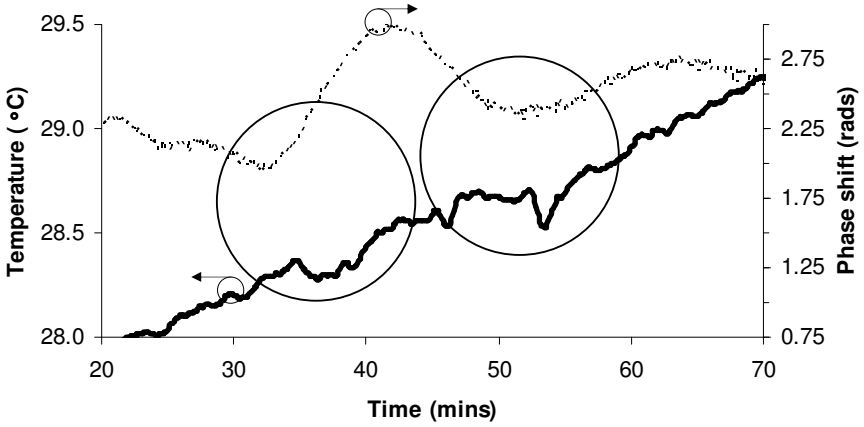

(b)

Fig 5.12 (a) Measured phase shift (dashed), measured with LPG-MZI, of sinusoidal channelled spectrum in band 5 of LPG based MZI. Expanded versions of the circled areas are shown in (b). Temperature (solid) of EpoTek OG-134 resin during cure.

There are two main advantages of LPG based MZIs over simple LPGs. Firstly, the frequency component of the channelled spectrum is governed by the separation of the

LPGs, equation 5.3 and this allows for multiplexed sensors on a single host fibre. LPG-MZIs with different separation lengths will exhibit different frequency spectra and using the FFT techniques presented here can be separated [4]. Secondly, LPG based MZIs exhibit large shifts in phase, greater than 4 radians, for small changes in refractive index, -0.004 rius [4] for indices close to that of the cladding and thus may be useful where measurements of small changes in index are required.

5.3.5 Summary

A cascaded LPG Mach-Zehnder interferometer was demonstrated as a potential cure monitor sensor with an ultraviolet cured epoxy resin. The phase shift and amplitude of the Fourier transform spectral peak of the associated interferometric fringes were calculated using Fourier analysis. The results were compared with the changing refractive index of the resin during cure; calculated with a Fresnel based refractometer. The results compare favourably and indicate the possibility of a highly sensitive cure sensor.

5.4 Resin Cure Monitoring using a Tilted Fibre Bragg Grating Refractometer.

5.4.1 Introduction

The work presented in this section was completed with Dr. Edmond Chehura, Engineering Photonics Group, Cranfield University.

As an alternative to LPG techniques a shorter gauge length device with multi parameter and multiplexing capabilities was investigated. A TFBG produces numerous resonances in the transmission spectrum of the optical fibre, the monitoring of which has been used to demonstrate a refractometer [20] without the requirement for etching, side polishing [21] or tapering [22] the fibre. In this section the ability of a TFBG to monitor changes in refractive index was compared with those of both a Fresnel refractometer and an LPG based refractometer.

5.4.2 Tilted Fibre Bragg Gratings

A standard fibre Bragg grating (FBG) consists of a refractive index modulation in the core of an optical fibre that acts to couple the fundamental forward propagating mode to the contra-propagating core mode. A tilted FBG (TFBG) [23,24] consists of a refractive index modulation that is purposely tilted or blazed relative to the fibre axis in order to enhance coupling between the forward-propagating core mode and contra-propagating cladding modes, as illustrated in figure 5.13. The contra-propagating cladding modes are poorly guided and attenuate rapidly and are therefore not observable in reflection but are observed as numerous resonant bands in the transmission spectrum. A typical TFBG transmission spectrum is shown in figure 5.14.

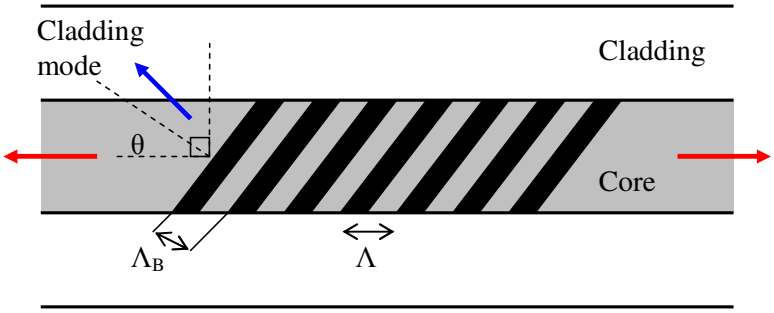

Figure 5.13 Schematic diagram of a tilted fibre Bragg grating (TFBG). Λ grating period, Λ_B blaze period and θ blaze angle.

The spectral response of the TFBG is governed by the phase matching condition [23]:

$$\lambda_i = \left(n_{eff\_co} + n^i_{eff\_cl}\right) \cdot \Lambda_B, \quad where \quad \Lambda_B = \frac{\Lambda}{\cos\theta} \qquad 5.7$$

where λ_i, n_{eff_co}, $n^i_{eff\_cl}$, θ, Λ and Λ_B are the ith cladding mode resonance wavelength, effective index of the core, effective index of the ith cladding mode, tilt angle, grating period and blaze period respectively.

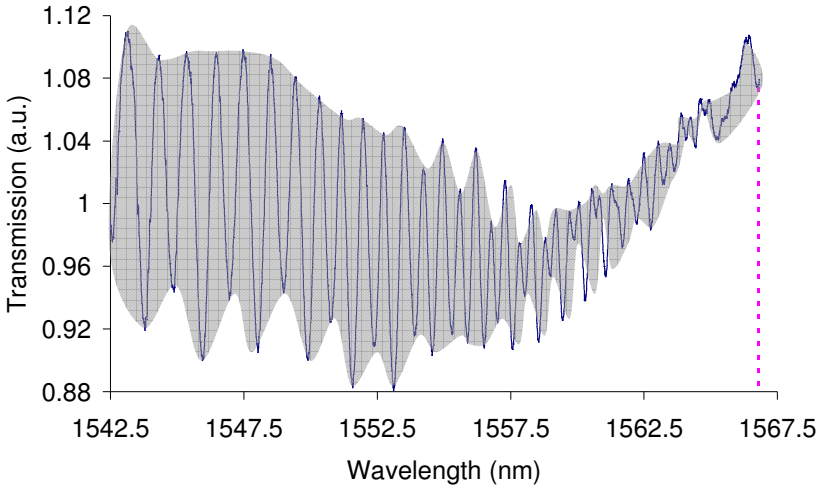

Figure 5.14 Transmission spectrum of a TFBG of length 5mm and blaze angle 4.5°, fabricated in boron-germanium co-doped optical fibre (Fibercore PS1250). The dotted line indicates the position of the Bragg wavelength. The shaded area illustrates the envelope technique used for area calculation.

The TFBG spectral resonances are complex and a method of analysis is to construct an envelope that completely surrounds the spectral resonances [20]. The area that is enclosed by the envelope varies with changes in the refractive index of the surrounding environment. By monitoring this change and relating it to the refractive index it is possible to use the TFBG as a refractometer.

The TFBG response to changes in surrounding refractive index, shown in figure 5.15, was characterised by immersing the section of fibre containing the TFBG in a series of Cargille refractive index oils of differing refractive index. The refractive index at the wavelength of operation was calculated using the Sellmeier equation. The wavelength response was then fitted with a 3rd order polynomial (lowest R^2 error) to generate a function relating wavelength shift to refractive index.

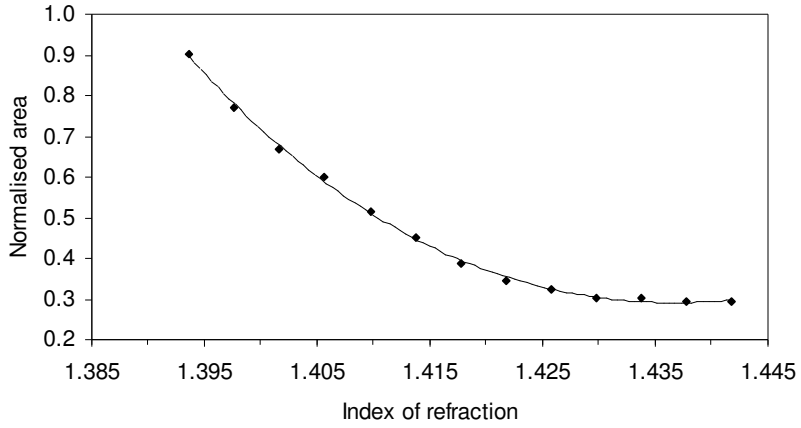

Figure 5.15 Normalised area of the envelope of the TFBG resonances (with reference to that when the TFBG is in air) plotted as a function of the refractive index of the surrounding medium.

Here, the use of a TFBG as a resin cure monitoring sensor is investigated. The sensitivity of a TFBG to changes in refractive index is exploited with the aim of developing a method of measuring the degree of cure. To aid cross comparison of results, a Fresnel reflection based refractometer is also implemented [25].

5.4.3 Experiment

A TFBG of length 5mm and blaze angle 4.5° was fabricated in boron-germanium co-doped optical fibre, Fibercore PS1250 with a cut-off wavelength of 1240 nm, using the near-field interference pattern of a tilted phase-mask. It was noticed that with this fibre it was necessary to improve its photosensitivity to achieve a reasonable spectrum. This was enhanced by pressurizing it in hydrogen for a period of 2 weeks at a pressure of 150 bar at room temperature. The phase mask was illuminated by the output from a UV laser operating at a wavelength of 248nm and with an average power of 40 mW. The TFBG was interrogated by coupling the output from a super-luminescent diode of bandwidth 60 nm into the optical fibre, and monitoring the transmission using a scanning fibre Fabry-Perot interferometer of free spectral range 43 nm and of finesse 900 [26].

The response of the TFBG based refractometer to the refractive index change was compared with refractive index measurements made using a Fresnel based refractometer operating at 1575nm [25] .This was to aid correlation with the wavelength region used by the fibre grating and to reduce the differences introduced by the dispersion of the resin.

A UV cured epoxy resin, EpoTek OG134, with an uncured refractive index of 1.4163, measured at 589nm [19], was used as the test resin. A UV lamp, with output power 4W and with a spectral peak at 365nm, was positioned to provide a fluence of 6.57mW/cm^2 in order to cure the resin. The TFBG spectrum and the reflection signal from the Fresnel probe were recorded at 0.5s intervals during the cure. The setup is shown in figure 5.16.

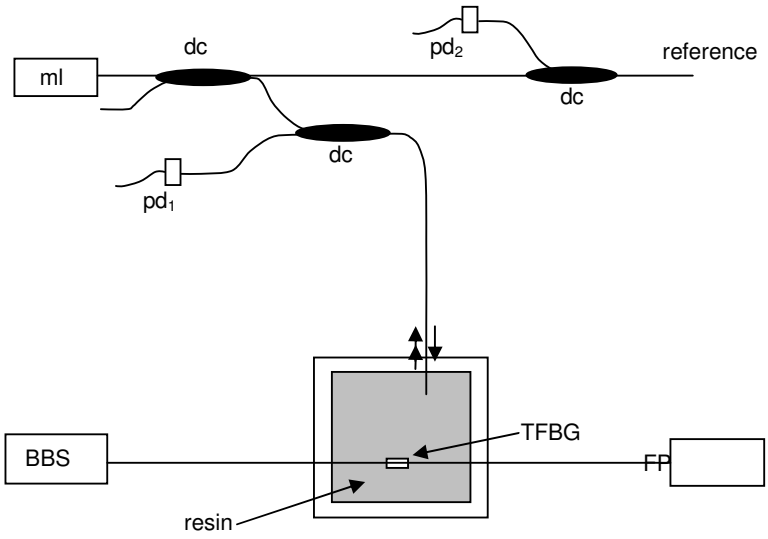

Figure 5.16 Experimental configuration. ml, modulated laser diode light source; pd, photodiode; dc, directional coupler; BBS, broadband source; FP, scanning Fabry-Perot interferometer; LPG, long period grating; TFBG, tilted fibre Bragg Grating.

5.4.5 Results and discussion

The refractive index change determined over the cure cycle by the TFBG is shown in figure 5.17. The form of the curve agrees well with the results from the Fresnel refractometer. The refractive index starts to increase 5 minutes after the UV lamp was

switched on. The initial thermo-optic effect of the resin heating due to an exothermic reaction is clearly evident immediately at UV switch on. The TFBG sensor indicates a refractive index of 1.437 at 1550nm when the resin is fully cured, achieved after 180 minutes. This agrees, to within 5 x 10^{-4} rius (refractive index units), with the measurement from the Fresnel refractometer operating at 1575nm. The calibration discussed in section 5.3.2 revealed that the sensitivity of the TFBG decreases rapidly for refractive indices greater than 1.43, and it is apparent that the response curve starts to flatten after 60 minutes as the TFBG starts to lose sensitivity. Both sensor types show that most of the reaction takes place in the first 90 minutes, after which there is a gradual reduction in the rate of change of refractive index. The reaction is almost complete after 2 hours.

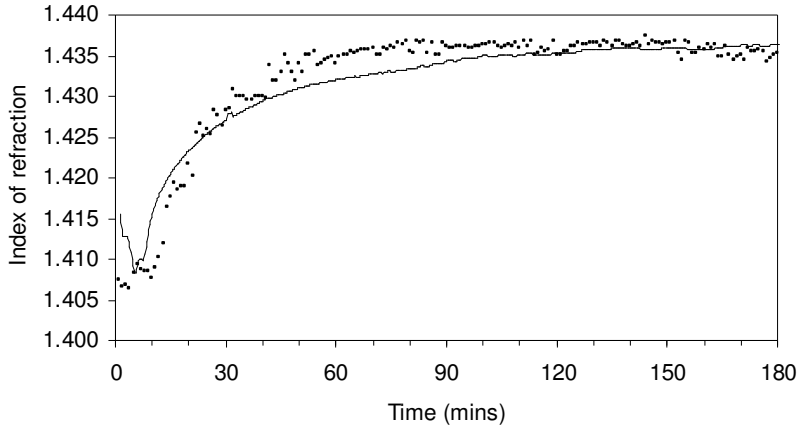

Figure 5.17 Tilted Fibre Bragg Grating (TFBG) calibrated response to refractive index change at 1550nm for the OG-134 UV cured epoxy during cure (■). The Fresnel response at 1575nm (dashed) is also shown for comparison.

The discrepancy between results obtained using the Fresnel and TFBG based refractometers may be attributed to the temperature and strain sensitivities of the TFBG sensor.

5.4.6 Summary

In summary, the core-cladding mode coupling resonances of a tilted fibre Bragg grating (TFBG) has been shown to be sensitive to the cure of an epoxy resin. The measurements made using the grating refractometer were compared with those made using a fibre optic Fresnel reflection based technique, and were found to be in agreement to within 5 x 10^{-4} rius. The TFBG results indicate a sensitivity region compatible with the LPG technique as the refractive index sensitivity is high at the initial stages of the cure before becoming less so as the index approaches that of the fibre, in contrast to the LPG. The results indicated that a TFBG sensor could be developed for the purposes of cure monitoring and resin presence detection. This is developed further in chapter 7. The TFBG has the further advantage of strain and temperature measurement capabilities using the reflected Bragg peak.

5.5 Concluding summary

Comparative techniques for monitoring the cure of resins were discussed in this chapter. The potential to monitor the flow of a resin was demonstrated using a chirped grating. It was demonstrated that the spectrum of such a device changes when gradually covered by an oil of a high refractive index and that the spectral changes are direction dependent, i.e. reliant on the axial direction of the oil flow. Cascaded gratings forming a Mach-Zehnder interferometer were considered for cure monitoring with the possibility of an increase in sensitivity to refractive index but they also offer up the potential for multiplexing. A further method of cure monitoring was demonstrated using a tilted fibre Bragg grating. The device allows for the Bragg peak to be monitored in reflection and thus monitor temperature and/or strain changes. However the cladding mode resonances can be monitored in transmission and these display a refractive index response to the surrounding medium. The sensor thus offers a multi-parameter capability. The performances of the different techniques are summarised and compared with that of an LPG in tables 5.1 and 5.2.

Table 5.1 Comparison of refractometer methods.

Refractometer	Gauge Length	Sensitivity Range
LPG	10-1000mm	1.400-1.45
LPG MZI	10-1000mm	1.438-1.45
TFBG	0.1-12mm	1.405-1.437
Fresnel	2-10mm	1-1.456 (and greater)

Table 5.2 Comparison of refractometer methods.

Refractometer	Measurement	Resolution capabilities
LPG	Wavelength shift	20nm/0.06rius
LPG MZI	Phase shift	4rads/0.004rius
TFBG	Normalised area change	90%/0.03rius
Fresnel	Intensity change	1 x 10^{-3}rius

Each method demonstrates a different parameter for change in refractive index. The intensity based measurements from the Fresnel technique are contrasted by the wavelength and phase shift responses of the LPG based sensors. It could be argued that the TFBG measurement is also intensity based however the multiple resonances of a TFBG spectrum also exhibit wavelength shift with index change. The resolution capabilities as presented provide an indication of the ability of the different technologies. Clearly the LPG based MZI indicates a very high resolution capability; this is offset however by its very narrow sensitivity range. The LPG has a broad measurement range with a high sensitivity region as the index approaches that of the cladding. The TFBG has a narrower sensitivity region however its working measurement region is below that of the LPG. The gauge lengths are constrained by the coupling mechanism of each sensor type, i.e. over-coupling can occur for longer length LPGs and reduce the spectral feature visibility. The LPG based sensors have the longest gauge length and differ to the TFBG and Fresnel based sensors which may be considered here as point sensors. As a method for monitoring the change in refractive index of a resin undergoing cure, the LPG appears to have advantages over the other techniques to suggest its use in composite materials. The applications of LPGs in composite materials in practical trials are the focus in chapters 6 and 7.

5.6 References

1. Duhem, O., Henninot, J.F. and Douay, M. (2000), 'Study of in fiber Mach-Zehnder interferometer based on two spaced 3-dB long period gratings surrounded by a refractive index higher than that of silica', *Optical Communications*, 180, p. 255–262.
2. Han, Y.G. Lee, B.H. Han, W.T. Paek U.C. and Chung Y. (2001), 'Fibre-optic sensing applications of a pair of long-period fibre gratings', *Measurement Science and Technology*, 12, p. 778–781.
3. Lee, B.H. and Nishii, J. (1998), 'Bending sensitivity of in-series long-period gratings', *Optics Letters*, 23, p. 1624–1626.
4. Murphy, R.P., James, S.W. and Tatam, R.P. (2007), 'Multiplexing of Fiber-Optic Long-Period Grating-Based Interferometric Sensors', *Journal of Lightwave Technology*, 25(3), p. 825-829.
5. Kashyap, R. Wyatt , R. and Campbell, R.J. (1993), 'Wideband gain flattened erbium fibre amplifier using a photosensitive fibre blazed grating', *Electronics Letters*, 29(2), p. 154-155.
6. S. C. Kang, S. Y. Kim, S. B. Lee, S. W. Kwon, S. S. Choi and B. Lee (1998), Temperature-independent strain sensor system using a tilted fiber Bragg grating demodulator', *IEEE Photonics Technology Letters*, 10(10), p. 1461.
7. Westbrook, P.S. Strasser, T.A. Erdogan, T. (2000), 'In-line polarimeter using blazed fiber gratings', *IEEE Photonics Technology Letters*, 12(10), p. 1352-1354
8. Caucheteur, C.; Chah, K.; Lhomme, F.; Debliquy, M.; Lahem, D.; Blondel, M.; Megret, P. (2005), 'Enhancement of cladding modes couplings in tilted Bragg gratings owing to cladding etching', 2005. Proceedings of 2005 IEEE/LEOS Workshop on Fibres and Optical Passive Components, 22-24 June, p. 234 – 239.
9. Chen, X., Zhou, K., Zhang, L. And Bennion, I. (2005), 'Optical chemsensor based on etched tilted Bragg grating structures in multimode fiber', *IEEE Photonics Technology Letters*, 17(4), p.864-866 .

10. Allsop, T., Zhang, L. and Bennion, I. (2001), 'Detection of organic aromatic compounds in paraffin by a long-period fiber grating optical sensor with optimized sensitivity', *Optics Communications,* 191, p. 181-90.
11. Wang, Z. Heflin, J.R. Vancott, K. Stolen, R. H. Ramachandran S. and Ghalmi, S. (2005), 'Sensitivity of Long Period Fiber Gratings to Nanoscale IonicSelf-Assembled Multilayers', *Proceedings of the SPIE*, 5925, p. 121-30.
12. Dunkers, J. P. Lenhart, J. L. Kueh, S. R. van Zanten, J. H. Advani S. G. and Parnas, R. S. (2001), 'Fiber optic flow and cure sensing for liquid composite molding', *Optics and Lasers in Engineering,* 35, p. 91-104.
13. Khaliq, S. James S. W. and Tatam, R. P. (2001), 'Fibre optic liquid level sensor using a long period grating', *Optics Letters*, (6), p. 1224-6.
14. Stegall, D. B. and Erdogan, T. (2000), 'Dispersion control with use of long-period fiber gratings', *Journal of the Optical Society of America A*, 17(2), p. 304-312.
15. Kashyap, R. (1999), Fiber Bragg Gratings, Academic Press, San Diego, USA.
16. Patrick, H. J., Kersey A. D. and Bucholtz, F. (1998), 'Analysis of the response of long period fibre gratings to external index of refraction', *Journal of Lightwave Technology*,16, p. 1606–12.
17. Fujita, K., Masuda, Y., Nakayama, K., Ando, M., Sakamoto, K., Mohri, J., Yamauchi, M., Kimura, M., Mizutani, Y., Kimura, S., Yokouchi, T., Suzaki, Y. and Ejima S. *(*2005), 'Dynamic Evolution Of The Spectrum Of Long-Period Fiber Bragg Gratings Fabricated From Hydrogen-Loaded Optical Fiber By Ultraviolet Laser Irradiation', *Applied Optics,* 44(33), p. 7032-7038.
18. Ye, C.C., James, S.W. and Tatam, R.P. (2000), 'Long period fibre gratings for simultaneous temperature and bend sensing', *Optics Letters*, 25, p. 1007-1009.
19. Epoxy Technology, http://www.epotek.com
20. Laffont, G. and Ferdinand, P. (2001), 'Tilted short-period fibre-Bragg-grating-induced coupling to cladding modes for accurate refractometry', *Measurement Science & Technology*, 12(7), p. 765-70.
21. Asseh, A., Sandgren, S., Ahlfeldt, H., Sahlgren, B., Stubbe, R. and Edwall, G. (1998), 'Fiber Optical Bragg Grating Refractometer', *Fiber and Integrated Optics*, 17, p. 51-62.

22. Grobnic, D., Mihailov, S. J., Huimin, D. and Smelser, C. W. (2006), 'Femtosecond IR laser fabrication of Bragg gratings in photonic crystal fibers and tapers', *IEEE Photonics Technology Letters*, 18, p. 160-2.

23. Erdogan, T. and Sipe, J. E. (1996), 'Tilted fiber phase gratings', *Journal of the Optical Society of America A*, 13, p. 296-313.

24. Brilland, L., Pureur, D., Bayon, J. F. and Delevaque, E. (1999), 'Slanted gratings UV-written in photosensitive cladding fibre', *Electronics Letters*, 35, p. 234-236.

25. Kim, C. B. and Su, C. B. (2004), 'Measurement of the refractive index of liquids at 1.3 and 1.5 micron using a fibre optic Fresnel ratio meter', *Measurement Science and Technology,* 15, p.1683-1686.

26. Ye, C-C, Staines, S. E., James, S. W. and Tatam, R. P. (2002), 'A polarisation maintaining fibre Bragg grating interrogation system for multi-axis strain sensing', *Measurement Science and Technology*, 13, p. 1446-9.

Industrial trials - long period grating sensors

6

6.1 Introduction

Research of LPGs in controlled laboratory experiments is crucial to develop the understanding of the mechanics and the limitations of using such devices in real world applications. Much published work to date looks at exploiting the evanescent nature of LPGs in varied fields [1] but little has been done in developing this knowledge to make use of the devices in an industrial sense. The focus of this chapter is primarily to demonstrate LPG devices in an industrial trial where the application environment is not easily controlled. The chapter looks at two industrially directed trials involving the integration of LPG sensors into composite structures. The aims are threefold; firstly to demonstrate the viability of such sensors in an industrial application, secondly to develop an understanding of the problems associated with such an undertaking and finally to obtain critical data from such structures during manufacture and testing. Due to time constraints imposed by the project, analyses of the data was not conducted consecutively but after both industrial trials were completed. Thus any lessons learned from the first trial were not be addressed by the second trial and the results appear repetitive. This chapter is broadly divided into two sections, each one focussing on an individual trial these are discussed briefly here. Both trials involve the integration of

optical fibre sensors in superconducting magnetic coils. Two of the project partners Oxford Instruments NanoScience (OINS) and Siemens Magnet Technology (SMT) manufacture magnetic coils of different dimensions and use, however the fundamental physics is the same and a brief description is given here to aid with the overall understanding of the application.

6.2 Superconducting magnets

The history behind superconductivity stems from the early work by Heike Kamerlingh Onnes with his discovery that at 4.2K the resistance of a mercury sample disappeared. He identified this phenomenon as superconductivity and was awarded the Nobel prize in physics shortly after this, in 1913 [2]. From this seminal work sprung a host of new research into the physics of materials and the application of superconductivity. One such application are superconducting magnets which take advantage of the ability of superconductors to carry large currents without generating resistive heat. Figure 6.1 illustrates the consequence of this with a comparison between conventional copper conductors and a superconductor carrying 12.5kA.

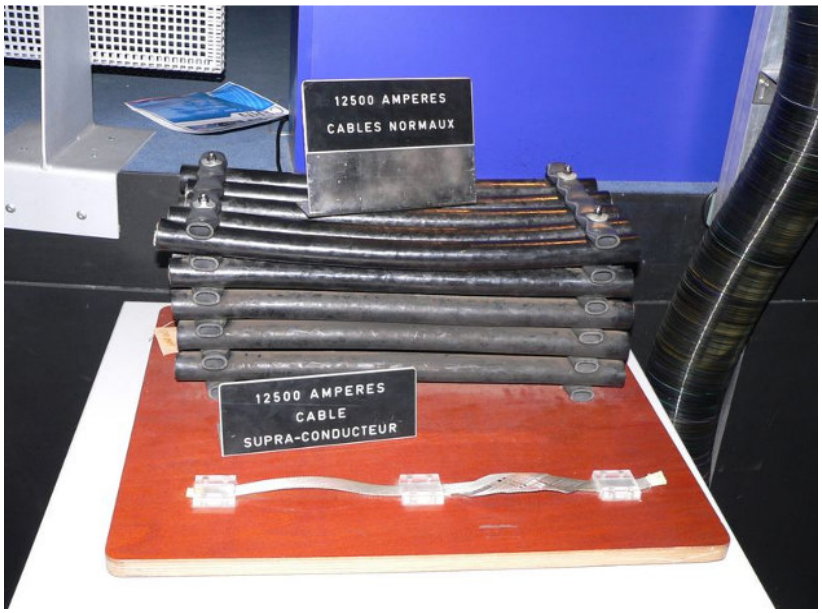

Figure 6.1 Superior current carrying capability of a superconducting cable when compared with conventional conductors.

The advantage then is the ability to create smaller magnetic systems that have larger magnetic fields. They also exhibit more stable magnetic fields over conventional magnetic systems. There are two types of superconducting materials, type I are pure metals and type II, or hard superconductors, are alloys or inter-metallic compounds. Two parameters describe their fundamentals; T_c, the critical temperature where the materials exhibit zero resistance and H_c, the maximum critical field where in the presence of an applied magnetic field a superconductor can become resistive. Type II conductors exhibit far higher H_c values than type I conductors with field strength in excess of 20T not uncommon [3]. The maximum current density of a conductor increases with decreasing temperature. However it also decreases with increasing magnetic field strength. Thus the three parameters are interrelated and consequently careful design of a magnetic is critical to ensure that a magnet operates within these critical current, temperature and magnetic field constraints.

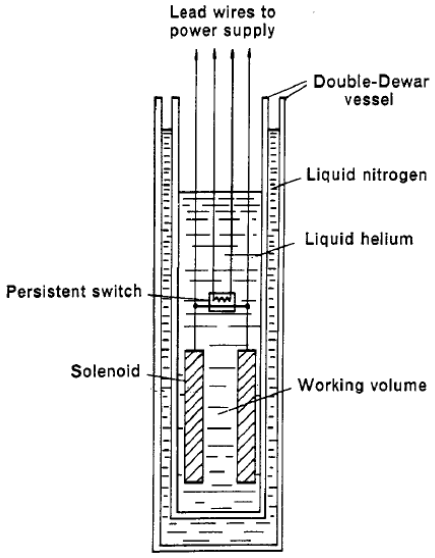

Figure 6.2 Schematic showing section through a superconducting magnet system [3]. The persistent switch allows the energising current to be disconnected from the system once the magnet is run up.

Figure 6.2 shows the basic superconducting magnet system [4]. It consists of a solenoid constructed from superconducting wires placed in liquid helium at 4.2K or below. The system is maintained in a cryostat or Dewar comprised of a liquid nitrogen jacketing

system. The superconducting wires used by the project partners OINS and SMT are type II conductors of Niobium-titanium (NbTi) or Niobium-tin (Nb_3Sn). The application and basic design of the magnetic systems are discussed separately in each section related to the individual tests. However an important phenomenon exhibited by superconducting magnets is quenching and this is discussed here separately.

6.2.1 Quenches in superconducting magnets

As mentioned previously, superconducting magnets generate large magnetic fields of 20T or more because of the ability of superconducting metal windings (NbTi or Nb_3Sn) to carry large currents. A magnet only functions properly should all conducting parts within it remain superconducting. If any part of a winding becomes resistive then ohmic heating will result. This heat can cause windings in the close vicinity to become non-superconducting and therefore resistive and in turn heat further areas of the coil. The resistive area can propagate rapidly through the coil and cause the stored energy (the magnetic field) to dissipate as thermal energy and rapidly heat the liquid helium. In many cases the helium will boil off and try to escape from the cryostat under pressure. This effect is termed a quench. Because of the high energy fields involved with such magnets, small movements of the coil windings can be enough to cause a quench and this is partly the reason why superconducting coils are encased in resins. The detrimental effects of cryogenic temperatures to resin systems, e.g. brittleness leading to fracture [5] ensure that total prevention of winding movement in high energy fields is impossible. Following a quench, it is often the case that windings settle and after re-cooling a system, quenches occur at progressively higher fields. This procedure is known as ‘training a magnet’ [5]. The ability to detect the localised thermal response of a magnetic system to quench was the focus of the research to integrate LPGs. The current temperature sensor technologies implemented are Cernox™ RTDs (resistance based temperature detectors). These devices although functional are not possible to integrate within a magnet system because of their bulk, typically 3.2 x 1.9 x 1 mm. They are also affected to a small extent by magnetic fields. Optical fibre sensors are attractive alternatives to these more traditional techniques due to their inherently high electrical insulation and relative immunity to electromagnetic interference [6]. For

example, FBG sensors have been reported as alternative sensing elements for the measurement of strain because of non-linear effects at cryogenic temperatures exhibited by restive foil strain gauges [7]. Here LPGs are located within a coil structure for the purpose of recording temperatures during quench.

6.3 OINS trial

6.3.1 Introduction

Oxford Instruments NanoScience (OINS) specialise in superconducting magnets and cryogenic technology [8]. They manufacture a broad range of products across both technology fields, developing turnkey and bespoke systems.

6.3.2 Proposal

OINS provided a superconducting magnet with the proposal to integrate LPG sensors. These were to be placed within the magnetic structure to firstly, learn and develop methods for attaching fibre sensors within the composite structure and secondly to access temperature data from the magnet during test and operation. The sensors were to be placed on the uppermost coil layer of the magnet to reduce the risk of the sensors compromising the integrity of the coil structure.

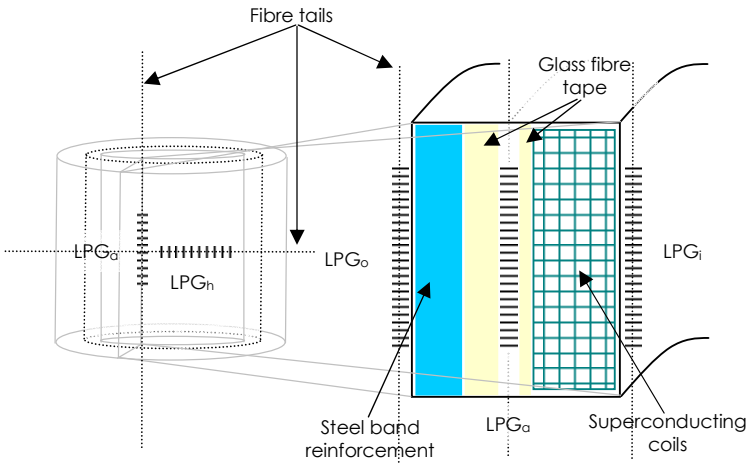

Figure 6.3 Simplified diagram showing locations of LPG sensors on test coil where, LPG_a = axially mounted LPG, LPG_h = hoop or circumferentially mounted LPG, LPG_o = LPG mounted on the outer surface of the coil and LPG_i = inner surface mounted LPG.

A composite construction of glass fibre, resin and steel reinforcement would then encase the structure. To obtain temperature data of the quench process at different locations of the magnetic structure, it was proposed to deploy four LPG sensors at specific points; two within the magnet, an axially placed LPG, LPG_a and a circumferentially placed LPG, LPG_h and two external to it, one on the outer surface, LPG_o and one on the inner surface, LPG_i. For the purposes of aiding the discussion points, LPG_a and LPG_h will be termed the integrated sensors and LPG_o and LPG_i the outer sensors. The aim is to successfully achieve integrating the sensors and undertake a testing schedule to achieve measurable temperature data. Figure 6.3 details the location of the sensors on the magnetic structure.

6.3.3 LPG fitting trial

A preliminary test was completed to resolve the best method for attachment of the outer LPGs. Three different methods were tested and are detailed in table 6.1.

Table 6.1 Fitting methods for outer surface LPG sensors

Test	Detail
1	LPG fitted to polished aluminium surface with epoxy surround
2	LPG fitted to polished aluminium surface with epoxy anchor points
3	LPG fitted to sanded aluminium surface with epoxy anchor points and aluminium tape surround

The three attachment methods are shown in figure 6.4 with the test layout. Each test involved fitting the LPG to the substrate (a smooth surfaced aluminium plate) and placing the substrate in liquid nitrogen. The epoxy used was a standard two part epoxy used by OINS called Double/Bubble™. The spectra for each method were acquired using a broadband light source to illuminate the gratings and an Ocean Optics HR4000 CCD spectrometer for spectra capture with a computer.

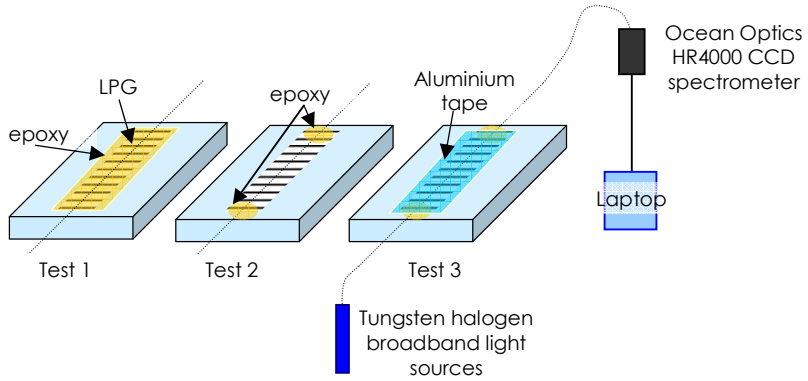

Figure 6.4 Outer surface LPG attachment methods for fitting test.

6.3.3.1 Results

Test 1: Epoxy coat

Figure 6.5 shows the LPG spectral response at cryogenic temperatures (liquid nitrogen, 77K).

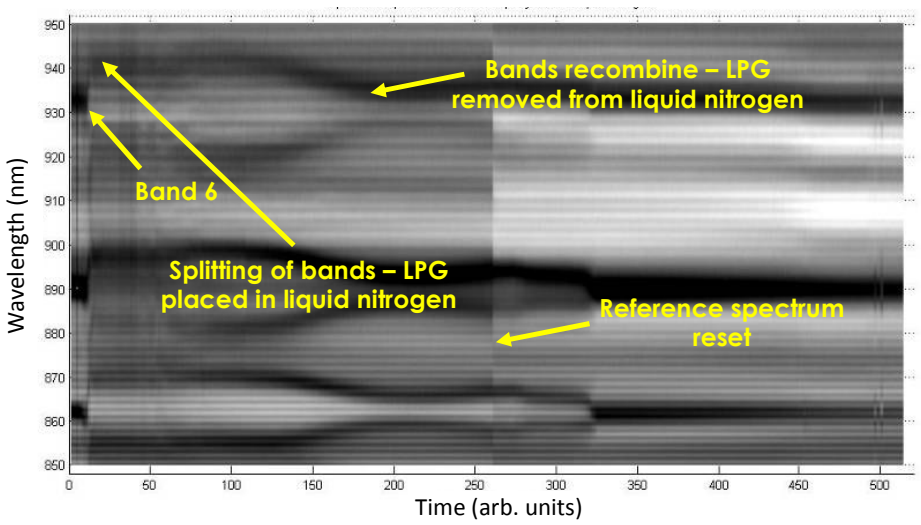

Figure 6.5 Spectral response of LPG coated with epoxy to immersion in liquid nitrogen. The chart shows the wavelength spectra against time with transmission represented in greyscale where black is 78% and white is 138% (percentage relative to reference spectrum).

The test demonstrated a thermal reaction which forced the epoxy to detach itself from the substrate and bend the sensor outwards. This effect is noticeable after time = 0 where the bands are shown to split, due to mechanically imparted birefringence. The bands then start to rejoin as the substrate and LPG are removed from the nitrogen and allowed to warm up to ambient. Bands 4, 5 and 6 are shown in the figure with band 6 annotated.

Test 2: Epoxy anchor points

Figure 6.6 shows the LPG spectral response at cryogenic temperatures. In this case contraction of the substrate forced the two anchor points towards each other and with this the LPG started to bend outwards. The spectral response indicates split attenuation bands appearing shortly after time = 0. As the substrate contracts further and the LPG continues to bend the wavelength separation between the split bands reaches a turnaround point and a dominant split band from each attenuation band shows a negative shift. In this test the LPG was left in the nitrogen and the dominant split band exhibited a turnaround point before slowly retracing to a spectral location below that of

the original band position. Bands 4, 5 and 6 are shown in the figure with band 6 annotated.

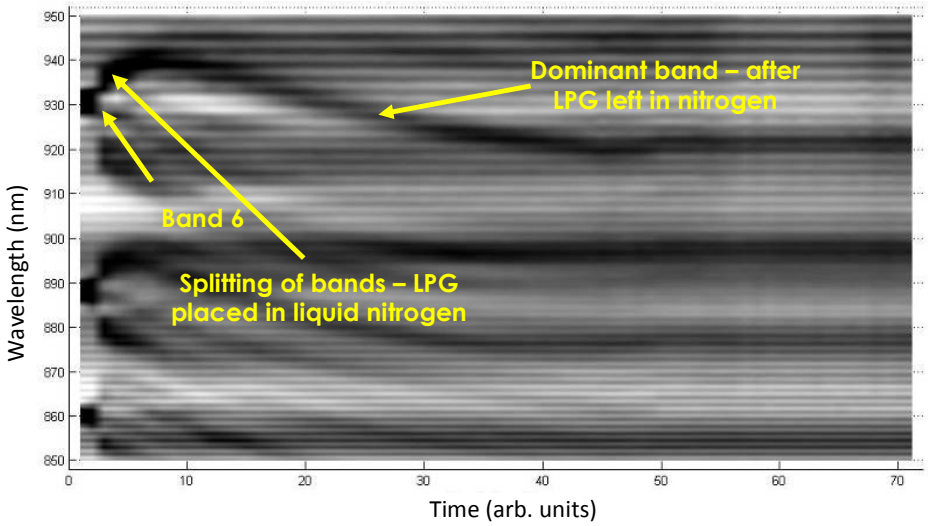

Figure 6.6 Spectral response of LPG coated with epoxy to immersion in liquid nitrogen. The chart shows the wavelength spectra against time with transmission represented in greyscale where black is 80% and white is 120% (percentage relative to reference spectrum).

Test 3: Epoxy anchor points with aluminium tape

Figure 6.7 shows the LPG spectral response at cryogenic temperatures. The effect of the contraction of the substrate on the LPG in this case is restricted due to the aluminium tape. The bands are evident at room temperature (time = 0) but at cryogenic temperatures the bands disappear at time ≈ 90 (arb. units), the bands then reappear as the substrate warms up to ambient. The band disappearance may be as a result of induced micro bends on the fibre as the aluminium tape contracts. Thermal contraction of aluminium at around 0.4% at cryogenic temperatures will impart a significant transverse load on the fibre [5]. LPGs have been demonstrated as load sensors utilising the spectral separation of the resultant split attenuation band as a load parameter [9]. They report on the effects of side loading a fibre with a force generated from a 4kg weight.

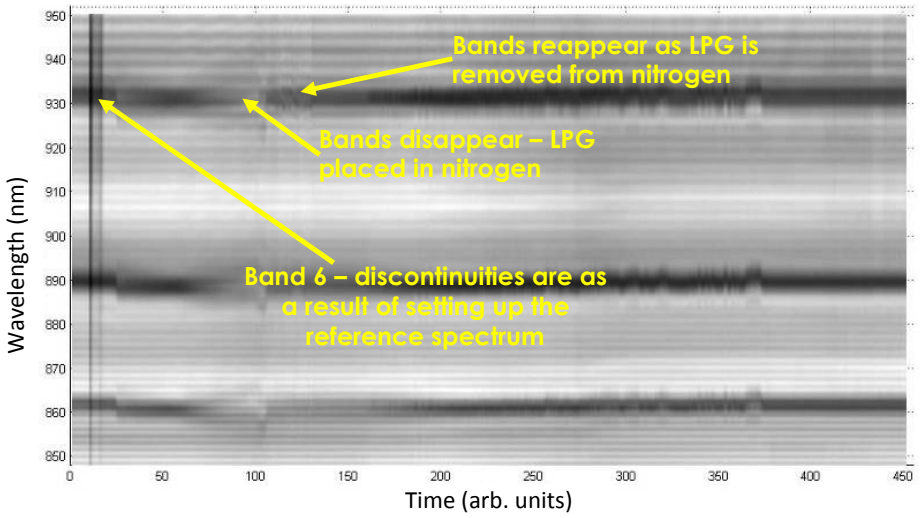

Figure 6.7 Spectral response of LPG coated with epoxy to immersion in liquid nitrogen. The chart shows the wavelength spectra against time with transmission represented in greyscale where black is 41% and white is 122% (relative to reference spectrum).

An approximation of the change in dimension of the glass can be determined from Young's modulus for a 125µm cube [10] which for silica (quartz) is 73 GPa [11]:

$$E = \frac{FL_0}{A_0 \Delta L} \qquad 6.1$$

Where F=39.24N (4kg x 9.81m/s^2), L_0=125µm, A_0=125µm^2 and E=73GPa

From this we deduce ΔL to be 3.34µm which suggests a contraction of 0.03%, much smaller than that for aluminium contraction at cryogenic temperature. Therefore, the transverse loading to the fibre is significant in this instance and attributable to the loss of attenuation bands. Bands 4, 5 and 6 are shown in the figure with band 6 annotated.

6.3.3.2 Discussion

The attachment tests demonstrated an important consideration when deploying LPGs in composites. The nature of the evanescent sensor determines that interaction with the method of attachment is possible and therefore a benign technique is critical for the

sensor to function. From the small sample of tests completed a decision was made to utilise the method of test 2 (epoxy anchor points) for the external sensors. The small amount of epoxy used ensured that thermal contraction effects were negligible however the bending moment created from the contraction of the substrate is an issue. It was clear however that spectral features remained and it may be possible to use these for measurement purposes. The sensors integral to the magnet were fixed initially with double sided Kapton tape and the composite structure provided a secure environment post resin impregnation and cure.

6.3.4 OINS - Experiment

A layout of the test arrangement is detailed in figure 6.8. The essential elements comprise; a test coil and associated background field magnets, a cryostat and an optical sensing system, LPGs. The LPG setup consists of four, 40mm length LPGs of 400μm period written on Fibercore SM750 fibre using the amplitude mask method discussed in section 3.6.2. Each sensor had 4m fibre tails to allow the fibre to be routed from the magnet through the cryostat to the data capture measurement equipment. It was necessary to maintain an effective distance (~2m) from the energised magnet to ensure both the equipment and personnel would not be affected by emitted magnetic fields. The fitting locations for each of the individual sensors were shown previously in the simplified diagram of the magnet in figure 6.3.

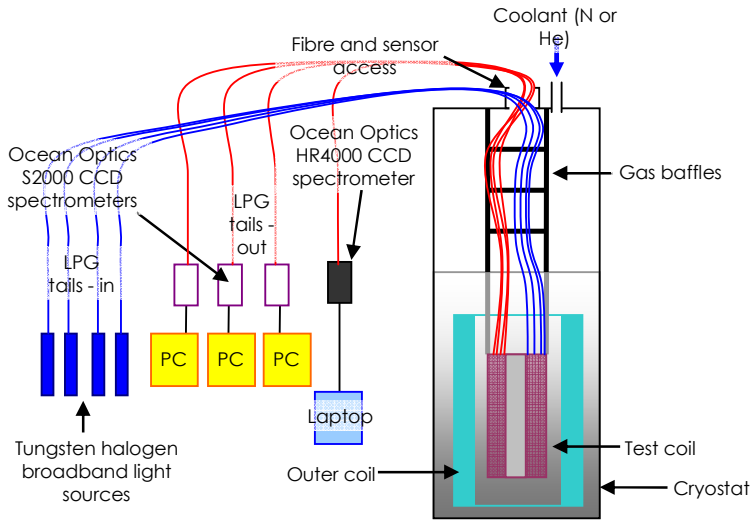

Figure 6.8 Experimental layout of Oxford Instruments NanoScience industrial trial.

The LPGs were located in the coil structure and on both surfaces in order to determine a thermal gradient across the magnet during quench. A test coil was used as a test bed for the industrial trial. The sensors were fitted directly to a closely woven glass fibre tape over bind. The tape was wound around the top layer of the coils for protection and to create a base layer for the reinforcement composite that surrounds the magnetic coils. A double sided Kapton tape was used to place anchor locations either side of the LPG sensors and to route the fibre over the surface of the magnet. Figure 6.9 (a) shows the location of the two LPG sensors on the magnet. The LPGs were placed in orthogonally to each other, to determine what effect this would have on the LPG spectra during tests and to provide an element of redundancy.

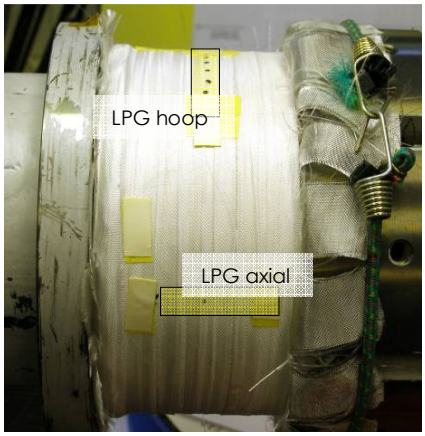

Figure 6.9 Fitting of the optical sensors; the two LPG sensors are fitted in orthogonal orientations with double sided Kapton.

A lead through was designed by OINS to route the fibre safely out of the coil for attachment to a super conducting joint post. The feed through was flared to prevent damage to the fibre and was slotted to provide a barrier for resin flow during impregnation. The lead through is shown in figure 6.10 (a). The fibre tails were then wound onto a bobbin to prevent damage, figure 6.10 (b).

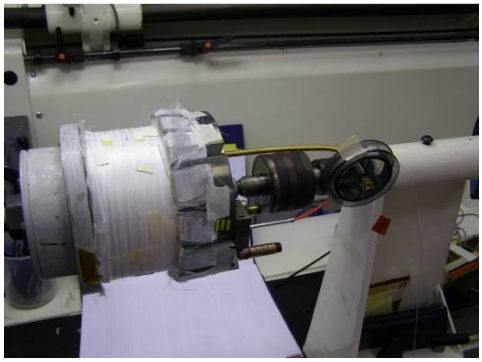

(a) (b)

Figure 6.10 The fibre feed through with flare (a) and bobbin mount (b).

After the sensors were fitted to the magnet they were embedded within the structure. An over bind glass fibre tape was then wound over the LPGs and magnet. Figure 6.11 (a) shows the magnet with over bind. The stanchion holding the fibre bobbin (plastic cover) is also shown.

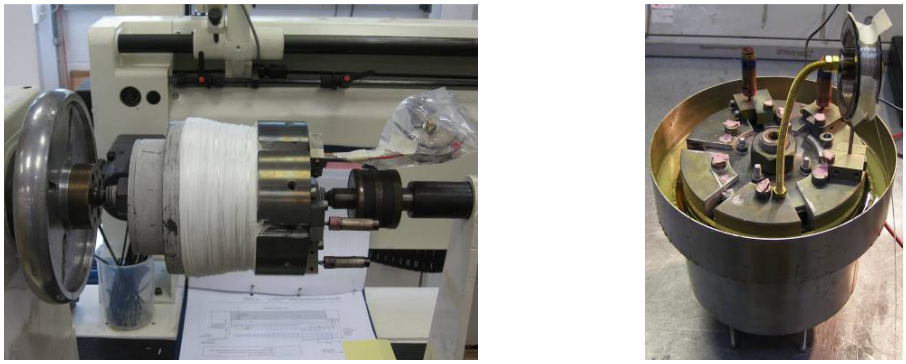

(a) (b)

Figure 6.11 Glass fibre tape wound over sensor locations and built up (a). Magnet in resin pot, post cure (b).

The coil was then impregnated with a diglycidyl ether of bisphenol A (DGEBA) resin and hardener. The coil was placed in an autoclave and cured at 80°C for 12 hours. Figure 6.11 (b) shows the magnet post impregnation in a potting container. After impregnation and cure the surface of the coil was machined to fit steel over binding or reinforcement. The reinforcement provides a mechanical constraint for the coil whilst energised to prevent movement. Figures 6.12 and 6.13 show the spectra for the integrated LPGs during specific times in the coils production cycle.

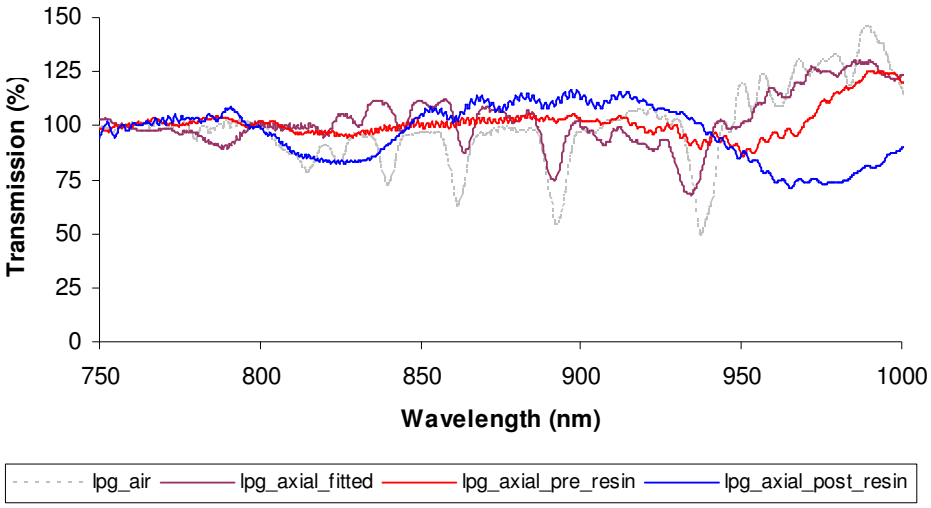

Figure 6.12 Spectra for the axially placed LPG, LPG_a at 4 different stages of the magnet production cycle.

Figure 6.12 illustrates the affect on the spectrum of the axially placed LPG, LPG_a. The bands are clearly visible for the LPG surrounded by air. Once the LPG is fitted to the coil a slight distortion is evident. This may be due to the insecure and moveable surface the sensor was fitted to, the glass weave tape. The small amount of movement in the cloth may cause the sensor to bend slightly and produce a broadening effect [12]. Also shown is the disappearance of the bands once the sensors have been over wound with a further layer of glass weave tape, this is shown as the spectrum annotated as, *lpg_axial_pre_resin*. Finally, once the coil has been impregnated, further change to the spectrum is evident.

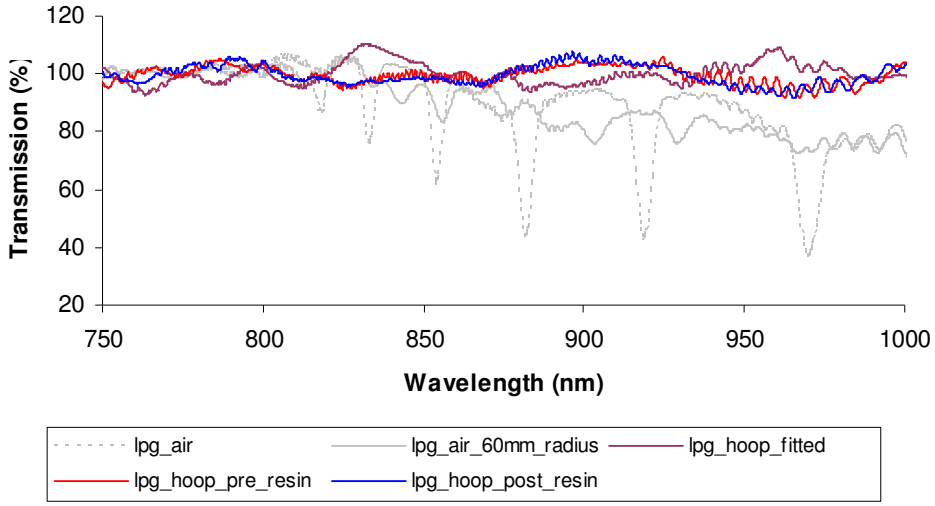

Figure 6.13 Spectra for the circumferentially placed LPG, LPG_h at 4 different stages of magnetic coil production cycle.

Figure 6.13 illustrates a similar change to the spectrum of the circumferentially placed LPG at stages during the coil manufacture. Also shown is the spectrum for the LPG held in air on a 60mm radius circular former. This is shown to demonstrate the expected spectrum for the LPG fitted to the magnet. Clearly, the effect of the sensor in contact with the glass cloth and the induced bend leads to a degradation of the spectrum from which little information is available. The pre and post resin impregnation spectra show little change. This effect is investigated and discussed in section 6.5. The outer sensors were then placed on the inner and outer diameter surface of the coil as shown previously

in figure 6.3. The attachment method was directed from the initial tests in section 6.15. The surface of the magnet was polished with a fine sand paper and a two part epoxy was used to fix two anchor locations of the fibre, either side of the LPG. The spectra of these sensors fitted to the outermost surfaces of the magnet did not exhibit the effects shown by LPG_a and LPG_i and their spectra are shown in figure 6.14. This is due to the secure anchor points of the epoxy with the magnet surface and the minimal contact between the magnet surface and the bare glass fibre.

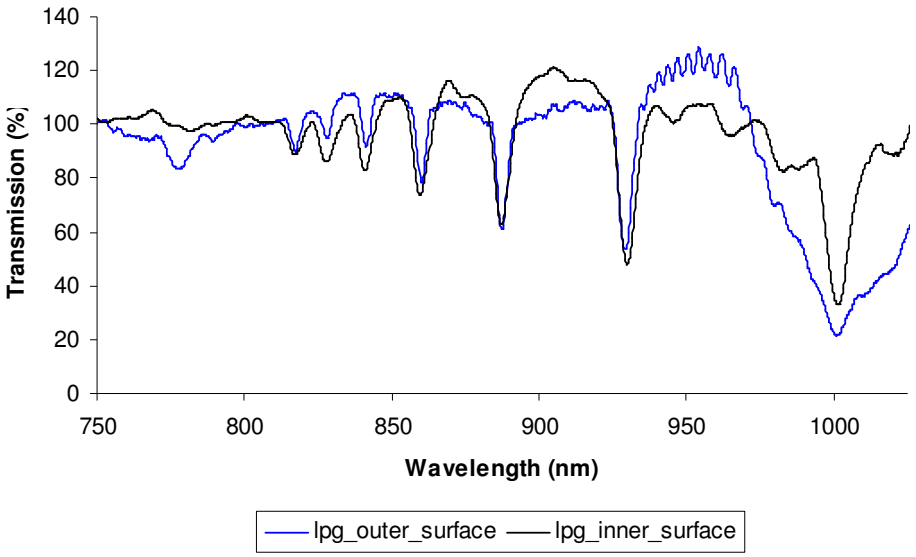

Figure 6.14 Spectra for the externally located sensors, lpg_outer_surface = LPG_o and lpg_inner_surface = LPG_i.

In this system the test coil is part of a larger magnetic system, figure 6.15 (a). The coil is placed inside an outer magnet which provides a background magnetic field to enhance and develop the field generated from the test coil. Figure 6.15 (b) shows the system in preparation for placement in the cryostat. A superstructure is mounted to the magnets as part of the thermal insulation mechanism it also aids placement in the cryostat. The gas baffles act as radiation shields and prevent convection losses in the cryostat [8].

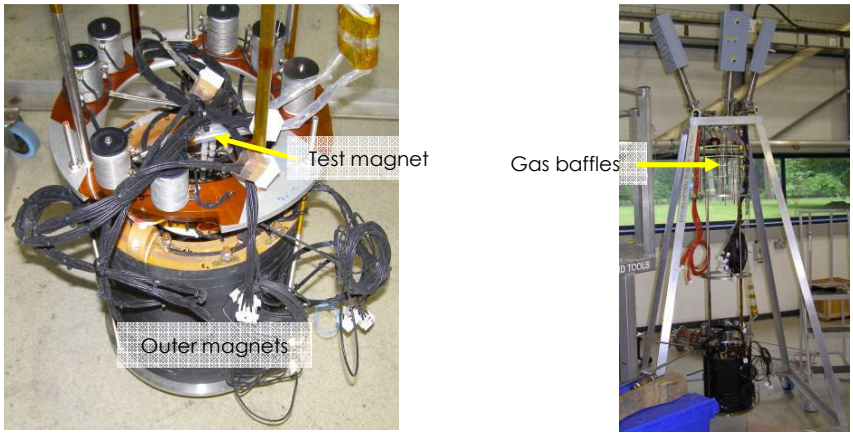

(a) (b)

Figure 6.15 The test coil is placed inside two larger magnets which provide a background magnetic field during testing (a). A superstructure is added to aid thermal insulation and provide routing for sensor and power lines in the cryostat (b).

Table 6.2 Test schedule

Test	Conditions	Notes
0	Monitor cool down	
1	Outer coil to 110A @ 2A/min	Spontaneous quench
2	Outer coil to 100A @ 2A/min	
3	Outer coil held at 100A and test coil to 200A and back @ 5A/min	
4	Outer coil to 110A from 100A above	
5	Outer coil to 110A @ 10A/min	
6	Outer coil to 110A and test coil to 400A and back @ 20A/min to 200A, 10A/min to 400A	Spontaneous quench
7	Outer coil to 110A and test coil to 400A and back @ 20A/min to 200A, 10A/min to 400A	Spontaneous quench
8	Outer coil to 110A and test coil to 100A and force quench on outer coil	

After placement in the cryostat, each LPG was illuminated with a tungsten halogen broadband light source and three of them were interrogated with Ocean Optics S2000 CCD spectrometers. A fourth LPG was interrogated by an Ocean Optics HR4000 CCD spectrometer (this arrangement was driven by availability of the spectrometers). The setup was shown previously in figure 6.8. The CCD spectrometers provide a resolution of 0.25nm. The LPG spectra were captured at 3Hz, the capture rate determined by the light levels achievable from the light sources and inherent losses in the system. Capture rates of up to 100Hz are achievable with the CCD spectrometers dependent on light levels.

A test schedule was detailed, table 6.2, to develop measurable temperatures during energise and quench times.

6.3.5 OINS - Results

Test 0: Cool down

The first stage of the test involved cooling down the magnet to cryogenic temperatures (below -150°C). The cryostat is made up of an outer vacuum jacket (OVC), a sample space which is a liquid helium reservoir and a cylindrical liquid nitrogen jacket which is built into the OVC and surrounds the liquid helium can [7]. The process involved pre-cooling of the cryostat with liquid nitrogen. The nitrogen is typically left overnight before being purged from the system with helium gas and is then filled with liquid helium which lowers the temperature of the cryostat to 4.2K. During this process the LPG spectra were monitored to determine their response to temperature. Due to the poor quality spectra obtained, it was necessary to track spectral changes by playing through the spectra and visually checking for spectral shifts or changes in transmission. These are more clearly visible in the gray scale images shown in figures 6.16 and 6.17. Once a spectral feature was identified, a matlab program was used to track it during each set of test results. This was achieved by fitting a 6^{th} order polynomial to the spectral dip and recording the wavelength and transmission depth of its minimum point. It was found that a 6^{th} order polynomial was the best fit throughout each test.

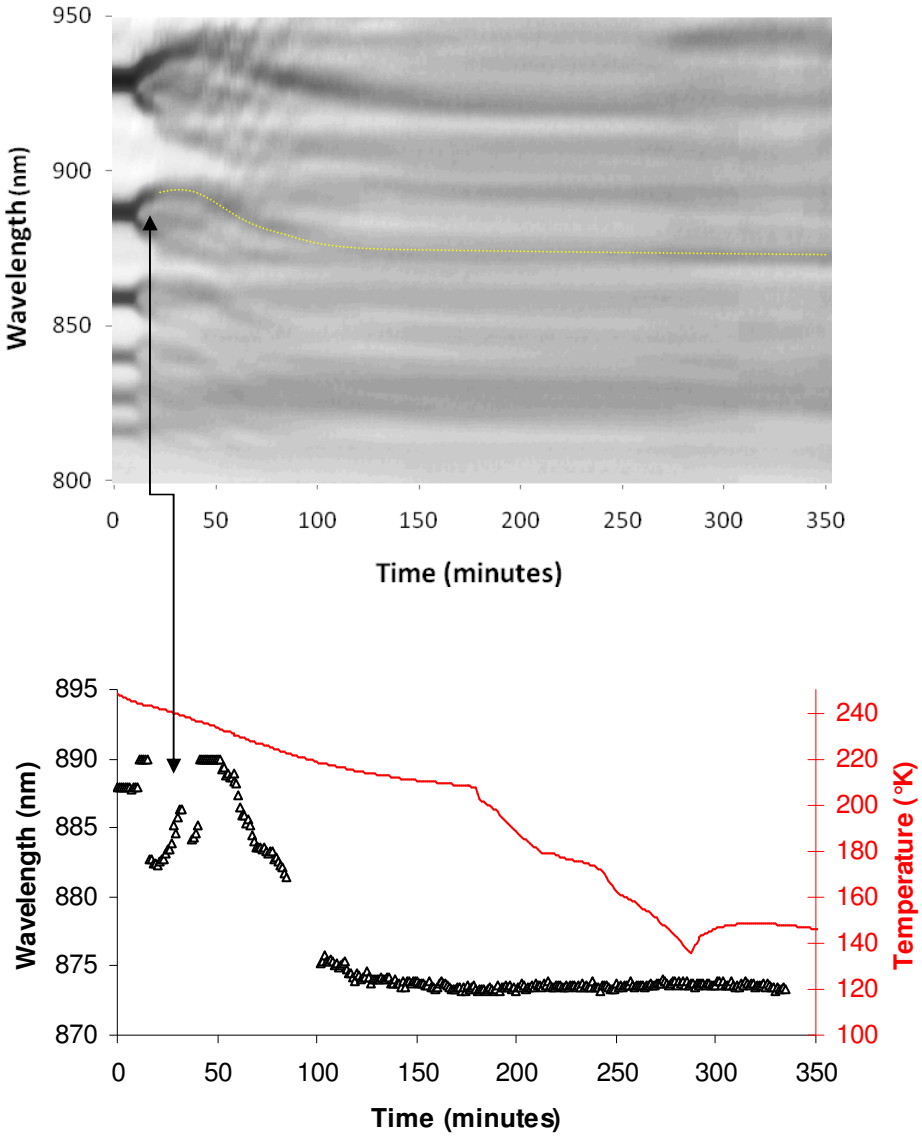

Figure 6.16 Spectral response of inner surface LPG to cool down. The first order coupled attenuation bands are shown from 800nm to 950nm. The black arrow in the upper chart annotates a part of the spectrum that is described in more detail in the lower graph. The yellow dotted line is a visual aid to indentifying the spectral movement during the period.

Figures 6.16 and 6.17 show the spectra response to cool down for the two LPGs mounted on the outer surface of the magnet, LPG_o and LPG_i. The spectra are described in grey scale with white representing 100% and black representing 0%. The spectra

show the destruction of the bands due to thermo-mechanical contraction of the magnet causing the anchor points of the LPGs to move towards each other. This agrees with fitting test 2, discussed in section 6.3.3. The bend sensitivity of the LPGs is evident where sudden contraction of the sensor substrate (in this case the magnet) causes splitting of the attenuation bands.

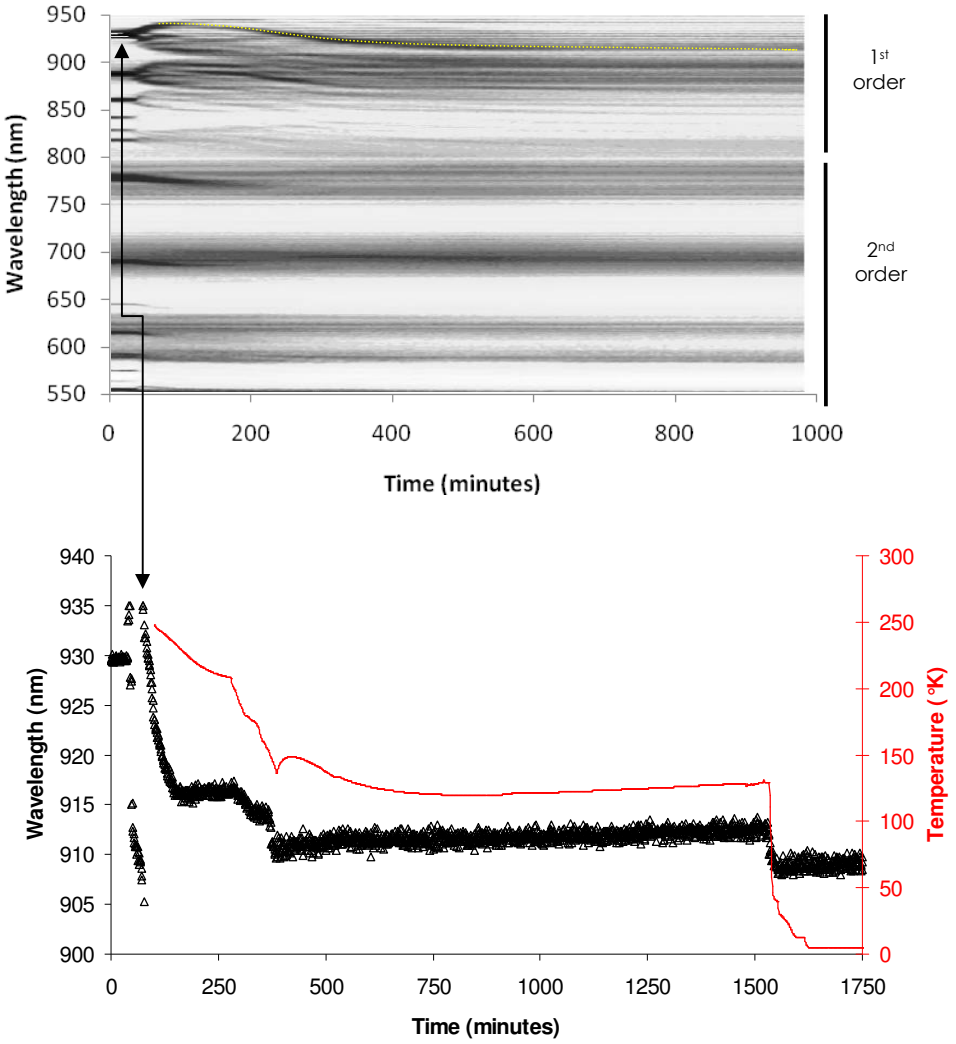

Figure 6.17 Spectral response of outer surface LPG to cool down. The first and second order coupled attenuation bands are shown from 550nm to 950nm. The upper graph only shows the first 1000 minutes. The black arrow in the upper chart annotates a part of the spectrum that is described in more detail in the lower graph. The yellow dotted line is a visual aid to indentifying the spectral movement during the period.

By tracking a particular spectral feature derived from the attenuation band it is possible to compare the wavelength response with temperature for LPG_i and LPG_o. The figures show the response for band 5 and band 6 of LPG_i and LPG_o respectively during cool down. LPG_i suffers a loss in transmission during cool down at around 340 minutes. This may be attributed to defects on the glass surface caused by the UV writing process [13]. Small defects may propagate across the fibre due to the bending moment at cryogenic temperatures and lead to failure.

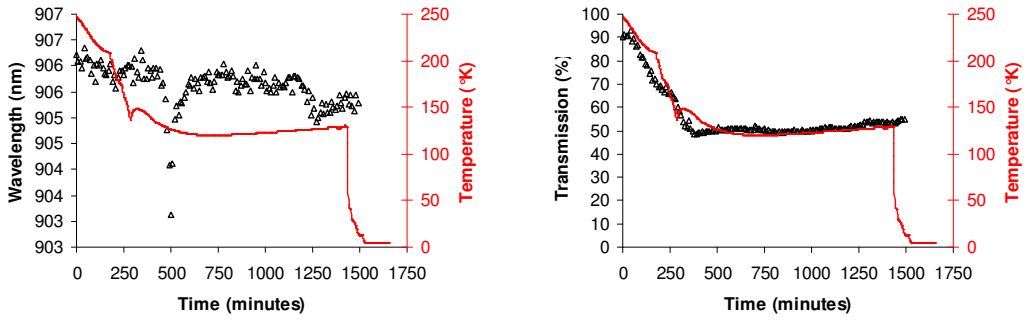

(a) (b)

Figure 6.18 Wavelength shift (a) and transmission change (b) of a spectral feature of LPG_a during cool down.

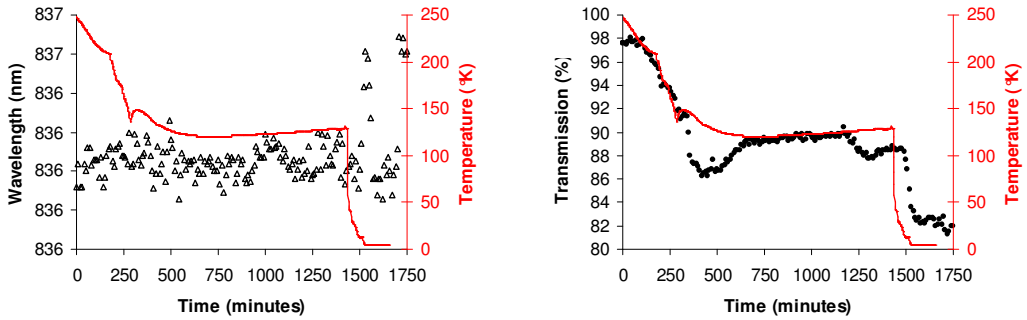

(a) (b)

Figure 6.19 Wavelength shift (a) and transmission change (b) of spectral feature of LPG_h during cool down.

Figures 6.18 and 6.19 show the responses from the integrated LPGs. They appear to show very little wavelength response to changes in temperature. However as previously discussed the bands are destroyed by the interaction of the LPG with the glass tape,

resin and high mechanical strains imparted on them by the magnetic structure. What is evident however is the transmission change that matches closely with the temperature change during cool down. This effect may be due to micro-bending of the fibre, caused by thermal contraction of materials in direct contact with the LPG. The transmission change illustrates the effect cryogenic temperatures on the materials surrounding the fibre, however as the spectra are poorly resolved and provide no consistent wavelength shift to observe, it cannot be directly attributed to an LPG band response. To appreciate the effects of integrating LPGs within composites evidenced in this chapter and the next, experimental work is considered in section 6.5, investigating these problems.

Tests 1 – 8: Energise and quench tests

The purpose for the placement of the LPG sensors within the structure of the magnet was to access temperature data during a quench. At present, Cernox™ RTDs (resistance temperature detector) provide this information placed within the cryostat on the outer surfaces of the magnet. The advantage of LPG sensors is the ability to be integrated within the magnet, without compromising the structure and to access this temperature data at critical locations of a structure. A typical quench temperature response captured from rhodium iron sensors is shown in figure 6.20.

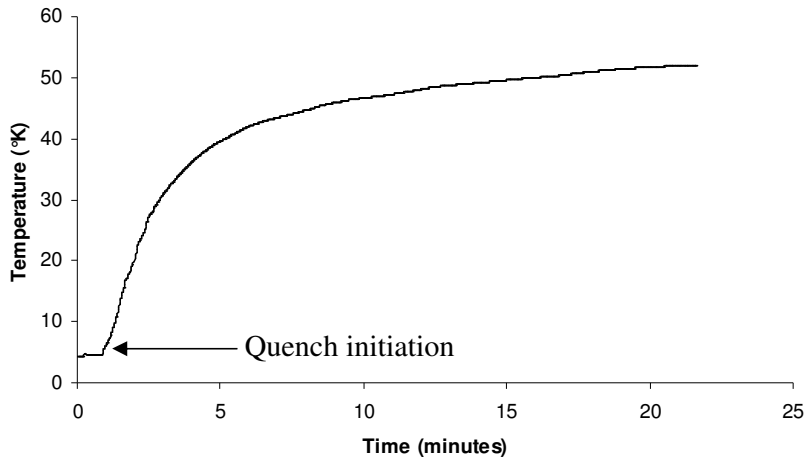

Figure 6.20 Typical temperature response during a forced quench.

It was noted that the outer surface sensors, LPG_i and LPG_o, were unable to provide sufficient spectral information during energise and quench. This was due to their compromised placement and resultant bending which appears to have destroyed any visible attenuation bands. LPG_i also failed to transmit light during cool down. The results presented here therefore concentrate on the integrated sensors, LPG_h and LPG_a.

Test 1

The initial test was conducted to enable checks on the background magnets. The magnets were energised to 110A at a ramp rate of 2A/min. At 102A the magnets experienced a spontaneous quench. The results from LPG_h and LPG_a are shown in figures 6.21 and 6.22. A spectral feature from both sensors is monitored during the energising of the coil and the results show a spectral response at quench. LPG_h appears to follow energise with a positive transmission response of 4%. Both sensors indicate a sharp wavelength dip, corresponding to the quench, before a turnaround point where the wavelength shifts back towards the original spectral location with a slower time response.

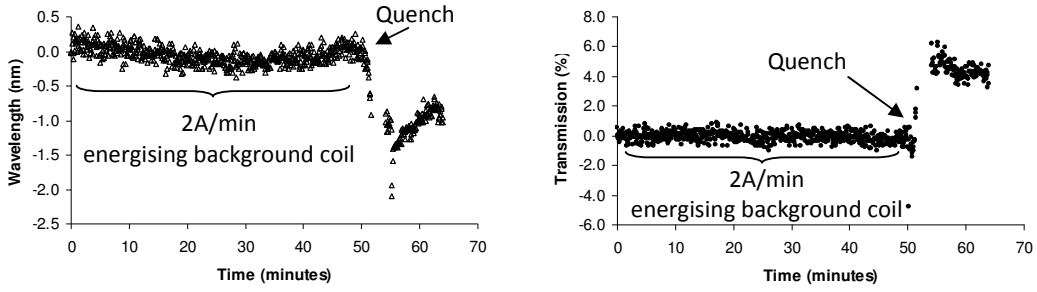

Figure 6.21 LPG_a spectral response to test 1

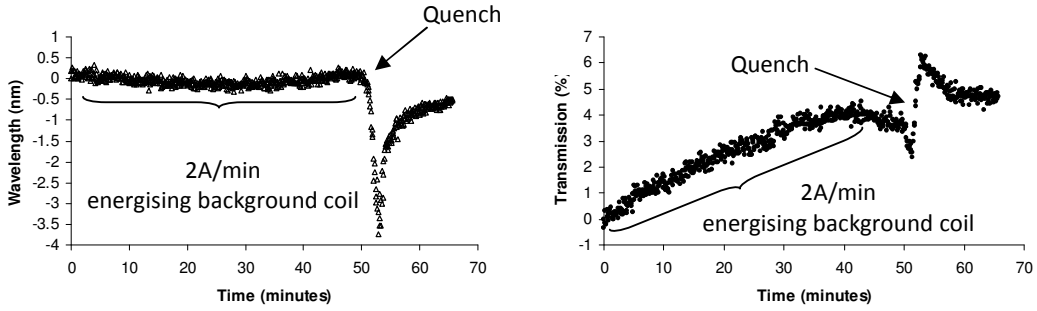

Figure 6.22 LPG_h spectral response to test 1.

Test 2

A second test was conducted on the background magnets with the purpose of energising the coil whilst avoiding a spontaneous quench. The magnets were taken to 100A at a ramp rate of 2A/min. The results for both sensors are shown in figures 6.23 and 6.24. LPG_a shows very little wavelength or transmission response to the energising of the outer magnets. LPG_h again shows a transmission response to the ramp rate with a positive change of 4%. An apparent positive wavelength shift over the first 20 minutes is evident before a negative shift up to 30 minutes where the transmission change is no longer evident. The wavelength noise of ±0.2nm cannot be explained however a possible cause may be due to the high EM fields from the superconducting magnets, although this was not investigated.

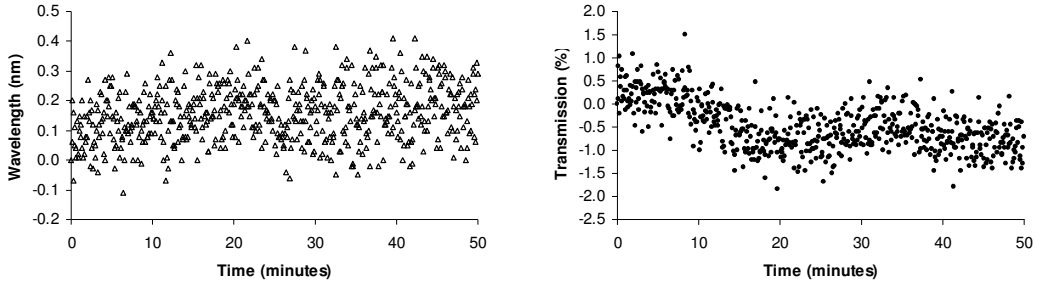

Figure 6.23 LPG_a spectral response to test 2.

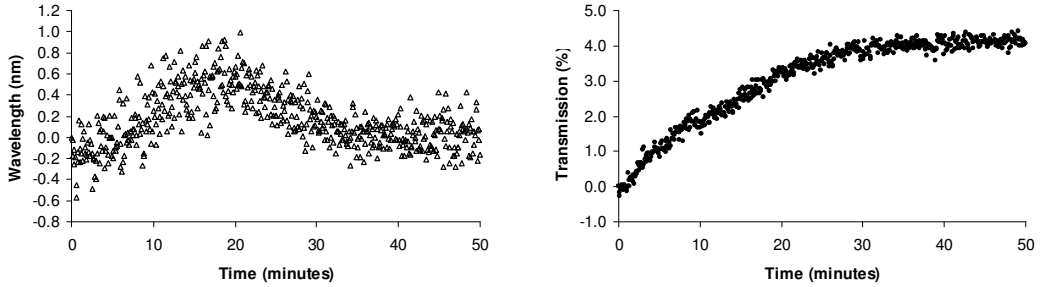

Figure 6.24 LPG_h spectral response to test 2.

Test 3

Test three involved energising of the test coil. The outer magnet was maintained at a background field with 100A whilst the test coil was ramped from 0 to 100A at a ramp

rate of 5A/min and from 100A to 200A at a ramp rate of 10A/min. Both sensors (figures 6.25 and 6.26) show a negligible wavelength response but the transmission response of both shows a drop in attenuation as the test coil is energised and a positive change in transmission as the coil is de-energised. The ramp rate change is evident from the transmission graphs were a change in slope occurs at ~22 minutes for both sensors. LPG_a shows a sharper transmission change (~18%) and this may be as a result of micro-bending induced on the sensor by the magnetic coils that are forced outwards and compress the fibre against the composite reinforcement.

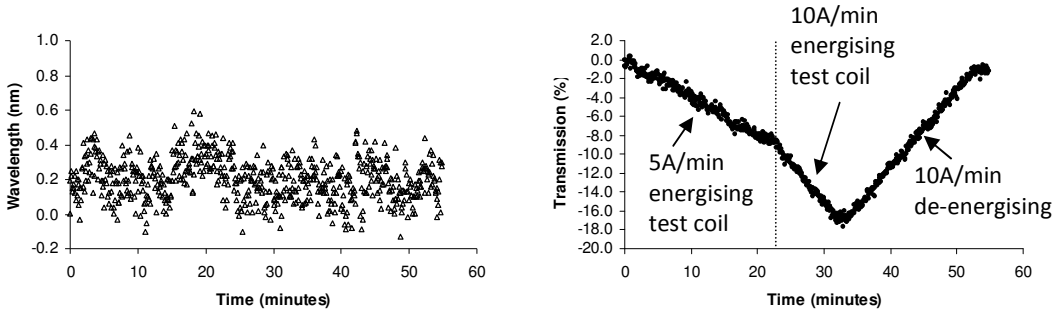

Figure 6.25 LPG_a spectral response to test 3.

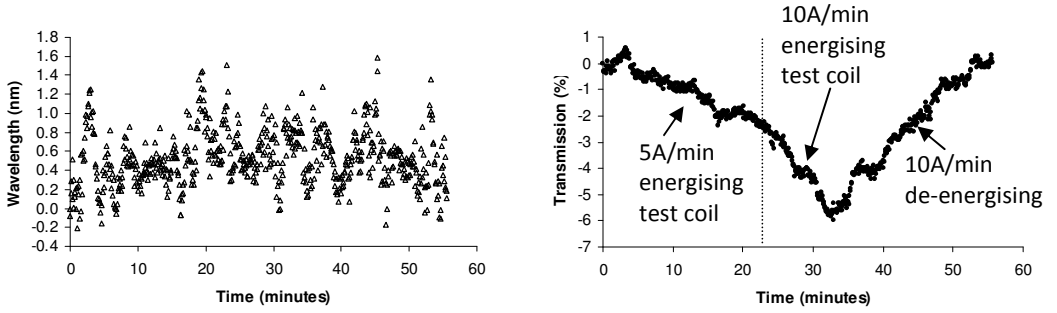

Figure 6.26 LPG_h spectral response to test 3.

Test 4

Test 4 was carried out to test the outer magnet for spontaneous quench. The outer magnet was taken to 110A from the 100A position of test 3. The results shown in figures 6.27 and 6.28 exhibit little change as would be expected from the results of test 1 and 2. Both sensors exhibit no wavelength response and negligible transmission response. LPG_h shows a small change in transmission ~0.2% but this is well within the

noise level and is not significant. A spontaneous quench did not occur and this is demonstrated in the results as there is no significant change in wavelength.

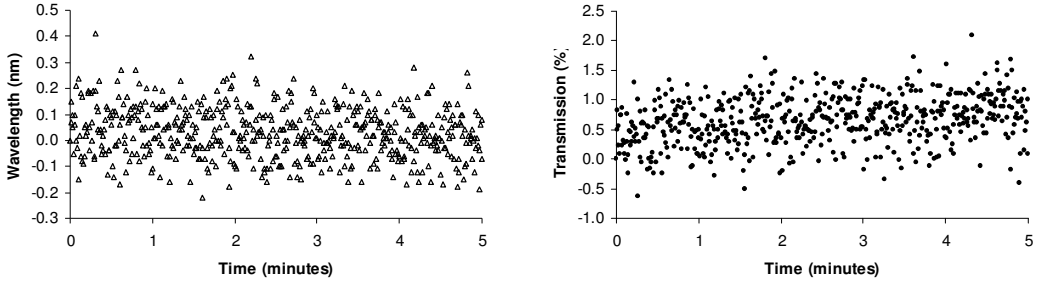

Figure 6.27 LPG_a spectral response to test 4.

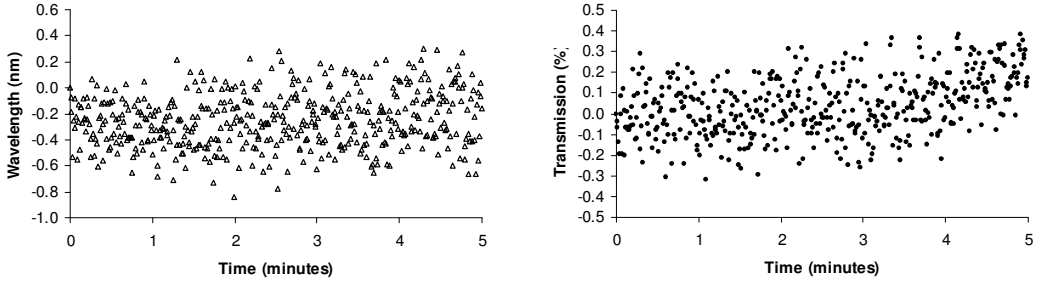

Figure 6.28 LPG_h spectral response to test 4.

Test 5

Test 5 was a repeat of test 1. The outer magnet was ramped to 110A from 0A. This demonstrated that the outer magnet had been quench trained, i.e. there was no quench during the ramp. The results in figure 6.29 show the response of LPG_a. In this case there appears to be a wavelength correspondence with the outer coil being energised, there is a positive wavelength shift of ~0.7nm over the ramp time. A similar transmission profile as test 2 is demonstrated by the sensor.

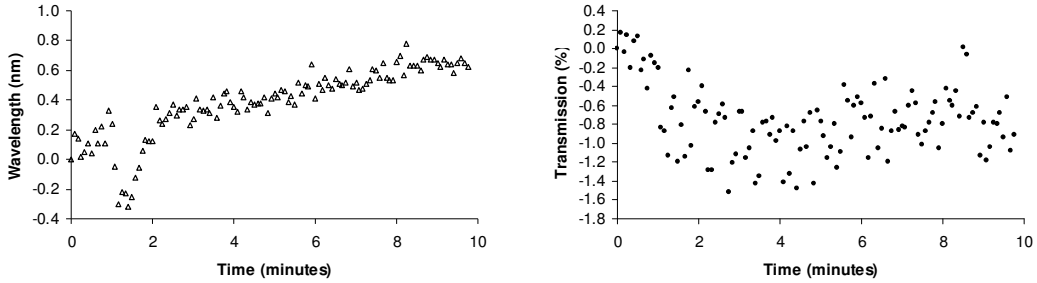

Figure 6.29 LPG_a spectral response to test 5.

Test 6

The outer magnet was maintained at 110A and the test coil was energised at a ramp rate of 20A/min from 0A to 200A and 10A/min from 200A to 400A. Figure 6.30 shows a negative transmission change of 16% for the first 10 minutes which corresponds with the initial ramp rate at 10 minutes. There is a change in slope that coincides with the change in ramp rate. In this test the transmission shows a dramatic change as a spontaneous quench occurs at 12.5 minutes. A large positive change of 18% is measured, that may be due to the addition of the energised test coil. The form of the response is also different to that of the test 1 and the lack of any notable wavelength response is contrary to the previous result.

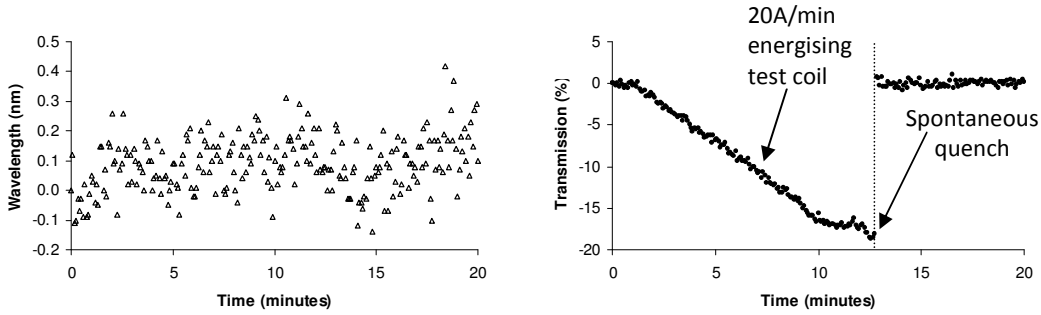

Figure 6.30 LPG_a spectral response to test 6.

Test 7

The background magnets were maintained at 110A and the test coil was energised from 0 to 200A at 20A/min and then from 200A to 400A at 10A/min. A spontaneous quench occurred shortly after the change in ramp rate at about 12 minutes into the test. Figures

6.31 and 6.32 illustrate the sensor response showing both wavelength and transmission changes at 12 minutes. The quench occurred at the same time as the previous test which may indicate a critical flaw with the magnet system. The transmission response of both sensors shows the energising of the coil with the change in ramp rate at 10 minutes. The wavelength response provides more information about the quench. The initial negative shift in wavelength over a 2 minute period is followed by a slower (>28 minutes) positive wavelength shift. The spectral feature appears to return to the spectral location at t = 0. As shown previously in test 1, LPG_h shows a larger wavelength shift.

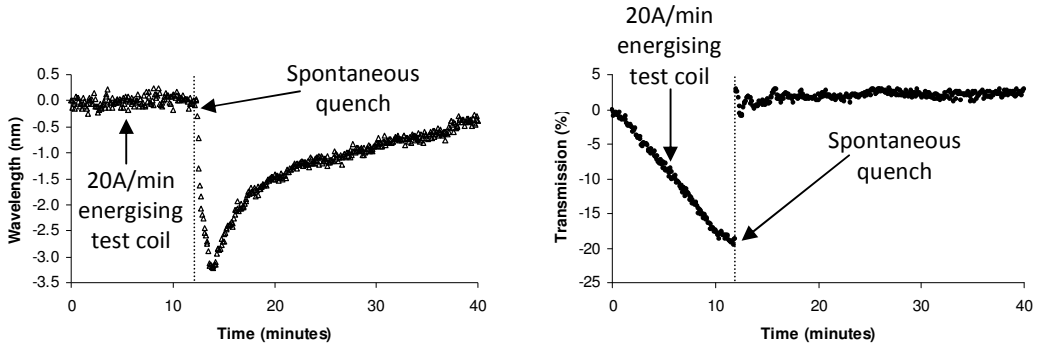

Figure 6.31 LPG_a spectral response to test 7.

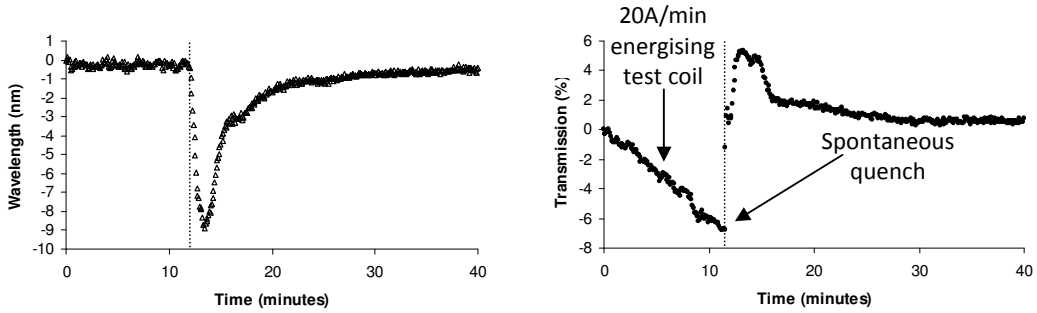

Figure 6.32 LPG_h spectral response to test 7.

Test 8

To determine the quench response at a higher resolution data rate, a forced quench test was initiated. The background magnets were held at 110A and the test coil was held at 100A. A forced quench was carried out by switching on heating elements in the outer magnets. The recording equipment was started a few minutes before the quench was initiated. Figures 6.33 and 6.34 show the transmission and wavelength response of the

spectral features for both sensors. The results show that LPG_a experiences a greater change in transmission whilst LPG_h has a greater wavelength shift.

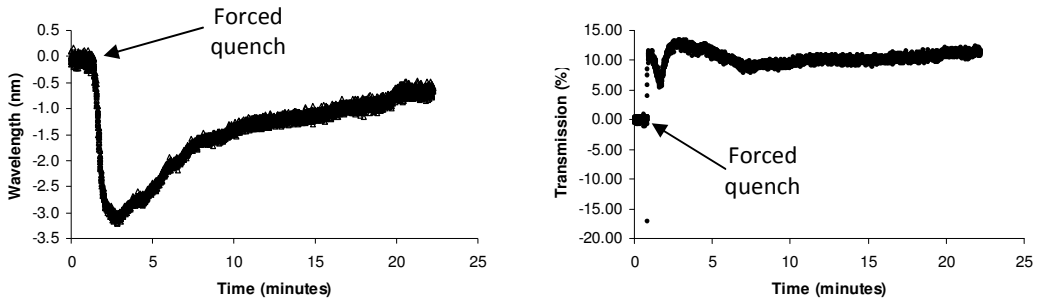

Figure 6.33 LPG_a spectral feature at 800nm response to test 8.

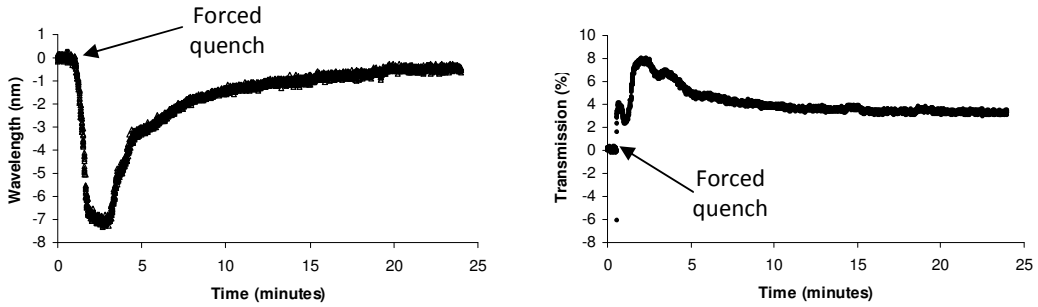

Figure 6.34 LPG_h spectral feature at 840nm response to test 8

6.3.6 Preliminary discussion on results

The spectral responses from the tests show different results for separate sensor locations. The discussion of the results however will focus on the final forced quench test. A forced quench was conducted with parameters given in table 6.2. A surface plot of the spectral changes over a broader wavelength range is shown in figure 6.35. The results for test 8 in the results section are derived from this spectrum. From the discussion in section 6.3.4 and the cool down test, it was shown that the original LPG attenuation bands were destroyed. The location of the new spectral features does not appear to have any wavelength correlation with the original attenuation bands. The features in figure 6.35 however, appear to emulate an LPG spectrum, with broadening bands and greater wavelength separation at longer wavelengths. I postulate that these

spectral features monitored here may be as a result of mechanical birefringent effects imposed on the fibre by the magnets construction.

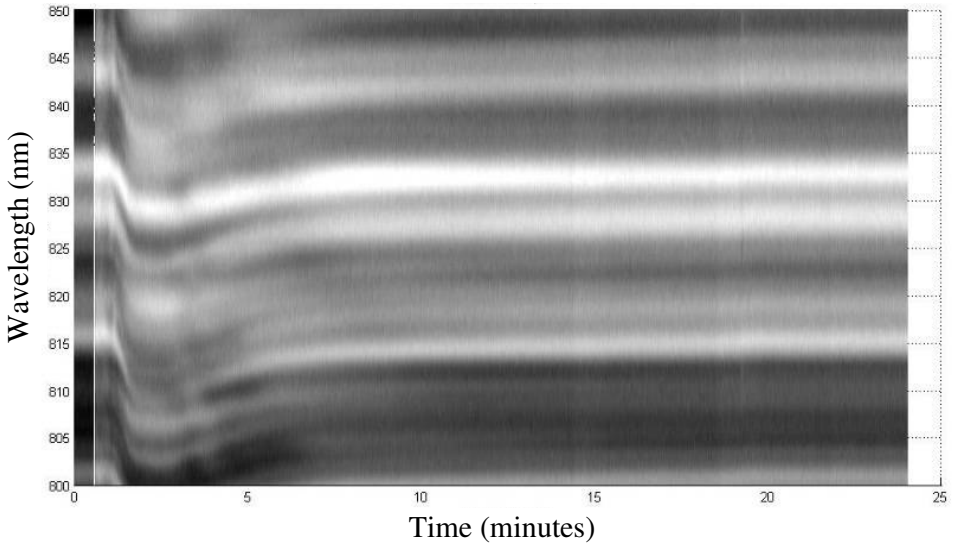

Figure 6.35 LPG_h spectral response to test 8.

The typical periods of LPGs range from 1μm to 1000μm in order to facilitate coupling to specific cladding modes, at certain wavelengths and/or to accommodate certain fibre types. The spectral features reported here may be a product of mechanically induced refractive index changes to the fibre. Mechanically induced LPGs have been reported previously [14,15,16,17] using differing methods to apply periodicity.

In the work presented in this trial, the fitting of the sensors is critical. Each of the fibre sensors were placed on glass fibre tape which was wound around the top coil layer to protect the superconducting coils from damage. A further layer of glass fibre tape was wound over the LPGs after fitting to build up the coil for steel reinforcement fitting. The glass fibre tape was of a plain weave with a period of ~900μm. The tension applied to the tape during winding and the contraction of the resin system during cure (shrinkage) causes the tape to place pressure directly on the bare fibre surface. The averaging effect of this pressure may impart birefringent effects [9] which cause band splitting and erosion of the original attenuation bands. The steel reinforcement windings are added post cure and provide mechanical constraints on the magnet which may result in further pressure applied to the fibre. During cool-down the results show no wavelength correlation with temperature which suggests the absence of any real LPG

bands, however the process of cool-down transmits more pressure on the LPG sensors due to thermal contraction of the magnets material parts. Resin has a high mechanical thermal contraction of ~1% and stainless steel ~0.3% [5]. This would impart significant forces on a fibre to induce a periodic pattern of the glass tape weave. To demonstrate this possibility a simple experiment, described in the following section was undertaken.

6.3.6.1 Experimental investigation of mechanically induced LPGs

The experimental layout is shown in figure 6.36. A fibre (Fibercore SM750) with a cut-off wavelength of 650nm, with the coating removed from a 5cm section, was placed on a flat plate bed and held down with two anchor points to ensure the fibre was taut and straight. The fibre was coupled to a tungsten halogen broadband light source and the spectrum is captured with an Ocean Optics S2000 CCD spectrometer. A section of glass fibre tape of 15cms in length was then placed on the fibre. A straight edged aluminium plate was then placed on the tape to hold it in place and ensure clean contact between the tape and fibre. Increasing loads were then placed on the fibre from 0kg to 20kg and the spectra were captured. For comparison the glass tape was replaced with lens tissue and the experiment repeated.

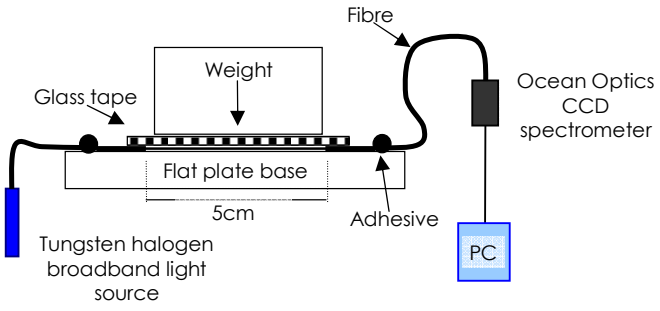

Figure 6.36 Experimental setup of mechanically induced LPG.

6.3.6.2 Results and discussion

Figure 6.37 (a) and (b) shows the spectra obtained from the experiment. Figure 6.38 focuses on the wavelength region of interest with reference to the test coil. The spectra show the growth of spectral features with increasing weight applied to the glass fibre tape.

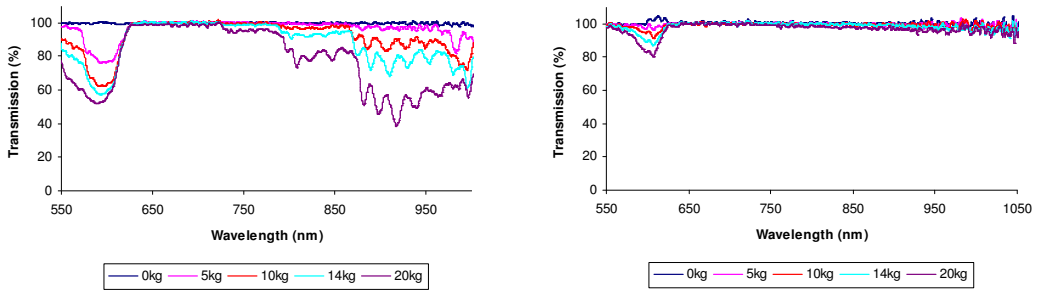

Figure 6.37 (a) Spectral features developed on bare fibre with glass fibre tape imprint, (b) features developed with lens tissue imprint.

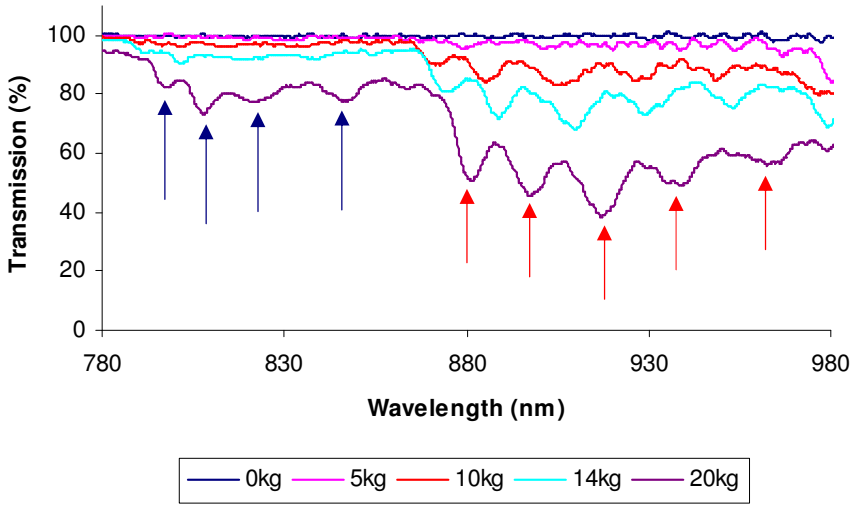

Figure 6.38 Spectral features of mechanically induced LPG with glass fibre tape imprint from 750 – 950 nm. Blue arrows indicate possible origin of bands evident in fibres of the test coil. Red arrows indicate longer wavelength bands not evident in test coil.

The results indicate that the presence of the glass tape with applied pressure creates spectral features. The periodic profile of the weave acts to generate an LPG on the fibre and the spectral features may be attributed as attenuation bands. The lens tissue with a random weave pattern does not generate spectral features for similar applied loads. The spectral features of interest (blue arrows in figure 6.2.38) also appear in the same wavelength region as those visible on the test coil. The stronger features at longer wavelengths, indicated by the red arrows, with cladding modes of longer evanescent tails may be more susceptible to interaction with the impregnating resin and further mechanical constraints associated with the magnet, i.e. the coil structure and steel over bind and are consequently destroyed.

6.3.7 Concluding discussion

Considering the spectral features as mechanically induced attenuation bands it is possible to compare the wavelength shift with the temperature response from the rhodium iron temperature sensors. Figure 6.39 illustrates the response of one of the spectral features against temperature for LPG_h, with less data points for clarity. Temporal analysis shows that both the temperature and wavelength response are similar. The results show a positive shift for positive temperature change from ~3 minutes. Although previous characterisation of the UV induced LPGs written in Fibercore SM750 fibre revealed a negative coefficient for temperature and wavelength response for a period of 400μm, a mechanically induced LPG has been demonstrated

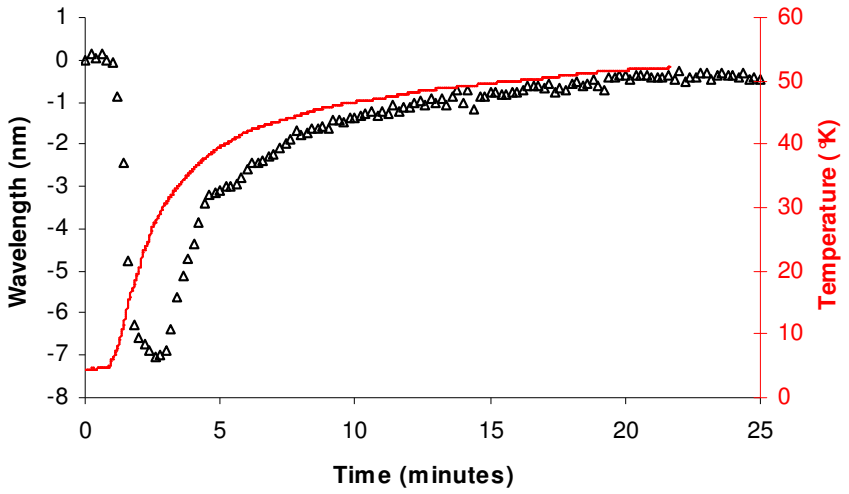

Figure 6.39 LPG_h spectral feature at 840nm, response to test 8 (with less data points for clarity) also shown is the temperature response from one of the rhodium iron sensors in the cryostat.

with a positive coefficient for a period of 600μm on telecoms grade fibre [13]. Published work on LPGs at cryogenic temperatures demonstrate a linear relationship between wavelength and temperature down to 77K with decreasing sensitivity to 20K [7]. A sign change for wavelength shift at temperatures below 20K is suggested from the work and this may explain the sign change evident from the results.

Figure 6.40 shows a correlation of wavelength shift with temperature. Two linear regions may be interpreted from the data either side of the trough from 18K to 37K. Below 18K the LPG has a temperature coefficient of -0.47nm/K and above 37K the coefficient is positive 0.21nm/K.

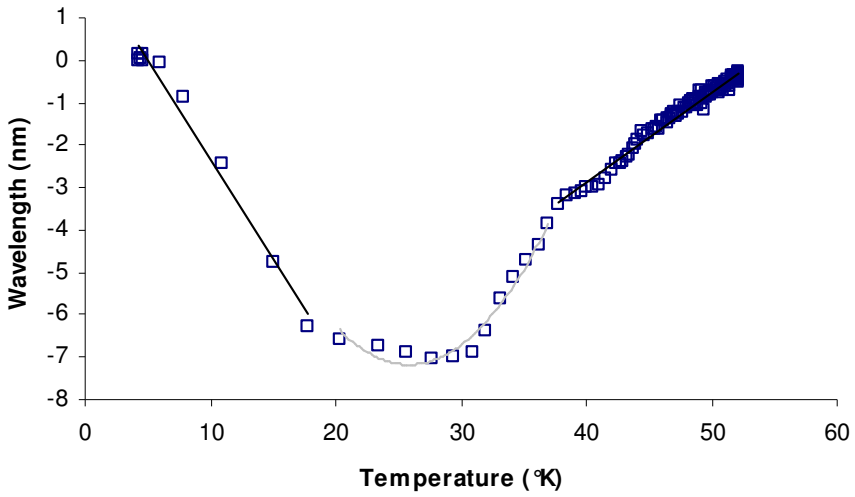

Figure 6.40 Correlation of wavelength shift and temperature from LPG_h. Below 18°K the LPG shows a good linear fit with a temperature coefficient of -0.47nm/°K and above 37K the coefficient is positive 0.21nm/°K.

Figure 6.41 is the response of LPG_a for the same quench event. The spectral location of this feature at 800nm was 40nm shorter than that shown for LPG_h (840nm). What is clear and what was shown previously, is the wavelength shift for LPG_a is less than that of LPG_h, although the temporal characteristics are similar. This may indicate a significant temperature difference between the sensors but what is a more likely explanation is that the LPGs are being subjected to different mechanical constraints and hence have different period designs with different temperature characteristics.

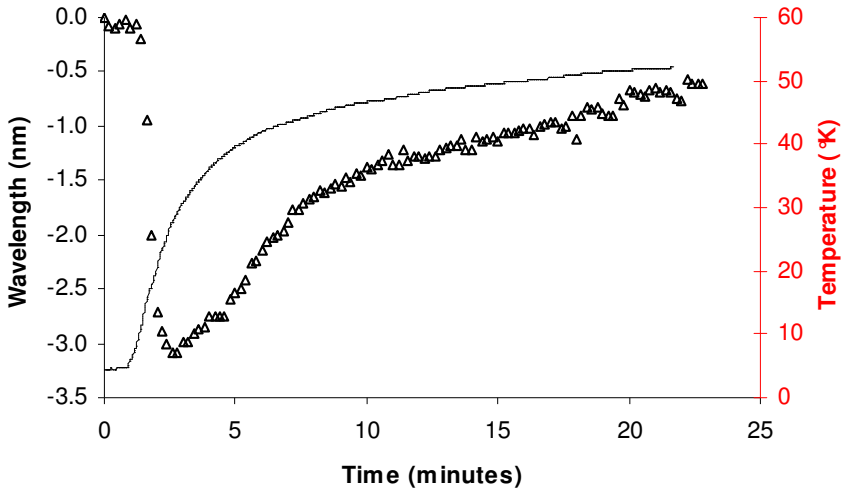

Figure 6.41 LPG_a spectral feature at 800nm, response to test 8 (with less data points for clarity) also shown is the temperature response from one of the rhodium iron sensors in the cryostat.

The correlation of wavelength and temperature is shown in figure 6.42.

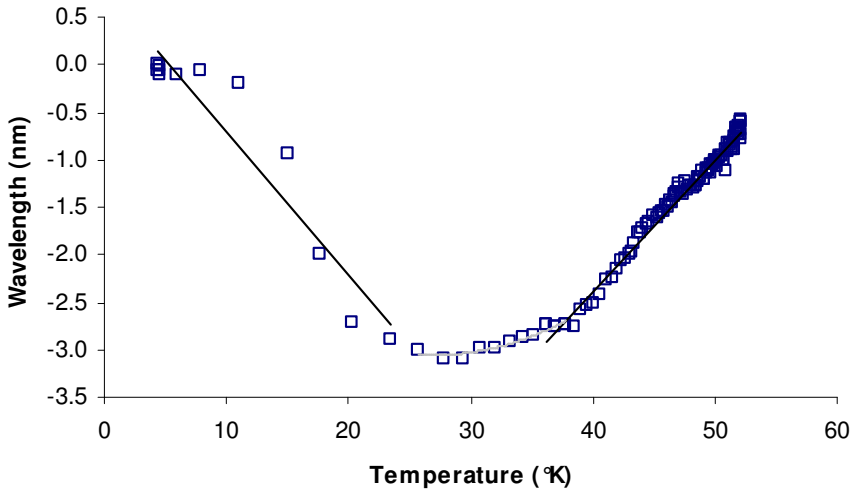

Figure 6.42 Correlation of wavelength shift and temperature from LPG_a. Below 23K the LPG shows a poor linear fit with temperature and a derived coefficient of -0.47nm/K and above 37K the coefficient is positive 0.21nm/K.

What is not considered here and may be significant, are the cryogenic effects on resin. Although the resin is used to impede the movement of individual coils within the magnet - to prevent the electromagnetic energy being converted to heat and initiate a quench – at cryogenic temperatures it becomes brittle [5]. Minor imperfections in the resin may lead to small cracks which can propagate with added stress (from energising the coil). This effect may result in a fibre sensor that is not uniformly surrounded by the resin and therefore give rise to a chirped spectrum. Chirped spectra require more bandwidth as the bands are broader and more complex and consequently more difficult to analyse. Chapter 5 demonstrates the potential use of chirped sensors as flow sensors and this initial work is discussed further in chapter 8. However dependant on the need for the sensor, the chirping of standard LPG spectra is detrimental as in the worst case the spectral bands could become too broad to analyse [18].

6.4 Integration issues of LPGs with composites.

6.4.1 Introduction

As discussed in chapters 2 and 3, the evanescent nature of LPGs has seen them demonstrated as sensors for temperature, strain, refractive index and bending. Their sensitivity to their surrounding however poses problem with application. Issues arrived at when integrating such sensors in industrial applications have been highlighted in section 6.3.4. Preliminary investigative work was carried out and the results highlight critical issues deploying such sensors in composites.

6.4.2 Experiment

The experimental layout is shown in figure 6.43. A fibre (Fibercore SM750) with a cut-off wavelength of 650nm was stripped of its protective jacket over a 40mm section. The UV writing method with amplitude mask as described in section 3.6.2 was used to inscribe an LPG of 400μm period over the 40mm length. The fibre was then placed on a flat plate bed and held down with two anchor points to ensure the sensor was taut and

straight. The fibre is illuminated with a tungsten halogen broadband light source and the spectrum is captured with an Ocean Optics S2000 CCD spectrometer.

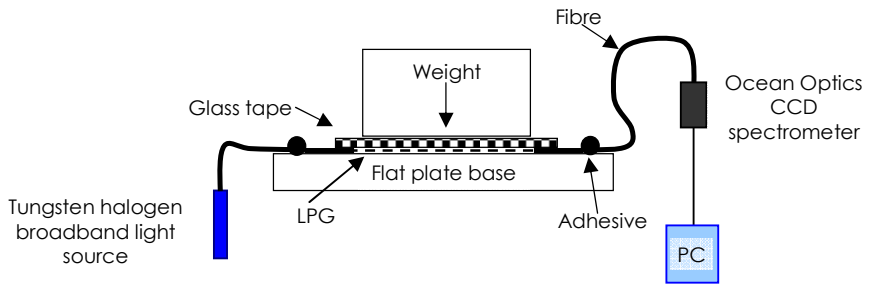

Figure 6.43 Experimental setup to investigate the interaction effects of LPG sensors with composite materials.

The tests involved subjecting the LPG to different contact environments, these were: glass fibre tape (as used by OINS and SMT), glass fibre weave, carbon fibre weave and metal (brush polished aluminium). A section of each material was used to cover the LPG and a load of 100g was placed to ensure direct contact of the material with the glass. The LPG spectrum was then captured. A further test involved placing an appreciable load of 7kg, to determine any loading effects. In some cases a combination of materials was used, these are indicated in the relevant spectral results. In this case a section of material was placed underneath the fibre on the flat plate base before the uppermost material was laid on top. The materials used are detailed in table 6.3

Table 6.3

Material	Code
Glass fibre tape	glasst
Glass fibre weave	glasw
Carbon fibre weave	carbonw
Brushed aluminium	metal

6.4.3 Results

Figure 6.44(a) shows the results for an LPG surrounded by air. The results for the same LPG are also shown for the cases where either a glass tape or metal is on the uppermost surface and the bottom surface of the LPG is in contact with the metal surface of the base plate. The bands are still visible.

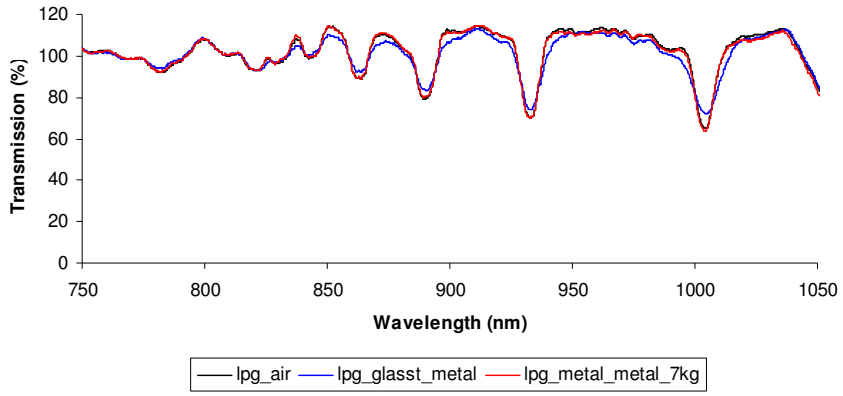

(a)

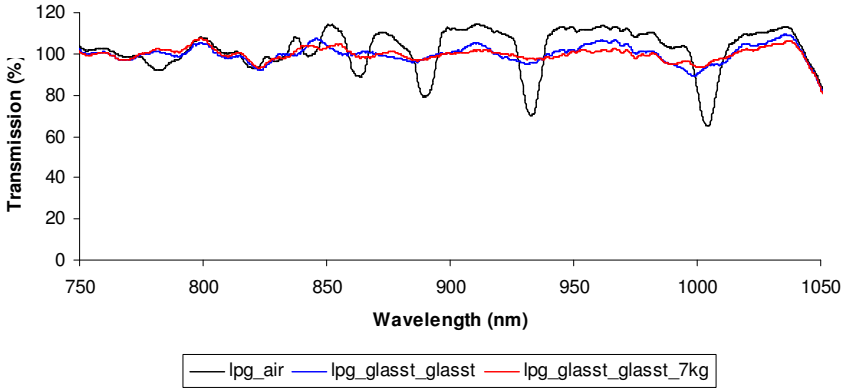

(b)

Figure 6.44 (a) LPG spectra for air, glass tape and metal, metal and metal (b) LPG spectra for air, glass tape top and bottom and glass tape with a 7kg load.

Conversely, figure 6.44(b) and 6.45(a) and (b) show the destruction of these bands when the fibre is in contact with a periodic surface on both the upper and lower surfaces. Here the bands are shown to disappear for a glass fibre tape on the lower

surface and glass tape, 6.44(b) glass weave, 6.45(a) and carbon weave, 6.45(b) on the uppermost surface.

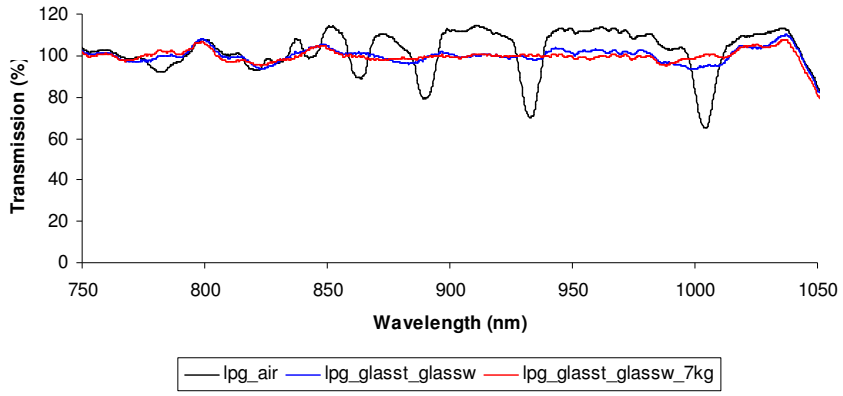

(a)

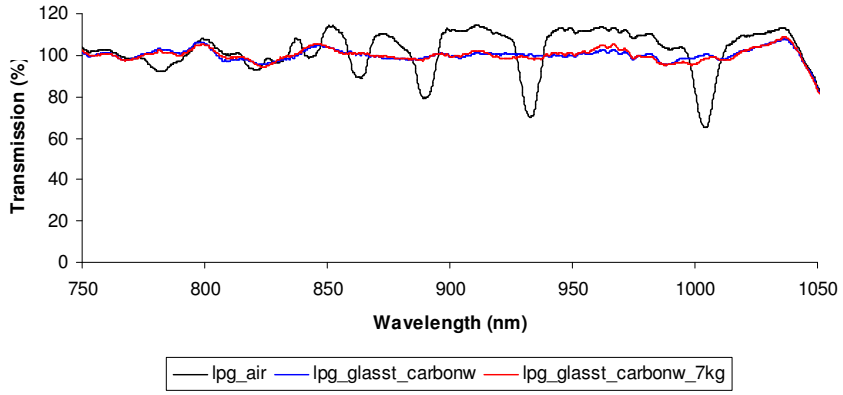

(b)

Figure 6.45 (a) LPG spectra for air, glass tape and glass weave, glass tape and weave with a 7kg load (b) LPG spectra for air, glass tape and carbon weave, glass tape and weave with a 7kg load.

6.4.4 Discussion

The results indicate that the presence of the glass tape, glass weave or carbon weave disrupts the coupling ability of the LPG. The effect appears to occur irrespective of whether the fibre is under load or not. The implication is that the LPGs are very sensitive to direct contact and care must be taken with deployment within a composite.

Figure 6.44 (a) also shows that disruption of the spectra is not complete if only one side of the LPG is in contact with a filament material. The smooth surface of the metal ensures that the cladding modes are still supported to enable coupling from the core mode. The results clearly show loss of LPG spectral features for sensors placed in direct contact with filament materials. It is therefore imperative for future deployment to develop methods for disassociating the sensor from the contact material into which it is placed without affecting its sensing capability.

6.5 Siemens trial

6.5.1 Introduction

Siemens Magnet Technology manufactures magnetic resonance imaging (MRI) systems for the medical industry. MRI scanners are superconducting magnet based systems that generate large fields (typically 0.3T to 3T, as opposed to Oxford Instruments typically from 5T to 22T) to enable analysis of human tissue. The superconducting coils which form the basis of the MRI scanners are of a composite structure and typically weigh 300Kg and of 1.5m diameter with an operating current of 600-800A. The particular focus for the industrial trial discussed here was integration of optical fibre sensors in a composite magnetic structure to enable both temperature measurement and the possibility of resin flow and cure during the production process.

6.5.2 Proposal/Aim

The test proposed placing optical fibre sensor within a 1/3rd scale production coil to access thermal data from the magnet during test and operation. It was proposed that two LPG sensors be deployed for the purposes of temperature measurement. The sensors were to be placed on the uppermost layer of the magnet for two reasons; firstly to speed up the development process by removing the obstacle of winding in fibre on the production line and secondly to reduce the risk of compromising the coil structure. The fibres would then be encased within the magnets composite structure. The aim is to

successfully achieve integrating the sensors and undertake a testing schedule to achieve measurable temperature effects.

6.5.3 Experiment

The test setup is detailed in figure 6.46. Two 40mm length LPGs of 400µm period were written on Fibercore SM750 fibre using the amplitude mask method discussed in section 3.6.2. Each sensor had 6m fibre tails to allow the fibre to be routed from the magnet through the cryostat to the measurement equipment and personnel. It was necessary to maintain an effective distance (~2m) from the energised magnet to ensure the equipment would not be affected by the emitted magnetic field.

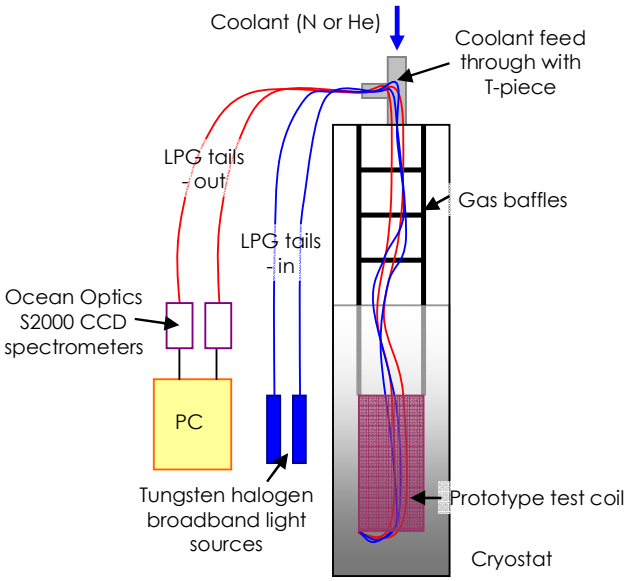

Figure 6.46 Experimental layout of Siemens trial.

Figures 6.47 and 6.48 show the spectra for both of the LPGs at specified times in the coils production life cycle.

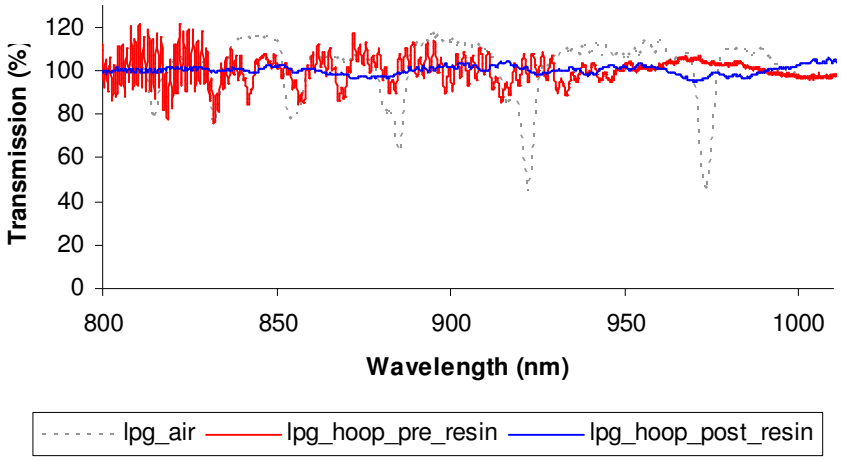

Figure 6.47 Spectra for the hoop or circumferentially placed LPG, LPG_h. lpg_air shows the original spectrum before attachment whilst the LPG is maintained axially straight with an air surround. Pre-resin impregnation and post-resin impregnation spectra are shown as lpg_hoop_pre_resin and lpg_hoop_post_resin.

As was the case with the integrated LPGs in section 6.3, the spectra are directly affected by the contact with the composite materials.

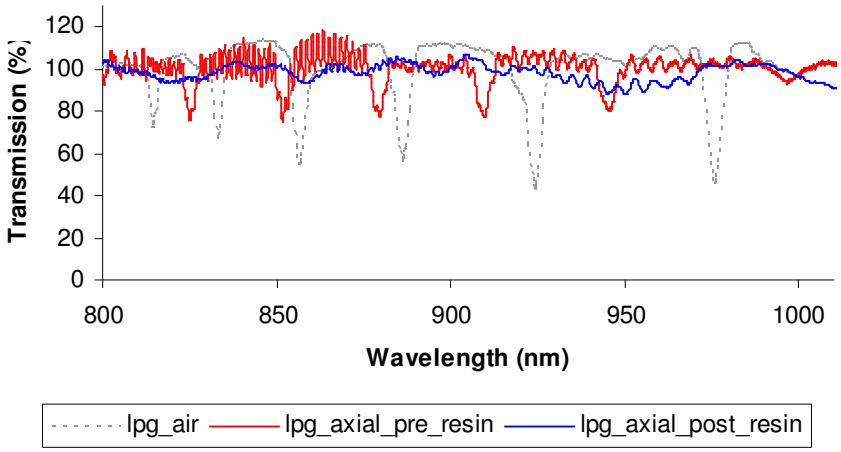

(b)

Figure 6.48 Spectra for the axially placed LPG, LPG_a. lpg_air shows the original spectrum before attachment whilst the LPG is maintained axially straight with an air surround. Pre-resin impregnation and post-resin impregnation spectra are shown as lpg_axial_pre_resin and lpg_axial_post_resin.

A prototype coil was used as a test bed for the application. Each LPG was coupled to a tungsten halogen broadband light source and interrogated with an Ocean Optics S2000 CCD spectrometer. The fitting locations for each of the individual sensors are shown in the simplified diagram of the magnet in figure 6.49. The sensors were placed on the top layer of the coils. A double sided Kapton tape was used to place anchor locations either side of the LPG sensors and to route the fibre over the surface of the magnet. After fixing a closely woven glass tape over bind was applied to protect the coils and sensors and to provide a mechanical structure to resist the coils natural tendency to expand and uncoil whilst energised. The LPGs were placed in two orientations to determine what effect this would have on the LPG signal during tests and to provide an element of redundancy.

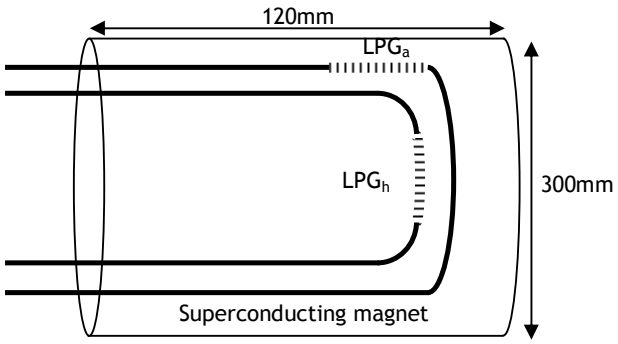

Figure 6.49 Simplified schematic showing LPG placement on prototype coil (not to scale). Axially mounted LPG termed LPG_a and circumferentially mounted LPG termed LPG_h.

Figure 6.50 is a photograph showing the location of the fibre, voltage and temperature sensors and heating elements. The fibres were accessed through a lead through shown on the right hand side and protected by small diameter (12mm) plastic tubing. The tubing was slit lengthways to reduce the risk of creating a pathway for the cryogens when the coil was placed in the cryostat.

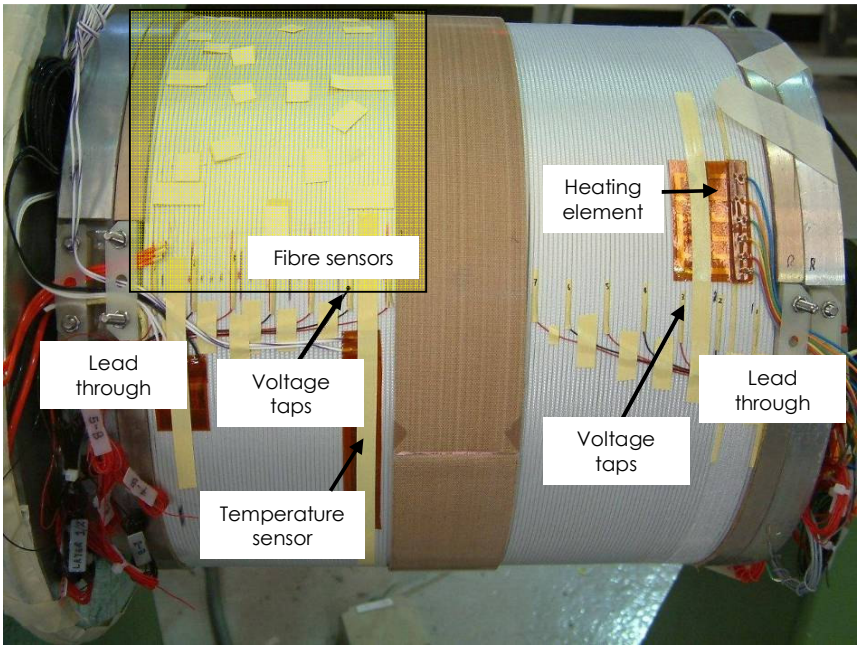

Figure 6.50 Photograph of magnet with optical and temperature and voltage sensors attached.

Figure 6.51 is a close up of the fibre sensor region and shows the two LPGs in orthogonal placements. LPG_h is on the circumference of the outer coils in the interstices of two adjacent windings. LPG_a is placed across the coil axially, bridging the interstitial gap.

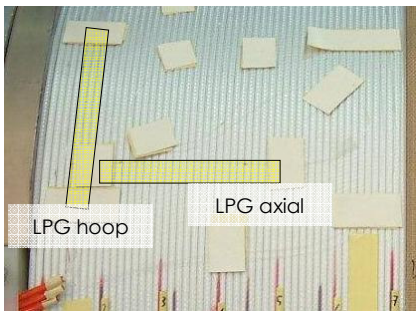

Figure 6.51 Close up of fibre layout area highlighting the LPG locations.

The glass fibre tape over bind was then wound around all sensors, figure 6.52 and built up to the edge of the tooling. The bulk glass fibre tape and resin composite provided a rigid mechanical structure to contain the movement of the magnet coils during energise.

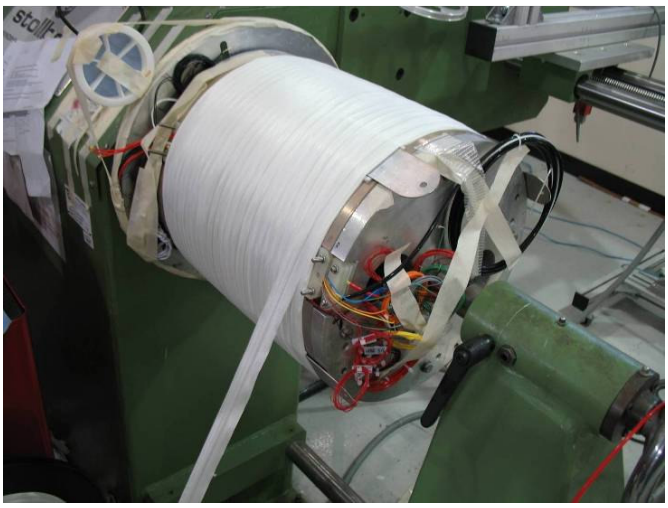

Figure 6.52 Prototype coil with glass fibre tape (over bind) being wound over coils and fibre sensors.

The coil was then impregnated with a diglycidyl ether of bisphenol A (DGEBA) based resin (MY 750) and hardener (HY 6552). The coil was placed in an autoclave and cured at 80°C for 12 hours. Figure 6.53 shows the magnet being prepared for impregnation placed in a potting vessel.

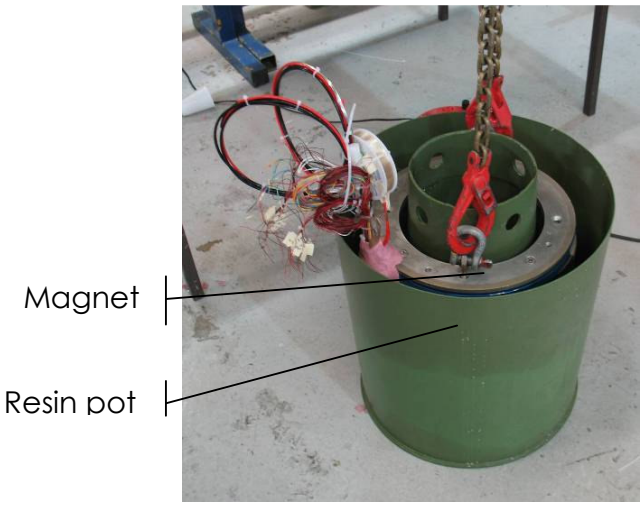

Figure 6.53 Test coil being prepared for resin impregnation.

(a) (b)

Figure 6.54 (a) Test coil with tooling attached post resin impregnation. The fibre is shown in the red plastic tubing and the tails are wound on spools for protection. (b) The lead through at the bottom of the magnet.

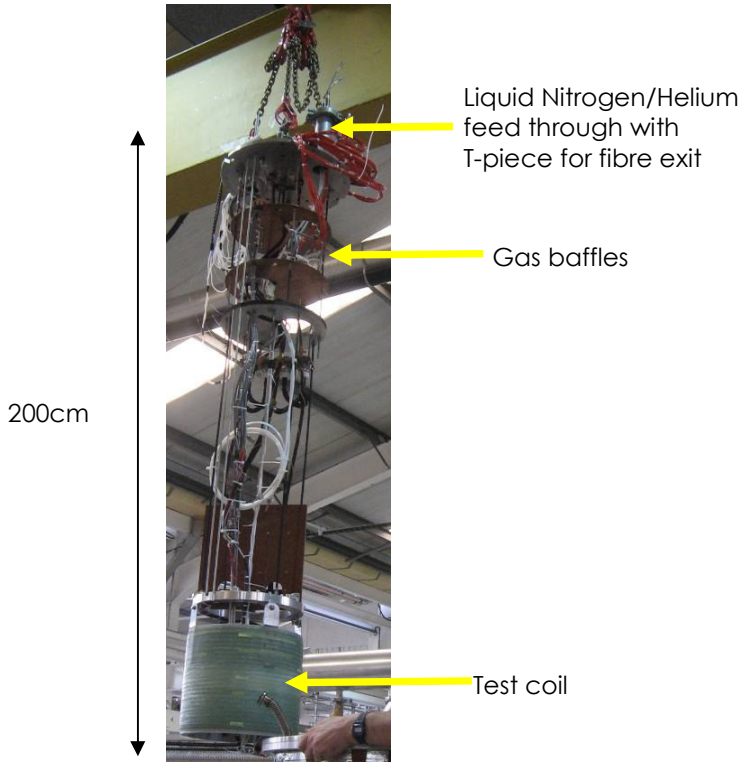

Figure 6.55 Test coil and cryogenic superstructure being readied for placement into the cryostat.

After impregnation and cure, figure 6.54 (a), the tooling was removed and any excess resin was machined from the coil. Continuity checks were made to ensure the fibres and ancillary sensors were intact and working. A lead through was designed, figure 6.54 (b), and incorporated to the base of the magnet to safely route the fibres with the other sensors through the centre of the magnet. This was to aid with the placement of the magnet and sensors in the cryostat.

The fibre tails were sheathed in 10mm nylon spiral bound from the lead through to the connection made at the spectrum analysers. Figure 6.55 shows the system in preparation for placement in the cryostat. A superstructure is mounted to the magnets as part of the thermal insulation mechanism, it also aids placement in the cryostat. The gas baffles act as radiation shields and prevent convection losses in the cryostat [8]. The fibres were accessed from the top of the cryostat via an adapted T-piece attached to the feed through for the cooling line. Figure 6.56 shows the system ready for test with the test coil placed in the cryostat.

Figure 6.56 Cryostat containing prototype magnet.

After placement in the cryostat, each LPG was coupled to a tungsten halogen broadband light source and the spectra captured using an Ocean Optics S2000 CCD. The setup was shown previously in figure 6.46. The CCD spectrometers provide a resolution of 0.25nm. The LPG spectra were captured at 3Hz, the capture rate determined by the light

levels achievable from the light sources and inherent losses in the system. Capture rates of up to 100Hz was achievable with the CCD spectrometer dependent on light levels. A simple test was detailed, table 6.4, to demonstrate the magnet during energise and quench.

Table 6.4 Test schedule	
Test	**Conditions**
0	Monitor cool down
1	Energise to 350A @ 100A/min
2	Force quench

6.5.4 Results

Test 0: Cool down

The first stage of the test involved cooling down the magnet to cryogenic temperatures. The cryostat is made up of an outer vacuum jacket (OVC), a sample space which is a liquid Helium reservoir and a cylindrical liquid nitrogen jacket which is built into the OVC and surrounds the liquid helium can [7]. The process involved pre-cooling of the cryostat with liquid nitrogen. The nitrogen is typically left overnight before being purged from the system with helium gas and is then filled with liquid helium which lowers the temperature of the cryostat to 4.2K. During this process the LPGs spectra were monitored to determine their response to temperature.

Because of the poor spectral information obtained from the LPG sensors it was difficult to derive a wavelength dependent response for cool down. Figures 6.57 and 6.58 show the change in transmission of both LPG spectra for the cool down process. The change in transmission may be as a result of thermo-mechanical contraction on the fibres inducing micro-bends on the fibre which affect the transmission characteristics of the fibre. The change in transmission matches well with the drop in temperature which was measured using carbon resistors glued at the midpoint along the inside diameter of the coil with Stycast™.

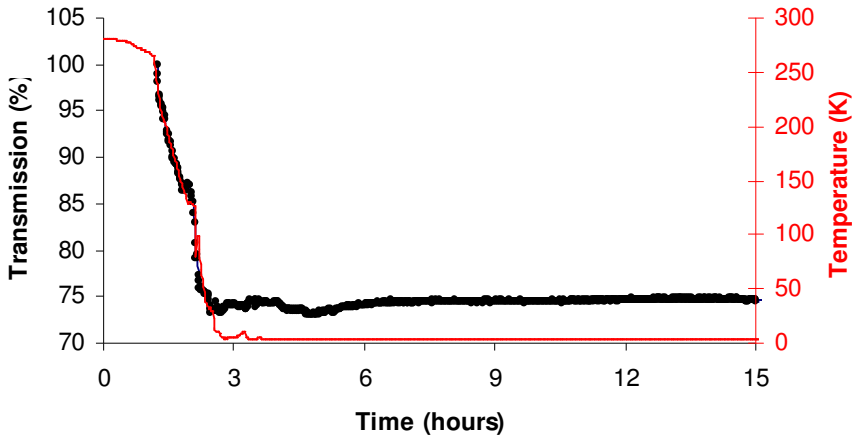

Figure 6.57 Average transmission change of spectrum (•) for LPG_a during cool down with liquid Helium to 4.2K. The actual temperature from a rhodium iron temperature sensor in the cryostat is also shown (–).

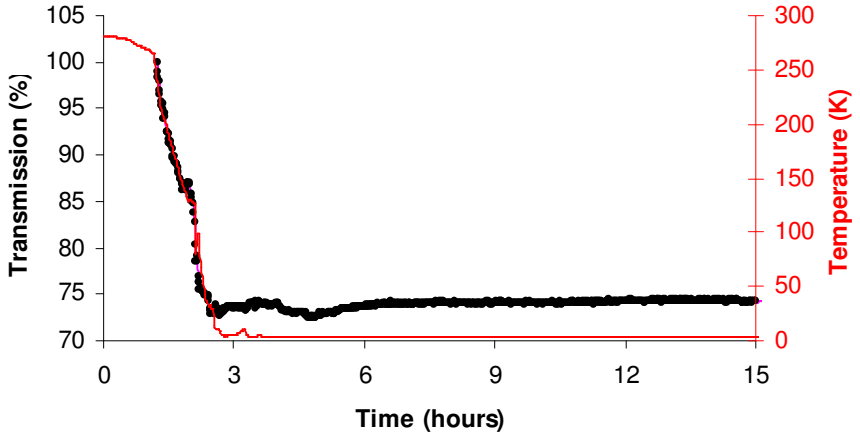

Figure 6.58 Average transmission change of spectrum (•) for LPG_h during cool down with liquid Helium to 4.3K. The actual temperature from a rhodium iron temperature sensor in the cryostat is also shown (–).

Tests 1 and 2: Energise and quench tests

The integrated fibre sensors were placed to access data from the magnet during energising of the coil and quench. The LPG sensors prime purpose was to access

temperature information during a quench. However, as indicated from the spectra shown in figures 6.47 and 6.48 previously the LPG bands appear to have been erased by interaction effects between the fibre and the surrounding environment of glass fibre tape, resin and mechanical and thermo-mechanical pressure. The following results refer to spectral features of the fibres un-related to those features ascribed to the original LPGs. The typical wavelength shift analysis associated with temperature changes exhibited by LPGs was unworkable due to the absence of attenuation bands. An alternative method of analysis was employed to determine the transient spectral effects. This involved referencing each subsequent spectrum during a test to an initial spectrum at time = 0. Using this technique it was possible to track very small changes of less than 1% to spectral features. This method although simple, required careful selection of the spectral bandwidth to improve the detection of spectral changes.

As discussed in 6.3.6.2 and section 6.4, the origin of the band loss may lie with the mechanical periodic perturbations induced from the glass fibre tape and pressure from the resin and thermal contraction effects. The results discussed here also concentrate on the response from, LPG_h. The spectral data from the axially mounted sensor, LPG_a, was poor although some information was gathered from the quench data. This may be explained by close inspection of the environment into which both sensors where placed. LPG_a was fitted bridging the interstitial gaps of the winding coils. This is illustrated in figure 6.59.

These coils were of a larger dimension than those of OINS, section 6.3, and consequently have a higher resin content. The high thermal contraction for resin [5] and brittleness at cryogenic temperatures may contribute birefringent and chirp effects on the fibre and alter the LPG spectra. These effects may be large enough to erase the LPG bands.

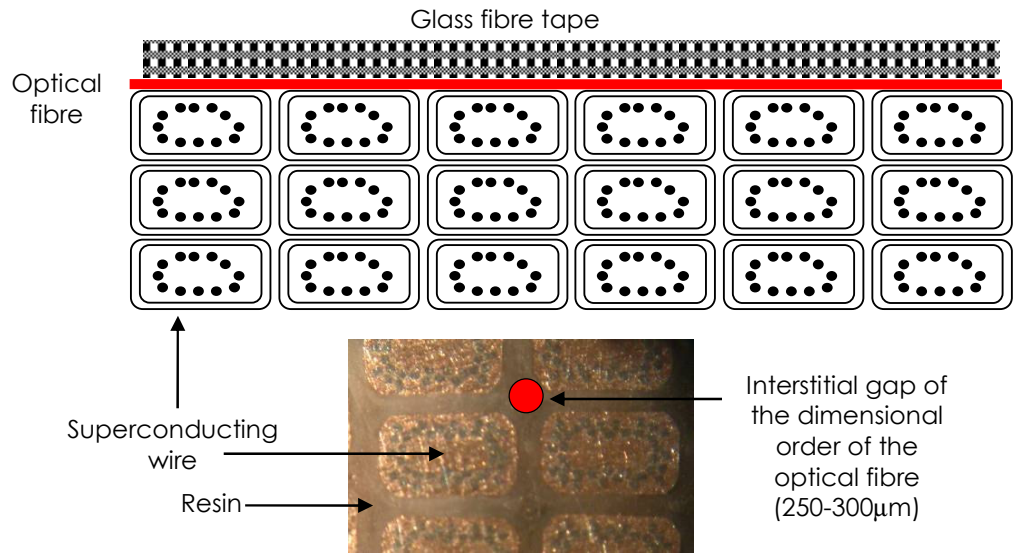

Figure 6.59 Pictorial and schematic layout of coils and LPG_a. The photograph shows a plane view of the coils and the interstitial gap. This is of the order of the dimensions of a fibre optic (courtesy of Dr. Adam Johnstone, Siemens Magnet Technology).

Test1: Energise

A spectral feature from 780nm to 790nm during the energising of the magnet is shown in figure 6.60 to develop a small transmission dip as the current is increased to 350A.

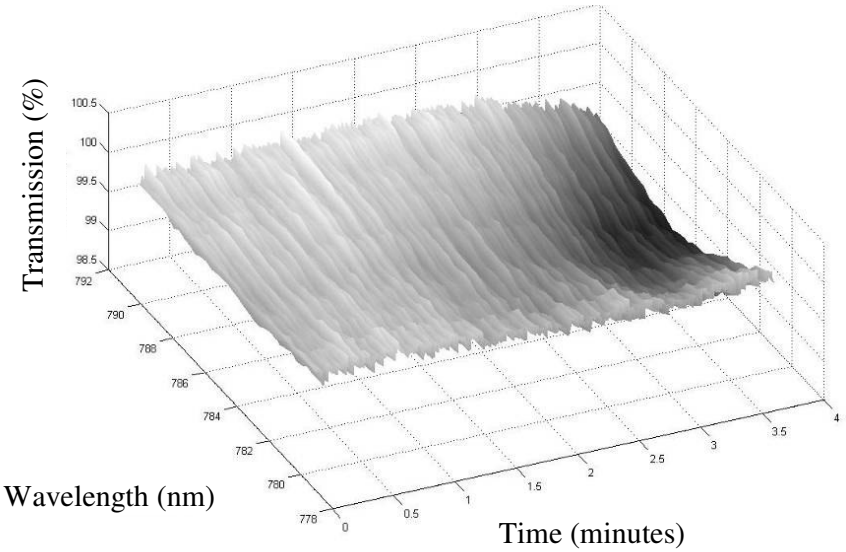

Figure 6.60 Spectral response of LPG_h from 778nm to 792nm during energising of the magnet.

This representation, in greyscale with black representing 0% and white representing 100% transmission, shows in 3D the effect of the energising current on the spectrum. Figure 6.61 shows the wavelength response of the feature against time. This was achieved by fitting a 6^{th} order polynomial and finding its minimum point.

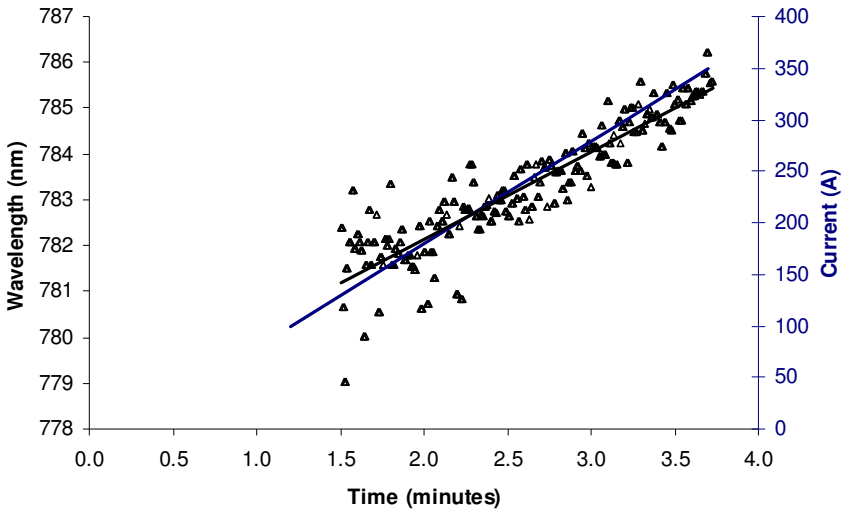

Figure 6.61 Wavelength shift (△) of attenuation dip in spectrum from 779nm to 787nm of LPG_h and current (–) during energising of magnet (test 4). Also shown is the trend line (–) for the transmission change for comparison with the current change.

The wavelength response of the feature shows that the fibre sensor responds to the energising current. The feature is traceable from about 1.5 minutes and the difficulty in tracking the minimum is evident as the noise is initially of the order of 4nm (standard deviation) before reducing to about 1nm. Comparison of the two trend lines in figure 6.61 shows a linear response with an approximate 4nm shift. The transmission response is shown in figure 6.62. The transmission change over the current ramp time shows a linear response also, however the change is very small, ~1% with a 0.2% noise error.

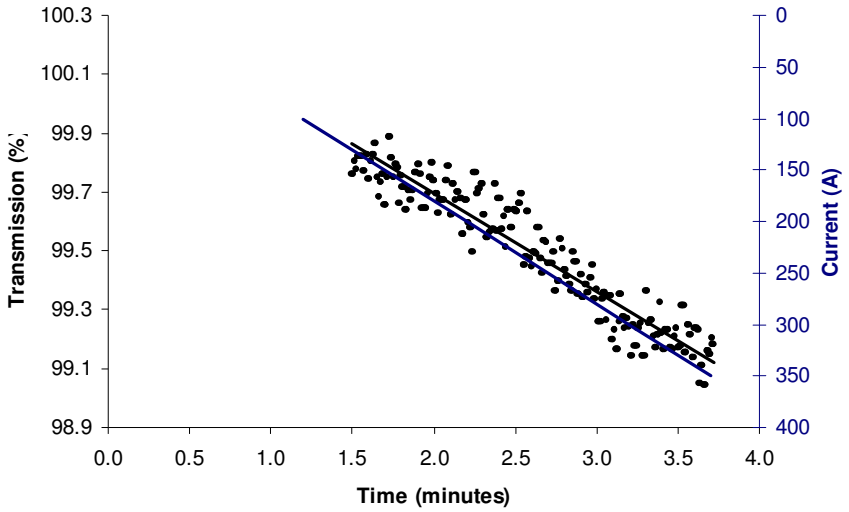

Figure 6.62 Transmission change (•) of attenuation dip in spectrum from 779nm to 787nm of LPG_h and current (–) during energising of magnet (test 4). Also shown is the trend line (–) for the transmission change for comparison with the current change.

Test 2: Quench

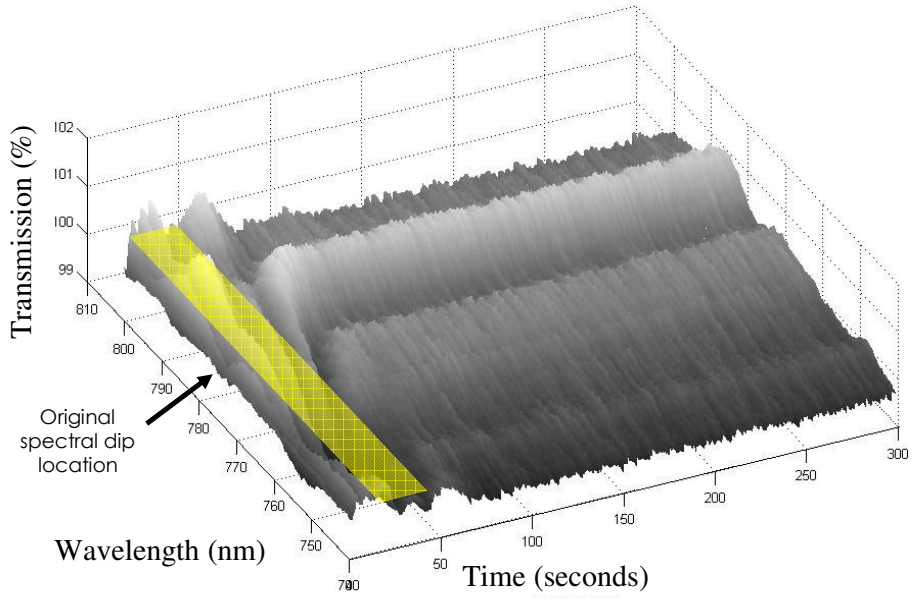

Figure 6.63 Spectral response of LPG_h from 740nm to 810nm during quench 4. The original spectral dip is visible at t = 0s. The shaded region in yellow highlights an area of rapid spectral change up to t = 23s.

A forced quench was initiated by heating a small area of the magnet using built in resistive elements on the magnet. Figure 6.63 is a 3D representation in time of the change in the spectrum from 740nm – 800nm of LPG_h. The figure shows a rapid change in spectral features at the initiation of a quench. From 20 seconds onwards a spectral dip (and associated peak) is seen to track from about 745nm towards 780nm for a period of approximately 1 minute.

Figure 6.64 illustrates this by showing the relative wavelength shift of the minimum point of the spectral dip. Also shown is the actual temperature response from a carbon resistor temperature sensor, the data logging system used updated every minute. A total wavelength shift of ~25nm is evident over the 90 second time period. The initial region up to approximately 28 seconds, annotated as the un-correlated region in the figure does not show any direct relationship with the temperature sensor. Preliminary results using highly birefringent FBG sensors to monitor the induced strain in a magnet show large spectral changes during this part of a quench. These results are yet to be evaluated but they may suggest that at this stage the fibre undergoes significant thermally induced mechanical deformation [18]. For this reason this part of the graph is not correlated with the temperature profile. The temporal comparison of the spectral change with temperature, for the correlated region is shown in figure 6.65.

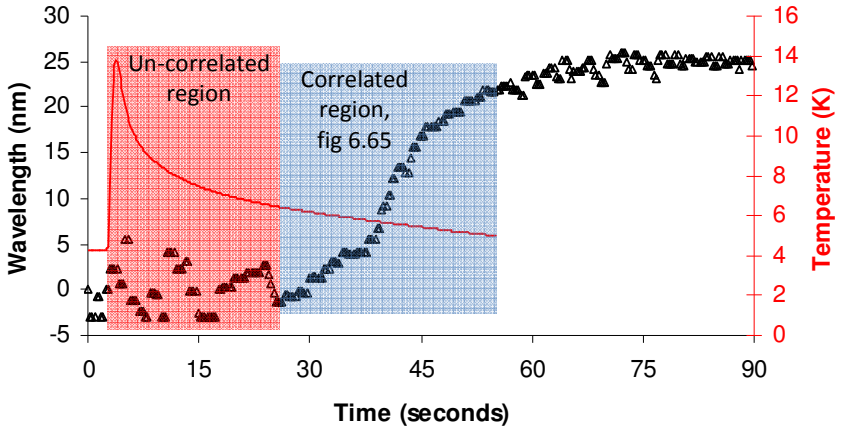

Figure 6.64 Wavelength shift of attenuation dip in spectral response from 745nm to 780nm (△) of LPG_h. The temperature response from a carbon resistor sensor in the cryostat is also shown (–).

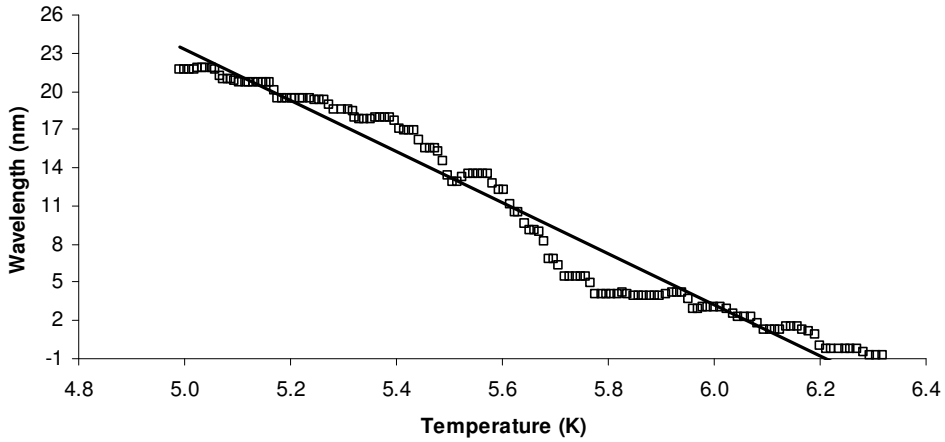

Figure 6.65 Correlation of temperature and wavelength shift for spectral feature in figure 6.64 for forced quench. $R^2 = 0.9627$.

Figure 6.66 shows a similar response for the same event for the axially mounted sensor, LPG_a. A total wavelength shift of ~20nm is evident over the 90 second time period. A 10 second period of data appears to be missing around 30 seconds. This is due to such small spectral changes that the feature becomes difficult to resolve.

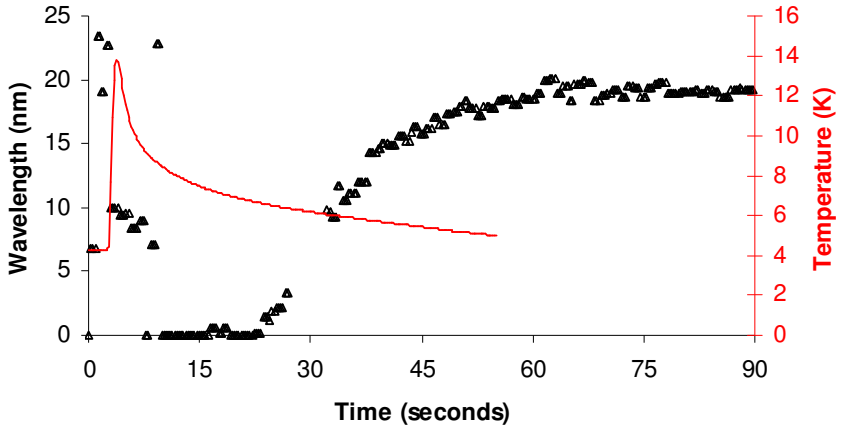

Figure 6.66 Wavelength shift of attenuation dip in spectral response from 700nm to 760nm (△) of LPG_a. The temperature response from a carbon resistor sensor in the cryostat is also shown (–).

6.5.5 Discussion

The original attenuation bands of the LPG written in the fibre using UV light appear to have been erased and the spectral features investigated in the results have no wavelength correlation with the original bands. As was shown in section 6.3 with the OINS LPG sensors the assumption is that the LPGs have been destroyed through the interaction of the fibre with its immediate environment. However there are small spectral features that are discernable and appear to have a wavelength response to energising and quenching of the coil. To aid with the understanding of the results, it is useful to compare these with those of section 6.2. This is acceptable due to the nature of the application (both are superconducting magnets), the materials used (the same resin and glass fibre tape) and the currents involved (100-300A). It is helpful to consider the differences between the two applications. The magnet in this case was bigger, dimensionally at least three times the size. The magnet was also a single magnet system as opposed to the OINS test. The reinforcement conditions for both were also different with a steel over bind utilised in the OINS magnet whilst the SMT magnet relied purely on the mechanical integrity from the composite construction of the coil with no added reinforcement. Following on from the discussion of results in section 6.2 and considering the spectral features as the result of a mechanically induced LPG we can interpret the results for energising and quench as attenuation band wavelength shifts. The bands respond to both temperature and strain.

The current energising results show a wavelength shift of 4nm. If this were purely a temperature effect, the results in section 6.2 and suggested here would indicate a resultant negative shift at very low temperatures (<20K). However, it may be as a result of strain imparted on the fibre altering the mechanically induced period; the restriction of coil movement in this case, not as stringent due to the lack of steel reinforcement. The small transmission drop (0.7%) may be attributed to micro bend losses induced by the coils.

Figures 6.64and 6.66 show a wavelength response to quench that follows that of the quench results in section 6.2. Although not shown in figure 6.62, the location of the spectral dip at t=0s is highlighted in figure 6.63. An area of rapid spectral change is highlighted in yellow before a wavelength trend is noticeable from time t=23s. This area

of rapid change may suggest movement to the immediate environment resulting in chirp and birefringent effects, e.g. band splitting, as discussed previously. A slower thermal response then starts to dominate as the spectral dip seeks to return to its original location.

6.6 References

1. James, S. W. and Tatam, R. P. T. (2003), 'Optical Fibre Long-period Grating Sensors: Characteristics and Application', *Measurement Science and Technology*, Vol. 14, pp. R49-R61.
2. Goodstein, D. and Goodstein, J. (2000), 'Richard Feynman and the History of Superconductivity', *Physics in Perspective (PIP)*, 2(1), p. 30-47
3. Brown, F.J., Kerley, N.W., Knox, R.B. and Timms, K.W. (1996), 'Review of high field superconducting magnet development at Oxford Instruments', *Physica B*, 216(3-4), p. 203-208.
4. Goldsmid, H. J. (1966), 'The physics of superconducting magnets', Physics Education, 1, p. 24-33.
5. Wilson, M. (1987), 'Superconducting magnets', Oxford University Press, Oxford, UK.
6. Culshaw, B. Dakin J., (Editors), Optical Fiber Sensors: Systems and Applications, ,Vol. 2, Artech House, Boston, USA.
7. James, S. W., Tatam, R. P., Bateman, R., Twin, A. and Noonan, P. (2003), 'Cryogenic Temperature Response of Fibre Optic Long Period Gratings', *Measurement Science and Technology,* 14, p. 1409-1411, 2003
8. Balshaw, N., (2007), Oxford Instruments Nanoscience literature (unpublished).
9. Zhang, L., Liu, Y., Everall, L., Williams, J. A. R. and Bennion, I. (1999), 'Design and Realization of Long-Period Grating Devices in Conventional and High Birefringence Fibers and Their Novel Applications as Fiber-Optic Load Sensors',*IEEE journal of selected topics in quantum electronics*, 5(5), p.1373-1378
10. Bunsell, A. R., (2005), 'Fundamentals of fibre reinforced composite materials', IoP publishing, London, UK

11. Kay and Labyhttp://www.kayelaby.npl.co.uk (accessed 26th May 2007).
12. Ye, C. C,. James, S. W. and Tatam, R. P. (2000), 'Simultaneous temperature and bend sensing using long period fibre gratings', *Optics Letters*, 25 , p 1007-1009, 2000.
13. Wei, C. Y., James, S. W., Ye, C. C., Tatam, R. P. and Irving, P. E. (2000), 'Application issues using fibre Bragg gratings as strain sensors in fibre composites, *Strain*, 36 , p.143-150.
14. Yokota, M., Oka, H. Yoshino, T. (2002), 'Mechanically induced long period fiber grating and its application for distributed sensing', 15th Optical Fiber Sensors Conference Technical Digest, 2002. OFS 2002,
15. Regoa, G. Fernandes, J.R.A. Santos, J.L. Salgado, H.M. P.V.S. (2003), 'Marques New technique to mechanically induce long-period fibre gratings', *Optics Communications*, 220, p. 111–118.
16. Mishra, V, Singh, N., Jain, S.C., Kaur, P., Luthra, R., Singla, H. Jindal, V.K., Bajpai, R. P. (2005), 'Refractive index and concentration sensing of solutions using mechanically induced long period grating pair', *Optical Engineering*, 44(9), p 094402-1-4.
17. Joon Yong Cho, J.Y. and Lee K.S. (2004), 'PDL-Compensated Mechanically Induced Long-Period Grating for EDFA Gain Flattening', *Fiber and Integrated Optics*, 23(6), p. 447-451.
18. Private communication with Dr. Edmond Chehura, Engineering Photonics Group, Cranfield University, Cranfield.

Resin transfer trials 7

7.1 Introduction

Resin transfer moulding (RTM) and vacuum infusion moulding are processes that involve the transfer of a resin system into a mould for impregnation of a dry fibre reinforcement material. Post impregnation the mould is taken up to temperature to initiate the cure process. The filling stage of such processes are understood theoretically [1], however in the more typical case where no clear definition can be made of the constituent materials properties, visual measurement techniques have been reported for the purpose of flow measurement [2]. Such methods are not practical in an industrial sense as they require transparent tooling. A dielectric measurement based flow sensor in an RTM process was reported by *Skordos et al* [3]. A dielectric sensor was used to create an electric field that emanated into the reinforcement fabric. The sensor was aligned parallel to the expected direction of the resin flow, figure 7.1. As the sensor was covered the dielectric response was monitored and revealed quantitative information about the filling process.

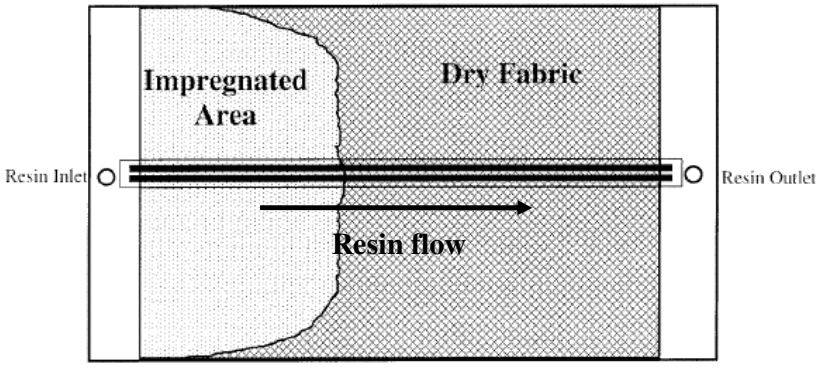

Figure 7.1 Working principle of dielectric flow sensor.

The sensor was also able to provide quantitative information about the cure process once the fibre was 'wetted' (process of impregnating the reinforcement fibre). In the following sections, LPG based optical fibre sensors are investigated as possible flow and cure sensors in an RTM trial and a vacuum infusion process. The results are compared with dielectric sensors for both flow and cure and with cure kinetic models.

7.2 Resin transfer moulding (RTM)

7.2.1 Introduction

Resin transfer moulding (RTM) is an industrial method of composite manufacture. The process involves pumping a resin which is mixed with a hardener (pre-catalysed) under pressure into a closed mould containing the fibre reinforcement. The mould is often heated to initiate and maintain the cure of the resin or matrix. The fibre reinforcement is typically a preformed woven or non-crimped fabric (NCF) of glass or carbon [4]. The engineering problems lie in ensuring an even wet of the reinforcement, a difficulty imposed by the non-Newtonian flow of the resin, and the uneven flow paths through the composite fibre and ensuring a homogenous cure [4,5]. Because of this specialised resins and thermal cycles are required.

7.2.2 Outline

An RTM mould was to be instrumented with optical fibre sensors and dielectric cure and flow monitoring sensors. In this proposal three types of LPG sensor were deployed to determine flow and cure and a TFBG for the determination of flow (see chapter 5). A Fresnel based refractometer, operating at 1581nm (as discussed in section 4.2.4) was used to measure the refractive index of the resin during cure. The aim was to establish the viability of placing fibre optic sensors in a semi-industrial machine, e.g. RTM and to measure the flow and cure of the resin.

7.2.3 Experiment

Figure 7.2 shows the experimental setup of the RTM. Based on the experimental results discussed in chapter 5, the flat plate mould was instrumented with LPG sensors, a TFBG sensor and with conventional dielectric cure and flow sensors. The optical fibre designs are summarised in table 7.1.

Table 7.1 LPG designs for RTM test.

Sensor	Design – length, period, fibre type	Purpose
LPG_{std}	40mm, standard 400μm, Fibercore SM750	Cure
LPG_{crp}	50mm, linear chirp 390-410μm, Fibercore SM750	Flow and cure
LPG_{cas}	40mm, 3 x standard LPGs cascaded non-interfering 360μm (LPG 1), 400μm (LPG 2) and 440μm (LPG 3), Fibercore SM750	Flow
TFBG	5mm, 4.5° blaze angle, Fibercore PS1250	Flow (resin presence)

The RTM setup consisted of an instrumented flat plate counter mould onto which the reinforcement material is carefully placed. The mould is closed and the resin is transferred to the mould by a pumping system that maintains the resin under a constant

positive pressure at 2bar. At the opposite end of the mould any resin residue that escapes from the mould is captured in a resin trap.

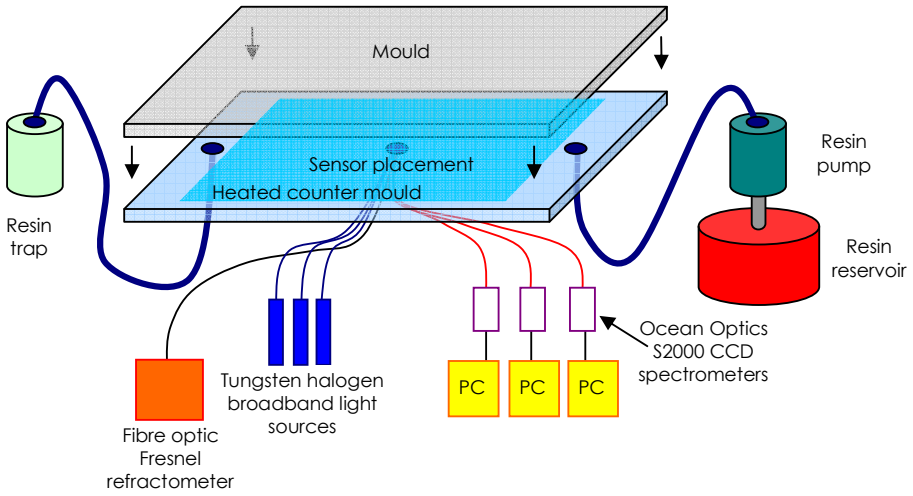

Figure 7.2 Experimental layout

Each of the sensors was designed to monitor a particular parameter of interest for composite material processing. All of the LPGs were written in Fibercore SM750, a single mode optical fibre with a cut off wavelength of 650nm. A standard LPG, LPG_{std} of length 40mm and period 400µm was written using the amplitude mask method described in section 3.6.2. A linearly chirped LPG, LPG_{crp}, was written using the point by point method described in section 3.6.3. The LPG was of length 40mm and its period ranged from 390µm to 420µm with a fixed UV exposed region of 200µm. An array of LPG sensors, LPG_{cas}, consisted of 3 LPGs of 3 different periods, 360µm, 400µm and 440µm. The sensor layout on the RTM mould is shown in figure 7.3.

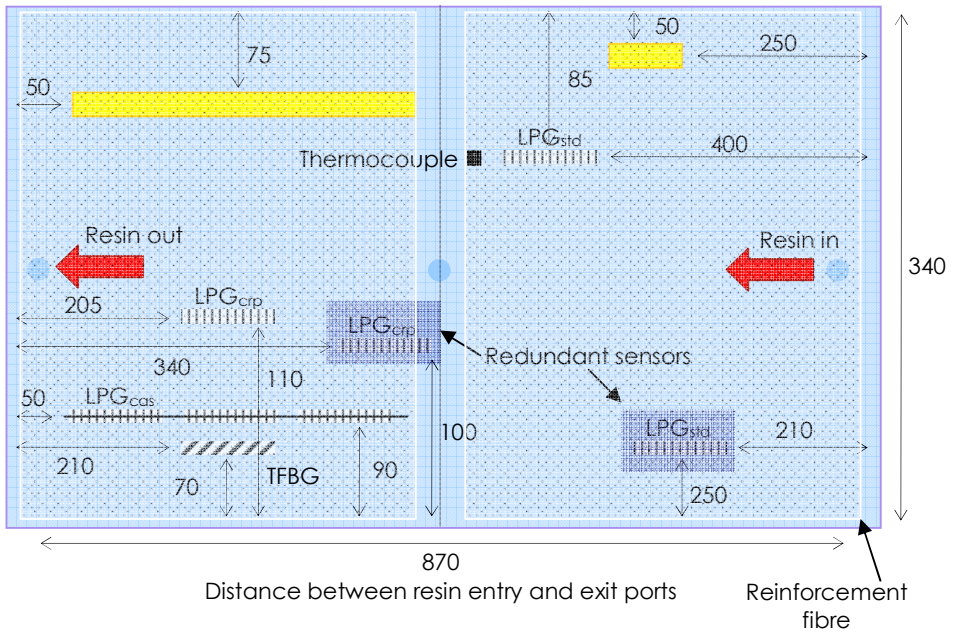

Figure 7.3 Layout of sensors on RTM flat plate mould. The reinforcement fibre was placed on top of the sensors, as shown. Two redundant sensors are also shown these were not used for analysis. All dimensions in mm.

The stages of preparation of the mould and sensors are shown in figure 7.4. The individual optical fibre sensors were fixed using thin section (10mm x 5mm) heat resistant Kapton tape (visible in figure 7.4 (b) as blue tape) on either side of the sensor whilst the fibre was held taut and straight. The optical fibre tip of the Fresnel refractometer was fixed using a single piece of Kapton. The dielectric sensors were fixed to the mould surface also using Kapton. An T-piece was adapted to allow the fibres to be safely routed out from the centre of the counter mould, highlighted in figure 7.4 (a). 5 layers of uni-axial non-crimp reinforcement fibre was placed on top of the sensors in the mould with a fibre orientation of 0°,±45°,90°,0° relative to the optical fibre axis, from the bottom layer upwards. The finished component would have a design V_f (equation 2.1) of 54%.

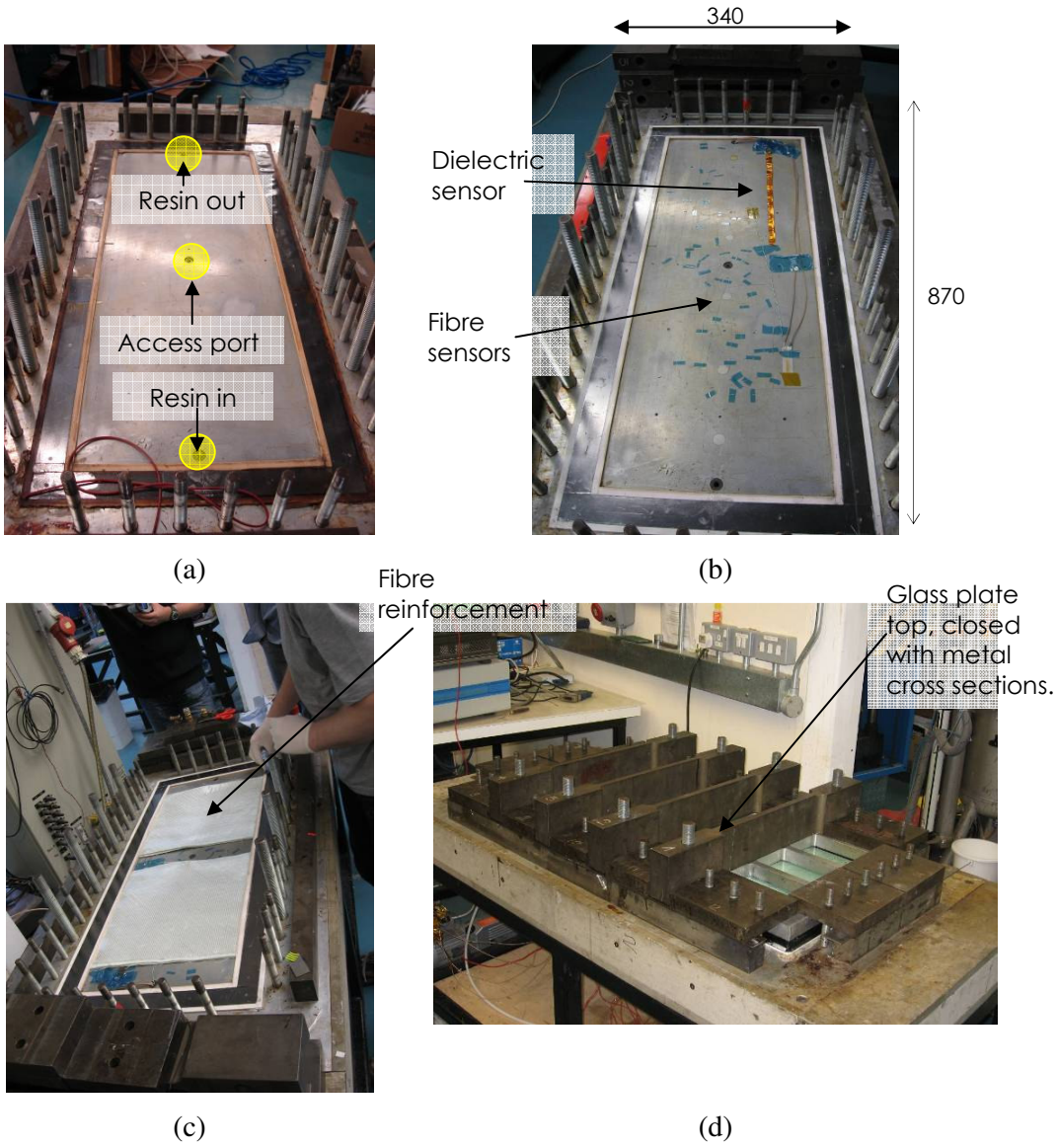

Figure 7.4 RTM at various stages of preparation: (a) shows counter mould in readiness for instrumentation, (b) the counter mould with fibre and dielectric sensors placed, (c) the reinforcement fabric placed on top of the sensors and (d) the mould closed. For this test a reinforced flat plate glass mould was used to visual measurement of the resin front during filling.

The spectra of each of the LPG designs: LPG_{std} LPG_{crp} and LPG_{cas}, are shown in figures 7.5, 7.6 and 7.7 respectively. The spectra are those captured before the RTM process was started. The sensors were placed within the mould and were in direct contact with the reinforcement fibres and the mould was closed.

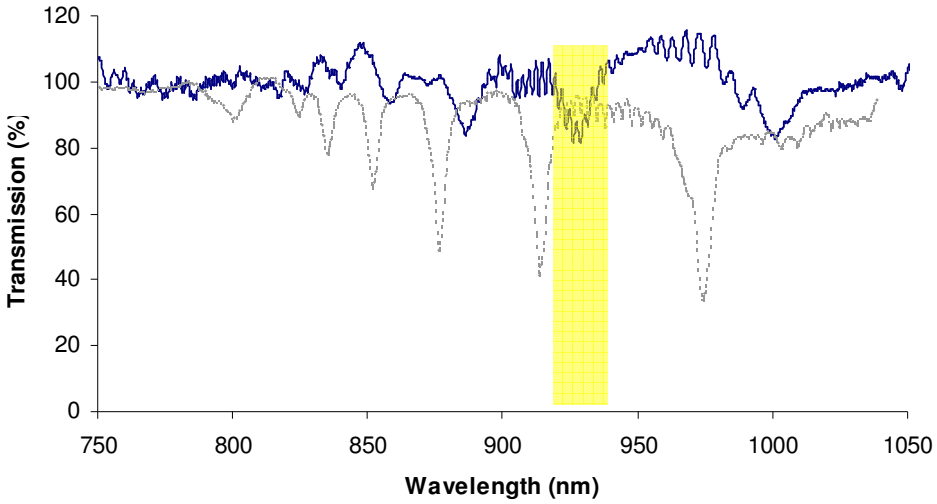

Figure 7.5 Shows the spectrum of LPG_{std} spectrum (—). Also shown is the typical LPG spectrum of a 400µm period LPG of 40mm length (▪▪▪). The spectrum shows the effects of interaction with the glass fibre weave with band depth diminished. The band highlighted is that which was used in the analysis of the results.

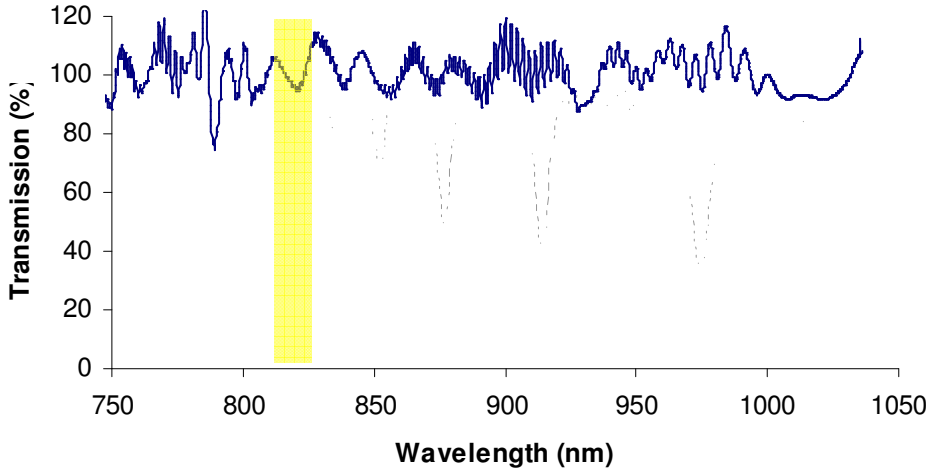

Figure 7.6 LPG_{crp} spectrum (—) for cure with typical LPG spectrum of 400µm period LPG of 40mm length (▪▪▪).The spectrum shows the effects of interaction with the glass fibre weave.

The chirped LPG, LPG_{crp} exhibits a similar spectrum to that of LPG_{std} however, because of the chirped period the bands are broadened and are not as easily distinguishable. This effect is compounded by the integration problems with the composite reinforcement, as discussed in chapter 6, and makes spectral analysis difficult.

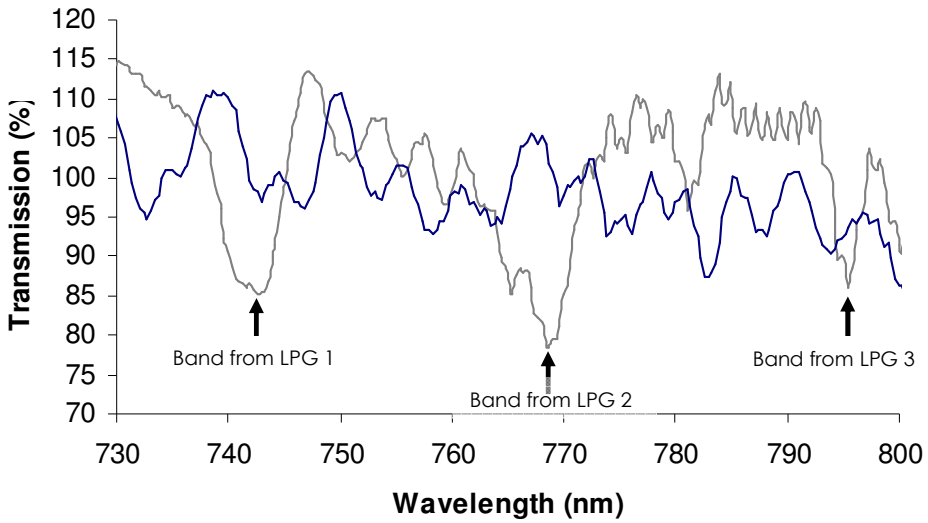

Figure 7.7 LPG_{cas} spectrum before placement in mould (—) and after(—). Three bands are annotated from the three different LPG designs, table 7.1, illustrating an example of a multiplexed LPG sensor.

Figure 7.7 shows three individual bands from the sensor spectrum that respond to measurands individually. This was demonstrated in the laboratory by heating sections of the single optical fibre containing the individual LPGs. An individual band corresponding to an LPG would respond independently of the others. It is a demonstration of the multiplexing ability of the LPG sensor. In practise however, the large bandwidth requirements restricts its application, for example in this case 70nm are necessary to encompass all three bands. Further complexity is added by the integration problem with LPGs and composites and this is highlighted by the difference between the spectra pre and post-placement in the mould.

After the reinforcement fabric was placed over the sensors on the counter mould, figure 7.4 (c), the mould was then closed with a reinforced glass plate, figure 7.4 (d). The glass plate allowed the position of the resin front to be tracked visually. The plate was annotated with timed measurements noting the resin front position and time to allow comparison with the flow sensors. The resin in the reservoir was maintained at a fixed temperature of 35°C. The resin transfer was initiated by pressurising the resin to 2 bar. During resin transfer the curing tool was maintained at a constant temperature of 40°C. Once the mould was filled with resin and the reinforcement fibre impregnated a 6 hour isothermal cure at 80°C was initiated and timed.

7.2.4 Results

The results are divided into two areas and discussed independently: flow measurement and cure monitoring.

7.2.4.1 Resin flow

The effects of the reinforcement fibre compressed on to the LPG array and the complexity of its spectra resulted in an inability to resolve any clear spectral features. The results shown are from LPG_{crp}. Figure 7.8 shows the wavelength shift and transmission change of the band highlighted in figure 7.5. There is a sudden wavelength shift at ~30 minutes, A, that correlates with the resin front reaching the LPG. At approximately 45 minutes, B, the attenuation shows a decrease of about 2%. This is consistent with the response of a band of a chirped grating as discussed in section 5.3, demonstrating the use of such a sensor as a directional liquid level sensor. The transmission decrease appears to occur at the same time as there is an apparent change in slope of the wavelength shift, C. This may indicate that the resin has coated the entire length of the sensor. The location of the start and end points from this analysis is shown in figure 7.9. The figure shows the visual measurement of the resin front together with the actual location of both the chirped LPG sensor and the TFBG sensor.

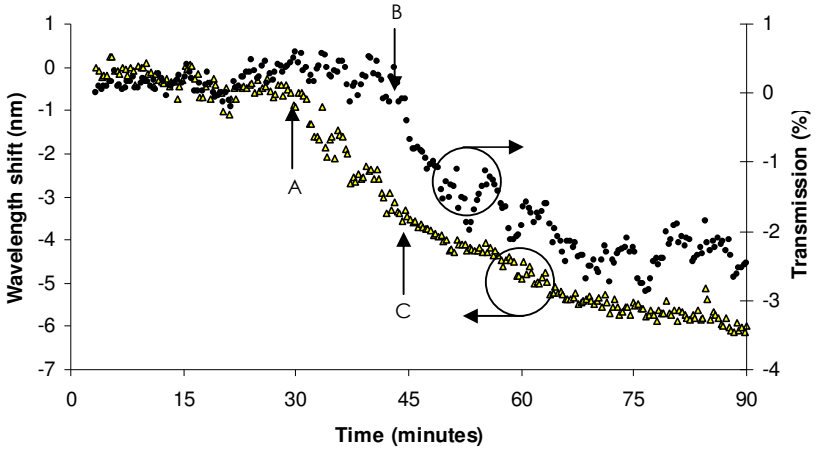

Figure 7.8 Chirped grating response to resin flow. A, resin front reaching LPG, B, transmission change as resin coats sensor and C, end of flow sensor.

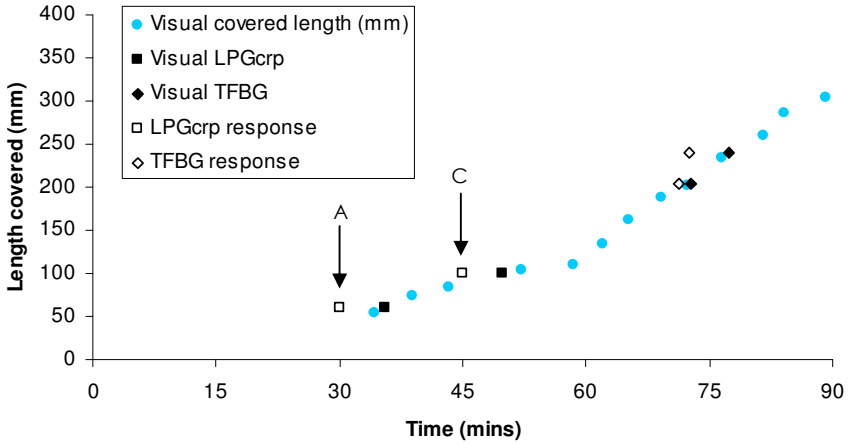

Figure 7.9 Flow sensor comparison of LPG sensors and visual measurements showing the calculated flow position from the LPG_{crp} (□), and TFBG(◇). The visual location of LPG_{crp} is shown as (■) and the TFBG is shown as (◆). The visual measurement of the flow is shown as (●). The points labelled A and C are those shown in figure 7.8.

The TFBG response is shown in figure 7.10. Points A and C correspond to temperature rises on the RTM hotplate to aid the progress of the resin through the reinforcement. At point B a clear drop in area of the enclosed spectrum is seen. This corresponds to the

arrival of the resin. The TFBG acts as a resin presence indicator with on/off sensitivity. The increase in area before this point (60 minutes) may be a feature of the temperature rise at point A. The temperature starts to stabilise at this point before the resin front arrives.

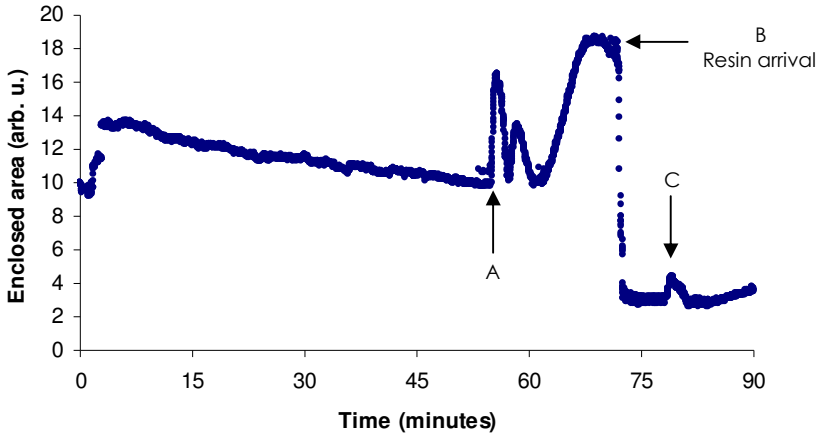

Figure 7.10 TFBG response to flow. Points A, B and C are discussed in the text.

7.2.4.2 Cure

Figure 7.11 shows the spectra for LPG_{std} at 0, 200 and 400 minutes. The spectra show the loss of band visibility during the cure process. This may be attributed to the resin shrinkage causing the reinforcement fibre to contract down on the fibre and affect the coupling efficiency of the UV induced LPG.

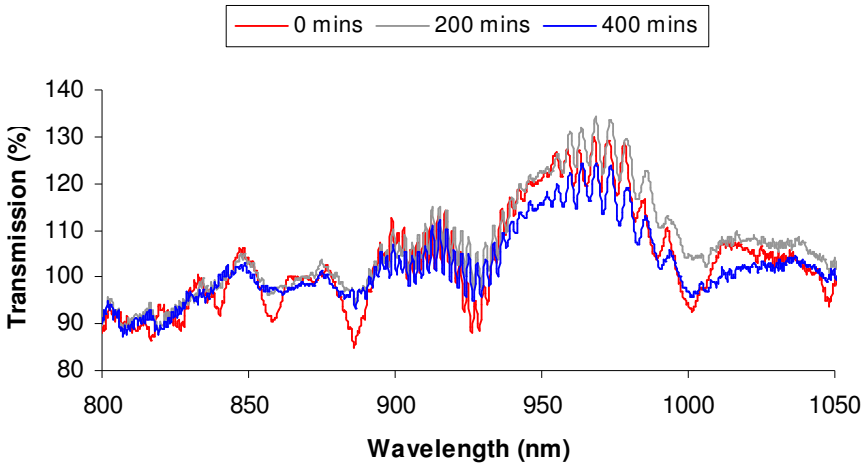

Figure 7.11 LPG_{std} at 3 points of time during the RTM process.

Figure 7.12 shows the wavelength response of band 6 in the spectrum. By fitting a 6th order polynomial to the band from 910nm to 940nm and finding the minimum it is possible to track the feature over time.

The wavelength response is shown against conversion as determined from the cure cycle and cure kinetics model [6]. The wavelength response is affected by the disrupted nature of the spectrum and the high refractive index of the resin. However, a trend with the conversion curve is noticeable. This demonstrates the use of the LPG as a cure sensor for resin systems with a refractive index above that of the sensing fibre. This result agrees well with that shown for the MTM 44-1 resin discussed in section 4.5 where a positive wavelength shift and high noise contribution are evident but the overall trend of the cure is still measured.

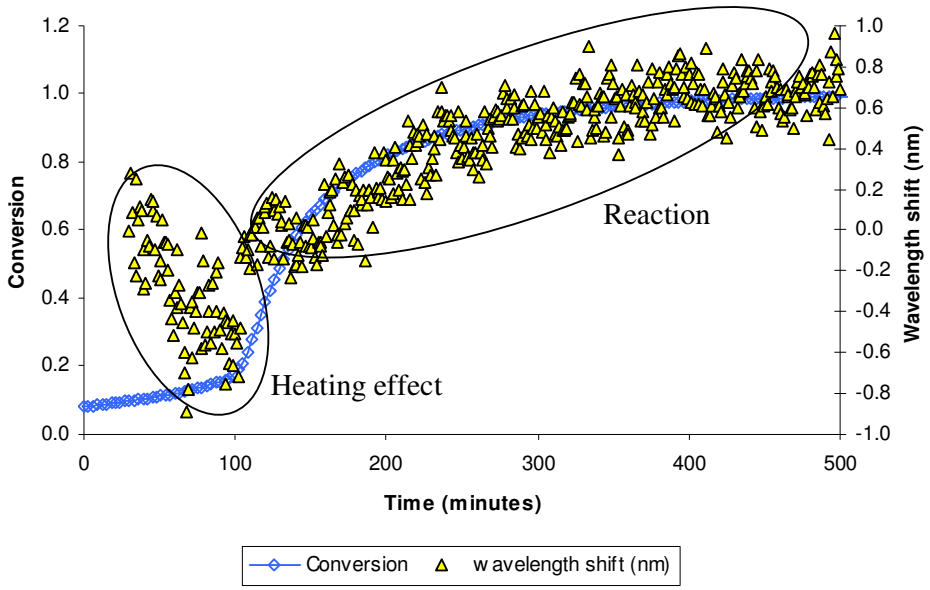

Figure 7.12 LPG_{std} band 6 wavelength response to resin cure and cure conversion model.

The small wavelength shift, 1nm, confirms the LPG is operating in the low sensitivity region of the LPG's refractive index response curve, figure 3.10. The initial dip in wavelength may be attributed to the temperature sensitivity of the sensor. This is further illustrated by analysis of the transmission response. Figure 7.13 shows the transmission response of the band over the cure time (500 minutes). The change in transmission of the band is shown to increase for the initial temperature ramps prior to the isothermal. At isothermal conditions the transmission decreases until it reaches another turning point at 300 minutes. The slight increase in transmission may indicate a small exothermal reaction during the latter stages of the cure.

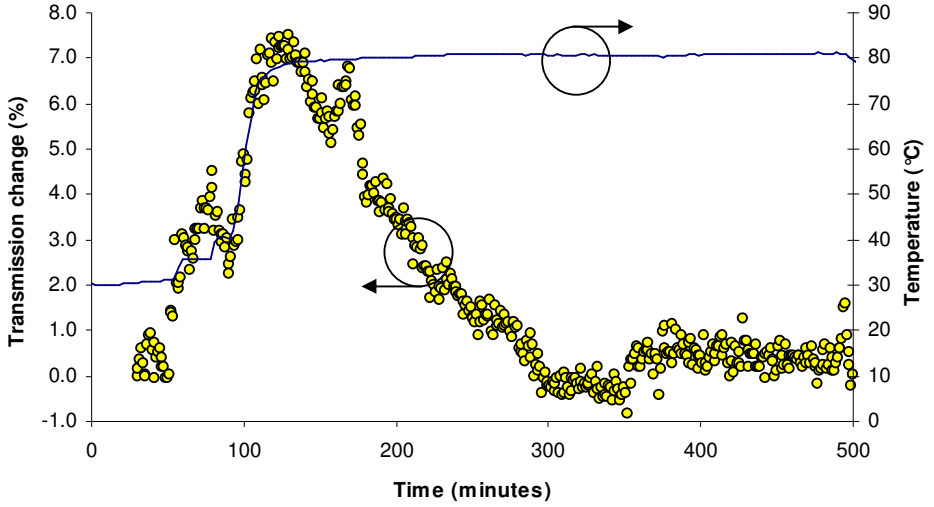

Figure 7.13 LPG_{std} band 6 transmission response to resin cure and cure cycle temperature.

The results from the optical fibre Fresnel refractometer are shown in figure 7.14.

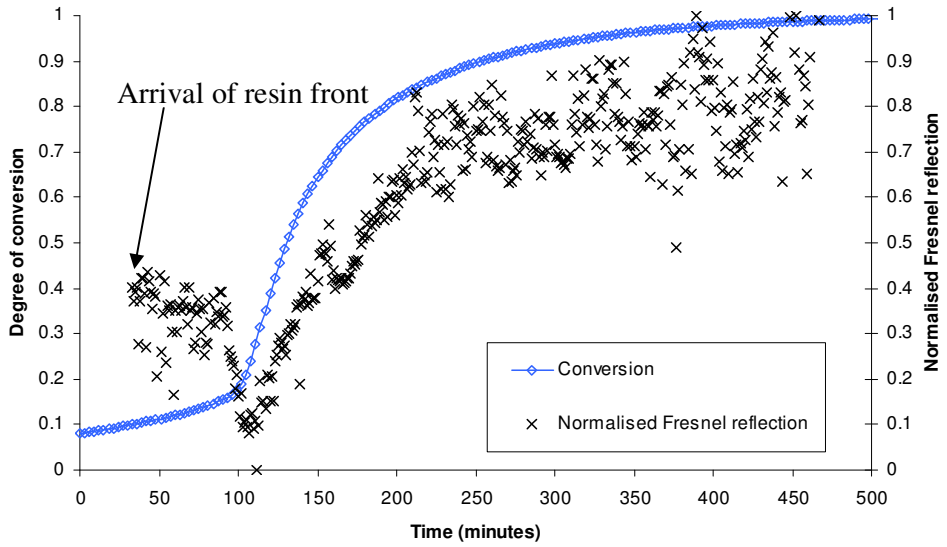

Figure 7.14 Fresnel refractometery measurements during resin cure.

These indicate the cure progression and show a good agreement with the cure kinetics model. The poor noise level may be due to a poor cleaved end on the fibre face caused by a fracture of the fibre during placement. It may also indicate mechanical interference

between the composite fibre and the sensing fibre. The Fresnel system also shows the arrival of the resin front at ≈32 minutes.

7.2.5 Discussion

The ability to deploy optical fibre flow and cure sensors has been demonstrated. Long period grating techniques, optical fibre Fresnel and tilted fibre Bragg grating methods were successfully realised in a manufactured composite using the RTM method. The results illustrate the possibility of incorporating such devices into industrial trials. The apparent incompatibility between the two technologies were overcome and with real design input a more rugged design for such devices would reduce integration concerns.

The results reveal a key issue which must be dealt with in future iterations of the work. The interaction between evanescent sensors and the environment into which they are placed is of critical importance. The advantages of such devices is clear, with their high sensitivity and multi-parameter sensing capability, however these abilities contribute to problems with integration, particular with high reinforcement fibre density composites. The LPG sensors experienced problems with distorted spectra.

The spectral information from the LPG sensors was poor and consequently the ability to detect the resin front for example was compromised, figure 7.8. However there was a clear indication of cure from the standard LPG place in the composite for the purpose but it also showed signs of spectral distortion. The effects of direct contact between an LPG and the reinforcement network of a composite have been reported before [7]. The solution proposed in the publication, encasing the LPG in a glass tube is interesting but the method precludes its use from integration within a composite material.

The spectral distortion effects, which are discussed and investigated to some extent in chapter 6 present an interesting research challenge as obvious solutions, e.g. mechanically seal the sensors from direct contact with the environment or placement in a capillary tube, inhibits the sensors full capabilities. Techniques to develop the sensor further to allow the sensor to integrate well with such composites are discussed further in chapter 8.

The optical fibre Fresnel refractometer results show the ability to detect cure online in an industrial system. The cure development was tracked through the Fresnel reflected light from the tip of what in this case is believed to have been a broken fibre. With a compromised sensor however the ability to 'see' the cure is still achievable. Point detection of the resin front is also achievable with such a system. Detection of the presence of resin was also demonstrated by the TFBG sensor. The enclosed area of the spectral resonances (as discussed in chapter 5) shows a dramatic decrease that corresponded to the arrival of the resin at the sensor location. Because the gauge length of the TFBG was 5mm the spectral response was of a point like sensor with an instant change to the spectra when the resin front had reached the device

The trial saw the successful incorporation of several different optical technologies for cure and flow measurement but further development work is needed to implement LPGs in direct contact with the reinforcement fibre.

7.3 Vacuum infusion trial

7.3.1 Introduction

Vacuum infusion is a method of composite manufacture that uses vacuum as an aid to resin impregnation of fibre reinforcement. Its main advantage over other manufacturing methods is its simplicity. It allows composites parts to be manufactured which have high fibre to resin ratios to develop greater strength to weight ratio characteristics. The vacuum infusion method employed in this trial uses a vacuum bagging technique which creates a mechanical pressure on the mould to increase the fibre to resin ratio and ensure there is no movement of fibres during the filling process. It also ensures that air is removed and that resin infuses throughout thus ensuring there are no dry locations.

7.3.2 Outline

A mould was to be instrumented with optical fibre sensors and dielectric cure and flow monitoring sensors. In this trial two types of LPG sensor were deployed to determine

flow and cure. An optical fibre Fresnel based refractometer, operating at 1581nm (as discussed in section 4.2.4) was also used to measure the refractive index of the resin during cure. The aim was similar to that stated for the RTM trial: the placement of optical fibre sensors and measurement of cure parameters in a quasi-industrial application, however in this case the test was applied to a more recognised industrial moulding technique.

7.3.3 Experiment

Figure 7.15 shows the experimental setup for the test. A flat plate mould was instrumented with LPG sensors and with conventional dielectric cure and flow sensors. The LPG designs are summarised in table 7.2. The purpose of the trial was to investigate the response of chirped gratings to both flow and cure in an industrial application.

Table 7.2 LPG design for vacuum infusion test.

LPG	**Design – length, period, fibre type**	**Purpose**
LPG_{A_100} LPG_{B_100}	2 x 100mm, linear chirp 390-410μm, Fibercore SM750	Flow
LPG_{40}	40mm, linear chirp 390-410μm, Fibercore SM750	Flow and cure

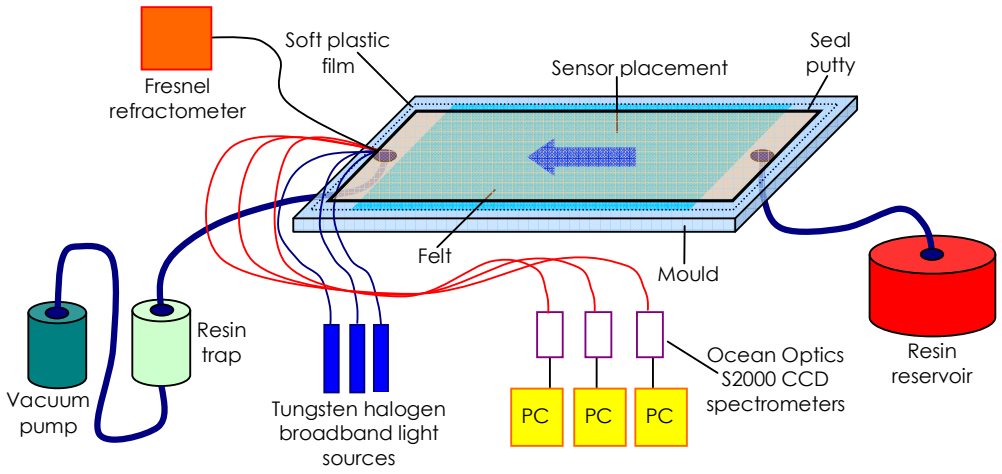

Figure 7.15 Experimental layout of vacuum infusion process. The blue arrow indicates the flow of resin.

The process consists of a mould onto which the reinforcement fabric and in this case the sensors are placed. The mould is sealed with a soft plastic film that acts to bag the entire mould. A resin reservoir is maintained at a constant temperature at one end of the mould. The infusion process is initiated by the application of a vacuum at the opposite end of the mould which causes the plastic bag to seal down onto the mould and 'suck' resin into the reinforcement fibre. A resin trap is placed before the vacuum system to prevent resin entering the vacuum pump and causing damage.

The sensors are coupled to tungsten halogen broadband sources and interrogated using Ocean Optics CCD spectrometers that are controlled using PCs. Each sensor was designed for a particular measurand. All the LPGs were written on Fibercore SM750 fibre with a cut off wavelength of 650nm. The linearly chirped LPGs, LPG_{A_100}, LPG_{B_100} and LPG_{40} were written using the point by point method described in section 3.6.3. The layout for the instrumentation is shown in figure 7.16. The black marks in the figure indicate the smaller period end of the fibre, i.e. 390µm. LPG_{A_100} and LPG_{B_100} were positioned such that their respective chirp directions were directly opposite to one another. This was to enable a direct comparison to be made of the directional resin flow effects across the sensors.

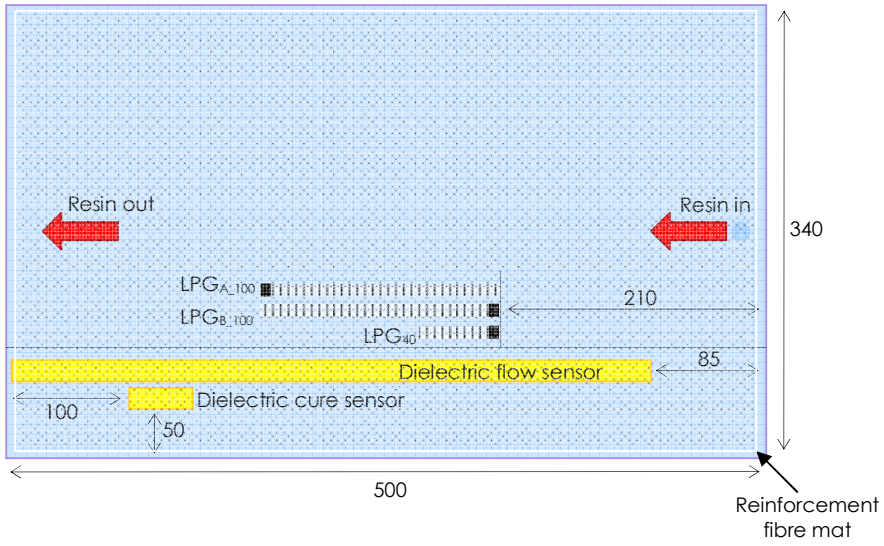

Figure 7.16 Layout of sensors on vacuum infusion flat plate mould. The reinforcement fibre mat was placed on top of the sensors. The black marks on the LPGs indicate the smaller period end, 390µm, with the period linearly increasing along the length.

The stages of preparation of the mould and sensors are shown in figure 7.17. The individual optical fibre sensors were fixed using thin section (10mm x 5mm) heat resistant Kapton tape on either side of the sensor whilst the fibre was held taut and straight. The optical fibre tip of the Fresnel refractometer was fixed using a single piece of Kapton. The dielectric sensors were fixed to the mould surface also using Kapton. The mould was placed on a heated curing bed and was then sealed with black sealing putty and the vacuum lines were fitted. Uni-axial glass NCF (discussed in more detail in the discussion) reinforcement was used and placed in 5 layers with the fibre lay at angles of -45°, 0°, +45°, 90°, and 0°, relative to the optical fibre axis. The finished component had a design V_f of 60%.

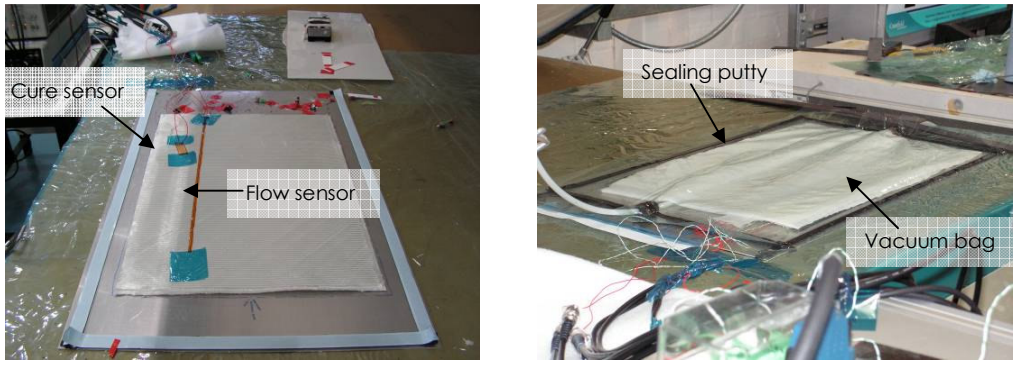

(a) (b)

Figure 7.17 Vacuum infusion at two stages of preparation: (a) shows counter mould with fibre sensors fitted and first layer of reinforcement placed on top. The dielectric cure and flow sensors are then placed on this layer. (b) The top layer of reinforcement mat is then placed and the plastic bagging is sealed around the mould.

The spectra of the LPGs are shown in figures 7.18 and 7.19. Figure 7.18 highlights the issue of LPG integration with composites discussed in chapter 6. The effects are compounded by the combined effects of poorly developed bands and the increased interaction length of the sensors (10cm) resulting in destruction of the spectral features.

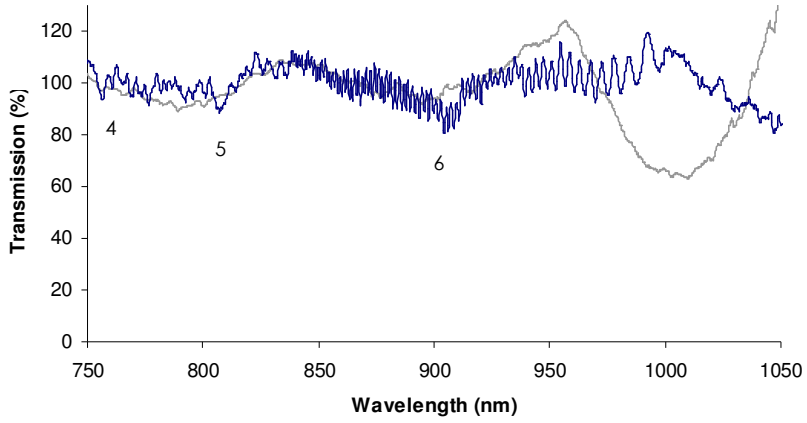

Figure 7.18 Spectrum of LPG_{A_100} (—). The spectrum shows the poorly developed bands (notated as bands 4 – 6). The spectrum of the sensor placed in the mould with the reinforcement fibres is also shown (—).

The spectrum of LPG_{40}, shown in figure 7.19, is that when the sensor is in contact with the reinforcement fabric. The spectrum exhibits prominent spectral distortions, for example, band 6, annotated on the figure, and has split into two bands. It is possible that this is due to a localised transverse load on the grating. This may be due to the stitching on the NCF reinforcement, which has a period of 4mm, being brought into direct contact with the grating when vacuum is applied.

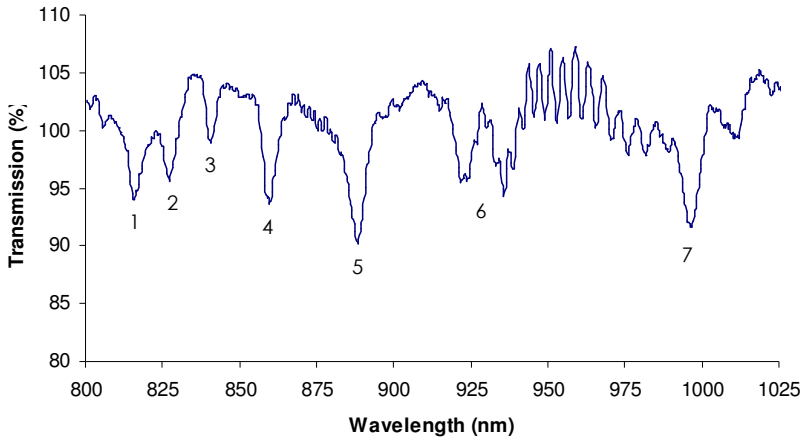

Figure 7.19 Spectrum of LPG_{40} after integration. The spectrum has the bands notated from 1 – 7. Band 6 appears to have split in two with two spectral features.

The MY750 (a diglycidyl ether of bisphenol A (DGEBA) based resin) was mixed with the HY5992 hardener and maintained at 30°C to prevent cure during the resin infusion and maintain a sufficiently low viscosity to improve the movement of the resin through the fabric. During the infusion process the mould was maintained at 40°C. To initiate cure the mould was then taken to 80°C for a 6 hour isothermal cure cycle.

7.3.4 Results

The results are divided into two main areas and discussed independently. Flow measurement is dealt with first followed by cure.

7.3.4.1 Flow

Initially partial vacuum is applied to smooth the bag surface before full vacuum is applied [8]. At full vacuum the resin is drawn through the reinforcement material in the mould. Figure 7.20, (a)-(l), shows the movement of resin through the flat plate mould with timed markings on the bag surface, these are the blue lines in the figure, this aids correlation between the dielectric cure sensors and the fibre sensors. A resin front straight and perpendicular to the flow direction is ideal but in this case the initial resin front exhibited a triangular formation.

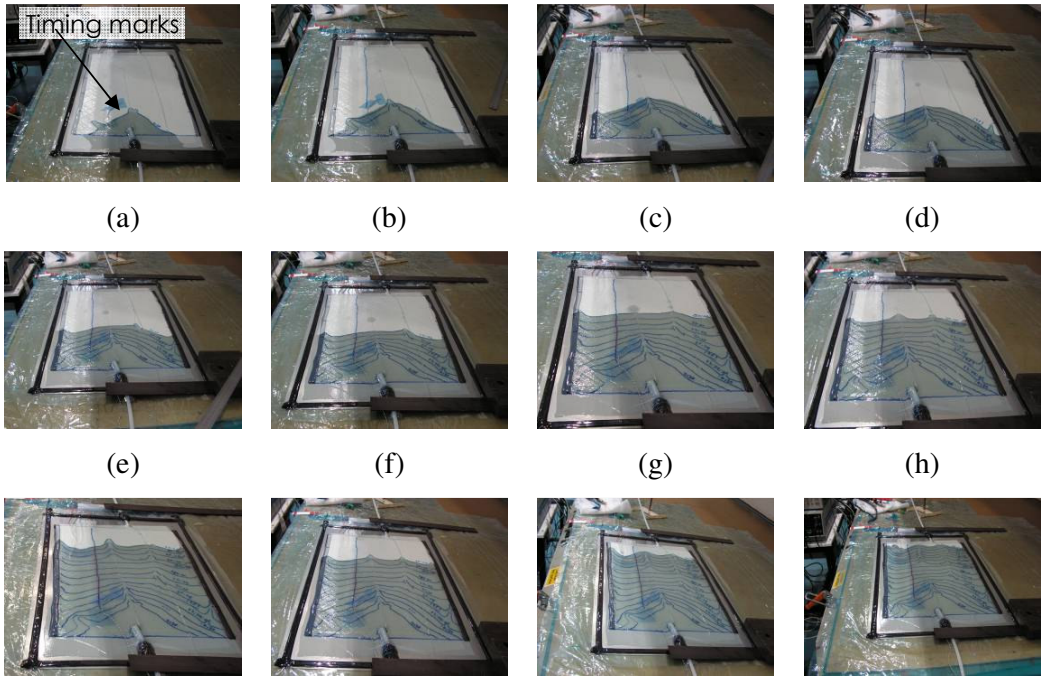

Figure 7.20 Shows progression of resin through reinforcement fibres during resin transfer. The vacuum outlet and inlet pipes are shown at the top and bottom of the figures respectively.

The combined results of the visual measurements and the dielectric sensor are shown in figure 7.21. They show very good agreement and demonstrate a measurement standard for resin flow equivalent to that achievable with non-fibre techniques [3].

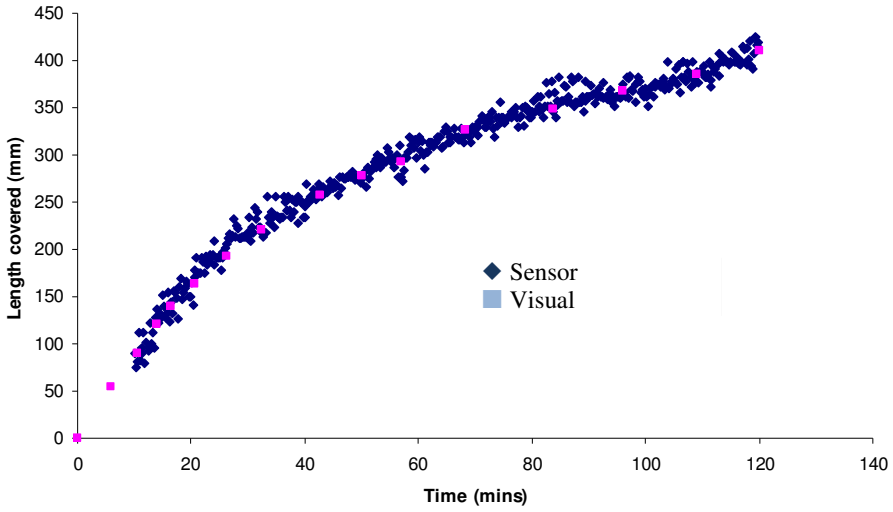

Figure 7.21 Correlation of visual resin front (■) and recorded resin front (◆) from the dielectric sensor.

A similar analysis technique, discussed in chapter 6, was used for the spectral anlaysis of the optical fibre sensors. This was driven by the poor spectral information available because of the integration problems of LPG sensors with composite materials. The results for both of the 100mm LPG sensors are shown in figures 7.22 and 7.23.

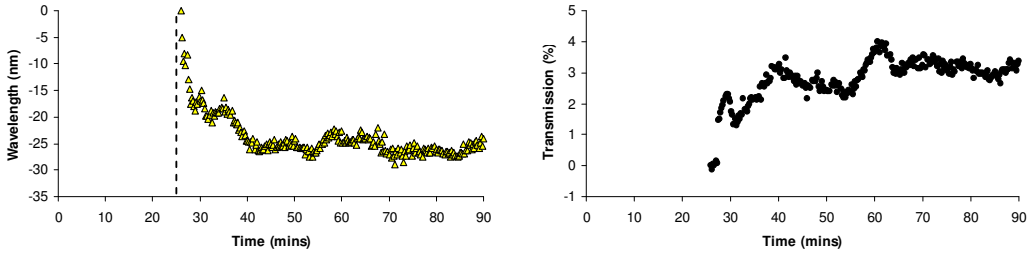

Figure 7.22 Wavelength (▲) and transmission (•) response of LPG_{A_100} to resin flow.

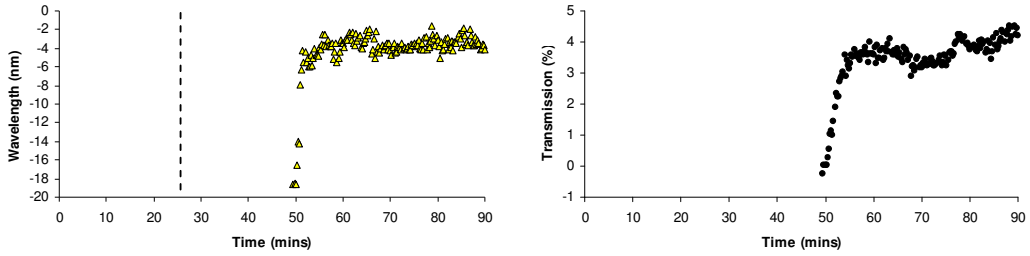

Figure 7.23 Wavelength (▲) and transmission (•) response of LPG_{B_100} to resin flow.

Spectral features at 925nm from LPG_{A_100} which may correspond to band 6 of figure 7.18 and 950nm from LPG_{B_100} are shown to exhibit wavelength shifts at different times during the infusion process. Chapter 5 introduced the concept of chirped LPG gratings as directional flow sensors and these results may be indicative of the resin coating the sensors as the reinforcement material is impregnated. The chirp direction of the two sensors are contra-directional to one another and perpendicular to the resin flow. This is evidenced by the opposing wavelength shift in the results of both sensors, e.g. a negative wavelength shift for $LPG_{A\_100.}$ A large wavelength shift, relative to the chirp results of chapter 5, is shown of greater than 20nm but this may be attributed to the long length of the sensor and the broad nature of the resultant bands. The change in transmission however is similar (~4%).

Figure 7.24 shows the spectra for band 5 at the start and end of the infusion process and at the early stages of the cure. The band experiences an apparent positive wavelength shift due to the presence of the resin as the longer wavelength edge is shifted to longer wavelengths. The initiation of the cure process, as the mould is ramped to an isothermal cure temperature of 80℃ is also apparent as the pre-cure spectrum shows the band wavelength shifted downwards. The transmission shift is also apparent with a reduction in transmission depth due to broadening of the band as the resin coats the sensor. As the temperature is increased to initiate the cure the attenuation band exhibits an increase in attenuation depth.

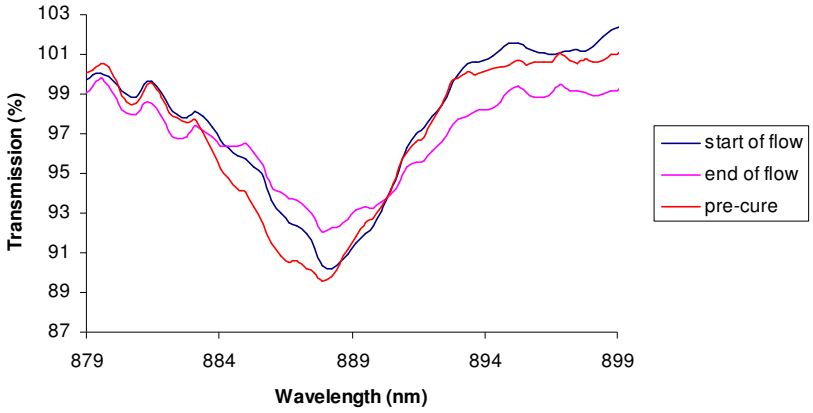

Figure 7.24 Wavelength spectra for band 5 of LPG_{40} at the start and end of resin flow and at the start of the isothermal cure cycle.

The positive shift for resin presence shown in the results for LPG_{B_100} is also exhibited by LPG_{40}, figure 7.25. As expected both sensors exhibit an apparent positive wavelength shift because their chirp orientations are in the same direction to the resin flow. The results show a small shift in wavelength, 1nm, relative to the longer LPG sensors. A large noise signal of ±0.5nm, ensures the detection of flow is compromised and the results should be treated with caution. The transmission change of 4% is similar to that of LPG_{A_100} and LPG_{B_100}.

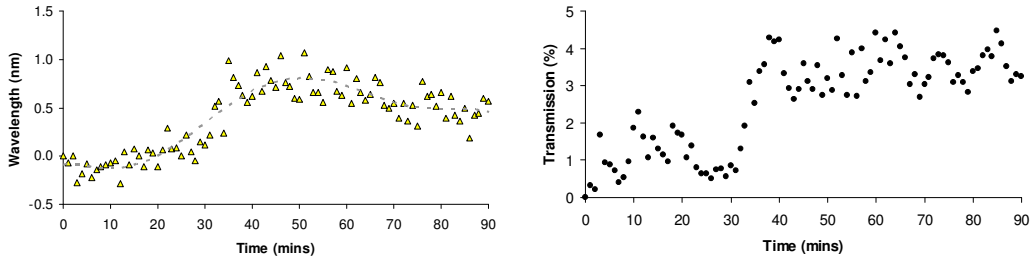

Figure 7.25 Wavelength (△) and transmission (•) response of LPG_{40} to resin flow. A 2nd order polynomial is shown with wavelength shift to aid correlation with the dielectric flow sensor.

Band 6 of LPG_{40} exhibited splitting, figure 7.19, and the effect of the resin coating the sensor on this band is shown in figure 7.26. It can be seen that the combination of the high index resin and increased temperature to isothermal conditions (80°C) creates a new band at the early stages of cure, formed by the combination of these two spectral features.

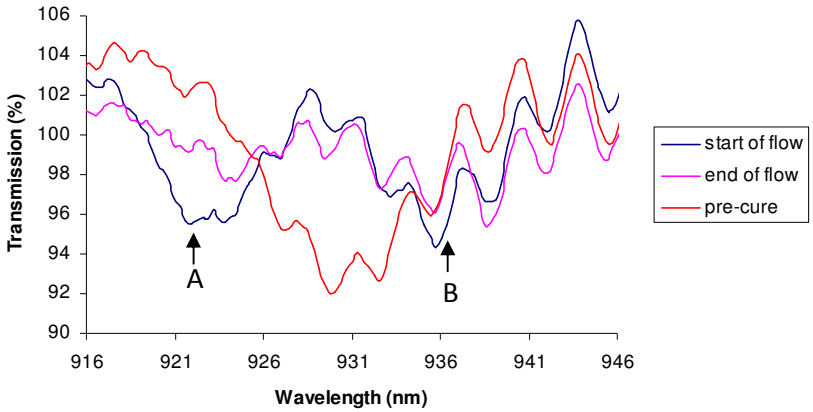

Figure 7.26 Wavelength spectra for band 6 of LPG40 at the start and end of resin flow and at the start of the isothermal cure cycle.

Analysis of these features, figure 7.27, reveals the nature of the new band as both features are shown to shift towards each other.

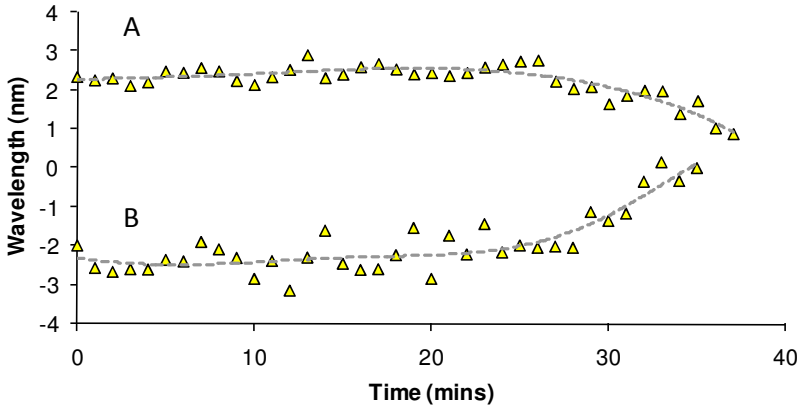

Figure 7.27 Wavelength (△) response of band 6 for LPG_{40} to resin flow. A 6^{th} order polynomial is shown for visual purposes. how the two bands moving towards each other to create a single band.

Demonstration of the flow monitoring capabilities of LPG sensors is shown in figure 7.28. The chirped LPGs responses are compared with the visual measurements over time. The LPG_{40} wavelength response is compared with the results from the dielectric sensor and fitted with a 3rd order polynomial. The fitted response is then compared with the visual results and show good agreement. The timings of the wavelength responses of LPG_{A_100} and LPG_{B_100} and their respective locations on the mould are also shown. The combined results indicate the possibility of using such devices as composite flow sensors. Differences between the visual and calculated results may be attributed to the non-uniform flow front indicated in figure 7.20. However the compromised nature of the sensor spectra due to the integration problems is likely to have a greater role over the quality of the results.

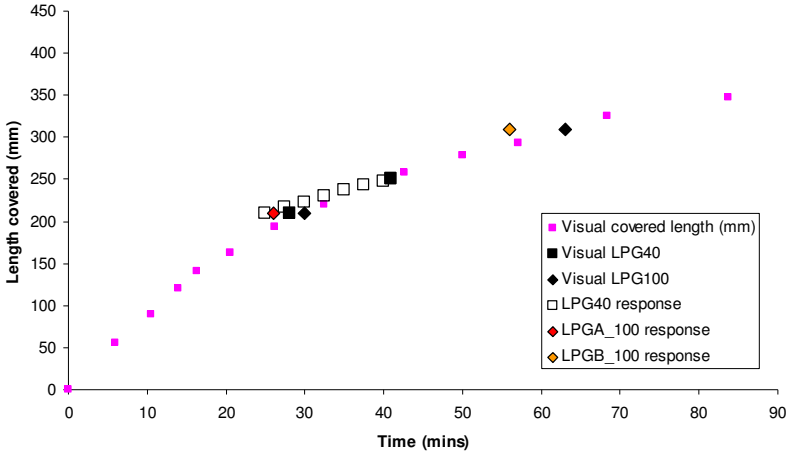

Figure 7.28 Flow sensor comparison of LPG sensors and visual measurements, LPG_{40} (□), LPG_{A_100}(◆) and LPG_{B_100}(◆). The visual start and end locations for all the sensors are shown as (◆) for LPG_{A_100} and LPG_{B_100} and (■) for LPG_{40}.

7.3.4.2 Cure

The cure results presented here are from LPG_{40}. The poor spectral information from the two 100mm length sensors provided no reportable evidence of the cure. Figure 7.29 shows the wavelength shift and transmission change attributed to the refractive index

change of the resin during the isothermal cure cycle for an attenuation band. The degree of cure is also shown for comparison.

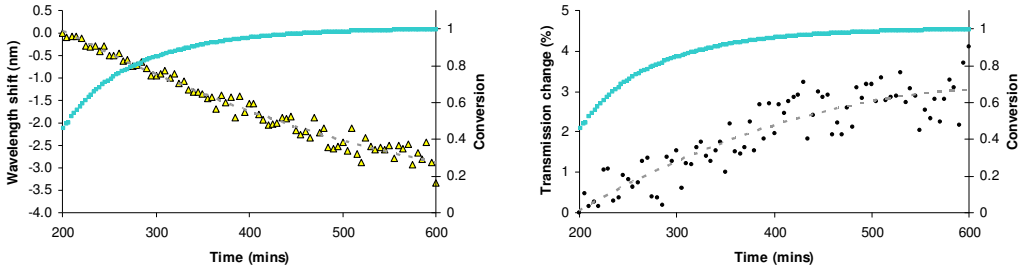

(a) (b)

Figure 7.29 Wavelength shift (▲) and transmission change (•) for band 5 of LPG40 to resin cure.

Band 4 shows a negative wavelength shift of 3nm. The results are problematic as they do not show a close wavelength relationship with the cure conversion. The almost linear appearance of the shift shown in figure 7.29(a) may be attributed to hydrogen out diffusion [9,10]. This would affect the cure results particularly due to the elevated temperature and relatively long cure time. It was believed a sufficiently long period of time was taken to allow the hydrogen to diffuse out without the need for heating the fibre to speed up this process. The effect of the cure is still discernible with the results revealing a slight change in slope at about 350 minutes and an apparent increase in noise. The transmission results, figure 7.29(b) seem to indicate a more favourable result although there is a significant noise contribution.

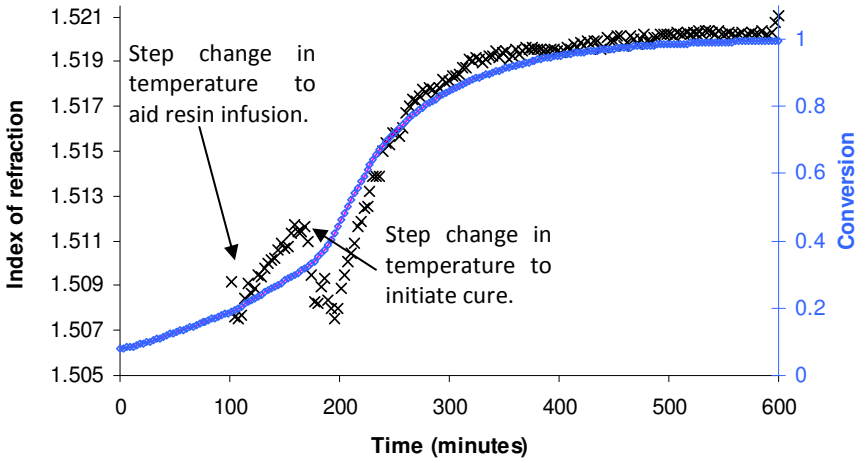

Figure 7.30 Cure conversion and refractive index change during cure calculated from the optical fibre Fresnel refractometer.

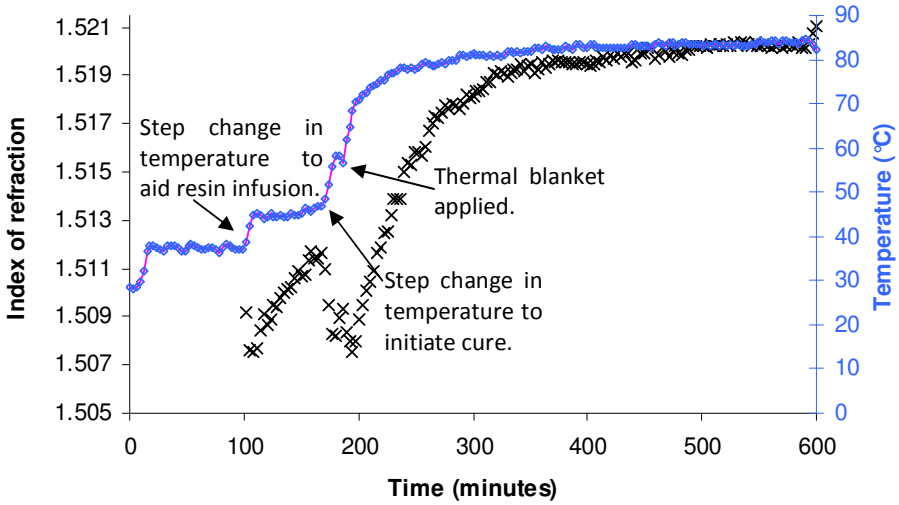

Figure 7.31 Temperature profile and refractive index change during cure calculated from the Fresnel refractometer.

The optical fibre Fresnel refractometer results are shown in figure 7.30 and 7.31. Temperature changes applied to the vacuum infusion process to aid the resin impregnation are annotated. This is evidenced as a sharp decrease in refractive index because of the negative thermo-optic coefficient of the resin. At each point, the

temperature stabilises and the cure effect starts to dominate where there is a turning point and the refractive index begins to increase sharply. The overall progression of the resins' refractive index is shown to closely match that of the cure kinetic model. This agrees well with the laboratory based trials discussed in chapter 4. A linear correlation between the Fresnel calculated refractive index and the conversion is shown in figure 7.32. The parameters measured are not necessarily expected to be linear in relationship as they correspond to different phenomena, namely refractive index change during cure and heat generation during the cure reaction. However the close agreement between the two indicates the possibility of using the resin refractive index change as a measurement for cure progression.

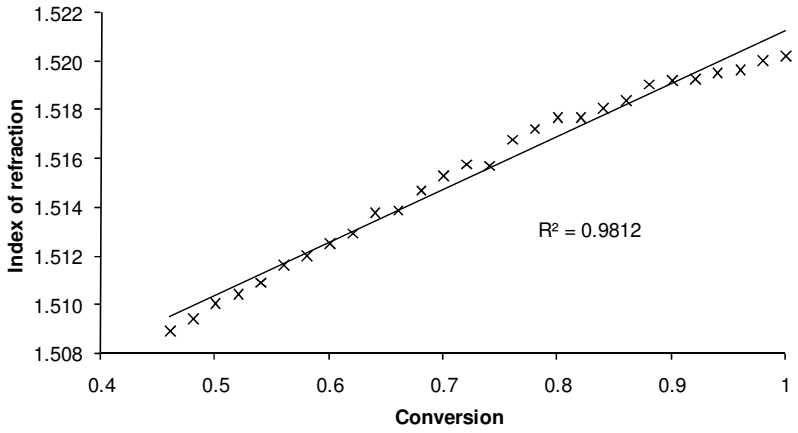

Figure 7.32 Linear correlation of band 5 for conversion and transmission change.

7.3.5 Discussion

Both flow and cure measurements were achieved with LPG sensors and the optical fibre Fresnel refractometer. The Fresnel measurements showed improved results compared with those of the RTM trial. The calculated refractive index change during cure showed very good direct correlation with later stages of the cure (>50%) compared with the cure conversion model. Allowing for a refractive index variation of ±0.001 from the linear correlation, it is possible to assess the cure of the resin in this trial utilising refractive index data with an error of ±5%. The improved results may be attributed to the experience gained with the first trial in fitting and placing the fibre sensors.

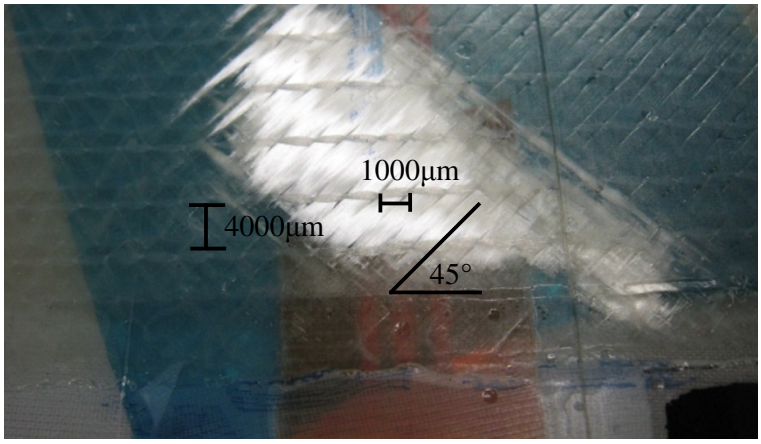

Figure 7.33 Bottom layer of fibre reinforcement in contact with optical fibre sensors. The sensors are not shown in the picture.

However the issue of spectral distortion of the LPG sensors in direct contact with the reinforcement fabric remains. Figure 7.33 shows the layer of reinforcement fibre that was in direct contact with the optical fibre sensors. The fibre was at an angle of 45° to the LPG sensors. A periodic structure is seen in the reinforcement material: of 4000µm period for the stitching between the fibre bundles and 1000µm between the individual bundles. The transverse load exerted by the weight of the material directly on top of the sensors and the application of vacuum may cause localised birefringent effects on the fibre at the stitching locations. This may lead to the spectral distortion evident in the results. Furthermore the shorter period defined by the fibre bundles of 1000µm may destroy the coupling of the LPGs by inducing a mechanical LPG profile on the fibre.

The flow detection results indicated the possibility of both detecting the presence of resin in a composite structure and the movement of the resin front in a single sensor. The results from the three LPG designs when compared with a visual measurement showed the sensors ability to detect the arrival of the resin front and the subsequent flow of the resin over the sensor length, despite the compromised nature of the spectra. A polynomial fit to the wavelength shift of a chirped LPG sensor appeared to correspond well with the visual data. Further work is necessary, to maintain the spectra of LPG sensors integrated in composite structures to improve the quality of the results. The cure results from the LPG sensors appeared to show the refractive index change as the cure progressed and demonstrated the possibility of utilising integrated fibre optic sensors as process monitoring sensors in the manufacture of composite components.

7.4 References

1. Liu, B. C., Bickerton, S. and Advani, S. G. (1996), 'Modelling and simulation of resin transfer moulding (RTM)-gate control, venting and dry spot prediction', *Composites A*, 27, p. 135–41.
2. Ferland, P., Guittard, D. and Trochu, F. (1996), 'Concurrent methods for permeability measurement in resin transfer moulding', *Polymer Composites*, 17, p. 149–58.
3. Skordos, A.A., Karkanas, P.I. and Partridge, I.K. (2000), 'A Dielectric Sensor for Measuring Flow in Resin Transfer Moulding', *Measurement Science & Technology*, 11(1), p. 25-31.
4. Gay, Daniel, Hoa, Suong V, and Tsai Stephen W. (2002). *Composite Materials: Design and Applications* (4th ed.), CRC press, Florida.
5. Harris Bryan (1998). *Engineering composite materials*, Maney publishing, London.
6. Dimopolous A. (2008). Effect of carbon nanotubes on epoxy, Cranfield University, Cranfield.
7. Dunkers, J. P., Lenhart, J. L., Kueh, S. R., van Zanten, J. H., Advani, S. G., Parnas, R. S. (2001), 'Fiber Optic Flow and Cure Sensing for Liquid Composite Molding', *Optics and Lasers in Engineering*, 35(2), p. 91.
8. Schwartz Mel (1983). *Composite Materials Handbook* (2nd ed.), McGraw Hill, USA.
9. Mizunami, T., Fukuda, T., (2006), 'FEM Calculation And The Effects Of Hydrogen Diffusion In Fabrication Processes Of Long-Period Fiber Gratings, *Optics Communications*, 259, p.581–586.
10. Masuda, Y.; Nakamura, M.; Komatsu, C.; Fujita, K.; Yamauchi, M.; Kimura, M.; Mizutani, Y.; Kimura, S.; Suzaki, Y.; Yokouchi, T.; Nakagawa, K.; Ejima, S. (2004), 'Wavelength Evolution Of Fiber Bragg Gratings Fabricated From Hydrogen-Loaded Optical Fiber During Annealing', *Journal Of Lightwave Technology*, 22(3), p. 934-941.

Conclusions and future work

8

8.1 Thesis summary

Composites are becoming an increasingly significant engineering material; in some modern engineering systems their use is critical. Because of this careful control during their manufacture is important and requires well considered process controls. In this thesis an LPG based sensor was investigated as a possible alternative to traditional sensing methods, used to monitor the processing of these materials. An LPG sensor was demonstrated as a refractive index sensor with the index parameter used as an indication of cure with a UV curable epoxy. This work and extensions of it, including industrial applications, were discussed and conclusions and possibilities for future work are developed in this chapter.

8.2 Thesis conclusions

The use of an LPG as a cure monitoring sensor with a UV curable epoxy was demonstrated. The closely matched but lesser refractive indices of the epoxy and the cladding of the host optical fibre ensured that a wavelength shift of the LPG attenuation bands was evident during the cure of the epoxy. The measured wavelength shift was

attributed to the changing refractive index of the curing resin. This was the first reported demonstration of the use of an LPG as a cure sensor and the technique opens up the possibility of using such sensors for in-situ cure monitoring. Critically, the resin being monitored must have a refractive index that is lower than that of the host optical fibre. Fresnel based refractometers working at 1581nm and 833nm showed that the calibrated response of an embedded LPG sensor agreed to within $6x10^{-4}$ refractive index units. This measurement capability is comparable with other optical fibre based refractive index measurement techniques and exceeds the specification of the oils used to calibrate the LPG sensors. Comparison with both dielectric spectroscopy and differential scanning calorimetric measurements revealed that the refractive index change agreed well over the full cure of the epoxy, figure 8.1. Close agreement with these industrially recognised measurement techniques provides good reason to further research the use of LPG sensors to monitor the cure of composite materials.

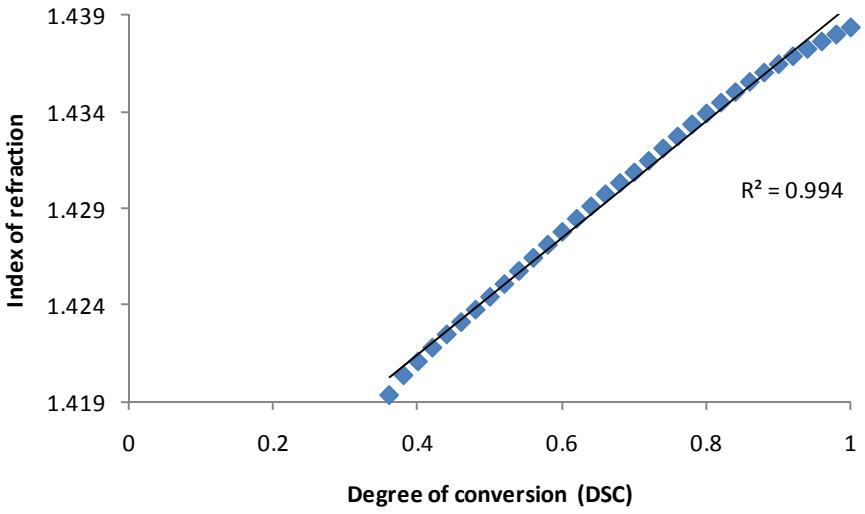

Figure 8.1 Comparison of index of refraction measurement with DSC. R^2 value of 0.994.

The results presented in chapters 4 and 5 illustrated the potential of LPG sensors as resin cure sensors. The ability to integrate such sensors in composite materials due to their small size and relative compatibility with the reinforcement fibres suggested their aptitude as cure monitoring sensors.

However the problem of measuring the refractive index change of the resin in composite systems compared with neat resin systems was evident in the subsequent results presented in chapters 6 and 7. The technical difficulties involved in integrating LPGs in a composite environment was confirmed by industrial applications in composite component manufacturing, e.g. RTM and vacuum infusion tests and composite products, e.g. superconducting magnet systems. The direct contact of composite reinforcing fibres with the LPG grating location (the stripped region of optical fibre where an LPG sensor is located), was shown to affect the transmission spectrum of the devices. The distortion of the spectra of LPG's integrated into the glass fibre composite structures within the superconducting magnets resulted in an inability to follow the cure or monitor the progress of a resin impregnating the reinforcement network. This is highlighted in figure 8.2 where the spectral bands synonymous with LPGs are shown to degrade when integrated in a composite structure.

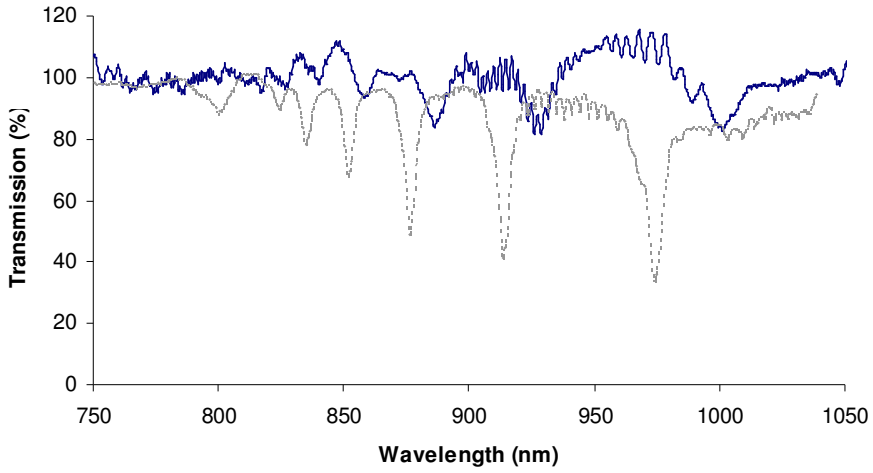

Figure 8.2 Distortion of LPG when integrated in a composite structure, in this case glass weave as discussed in chapter 7.

It was shown that this may be due in part to the localised mechanical effects caused by the periodic spacing of the reinforcement fibres. Thus future applications of LPG sensors require a method of both maintaining the structural homogeneity of the sensor and the component and preventing masking of the sensor's sensitivity to refractive index.

Adaptive grating techniques were also described in this work: a novel LPG based flow sensor with directional sensing capability and an in fibre Mach-Zehnder interferometer based refractometer. A directional sensing capability was demonstrated with a chirped LPG sensor when detecting the flow of resin across the sensor. The chirp to the period of the LPG acts to broaden the attenuation bands. Directional sensitivity is achieved by the wavelength selectivity of the band given by the central wavelength equation 8.1, discussed in chapter 3. The arrival of a high index resin from either axial direction of an LPG sensor placed perpendicular, figure 8.3, to an expected resin flow would manifest as a distortion to the attenuation band profile dependant of the direction. Such devices may provide useful in-situ sensors in complex moulds for composite components.

$$\lambda^i = \left[n_{eff} - n^i_{clad}\right]\Lambda \qquad 8.1$$

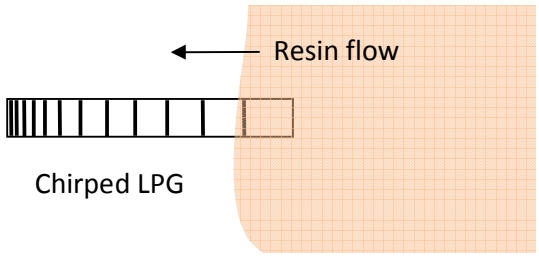

Figure 8.3 Directional LPG based flow sensor placed perpendicular to resin flow.

The ability of an LPG to couple light into and out of the cladding was used to create an in-fibre Mach-Zehnder interferometer. The phase sensitivity of the device was demonstrated to sense the refractive index of a curing resin. The device is shown in figure 8.4. The first LPG acts to couple the light into the cladding of the fibre at specific wavelengths governed by the characteristic equation of an LPG. Uncoupled light continues to propagate in the core. This cladding mode then acts as the sensing arm of the interferometer whilst the uncoupled light acts as a reference arm. The results showed that as the cure progressed and the refractive index changed, an associated phase change was measurable due to the change in effective index of the cladding modes.

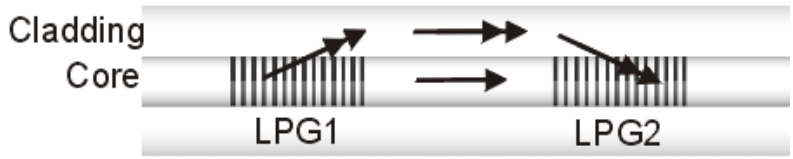

Fig 8.4 Operation of cascaded LPGs as an MZI. Discussed in chapter 5 [4].

The integration of LPGs within complex composite components was also achieved. A demonstration of the application of LPG sensors for temperature sensing in superconducting magnets and as cure and flow sensors in resin transfer process techniques was presented. The work demonstrated that, despite technological incompatibility, e.g. more robust tooling and machinery, between the composite manufacturing environment and optical fibres, a method of combining the two was achieved.

8.3 Future work

Arc induced LPGs have been reported with no sensitivity to bends imparted on the fibre for bend curvatures of up to $10m^{-1}$ with as few as 2 grating planes [1]. These types of LPGs may show improved resistance to spectral distortion due to integration issues with reinforcement fibres. The reduced number of grating planes creates a sensor with a much reduced interaction length with the reinforcement fibres. The small gauge length, ≈400µm, allows for a sensor to be placed within a resin rich area of a composite without affecting a components structural integrity.

Mechanically induced gratings in optical fibres were discussed in chapters 3 and 6. The ability to form long period gratings on an optical fibre without mechanical applied pressure systems was demonstrated by Yang et al. [2]. Here, a periodic structure was overlaid with an optical fibre with its protective jacket removed. The fibre was then coated with a curing epoxy and as the epoxy cured and contracted, an LPG was shown to develop as the cure progressed. This form of grating may provide a method of

incorporating fibre within composites. A periodic former could be encapsulated around a bare fibre section and placed within a mould. The curing epoxy will then cause the fibre to compact onto the former and create attenuation bands that reveal the progress of the cure.

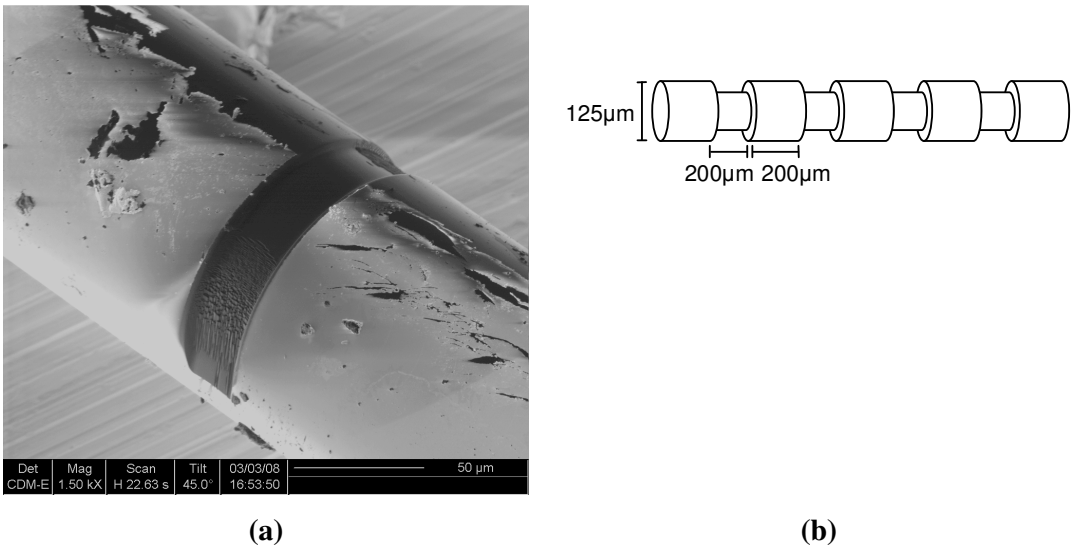

(a) **(b)**

Figure 8.5 (a) Etched surface of optical fibre showing a 25µm wide slot of 10µm depth. This was achieved using an FIB (focused ion beam) system at the School of Applied Sciences, Cranfield University. (b) Representation of microstructured LPG using an etching technique with example dimensions.

A similar technique may be achieved by using microstructured fibres. Figure 8.5 shows an SEM photograph of a fibre subjected to an ion beam etching process that has removed a 25µm long strip of cladding to a depth of 10µm on one side of the fibre. If a sufficient number of etched areas were periodically formed on the surface of the fibre it may be possible to induce a grating on the fibre through the affect of a curing resin. If the fibre were placed in a resin rich location within a mould, the curing reaction may cause concentrated stress regions due to shrinkage at these etched locations that in turn cause axial loading and localised birefringence along the fibre.

LPGs fabricated in double clad fibres have been proposed as temperature and strain sensors [3]. Figure 8.6, shows the response of the transmission spectrum of an LPG written in a double clad fibre. The figure shows the response of an LPG immersed in an

oil of refractive index that is matched to that of the cladding that is being heated. As the oil is heated from room temperature, the refractive index decreases and the bands associated to the outer cladding modes are seen to respond. This is because the effective indices of these modes are bound by the refractive index of the external environment. The bands associated to the inner cladding modes on the other hand exhibit less sensitivity as these modes are bound by the refractive indices of the core and cladding only. These devices may be more readily integrated in composite structures for strain and temperature sensing. The inner cladding modes may exhibit more defined spectral features as there is a degree of mechanical stability imparted by the outer cladding. Refractive index measurements using such sensors are still restricted by the same issue of the typical high index value of structural resins. The LPG sensor shows a poor refractive index sensitivity to indices higher than that of the fibre, chapter 3.

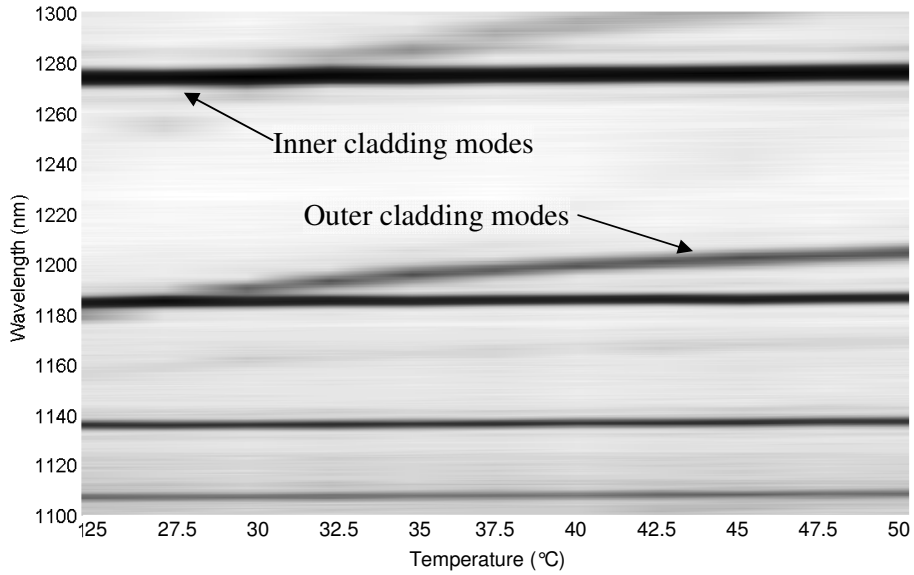

Figure 8.6 Spectrum of a 400μm period LPG written in double clad fibre (Fibercore SMM900). The graph shows the outer and inner cladding modes response to temperature. Temperature increments correspond to 2.5°C.

There is a great flexibility with the application of LPGs because of the ability to design, e.g. different fibre types, period, coatings. Chirped LPGs have been discussed and demonstrated in chapters 5, 6 and 7 as directional liquid level and flow sensors. This

technique could be further improved, with superior writing techniques, to increase their resolution capability and the possibility of sensitive flow sensors with a resolution determined by the period of the grating.

8.3 References

1. Nam, S. H., Zhan C., Lee, J., Hahn, C., Reichard, K., Ruffin, P., Deng, K-L, and Yin, S. (2005), 'Bend-insensitive ultra short long-period gratings by the electric arc method and their applications to harsh environment sensing and communication', *Optics Express,* 13(3), p. 731-737.

2. Yang, R.-C., San, K-C, Wu, E, Lin, C.H. and Lee, H.P. (2004), A thermal-curing induced long-period fiber grating on corrugated metal fixture. In: (CLEO) Conference on Lasers and Electro-Optics, San Jose, California, May 16-21 2004, Vol. 2, p. 280-282.

3. Shin, C.-S., Chianga C-C and Liaw S-K, (2006), Comparison of single and double cladding long period fiber grating sensor using an intensity modulation interrogation system', *Optics Communications,* 258, p. 23–29.

4. Murphy, R.P., James, S.W. and Tatam, R.P. (2007), 'Multiplexing of Fiber-Optic Long-Period Grating-Based Interferometric Sensors', *Journal of Lightwave Technology*, 25(3), p. 825-829.

Publications

Journals

1 Monitoring cure in epoxies containing carbon nanoparticles via optical fibre grating refractometers
A Dimopoulos, S J Buggy, A A Skordos, S W James, R P Tatam and I K Partridge
Polymer (accepted October 2008)

2 Optical fibre grating refractometers for resin cure monitoring
S J Buggy, E Chehura, S W James, R P Tatam
Journal of Optics A: Pure and Applied Optics, 2007, 9(6)

Conferences

1 A long period grating based directional flow sensor
S J Buggy, E Chehura, S W James, R P Tatam
19th International Conference on Optical Fibre Sensors, 14 – 18/04/2008, Perth, Australia

2 Cure monitoring of a UV cured epoxy resin using a LPG Mach-Zehnder interferometer
S J Buggy, R P Murphy, S W James, R P Tatam
European workshop on optical fibre sensors (EWOFS 2007), 4th–6th June, Naples, Italy

3 Fibre grating refractometer sensors for composite process monitoring
S J Buggy, E Chehura, A A Skordos, A Dimopoulos, S W James, I K Partridge and R P Tatam
Optical Metrology 2007, 18 – 21/06/2007, Munich, Germany

4 Fibre gratings for cure monitoring of epoxy resins
S J Buggy, E Chehura, S W James, R P Tatam
18th International Conference on Optical Fibre Sensors, 23 – 27/10/2006, Cancun, Mexico

5 Refractive index measurements using LPGs for cure monitoring applications
S J Buggy, E Chehura, S W James, R P Tatam
Britain's young engineers at the House of Commons, 13/03/2006, Houses of Parliament, UK

6 Fibre optic long period grating refractometer for resin cure monitoring
S J Buggy, E Chehura, S W James, R P Tatam
Physics – A Century after Einstein, 10 – 14/04/2005, University of Warwick, UK

7 Long period gratings (LPG's) for cure monitoring applications
S J Buggy, E Chehura, S W James, R P Tatam
Photon 06, 4 – 7/09/2006, University of Manchester, UK

8 Refractive index measurement using LPGs for cure monitoring applications
S J Buggy, S W James, R P Tatam
Photonex 05, 5 – 6/10/2005, Stoneleigh Park, Coventry, UK